MODELING AND SIMULATION OF PHOTOBIOREACTORS FOR BIOLOGICAL HYDROGEN PRODUCTION

A THESIS SUBMITTED TO
THE GRADUATE SCHOOL OF NATURAL AND APPLIED SCIENCES
OF
MIDDLE EAST TECHNICAL UNIVERSITY

BY

DOMINIC DEO ANDROGA

IN PARTIAL FULFILLMENT OF THE REQUIREMENTS
FOR
THE DEGREE OF DOCTOR OF PHILOSOPHY
IN
BIOTECHNOLOGY

APRIL 2014

Approval of the thesis:

MODELING AND SIMULATION OF PHOTOBIOREACTORS FOR BIOLOGICAL HYDROGEN PRODUCTION

submitted by **DOMINIC DEO ANDROGA** in partial fulfillment of the requirements for the degree of **Doctor of Philosophy in Biotechnology Department, Middle East Technical University** by,

Prof. Dr. Canan Özgen ______________________
Dean, Graduate School of **Natural and Applied Sciences**

Prof. Dr. Filiz Bengü Dilek ______________________
Head of Department, **Biotechnology**

Prof. Dr. İnci Eroğlu ______________________
Supervisor, **Chemical Engineering Dept., METU**

Asst.Prof. Dr. Başar Uyar ______________________
Co-supervisor, **Chemical Engineering Dept., Kocaeli University**

Examining Committee Members:

Prof. Dr. Ufuk Gündüz ______________________
Biological Sciences Dept., METU

Prof. Dr. İnci Eroğlu ______________________
Supervisor, Chemical Engineering Dept., METU

Asst. Prof. Dr. Gökhan Kars ______________________
Biology Department, Selçuk University

Asst.Prof. Dr. Harun Koku ______________________
Chemical Engineering Dept., METU

Asst. Prof. Dr. Tuba Hande Ergüder ______________________
Environmental Engineering Dept., METU

Date: 10th April, 2014

I hereby declare that all information in this document has been obtained and presented in accordance with academic rules and ethical conduct. I also declare that, as required by these rules and conduct, I have fully cited and referenced all material and results that are not original to this work.

Name, Last name: DOMINIC DEO ANDROGA

Signature :

ABSTRACT

MODELING AND SIMULATION OF PHOTOBIOREACTORS FOR BIOLOGICAL HYDROGEN PRODUCTION

Androga, Dominic Deo
PhD., Department of Biotechnology
Supervisor : Prof. Dr. İnci Eroğlu
Co-Supervisor: Asst. Prof. Dr. Başar Uyar

April 2014, 242 pages

In applications of photofermentative hydrogen production, maintaining optimal temperature, feed composition, pH range and light intensity is the most critical objective for growth and proper functioning of the photosynthetic bacteria. Response Surface Methodology was applied to optimize temperature and light intensity for indoor hydrogen production using *Rhodobacter capsulatus*. Surface and contour plots of the regressions models developed revealed a maximum hydrogen production rate of 0.566 mol $H_2/m^3/h$ at 27.5°C and 287 W/m^2 and a maximum hydrogen yield of 0.326 mol H_2/mol substrate at 26.8°C and 285 W/m^2.

For outdoor photofermentative hydrogen production many parameters are beyond manipulation, hence effective control of temperature in photobioreactors is a challenge. In this thesis, an internal cooling system was designed and built, and its performance in outdoor tubular photobioreactors was tested during summer months in Ankara, Turkey. Four tubular reactors with and without *Rhodobacter capsulatus* were operated in parallel. Counter-current and co-current cooling modes were implemented to stabilize the reactor temperature. The temperatures were found to be strongly influenced by the solar irradiance and the ambient air temperature during daytime; however, the surface temperature was found to be approximately constant along the reactor length. Counter-current cooling was found to be more effective compared to co-current cooling in controlling temperatures inside the reactor. High biomass growth rate (0.10 per hour) and hydrogen production rate (1.3 mol $H_2/m^3/h$) was achieved in the outdoor operations.

The flow distribution in tubular reactors operated at steady state conditions was analyzed using computational fluid dynamics. A one-dimensional dynamic thermal model to describe the variations of temperature in tubular reactors operated outdoors with or without internal cooling was developed and verified with experimental data. The transient model included the effects of convection and radiative heat exchange on the reactor temperature throughout the day. The model established is useful in estimating the cost-effectiveness of producing hydrogen in large scale outdoors.

Keywords: Photofermentation, biohydrogen, tubular photobioreactor, *Rhodobacter capsulatus* response surface methodology, computational fluid dynamics, dynamic thermal model

ÖZ

BİYOLOJİK HİDROJEN ÜRETİMİ İÇİN FOTOBİYOREAKTÖR MODELEME VE SIMULASYON

Androga, Dominic Deo
Doktora, Biyoteknoloji Bölümü
Tez Yöneticisi : Prof. Dr. İnci Eroğlu
Ortak Tez Yöneticisi: Yrd. Doç. Dr. Başar Uyar

Nisan 2014, 242 sayfa

Fotofermentatif hidrojen üretimi uygulamalarında en uygun ışık şiddeti, sıcaklık, besiyeri kompozisyonu vepH aralığında çalışılması fotosentetik bakterilerlerin üreme ve fonksiyonlarını yerine getirmeleri için zorunludur. Tepki yüzeyi yöntemiyle, sıcaklık ve ışık şiddeti, *Rhodobacter capsulatus* ile kapalı ortamda yapılan hidrojen üretimi deneyleriyle, optimize edilmiştir. İstatistiksel modellerin incenlemesiyle oluşturulan yüzey grafikleri en yüksek hidrojen üretim hızının, 0.566 mol $H_2/m^3/h$, 27.5°C and 287 W/m^2 ve en yüksek hidrojen veriminin, 0.326 mol H_2/mol besiyeri, 26.8°C and 285 W/m^2 olduğunu göstermiştir.

Açık havada fotofermentasyonla hidrojen üretiminde parametreleri ayarlamak mümkün değildir, özellikle fotobiyoreaktörlerde sıcaklık kontrolu çok zordur. Bu tezde borusal fotobiyoreaktör içine yerleştirilen iç soğutma borusu sistemiyle açık havada yaz aylarında Ankara Türkiye'de reaktörleri test etmek mümkün olmuştur.

Dörtlü parallel reaktör sistemiyle *Rhodobacter capsulatus* içeren ve içermeyen ortamlarda eş veya ters yönlü soğutma akışlarında çalışılarak reaktör sıcaklığı istenilen düzeyde tutulabilmiştir. Reaktör sıcaklığının, güneş ışıması ve çevre sıcaklığıyla gün boyu değiştiği, ancak reaktörün yüzey sıcaklığının reaktör boyunca sabit kaldığı görülmüstur. Ters yönlü soğutmanın eş yönlü soğutmaya nazaran reaktör sıcaklığının kontrölünde daha etkili olduğu bulunmuştur. Açık hava uygulaması esnasında, yüksek bakteri büyüme hızı (0.10 saatte) ve hidrojen üretim hızına (1.28 mol $H_2/m^3/h$) ulaşılmıştır.

Kararlı durumda akış dağılımı hesaplamalı akışkan dinamiği (CFD) ile analiz edilmiştir. İçten soğutmalı ve soğutma olmayan borusal reaktörlerdeki gün boyu değişen sıcaklık değerlerini hesaplayan tek boyutlu dinamik bir ısı modeli geliştirilmiş ve model sonuçlarının deneysel verilerle örtüştüğü gözlenmiştir kanıtlanmıştır. Oluşturulan zamana bağlı model gün boyu değişen konveksiyonel ve radyasyon ısı transferini dikkate almaktadır. Bu model büyük ölçekli açık hava hidrojen üretimi uygulamalarında maliyet verimliliği hesaplamalarına yardımcı olacaktır.

Anahtar Kelimeler: Fotofermentasyon, borusal fotobiyoreaktör, biyohidrojen, *Rhodobacter capsulatus*, tepki yüzeyi yöntemi, hesaplamalı akışkan dinamiği, dinamik ısı modeli

To My Family

ACKNOWLEDGEMENTS

I would like to express my sincere gratitude to my supervisor Prof. Dr. İnci Eroğlu for her guidance, advice, encouragements and support throughout the study. The numerous dicussions and criticisms gave me good insight on the research work. I also thank my co-supervisor Asst. Prof. Dr. Başar Uyar and Asst. Prof.Dr. Harun Koku for their counsel, suggestions and recommendations. The contributions of Prof. Dr. Ufuk Gündüz, Prof. Dr. Meral Yücel, Asst. Prof. Dr. Gökhan Kars and Asst. Prof. Dr. Tuba Hande Ergüder is greatly acknowledged.

I am grateful to my labmates Muazzez Gürgan, Emrah Sağır, Emine Kayahan, Pelin Sevinç, Sevgi Gökçe Avcıoğlu, Güneş Tuncay, Melih Can Akman and Engin Koç for their friendship, collaboration and assistance. The discussions, suggestions and help you gave in carrying out some of the procedures is greatly appreciated.

The technical assistance of Isa Çağlar at the Glass Workshop in the Chemical Engineering Department, METU and Gülten Orakçı is appreciated.

I am indebted to Bilgi Alver, Mert Oymak and Bariş Erdoğan for their friendship and support.

Lastly, I sincerely thank my family for their support and love. I especially thank my parents for their love, encouragement and trust.

This research study was supported by the METU Grant No: BAP-07-02-2012-002 and the EU 6th Framework Integrated Project 019825 (HYVOLUTION). Financial support by the Scientific and Technological Research Council of Turkey (TÜBITAK-BIDEB) through the PhD Fellowship for Foreign Citizens (Code 2215) is acknowledged.

TABLE OF CONTENTS

ABSTRACT v

ÖZ vii

ACKNOWLEDGEMENTS x

TABLE OF CONTENTS xi

LIST OF TABLES xvii

LIST OF FIGURES xx

LIST OF SYMBOLS AND ABBREVIATIONS xxxiii

CHAPTERS

1. INTRODUCTION 1

2. LITERATURE SURVEY 9
   - 2.1 Photofermentative Hydrogen Production by Purple Non-Sulfur Bacteria 9
   - 2.2 Optimization of Temperature and Light Intensity for Improved Hydrogen Production 13
   - 2.3 Reactor Design 16
      - 2.3.1 Types of Reactors 16
      - 2.3.2 Reactor Orientation, Mixing and Light Distribution 19
      - 2.3.3 Material of Construction 20
      - 2.3.4 Mode of Operation 20
      - 2.3.5 Temperature Control 20
   - 2.4 Modeling of the Reactor Systems 23
      - 2.4.1 Computational Fluid Dynamics Modeling 23
      - 2.4.2 Modeling Heat Transfer in the Solar Bioreactors 26

2.5 Outdoor Photofermentative Hydrogen Production....................................27
2.6 Aim of the Thesis 32
3. MATERIALS AND METHODS..35
3. 1 The Microorganisms..35
3. 2 Growth and Hydrogen Production Media 35
3. 3 The Experimental Procedure 36
3.3.1 Preparation of the Inoculum...36
3.3.2 Cleaning, Sterilization and Leakage Tests of the Photobioreactors 36
3.3.3 Inoculation of the Photobioreactor..36
3.3.4 Sampling 36
3.3.5 Shut-down of the Photobioreactors..37
3. 4 The Indoor Experiments 37
3. 5 The Outdoor Experiments 37
3.5.1 The Experiments Performed with Variable Flowrates.........................37
3.5.2 The Experiments Performed at Constant Flowrates 40
3.6 Analytical Methods...42
3.6.1 Cell Concentration 42
3.6.2 pH..43
3.6.3 Temperature 43
3.6.4 Light Intensity..43
3.6.5 Organic Acid Analysis..43
3.6.6 Gas Analysis 44
4. MODELING AND SIMULATION OF PHOTOBIOREACTORS 45
4.1 Response Surface Methodology 45
4.2 Dynamic Heat Transfer Model for the Outdoor Operated Tubular Bioreactors..47
4.2.1 Thermal Balance on the Reacting System 47
4.2.1.1 Radiative Heat Transfer 48
4.2.1.2 Convective Heat Transfer...51
4.2.1.3 Heat Removed by the Cooling Water 54

4.2.1.4 Work Done by the Pump 55
4.2.1.5 Metabolic Heat of the Reacting System 55
4.3 The Model Assumptions 57
4.4 The Model Algorithm 58
4.5 Heat Transfer at the Auxilliary Section of the Reactor System 61
4.6 The Overall Heat Transfer Coefficient 62
4.7 Modeling of Growth and Hydrogen Production by *Rhodobacter capsulatus* 63
5. OPTIMIZATION OF TEMPERATURE AND LIGHT INTENSITY FOR IMPROVED PHOTOFERMENTATIVE HYDROGEN PRODUCTION......... 65
5.1 Hydrogen Production Rate.. 65
5.2 Hydrogen Yield.. 70
5.3 Discussion.. 74
6. COMPUTATIONAL FLUID DYNAMICS MODELING OF FLOW IN TUBULAR BIOREACTORS 77
6.1 Meshing 78
6.2 Velocity Distribution and Pressure Drop in the Tubular Photobioreactors 79
6.3 Comparisons of the Volumetric Flow Rates in the Tubular Reactors 91
7. DYNAMIC MODELING OF TEMPERATURE CHANGE IN OUTDOOR OPERATED TUBULAR BIOREACTORS FOR HYDROGEN PRODUCTION 95
7.1 Dynamic Modeling of Temperature Change in Bioreactors Operated at Different Flow Rates in Outdoor Conditions.. 96
7.1.1 Temperature Variation in Bioreactors Operated at Different Flow Rates in Outdoor Conditions.. 96
7.1.2 Temperature Change Along the Bioreactors Operated at Different Flow Rates in Outdoor Conditions... 101
7.1.3 Dynamic Modeling of Temperature Change in Bioreactors Operated at Different Flow Rates in Outdoor Conditions 102

7.1.4 Energy Transfer in the Bioreactors Operated at Different Flow Rates in Outdoor Conditions............103
7.2 Radial Variation of Temperature in Bioreactors Operated Outdoors at Different Flow Rates 108
7.3 Dynamic Modeling of Temperature Change in Bioreactors Operated Outdoors With or Without *Rhodobacter capsulatus* YO3 109
7.3.1 Temperature Variation in the Outdoor Operated Reactors 109
7.3.2 Temperature Change Along the Reactor Surface 115
7.3.3 Dynamic Modeling of Temperature Change in the Outdoor Operated Bioreactors 118
7.3.4 Energy Transfer in the Outdoor Operated Reactors 124
7.3.5 Comparison of the Overall Heat Transfer Coefficients 129
8. PHOTOFERMENTATIVE HYDROGEN PRODUCTION BY RHODOBACTER CAPSULATUS IN OUTDOOR OPERATED PHOTOBIOREACTORS 133
8.1 Growth and Hydrogen production by *Rhodobacter capsulatus* YO3 in Outdoor Conditions............133
8.2 Modeling of Growth and Hydrogen Production by *Rhodobacter capsulatus* YO3 139
8.2.1 Modeling the Growth *Rhodobacter capsulatus* YO3 139
8.2.2 Modeling the Hydrogen Production by *Rhodobacter capsulatus* YO3 141
8.3 Comparison of Hydrogen Production Studies............144
9. CONCLUSIONS AND RECOMMENDATIONS............149
9.1 Conclusions 149
9.2 Recommendations 152
REFERENCES 153

APENDICES

A. FLOW THEORY 175

A.1 COMSOL: GENERAL SINGLE PHASE FLOW THEORY 175

A.2 ANALYTICAL SOLUTION OF PRESSURE DROP 176

B. THE COMPOSITION OF THE FEED MEDIUM 179

C. THE DIMENSIONS OF THE PHOTOBIOREACTOR................................. 181

D. HYDRODYNAMIC AND THERMAL ENTRY LENGTH IN THE TUBULAR PHOTOBIOREACTORS.. 183

E. ELEMENTARY BALANCE TO DETERMINE STOICHIOMETRIC COEFFICIENTS FOR BIOMASS FORMATION... 185

F. POLYMATH PROGRAM FOR CALCULATING THE METABOLIC HEAT ……..……………………………………………………………………………187

G. ABSORBANCE SPECTRUM OF RHODOBACTER CAPSULATUS AT DIFFERENT CELL CONCENTRATIONS 191

H. UNSTEADY STATE ONE_DIMENSIONAL THERMAL MODEL 193

Subsystem A: Calculation of the Total Radiative Heat Transferred 194

Subsystem B: Calculation of the Convective Heat transfer Coefficients in the Reactor 195

Subsystem C: Calculation of the Cooling Duty.. 196

Subsystem D: Calculation of the Amount of Energy in the Reactor 196

Subsystem E: Calculation of the Average Reactor Temperature 196

I. SAMPLE CALCULATIONS.. 197

I.1 Volume of the Outdoor Photobioreactor 197

I.2 Surface Area of the Photobioreactor and the Cooling Tube..................... 197

I.3 Determination of the Hydraulic Diameter.. 198

I.4 Reactor Medium Mass Flow Rate 198

I.5 Cooling Water Mass Flow Rate 199
I.6 Reynolds Number..199
I.7 Prandtl Number 199
I.8 Peclet Number 199
I.9 Hydrodynamic and Thermal Entry Length 200
I.10 Pressure Drop Calculation...200
I.11 Hydrualic Retention Time Calculation 201
I.12 Average Volumetric Flow Rate..202
I.13 Latitude (φ) of Ankara 202
I.14 Solar Declination (δ) 202
I.15 Solar Hour Angle (ω) 202
I.16 Angle of incidence (θ_z)..202
I.17 Work Done by the Pump..203

J. DATA RELATIVE TO CHAPTER 7…...205

CURRICULUM VITAE...239

LIST OF TABLES

TABLES

Table 2.1 Comparison of photofermentative hydrogen production performances in flat panel photobioreactors operated in outdoor conditions. 29

Table 2.2 Comparison of photofermentative hydrogen production performances in tubular photobioreactors operated in outdoor conditions...................................... 31

Table 2.3 Comparison of photofermentative hydrogen production performances in other types of photobioreactors operated in outdoor conditions. 31

Table 3.1 Summary of the experiments to determine the change temperature in the tubular photobioreactors circulated at different flow rates. 39

Table 3.2 Summary of the experiments to determine the change temperature in the tubular photobioreactors circulated at constant flow rate. The experimements were performed in the summer of 2013. 42

Table 4.1 Constants used in developing the transient thermal model. 60

Table 5.1 Experimental design table for the optimization of hydrogen production rate and yield. 66

Table 5.2. ANOVA for the rate of hydrogen production by *Rhodobacter capsulatus* DSM1710. 67

Table 5.3 ANOVA for hydrogen yield by *Rhodobacter capsulatus* DSM1710. 71

Table 6.1 Geometry of the tubular reactors. 77

Table 6.2 The number and quality of elements used in meshing the tubular reactors. 78

Table 7.1 Summary of the maximum air temperatures, ground temperatures and solar radiation recorded during the outdoor experiments. 97

Table 7.2 Summary of the maximum air temperatures, ground temperatures and solar radiation recorded during the outdoor experiments. 110

Table 7.3 The average values of the convective heat transfer coefficients between the reactor medium and the outer surface of the cooling tube (h_{co}) and the cooling water and the inner surface of the cooling tube (h_{ci})..131

Table 7.4 The minimum and maximum values of the thermal resistances between the reactor medium and the outer surface of the cooling tube (R_o), the cooling tube wall (R_{wall}) resistance and the thermal resistance between the cooling water and the inner surface of the cooling tube (R_i)...131

Table 8.1 The rate constants for acetic acid consumption and the coefficient of determination values (R^2) for the *Rhodobacer capsulatus* YO3 cultures grown on media containing 40 mM acetic acid reactors as carbon source and 4 mM sodium glutamate as nitrogen source..136

Table 8.2 Summary of the results showing the acetic acid and glutamate consumption for growth, maintenance and hydrogen production by *Rhodobacter capsulatus* YO3. The experiment was performed on the 5th of August, 2013.......138

Table 8.3 Logistic model parameters and the coefficient of determination values (R^2) for the growth *Rhodobacter capsulatus* YO3 cultures grown on media containing 40 mM acetic acid reactors as carbon source and 4 mM sodium glutamate as nitrogen source in outdoor conditions. 139

Table 8.4 Modified Gompertz model parameters and the coefficient of determination values (R^2) for the cumulative hydrogen produced by *Rhodobacter capsulatus* YO3 cultures in outdoor conditions...141

Table B.1 The composition of the standard basal, growth and hydrogen production medium.. 179

Table B.2 The composition of trace element solution. 180

Table B.3 The composition of the vitamin solution... 180

Table D.1 Summary of the hydrothermal entry lengths and thermal entry lengths of the different flow rates used in the outdoor experiments. 184

Table J.1 Summary of the results showing the acetic acid and glutamate consumption for growth, maintenance and hydrogen production by *Rhodobacter capsulatus* YO3. The experiment was performed on the 7th of August, 2013. 233

Table J.2 Summary of the results showing the acetic acid and glutamate consumption for growth, maintenance and hydrogen production by *Rhodobacter capsulatus* YO3. The experiment was performed on the 8th of August, 2013. 234

LIST OF FIGURES

FIGURES

Figure 2.1 Photofermentative hydrogen production 9

Figure 2.2 Photofermentative hydrogen production in purple non sulfur bacteria..12

Figure 2.3 Parameters affecting photofermentative hydrogen production. 14

Figure 2.4 Operation of the (A) Flat panel photobioreactor and (B) Tubular photobioreactor in outdoor conditions 18

Figure 2.5 The convoluted relationships between fluid dynamics, light energy and reaction kinetics in the photobioreactor 23

Figure 4.1 Schematic of the energy transfer in the reactor system. 47

Figure 4.2 Schematic of the annular section of the reactor system. 52

Figure 4.3 Solution algorithm of the thermal model...59

Figure 4.4 A schematic of the heat transfer in the reactor system. 61

Figure 5.1 Correlation between the predicted and observed values for hydrogen production rate using batch cultures of *Rhodobacter capsulatus* DSM1710. 67

Figure 5.2 Plots for the hydrogen production rate model using batch cultures of *Rhodobacter capsulatus* DSM1710. (A) Three-dimensional response surface plot and (B) Two-dimensional contour plot. The arrow on the response surface plot indicates the position of the maximum hydrogen production rate. 69

Figure 5.3 Correlation between the predicted and observed values of hydrogen yield using batch cultures of *Rhodobacter capsulatus* DSM1710. 72

Figure 5.4 Effects of temperature and light intensity on hydrogen yield for batch cultures of *Rhodobacter capsulatus* DSM1710. (A) Three dimensional response surface plot and (B) Two dimensional contour plot. The arrow on the response surface plot indicates the position of the maximum yield...................................... 73

Figure 6.1 The velocity distribution in the U-tube modular reactor. The inset shows the yellow streamlines, which are the paths taken by particles as they are carried by the flow.. 80

Figure 6.2 The change in velocity across the tube diameters of the U-tube modular reactor. The reactor consists of 2 tubes and the arc length is the horizontal distance between the tubes. 81

Figure 6.3 Pressure drop in the U-tube modular reactor. 82

Figure 6.4 The velocity distribution in the serpentine reactor. The yellow streamlines in the inset show the path taken by particles as they are carried by the flow. 83

Figure 6.5 The change in velocity across the tube diameters of the serpentine reactor. The reactor consists of 25 tubes and the arc length is the horizontal distance between the tubes. 84

Figure 6.6 Pressure drop in the serpentine reactor. 85

Figure 6.7 The velocity distribution in the manifold reactor with a single inlet and a single outlet. The yellow streamlines in the inset show the path taken by a particle as it is carried by the flow. 86

Figure 6.8 The change in the velocity across the tube diameters of the manifold type reactor with a single inlet and a single outlet. The reactor consists of 9 tubes and the arc length is the horizontal distance between the tubes............................. 87

Figure 6.9 Pressure drop in the manifold type reactor with a single inlet and a single outlet.. 88

Figure 6.10 Velocity distribution in the manifold type reactor with multiple inlets and a single outlet. The yellow streamlines in the inset show the path taken by a particle as it is carried by the flow. 89

Figure 6.11 The flow distribution across reactor tubes in the manifold type reactor with multiple inlets and a single outlet. The arc length is the horizontal distance between the tubes. The reactor consists of 9 tubes 90

Figure 6.12 Pressure drop in the manifold type reactor with multiple inlets and single outlet. 91

Figure 6.13 Comparison of the average volumetric flow rate in the U-tube modular reactor and the serpentine reactor. 93

Figure 6.14 Comparison of the average volumetric flow rate in the manifold type tubular reactor with a single inlet and single outlet and multiple inlets and a single outlet. 93

Figure 7.1 The change in the air temperature, the ground temperature and solar radiation with time. The reactor contained water circulated at Reynolds number 160, in co-current flow to the cooling water. The experiment was performed on the 28th of August, 2008. The start of the experiment (0th hour) corresponds to 7 a.m. and the end of the experiment (12th hour) corresponds to 7 p.m. 97

Figure 7.2 Comparisons of the changes in the reactor inlet temperatures, the reactor outlet temperatures, the cooling water inlet temperatures and the cooling water outlet temperatures with time. The reactors contained water circulated at Reynolds number 160, 1860 and 2700 in co-current flow to the cooling water. 99

Figure 7.3 Comparisons of the changes in the reactor inlet temperatures, the reactor outlet temperatures, the cooling water inlet temperatures and the cooling water outlet temperatures with time. The reactors contained water circulated at Reynolds number 160, 1860 and 2700 in counter-current flow to the cooling water...........100

Figure 7.4 The change in the surface temperature along the reactor tube at different times of the day. The experiment were performed on the 1st of September, 2012 using reactor with medium circulated at 5.8×10^{-2} kg/s (*Re* = 2700) and the reactor were co-currently cooled 102

Figure 7.5 Comparison of the changes in the reactor average temperatures, the reactor surface temperatures and the predicted (model) temperatures with time. The experiment was performed on the 29th of August, 2012. 103

Figure 7.6 Comparison of the energy gained or lost during the day time in the co-currently cooled reactors operated in outdoor conditions. 106

Figure 7.7 Comparison of the energy gained or lost during the day time in the counter-currently cooled reactors operated in outdoor conditions. 107

Figure 7.8 Temperature variation in radial direction for the reactor circulated at low flow rate. 108

Figure 7.9 Temperature variation in radial direction for the reactor circulated at high flow rate. 109

Figure 7.10 The change in the air temperature, the co-currently cooled reactor ground temperature, the counter-currently cooled reactor ground temperature and the solar radiation with time. The experiments were carried out on the 5th of August, 2013. The start of the experiment (0th hour) corresponds to 6 a.m. and the end of the experiment (14th hour) corresponds to 8 p.m. 110

Figure 7.11 Comparisons of the changes in the reactor inlet temperatures, the reactor outlet temperatures, the cooling water inlet temperatures and the cooling water outlet temperatures with time. The experiments were performed on the 5th of August, 2013 using co-currently cooled reactors with and without *Rhodobacter capsulatus* YO3 cultures operated in outdoor outdoors. 112

Figure 7.11 Comparisons of the changes in the reactor inlet temperatures, the reactor outlet temperatures, the cooling water inlet temperatures and the cooling water outlet temperatures with time. The experiments were performed on the 5th of August, 2013 using counter-currently cooled reactors with and without *Rhodobacter capsulatus* YO3 cultures operated in outdoor outdoors. 113

Figure 7.13 The change in the surface temperature along the reactor tube at different times of the day. The experiments were performed on the 5th of August, 2013 using co-currently cooled reactors with and without *Rhodobacter capsulatus* YO3 cultures operated in outdoor conditions 116

Figure 7.14 The change in the surface temperature along the reactor tube at different times of the day. The experiments were performed on the 5th of August, 2013 using co-currently cooled reactors with and without *Rhodobacter capsulatus* YO3 cultures operated in outdoor conditions 117

Figure 7.15 Comparison of the changes in the reactor average temperatures, the reactor surface temperatures and the predicted (model) temperatures with time. The experiments were performed on the 5th of August, 2013 using co-currently cooled reactors with and without *Rhodobacter capsulatus* YO3 cultures operated in outdoor conditions. 119

Figure 7.16 Comparison of the changes in the reactor average temperatures, the reactor surface temperatures and the predicted (model) temperatures with time. The experiments were performed on the 5th of August, 2013 using counter-currently cooled reactors with and without *Rhodobacter capsulatus* YO3 cultures operated in outdoor conditions. 120

Figure 7.17 Comparisons of the experimental reactor surface temperatures and the average reactor temperatures with the predicted reactor temperatures. The dashed lines indicate the 10 % temperature error margin. The experiments were performed on the 5th of August, 2013 using co-currently cooled reactors with and without *Rhodobacter capsulatus* YO3 cultures operated in outdoor conditions. 122

Figure 7.18 Comparisons of the experimental reactor surface temperatures and the average reactor temperatures with the predicted reactor temperatures. The dashed lines indicate the 10 % temperature error margin. The experiments were performed on the 5th of August, 2013 using counter-currently cooled reactors with and without *Rhodobacter capsulatus* YO3 cultures operated in outdoor conditions................ 123

Figure 7.19 Comparison of the energy gained or lost during the day time in the outdoor operated reactors. The experiments were performed on the 5th of August, 2013 using co-currently cooled reactors operated outdoors with and without *Rhodobacter capsulatus* YO3 cultures.. 125

Figure 7.20 Comparison of the energy gained or lost during the day time in the outdoor operated reactors. The experiments were performed on the 5th of August, 2013 using counter-currently cooled reactors operated outdoors with and without *Rhodobacter capsulatus* YO3 cultures.. 126

Figure 7.21 Comparison of the overall heat transfer coefficients between the medium in the reactors and the cooling water. The experiments were performed on the 5th of August, 2013, using reactors with and without *Rhodobacter capsulatus* YO3. 130

Figure 8.1 The change in the biomass concentration, the cumulative hydrogen production and acetic acid concentration in the outdoor reactors with time. The experiments were performed on the 5th of August, 2013 using reactors operated outdoors with and without *Rhodobacter capsulatus* YO3 cultures. (A) Biomass growth, (B) Cumulative hydrogen produced and (C) Acetic acid consumption. Co-currently cooled reactor and Counter-currently cooled reactor 134

Figure 8.2 Comparison of the experimental and predicted biomass growth in the outdoor operated reactors. Experimental value and predicted value using the logistic model. 140

Figure 8.3 Comparison of the experimental and predicted biomass growth in the outdoor operated reactors. Experimental value and predicted value using the logistic model. 143

Figure 8.4 Comparison of the hydrogen production rates in outdoor operated tubular reactors......145

Figure 8.5 Comparison of the hydrogen production rates in outdoor operated panel reactors and the present study reactors. 146

Figure C.1 Dimensions of the (A) photobioreactor and (B) reactor tube and the cooling tube......181

Figure G.1 Absorbance spectrum of *Rhodobacter capsulatus* YO3 at different cell concentrations. 191

Figure H.1 The dynamic thermal model solved using Matlab 2013_Simulink.....193

Figure H.2 The total radiative heat transferred in the dynamic thermal model.....194

Figure H.3. Calculation of the convective heat transfer coefficients in the reactor. 195

Figure H.4 calculations of the amount of heat removed by the cooling water......196

Figure H.5 Calculation of the amount of heat in the reactor. 196

Figure H.6 Calculations of the average reactor temperature. 196

Figure J.1 The change in the air temperature, the ground temperature and solar radiation with time. The reactors contained water circulated at Reynolds number 1860 and 2700, in co-current flow to the cooling water. The start of the experiment (0th hour) corresponds to 7 a.m. and the end of the experiment (12th hour) corresponds to 7 p.m......205

Figure J.2 The change in the air temperature, the ground temperature and solar radiation with time. The reactors contained water circulated at Reynolds number 1860 and 2700, in counter-current flow to the cooling water. The start of the experiment (0th hour) corresponds to 7 a.m. and the end of the experiment (12th hour) corresponds to 7 p.m. 206

Figure J.3 Comparison of the changes in the reactor average temperatures, the reactor surface temperatures and the predicted (model) temperatures with time. The experiment was performed on the 28th of August, 2012. 207

Figure J.4 Comparison of the changes in the reactor average temperatures, the reactor surface temperatures and the predicted (model) temperatures with time. The reactors were counter-currently cooled. 208

Figure J.5 The change in air temperature, the co-currently cooled reactor ground temperature, counter-currently cooled reactor ground temperature and solar radiation with time. The experiments were carried out on the 7th and 8th of August, 2013. The start of the experiment (0th hour) corresponds to 6 a.m. and the end of the experiment (14th hour) corresponds to 8 p.m. 209

Figure J.6 Comparisons of the changes in the reactor inlet temperatures, the reactor outlet temperatures, the cooling water inlet temperatures and the cooling water outlet temperatures with time. The experiments were performed on the 7th of August, 2013 using co-currently cooled reactors with and without *Rhodobactercapsulatus* YO3 cultures operated in outdoor conditions................. 210

Figure J.7 Comparisons of the changes in the reactor inlet temperatures, the reactor outlet temperatures, the cooling water inlet temperatures and the cooling water outlet temperatures with time. The experiments were performed on the 7th of August, 2013 using counter-currently cooled reactors with and without *Rhodobactercapsulatus* YO3 cultures operated in outdoor conditions................. 211

Figure J.8 Comparisons of the changes in the reactor inlet temperatures, the reactor outlet temperatures, the cooling water inlet temperatures and the cooling water outlet temperatures with time. The experiments were performed on the 8th of August, 2013 using co-currently cooled reactors with and without *Rhodobacter capsulatus* YO3 cultures operated in outdoor conditions. 212

Figure J.9 Comparisons of the changes in the reactor inlet temperatures, the reactor outlet temperatures, the cooling water inlet temperatures and the cooling water outlet temperatures with time. The experiments were performed on the 8th of August, 2013 using counter-currently cooled reactors with and without *Rhodobacter capsulatus* YO3 cultures operated in outdoor conditions. 213

Figure J.10 The change in the surface temperature along the reactor tube at different times of the day. The experiments were performed on the 7th of August, 2013 using co-currently cooled reactors with and without *Rhodobacter capsulatus* YO3 cultures operated in outdoor conditions 214

Figure J.11 The change in the surface temperature along the reactor tube at different times of the day. The experiments were performed on the 7th of August, 2013 using counter-currently cooled reactors with and without *Rhodobacter capsulatus* YO3 cultures operated in outdoor conditions 215

Figure J.12 The change in the surface temperature along the reactor tube at different times of the day. The experiments were performed on the 8th of August, 2013 using co-currently cooled reactors with and without *Rhodobacter capsulatus* YO3 cultures operated in outdoor conditions 216

Figure J.13 The change in the surface temperature along the reactor tube at different times of the day. The experiments were performed on the 8th of August, 2013 using counter-currently cooled reactors with and without *Rhodobacter capsulatus* YO3 cultures operated in outdoor conditions 217

Figure J.14 Comparison of the changes in the reactor average temperatures, the reactor surface temperatures and the predicted (model) temperatures with time. The experiments were performed on the 7th of August, 2013 using co-currently cooled reactors with and without *Rhodobacter capsulatus* YO3 cultures operated in outdoor conditions.. 218

Figure J.15 Comparison of the changes in the reactor average temperatures, the reactor surface temperatures and the predicted (model) temperatures with time. The experiments were performed on the 7th of August, 2013 using counter-currently cooled reactors with and without *Rhodobacter capsulatus* YO3 cultures operated in outdoor conditions.. 219

Figure J.16 Comparison of the changes in the reactor average temperatures, the reactor surface temperatures and the predicted (model) temperatures with time. The experiments were performed on the 8th of August, 2013 using counter-currently cooled reactors with and without *Rhodobacter capsulatus* YO3 cultures operated in outdoor conditions.. 220

Figure J.17 Comparison of the changes in the reactor average temperatures, the reactor surface temperatures and the predicted (model) temperatures with time. The experiments were performed on the 8th of August, 2013 using counter-currently cooled reactors with and without *Rhodobacter capsulatus* YO3 cultures operated in outdoor conditions.. 221

Figure J.18 Comparisons of the experimental reactor surface temperatures and the average reactor temperatures with the predicted reactor temperatures. The dashed lines indicate the 10 % temperature error margin. The experiments were performed on the 7th of August, 2013 using co-currently reactors with and without *Rhodobacter capsulatus* YO3 cultures operated in outdoor conditions................ 222

Figure J.19 Comparisons of the experimental reactor surface temperatures and the average reactor temperatures with the predicted reactor temperatures. The dashed lines indicate the 10 % temperature error margin. The experiments were performed on the 7th of August, 2013 using counter-currently reactors with and without *Rhodobacter capsulatus* YO3 cultures operated in outdoor conditions. 223

Figure J.20 Comparisons of the experimental reactor surface temperatures and the average reactor temperatures with the predicted reactor temperatures. The dashed lines indicate the 10 % temperature error margin. The experiments were performed on the 8th of August, 2013 using co-currently reactors with and without *Rhodobacter capsulatus* YO3 cultures operated in outdoor conditions 224

Figure J.21 Comparisons of the experimental reactor surface temperatures and the average reactor temperatures with the predicted reactor temperatures. The dashed lines indicate the 10 % temperature error margin. The experiments were performed on the 8th of August, 2013 using co-currently reactors with and without *Rhodobacter capsulatus* YO3 cultures operated in outdoor conditions 225

Figure J.22 Comparison of the energy gained or lost during the day time in the outdoor operated reactors. The experiments were performed on the 7th of August, 2013 using co-currently cooled reactors operated outdoors with and without *Rhodobacter capsulatus* YO3 cultures. 226

Figure J.23 Comparison of the energy gained or lost during the day time in the outdoor operated reactors. The experiments were performed on the 7th of August, 2013 using counter-currently cooled reactors operated outdoors with and without *Rhodobacter capsulatus* YO3 cultures. 227

Figure J.24 Comparison of the energy gained or lost during the day time in the outdoor operated reactors. The experiments were performed on the 8th of August, 2013 using co-currently cooled reactors operated outdoors with and without *Rhodobacter capsulatus* YO3 cultures. 228

Figure J.25 Comparison of the energy gained or lost during the day time in the outdoor operated reactors. The experiments were performed on the 8th of August, 2013 using counter-currently cooled reactors operated outdoors with and without *Rhodobacter capsulatus* YO3 cultures.. 229

Figure J.26 Comparisons of the overall heat transfer coefficients between the medium in the reactors and the cooling water. The experiments were performed on the: (A) 7th of August, 2013 and (B) 8th of August, 2013 using reactors with and without *Rhodobacter capsulatus* YO3 cultures 230

Figure J.27 The change in the biomass concentration, the cumulative hydrogen production and acetic acid concentration in the outdoor reactors with time. The experiments were performed on the 7th of August, 2013 using reactors operated outdoors with and without *Rhodobacter capsulatus* YO3 cultures. (A) Biomass growth, (B) Cumulative hydrogen produced and (C) Acetic acid consumption. Co-currently cooled reactor and Counter-currently cooled reactor 231

Figure J.28 The change in the biomass concentration, the cumulative hydrogen production and acetic acid concentration in the outdoor reactors with time. The experiments were performed on the 8th of August, 2013 using reactors operated outdoors with and without *Rhodobacter capsulatus* YO3 cultures. (A) Biomass growth, (B) Cumulative hydrogen produced and (C) Acetic acid consumption. Co-currently cooled reactor and Counter-currently cooled reactor 232

Figure J.29 The first order rate kinetics consumption of acetic acid by *Rhodobacter capsulatus* YO3 cultures grown in outdoor conditions. The experiments were performed on the 5th of August, 2013 235

Figure J.30 The first order rate kinetics consumption of acetic acid by *Rhodobacter capsulatus* YO3 cultures grown in outdoor conditions. The experiments were performed on the 7th of August, 2013 236

Figure J.31 The first order rate kinetics consumption of acetic acid by *Rhodobacter capsulatus* YO3 cultures grown in outdoor conditions. The experiments were performed on the 8th of August, 2013 237

LIST OF SYMBOLS AND ABBREVIATIONS

Symbols

A_{ro}	outer surface area of the reactor (m^2)
Cp_A	heat of capacity of acetate (kJ/mol/K)
Cp_{Glu}	heat of capacity of glutamate (kJ/mol/K)
Cp_{H_2O}	heat of capacity of water (kJ/mol/K)
Cp_{Glu}	heat of capacity of hydrogen (kJ/mol/K)
$Cp_{Biomass}$	heat of capacity of bacteria (kJ/mol/K)
Cp_{CO_2}	heat of capacity of carbon dioxide (kJ/mol/K)
Cp_r	heat capacity of the reactor medium (kJ/mol/K)
d_o	outlet diameter of the cooling tube (m)
Di	inlet diameter of the reactor tube (m)
f_A	form factor
$f(t)$	shading function
g	gravity acceleration (m/s)
G_d	intensity of the diffuse solar radiation (W/m^2)
G_D	intensity of the direct solar radiation (W/m^2)
G_s	intensity of the global solar radiation (W/m^2)
H^o_A	heat of combustion of acetic acid (kJ/mol)
H^o_{Glu}	heat of combustion of glutamate (kJ/mol)
$H^o_{H_2O}$	heat of combustion of water (kJ/mol)
$H^o_{H_2}$	heat of combustion of hydrogen (kJ/mol)
$H^o_{Biomass}$	heat of combustion of hydrogen (kJ/mol)
$H^o_{CO_2}$	heat of combustion of carbon dioxide (kJ/mol)

K_d	fraction of the diffuse radiation reaching the ground
K_h	clearness index
L	length of the reactor (m)
m	maintenance coefficient (1/h)
$\dot{m}_{cw}$	mass flow rate of the cooling water (kg/s)
$\dot{m}_r$	mass flow rate the reactor medium (kg/s)
N	day of the year
Nu_{ii}	coefficient for forced convection in annular tube with uniform flux at both surfaces
Nu_{oo}	coefficient for forced convection in annular tube with uniform flux at both surfaces
P_1	pressure at the inlet of the pump (bars)
P_2	pressure at the outlet of the pump (bars)
Pe	Peclet number
Pr	Prandtl number
Q_{ave}	average volumetric flow rate (m^3/h)
$\dot{Q}_{cw}$	the amount of heat removed by the cooling water (cooling duty) (W)
$\dot{Q}_{met}$	energy required by the bacteria for its metabolic activities (W)
$\dot{Q}_{conv}$	heat transferred through convection (W)
$\dot{Q}_{fconv,rw}$	convective heat transferred (W) from the reactor medium to the inner wall of the reactor
$\dot{Q}_{rad}$	heat transferred through radiation (W)
$\dot{Q}_{rad,a}$	radiation from the air surrounding the reactor (W)
$\dot{Q}_{rad,d}$	diffuse solar radiation (W)
$\dot{Q}_{rad,D}$	direct solar radiation (W)

$\dot{Q}_{rad,g}$	ground radiation (W)
$\dot{Q}_{rad,r}$	radiation energy emitted by the reactor (W)
$\dot{Q}_{re,a}$	reflected air radiation (W)
$\dot{Q}_{re,g}$	reflected radiation from the ground (W)
r_{A_1}	acetic consumption rate for hydrogen production (mol/L/h)
r_{A_2}	acetic consumption rate for biomass formation (mol/L/h)
r_{H_2}	hydrogen production rate (mol/L/h)
r_X	biomass formation rate (mol/L/h)
R_{ct}	outer radius of the cooling tube (m)
Re	Reynolds number
R_i	inner radius of the reactor tube (m)
R_o	outer radius of the reactor tube (m)
T_a	air temperature (K)
T_c	average of the cooling water inlet and outlet temperatures (K)
T_{ci}	cooling water inlet temperature (K)
T_{co}	cooling water outlet temperature (K)
T_g	ground temperature (K)
T_r	reactor bulk fluid temperature (K)
T_{ave}	average the reactor inlet and outlet temperatures (K)
u_1	velocity at the inlet of the pump (m/s)
u_2	velocity at the outlet of the pump (m/s)
V_r	volume of the reactor (m^3)
Y'_{A/H_2}	yield coefficient that relates the amount of acetic acid consumed (mol) to the amount of hydrogen formed (mol)
$Y'_{A/X}$	yield coefficient that relates the amount of acetic acid consumed (mol) to the amount of cells formed (mol)

z_1	elevation at the inlet of the pump (m)
z_2	elevation at the outlet of the pump (m)

Greek Symbols

α	kinetic correction factors
α_c	the ratio of the manifold header diameter to its length
α_d	the ratio of the manifold footer diameter to its length
δ	solar declination (rad)
ε_a	emissivity of air
ε_g	emissivity of the ground
ε_r	emissivity of the reactor medium
ω	solar hour angle
φ	latitude (rad)
τ	transmissivity of the reactor glass wall
θ_i^*	coefficient for forced convection in annular tube with uniform flux at both surfaces
θ_o^*	coefficient for forced convection in annular tube with uniform flux at both surfaces
θ_z	angle of incidence (rad)
ρ_r	density of the reactor medium (kg/m^3)
σ	Stefan-Boltzman constant (W/m^2/K^4)

Abbreviations

ATP	adenosine triphosphate
BP	Biebl and Pfennig
CCD	central composite design
DOE	design of experiments
GC	gas chromatography
gDCW	gram dry cell weight

HPLC	high performance liquid chromatography
HRT	hydraulic retention time
hup^-	membrane bound uptake hydrogenase deficient (mutant)
lx	lux
PNSB	purple non sulfur bacteria
OFAT	one-factor-at-a-time
RSM	response surface methodology
TCA	tricarboxylic acid cycle

CHAPTER 1

INTRODUCTION

Today, we are consuming the solar energy accumulated on earth in millions of years as fossil fuels at a rate which is much faster than it is formed. With rapidly growing power demand and concerns over the effects of pollution, global warming and energy security, alternative energy sources such as solar, wind, wave, geothermal and nuclear are carbon neutral technologies considered to substitute and/or supplement the existing major energy sources – petroleum, natural gas and coal. The deployment of renewables, particularly biofuels such as bioethanol, biodiesel and biohydrogen have been accelerated and are expected to constitute a substantial amount of the energy consumed for electricity generation and transportation in the near future. The global biofuels consumption is projected to increase from 1.3 millions barrels of oil equivalent per day (mboe/d) in 2011 to 2.1 mboe/d in 2020, and 4.1 mboe/d in 2035 (IEA report, 2013).

Hydrogen is considered to be a promising renewable energy carrier. It has a high energy content per unit weight (142 kJ/g), can be produced from readily available renewable resources and be efficiently used in fuel cells to generate power (Sakurai *et al.* 2013). The non-polluting nature of hydrogen, which produces energy and water when combusted, has resulted in numerous approaches to develop technologies to generate it feasibly in large scale.

At present, most of the hydrogen is generated from fossil fuels using thermo-chemical processes such as steam reforming and coal gasification. About 49% of hydrogen is produced from natural gas, 29% from liquid hydro carbons (heavy oil and naphtha), 18% from coal and 4% from other alternative resources such as hydroelectricity, wind, solar and biomass (Parthasarathy and Narayanan, 2014).

The market size of hydrogen production was estimated to be 53 million metric tons in 2010 with a market value of $82.6 billion. Production was forecasted to grow at an annual rate of 5.6% between 2011 and 2016 (Energy and Power, 2011). About 80 to 90% of the hydrogen generated is used in processing oil in refineries and producing chemicals such as methanol and ammonia. The remainder is used in industrial processes, chemical and the food industry (Levin and Azbar, 2011).

Although still in its early stage of development, laboratory and pilot-scale studies have demonstrated that biological hydrogen production has the potential to replace the current hydrogen production methods that rely on fossil fuels. It offers the prospect of producing hydrogen sustainably and at low costs. The processes involved are less energy intensive as they occur at ambient temperatures and pressures, and they utilize renewable resources such as sunlight, water and biomass, therefore promote the reduction and recycling of wastes.

Biohydrogen production can be categorized into two groups: the light-dependent processes (photolysis and photofermentation) and the light-independent process (dark fermentation). During photoautotrophic growth, microalgae and cyanobacteria use carbon dioxide as carbon source and sunlight energy to split water into hydrogen and oxygen - a process called photolysis. In microalgae, the reaction is catalyzed by the [Fe-Fe]-hydrogenase enzyme while in cyanobacteria, it is mediated by the nitrogenase enzyme (Show *et al.* 2011). Photofermentative hydrogen production occurs under anaerobic and nitrogen limited conditions. Photosynthetic bacteria such as the purple non sulfur bacteria (PNSB) break down small organic acids to produce hydrogen and water, using light energy. The process is primarily mediated by the nitrogenase enzyme, a metalloenzyme of which [Fe-Mo] and [Fe-Fe] proteins are the most common types (Vignais *et al.* 1985). In the dark fermentation process, organic substrates and wastewaters are decomposed under anaerobic conditions by anaerobic bacteria to form hydrogen and lower molecular weight organic acids (Hallenbeck and Ghosh, 2009).

Amongst the biological hydrogen production processes, photofermentative hydrogen production is favorable because it has high substrate conversion efficiency and the photosynthetic microorganisms are able to use a wide variety of substrates (Basak and Das, 2007). However, concerns regarding low hydrogen productivity and the costs of the reactor systems have been raised (Ljunggren *et al.* 2011). Research on photobioreactor development, strain selection and genetic manipulation of the hydrogen-producing microorganisms are going on to address these issues (Eroglu and Melis, 2011).

Photofermentative hydrogen production and growth of the photosynthetic bacteria in bioreactors involves complex mechanisms that are influenced by physiological parameters and the reactor design. Physiological parameters include the light intensity, temperature, feed composition and pH, while the reactor design contain the reactor geometry, mode of operation, mixing and flow regime (Koku *et al.* 2002). With most of the physiological parameters having been optimized in small scale laboratory experiments, reactor design remains a hurdle for scale-up. Scale-up of the reactors is necessary to produce hydrogen at competitive costs in industrial setting. However, the deviations in flow pattern under different reactor design geometries and operating conditions makes the task difficult (Bitog *et al*., 2011, Wild *et al*. 2003). Further studies are required to understand constraints such as the light distribution and mixing that become more pronounced as sizes of the reactors are increased.

The eventual goal of photobiological hydrogen production is to carry out the process in large scale photobioreactors operated outdoors, under natural sunlight. Solar light energy is a free resource that is abundant in nature. The earth receives about 5.7×10^{24} J of sunlight energy per year (Miyake *et al.* 1999) but the solar radiation varies according to the geographical location on the globe and the seasons. Turkey, which lies between 36° and 42 °N latitudes in the Meditterenean region, has a very high solar energy potential. It receives about 3.6 $kWh/m^2/day$ of solar radiation (on average) and a total of 2160 hours of radiation annually (Sözen *et al.* 2005). Therefore it is a suitable region for biological hydrogen production.

In outdoor conditions, photofermentative hydrogen production is greatly influenced by the physical variations in solar light energy and temperature, which are uncontrolled (Androga *et al.* 2012). Diurnal and seasonal variations in solar radiation affect the growth of the photosynthetic bacteria. PNSB require light energy to generate adenosine tri-phosphate (ATP) that is used for growth and hydrogen production (Koku *et al.* 2002). The quantity of light energy received by the culture is a function of the culture surface area, light path and shading caused by the cells in the reactor (Fernandez *et al.* 1998). Light is described to decay exponentially following Lambert-Beer's law inside the reactor (Katsuda *et al.* 2000). Strong irradiances, especially during the summer, result in photoinhibition and photolimitation. Photoinhibition occurs when excessive light damages the photosynthetic apparatus (Tandori *et al.* 2001) and photolimitation occurs when high biomass concentration prevents light from reaching all parts of the reactor (Barbosa *et al.* 2001). Low light irradiances experienced during the winter result in poor cell growth and hydrogen production (Androga *et al*. 2011a).

The changes in temperature within the reactors depend on the solar radiation and ambient temperature during outdoor operations. PNSB grow and produce hydrogen optimally between 30°C and 35°C (Sasikala *et al.* 1993). High solar irradiance and high ambient air temperatures experienced on summer days could lead to overheating of the culture and may denature cellular enzymes, reducing activity and/or causing death of cells (Goetz *et al.* 2011). This is likely in reactors with high surface to volume ratios, such as the panel and the tubular reactors, which are the main types of reactors used in photofermentative hydrogen production (Akkerman *et al.* 2012). Similarly, during winter, low radiation and cold outdoor temperatures reduce cell activity thus affecting growth and hydrogen production. Therefore control of the culture temperature is critical in outdoor operations.

Temperatures of the reactors have been regulated by water spraying, immersion in water baths and cooling using heat exchangers. The processes have been shown to be efficient, but they incur extra operating costs. Thermal balances can be made to determine the energy distribution within the system and to estimate the amount of energy needed for cooling.

The main bottleneck in photofermentative hydrogen production in large-scale is the total cost of the photobioreactor (Claassen *et al.* 2010). HYVOLUTION, the acronym for the 6th framework EU integrated project entitled “Nonthermal production of pure hydrogen from biomass” aimed to produce hydrogen from locally available biomass using integrated thermophilic dark fermentation and photofermentation processes. A variety of conventional crops and agro-industrial by-products such as potato steam peels, thick juice, molasses and barley straw were used as feedstock to produce hydrogen using dark fermentation. The effluent of the process was used in the subsequent photofermentation stage. The aim of the project was to achieve a total hydrogen production efficiency of 75 %. An economic analysis that included the capital costs for pretreatment of the feedstock, thermophilic fermentation, photofermentation and gas up-grading revealed that the photofermentors accounted for a large amount of the total capital costs. The final cost of photofermentative hydrogen production was estimated to be around 60 €/kg using tubular reactors and 390 €/kg by panel reactors, the major cost being the materials of construction of the reactors. During the project, tubular reactors made of low density polyethylene (LDPE) and flat panel reactors made from poly methyl methacrylate (PMAA) were designed, constructed and their performances evaluated (Androga *et al.* 2011a, Avcıoğlu *et. al.* 2011, Boran *et al.* 2010, Gebicki *et al.* 2010 and Boran *et al.* 2012). Comparable hydrogen production rates were obtained per illuminated surface area in both reactor types (Gebicki *et al.* 2010). The hydrogen production rate can be improved by making better reactor designs and the cost of the reactors can be reduced using construction material that is more durable and affordable.

Boran *et al.* 2012 operated a 90 L tubular photobioreactor outdoors and achieved stable hydrogen production at the rate of 0.40 mol $H_2/m^3/h$ using fed-batch cultures of *R.capsulatus* YO3. They reported that for long-term operation, more durable materials should be used to construct the reactor tubing – they had used tubes made from LDPE. The diameters of the tubes also needed to be optimized to allow better light penetration into the reactors – tube diameters below 6 cm are preferred. Moreover, they concluded that circulation of the medium in the reactors was necessary to improve mixing and enhance mass transfer and gas-liquid separation. Glass is considered to be very good material of construction for photobioreactors because it is transparent, has a low hydrogen permeability and a long lifespan (circa. 20 years) (Burgess *et al.* 2007).

Overall, a novel reactor that: (i) is made from a material that is durable and impermeable to hydrogen, (ii) has a suitable diameter which allows ample light penetration into the reactor, (iii) has a design which ensures uniform flow distribution for good mixing of cells and nutrients and easy gas separation and (iv) has a good temperature control is targeted. This would increase hydrogen productivity, reduce capital costs of the photofermentors and make the process more competitive with the other hydrogen production methods.

Within the scope of this study, temperature and light intensity were optimized using response surface methodology, a statistical modeling technique, in indoor experiments. U-tube reactors were constructed and their flow distribution investigated using computational flow dynamics. The U-tube reactors were made of glass and operated in outdoor conditions. Following the basic principles of thermodynamics and transport phenomena, dynamic models that included the effects of heat transfer through convection and radiation on the bulk temperature of the reactors were developed. The thermal models simulated the transient behavior of temperature in the system in response to the varying solar radiation, ambient air temperatures, biomass formation, hydrogen production and heat transfer inside the reactor. The general models are useful tools for the design and optimization of solar bioreactors.

In Chapter 2, a literature review on the optimization of temperature and light intensity, reactor design, reactor modeling and reactor operation outdoors is given. The experimental procedures for the indoor experiments and the outdoor experiments are discussed in Chapter 3. The modeling strategies used in this thesis are explained in Chapters 4 and the results and discussions are given in Chapters 5, 6, 7 and 8. Chapter 5 provides an in depth discussion on the optimization of temperature and light intensity using response surface methodology and Chapter 6 compares the flow distribution, based on the velocity profiles and pressure drops, in manifold tubular reactors and serpentine tubular reactors. In Chapter 7, the results of the dynamic thermal models are discussed and in Chapter 8, growth and hydrogen production by *Rhodobacter capsulatus* YO3 in outdoor conditions is given. The conclusions achieved from the studies and further recommendations are summarized in Chapter 9. Lastly, the publications cited in the thesis are listed in the References section. Additional data used in the studies are provided in the Appendices.

CHAPTER 2

LITERATURE SURVEY

2.1 Photofermentative Hydrogen Production by Purple Non-Sulfur Bacteria

Photofermentative hydrogen production is a microbial process in which electrons and protons generated through oxidation of organic compounds are used to produce molecular hydrogen under anaerobic, nitrogen-limited conditions, utilizing light as energy source (Figure 2.1). The process is mediated by the nitrogenase enzyme, which catalyzes the reduction of N_2 to NH_3. Hydrogen production is an inherent activity of the nitrogenase enzyme, which forms 1 mole of H_2 per mole of N_2 fixed as shown in Equation (2.1).

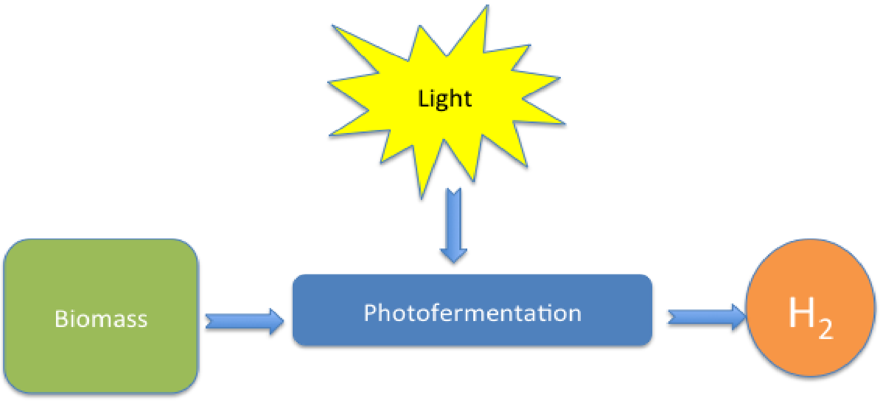

Figure 2.1 Photofermentative hydrogen production.

$$N_2 + 8H^+ + 8e^- \; 16ATP \rightarrow NH_3 + H_2 + 16ADP + 16P_i \qquad (2.1)$$

However, under limited nitrogen source, the enzyme functions as hydrogenase and catalyzes the reduction of protons to form molecular hydrogen at the expense of 4 moles of ATP as shown in Equation (2.2).

$$2H^+ + 2e^- + 4ATP \rightarrow H_2 + 4ADP + 4P_i \tag{2.2}$$

Hence, with the same energy requirement, 4 times more hydrogen can be produced under nitrogen-limiting conditions. There is also the membrane-bound H_2-uptake [Ni-Fe]-hydrogenase, which mainly catalyzes the oxidation of H_2 to protons and electrons, by the following reversible reaction. Deletion of this enzyme has shown increase in hydrogen production (Kars *et al.* 2008, Öztürk *et al.* 2006).

$$H_2 \rightarrow 2H^+ + 2e^- \tag{2.3}$$

A wide range of photosynthetic bacteria is reported to produce hydrogen. Among them, the PNSB is the most widely studied and well characterized. PNSB are facultative anoxygenic phototrophs belonging to the class of *Alphaproteobacteria* and include several genera within orders *Rhodobacterales, Rhodospiralles and Rhizobiales* (Dubbas and Tabitha, 2004). They are a diverse group of photosynthetic microorganisms that are capable of photobiological hydrogen production under anaerobic, nitrogen limiting conditions. Various species of PNSB were utilized in hydrogen production studies, *Rhodobacter capsulatus, Rhodobacter sphaeroides*, *Rhodoseudomonas palustris* and *Rhodospirillum rubrum* being the most used strains. They prefer photoheterotrophic growth in the presence of an organic carbon source, preferentially, small organic acids. Photoheterotrophic growth is the only growth mode that results in hydrogen production, however, PNSB are capable of growth under photoautotrophic, respiratory, fermentative or chemotrophic conditions, depending on the presence of light, type of carbon source and availability of oxygen (Koku *et al.* 2002).

This versatility of growth modes has attracted research interest for many years, and made PNSB a model organism to study metabolic regulations of carbon, nitrogen and energy metabolism. There are three important external factors that determine the metabolic route: the carbon source, light and oxygen availability. PNSB are capable of growth on a variety of organic carbon sources including sugars (glucose, sucrose), short chain organic acids (acetate, malate, succinate, fumarate, formate, butyrate, propionate and lactate), amino acids, alcohols and even polyphenols. They also grow on inorganic carbon (carbon dioxide) under photoautotrophy and chemoautotrophy. Under photoheterotrophic hydrogen production conditions, these bacteria preferentially use short chain organic acids as electron donors to obtain ATP for their metabolic processes. Short chain organic acids are assimilated through the tri-carboxylic acid (TCA) cycle, which yields carbon dioxide, protons and electrons, which are shuttled through electron transport chain that uses NAD/NADH and ferrodoxin (Figure 2.2) (Kars and Gündüz, 2010).

The photosynthetic apparatus in PNSB is located in the intracytoplasmic membranes the invaginations of cytoplasmic membrane, forming a parallel lamella underlying the cytoplasmic membrane. It is composed of a photosystem, a series of electron transport proteins (cytoplasmic cytochrome c, lipid soluble quinones (Q/QH), cytochrome b/c1 complex, and) and a transmembrane ATP synthase protein. The photosystem contains light harvesting complex 1 (LH1) and 2 (LH2) and a reaction center (Vermeglio and Joliot, 1999). LH complexes trap light in the visible (450-590 nm) and near infrared (800-875 nm) wavelength and transfers the excitation energy to the reaction center, and starts cyclic electron transfer. LH1, LH2 and the reaction center are protein-pigment complexes that contain different types of carotenoids and bacteriochlorophyll *a*. Biosynthesis of the photosynthetic apparatus is primarily controlled by presence of oxygen and light (Zhu and Heasrt (1986), Firsow and Drews, 1977, Pemberton *et al.* 1998). During aerobic growth, the synthesis of bacteriochlorophyll is repressed. Once the oxygen tension is removed, the synthesis resumes. Light intensity and quality also control the synthesis of the photosynthetic apparatus. Under low light intensity, photosystem biosynthesis increases to gather more light energy, and at high light intensity, less photosystem is biosynthesized.

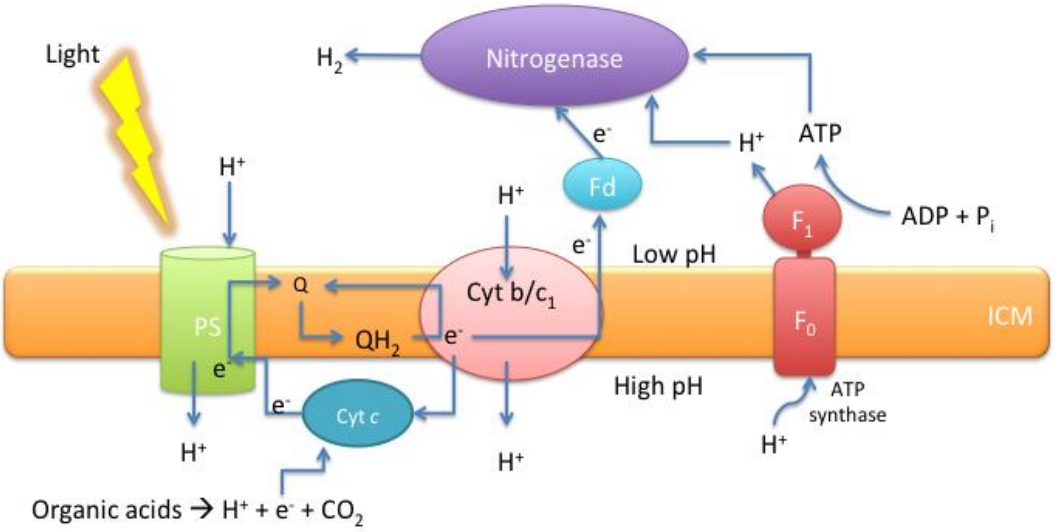

Figure 2.2 Photofermentative hydrogen production in purple non sulfur bacteria. Oxidation of organic acids generates electrons, which are delivered to cytochrome c and travels through the electron transport proteins (lipid soluble quinones (Q/QH), cytochrome b/c1) and are delivered to ferredoxin. During this process, protons are pumped through the membranes forming a proton gradient. This proton motive force drive ATP production by ATP synthase. Ferredoxin delivers electrons to nitrogenase, which catalyzes the reduction of protons to molecular hydrogen using ATP (Kars and Gündüz, 2010).

The photosystem of PNSB is not powerful enough to split water, therefore no oxygen is evolved and biohydrogen production can occur. Electrons that are liberated through oxidation of organic carbon are funneled through a series of electron carriers, during which protons are pumped through the membrane. This leads to a development of a proton gradient across the membrane, which drives ATP production by ATP synthase. The electrons are either used for replenishment of the quinone pool or donated to Ferrodoxin, which delivers electrons to nitrogenase enzyme to reduce molecular nitrogen to ammonia. When molecular nitrogen is not available, nitrogenase functions as hydrogenase and catalyzes the proton reduction with the electrons derived from ferrodoxin (Figure 2.2). By this way, electrons from organic compounds are extracted or discarded in the form of hydrogen by using light energy.

2.2 Optimization of Temperature and Light Intensity for Improved Hydrogen Production

Photofermentation is primarily influenced by nutritional and environmental factors, such as the choice of carbon and nitrogen sources, the carbon to nitrogen ratio, pH levels, temperature and light intensity. Shown in Figure 2.3 is a summary of the parameters affecting photofermentative hydrogen production. Two of these factors, temperature and light intensity, have been shown to strongly affect hydrogen production (Özgür *et al.* 2010, Androga *et al.* 2011a). PNSB grow and produce hydrogen optimally between 30 and 35°C (Sasikala *et al.* 1993) and fluctuating temperatures (15 – 40 °C) have been found to reduce hydrogen production significantly (Özgür *et al.* 2010). The rate of hydrogen production was demonstrated to increase with increasing light intensity, reaching saturation at 270 W/m^2 (Uyar *et al.* 2007). Therefore, optimization of temperature and light intensities is crucial to achieving high hydrogen production rates and yields.

Previous studies related to the optimization of light intensity and temperature have mostly been carried out using the “one-factor-at-a-time” (OFAT) method, where a single factor is varied while the others are kept constant (He *et al.* 2006, Uyar *et al.* 2007, Obeid *et al.* 2009, Sevinç *et al.* 2012). This approach is time-consuming and costly due to the large number of experiments that might be needed. In addition, as interactive effects between factors are not accounted for the obtained optima may differ from genuine multi-variate values.

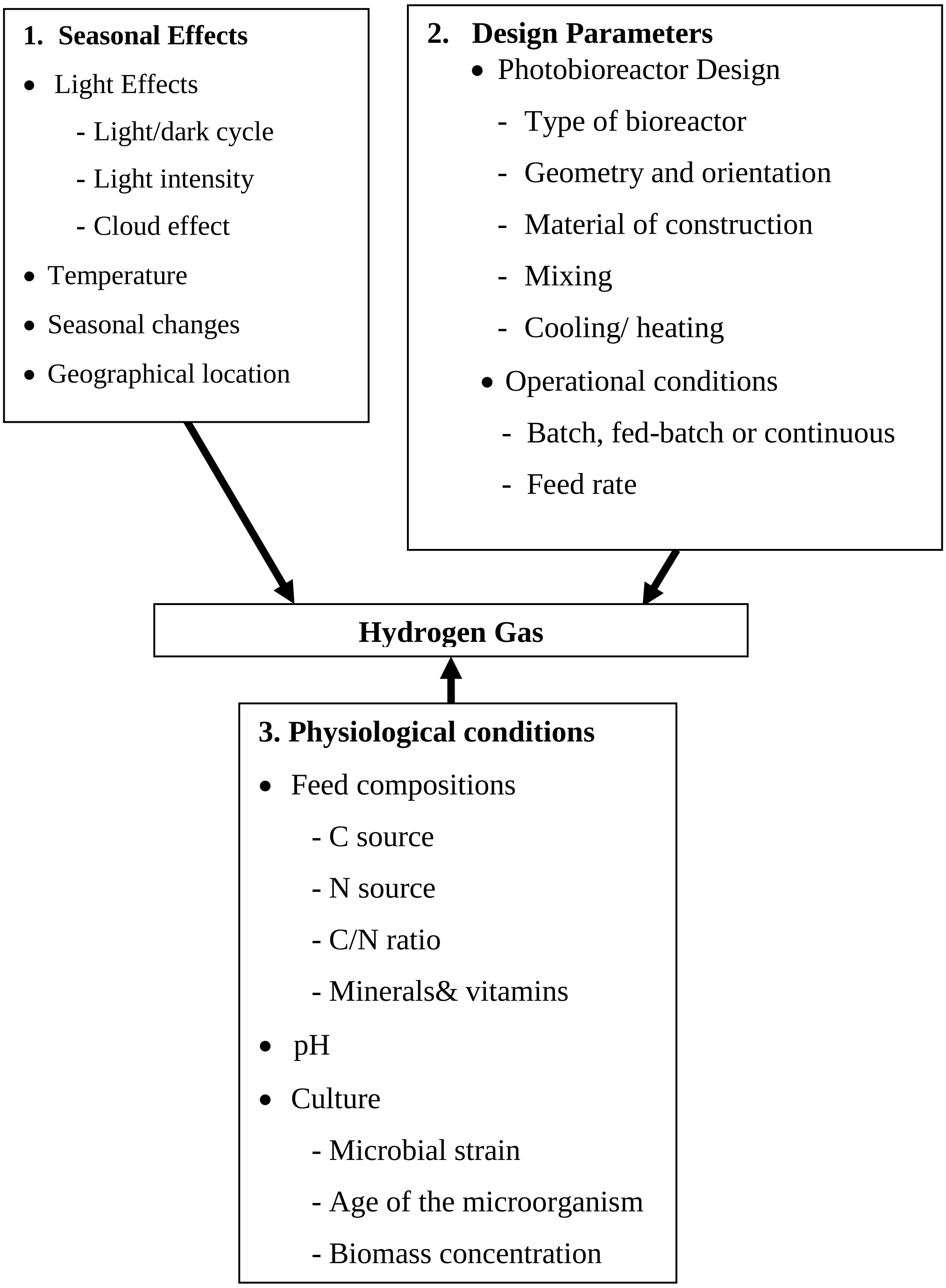
1. Seasonal Effects
• Light Effects
- Light/dark cycle
- Light intensity
- Cloud effect
• Temperature
• Seasonal changes
• Geographical location
2. Design Parameters
• Photobioreactor Design
- Type of bioreactor
- Geometry and orientation
- Material of construction
- Mixing
- Cooling/ heating
• Operational conditions
- Batch, fed-batch or continuous
- Feed rate
Hydrogen Gas
3. Physiological conditions
• Feed compositions
- C source
- N source
- C/N ratio
- Minerals& vitamins
• pH
• Culture
- Microbial strain
- Age of the microorganism
- Biomass concentration

Figure 2.3 Parameters affecting photofermentative hydrogen production.

To address these limitations, one alternative is to employ response surface methodology, a statistical modeling technique for the design of experiments (DOE) that accounts for interactions between factors. The procedure involves the development of a mathematical model that defines the relationships between a response and the independent variables studied, which in turn can be used to evaluate interactions between the factors and to determine optimal conditions (Montgomery, 2009). The application of the three level (3^k) general full factorial design allows the representation of the response by second-degree quadratic polynomials, which can be visualized as three-dimensional surface plots and two-dimensional contour plots (Box and Behnken, 1960, Wang and Wan, 2009).

Several studies on the use of DOE to optimize parameters for biohydrogen production are reported in literature: hydrogen production by green algae (Jo *et al.* 2006), dark fermentation (Mu *et al.* 2009, Infantes *et al.* 2011), photofermentation Shi and Yu 2005a, Chen *et al.* 2007, Obeid *et al.* 2009, Ghosh *et al.* 2012a, Ghosh *et al.* 2012b), and simultaneous dark and photofermentation using co-cultures (Sun *et al.* 2010). Shi and Yu (2005a) applied central composite design (CCD) in order to determine the effects of glutamate and pH on photofermentative hydrogen production using *Rhodopseudomonas capsulata*. CCD was also used to determine optimal concentrations of butyric acid, glutamic acid and iron (III) chloride for maximum hydrogen production using *Rhodopseudomonas palustris* WP3-5 (Chen *et al.* 2007). Ghosh *et al.* (2011a) used the Box-Behnken design to determine optimal light intensity and glucose and glutamate concentrations for photobiological hydrogen production using *Rhodobacter capsulatus* JP91 (hup^-).

Most optimization studies on photofermentative hydrogen production used different feed, inoculum sizes, light intensities and pH levels for different PNSB species. Due to the versatility in the growth and hydrogen production metabolisms of these bacteria (Das and Veziroğlu, 2001), it is important to carry out the optimization studies on a case-by-case basis, looking at important strains and operating parameters.

2.3 Reactor Design

2.3.1 Types of Reactors

Photobioreactors are systems designed to grow photosynthetic microorganisms under a given environmental condition (Tredici 2004). They can be classified as open (raceway ponds, lagoons and lakes) or closed (flat panel and tubular) systems. Open systems are mostly suited to biomass production since they cannot provide the anaerobic conditions required for hydrogen production. Also, control of parameters like temperature, nutrients and pH is poor in such systems. On the other hand, closed systems allow better control of these parameters and result in higher biomass and biohydrogen production (Dasgupta *et al.* 2010).

Different types of reactors are used in photofermentative hydrogen production studies (Figure 2.4). They are generally classified according to their: (i) Design – flat panel, tubular, horizontal, inclined, vertical or spiral and manifold or serpentine (Tredici, 1999) and (ii) Mode of operation – batch, fed-batch and continuous (Dasgupta *et al.* 2010). Flat panel and tubular types of reactors are commonly used in photofermentative hydrogen production (Figure 2.5). They have large illumination areas that result in high hydrogen production efficiencies (Akkerman *et al.* 2002).

Tubular reactors are made of long transparent tubes through which liquid culture is circulated using mechanical or gas-lift pumps. The tubes have diameters ranging between 3 and 6 cm and length between 10 to 100 m (Akkerman *et al.* 2002). The reactors fall under different categories: simple airlift or agitated bubble column (vertical type) (Eroglu *et al.* 1999, Carlozzi *et al.* 2009, Lee *et al.* 2011), horizontal or nearly horizontal tubular reactors (Tredici 2004, Gebicki *et al.* 2010, Boran *et al.* 2010) and helical type reactors (Hai *et al.* 2000, Sarı 2007).

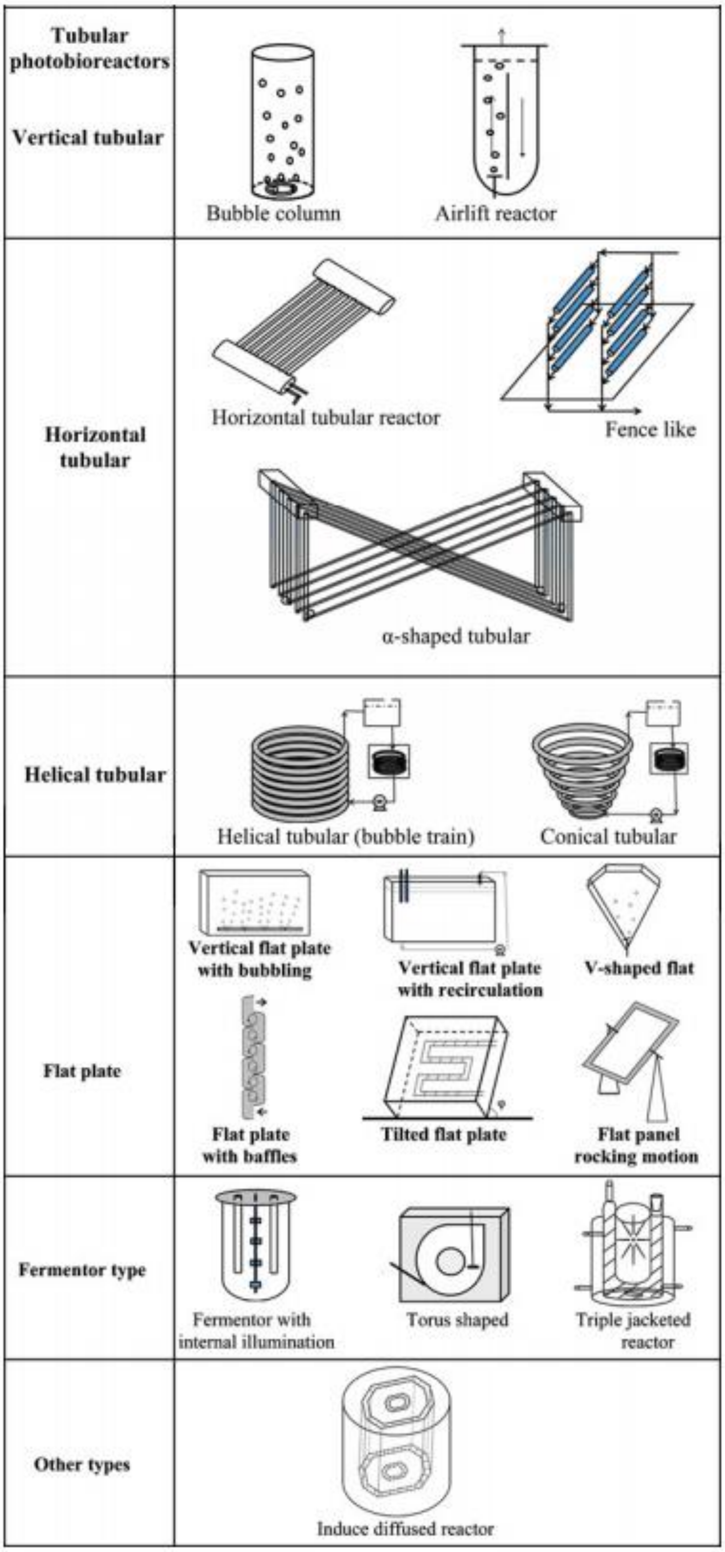
Tubular photobioreactors
Vertical tubular
Bubble column
Airlift reactor
Horizontal tubular
Horizontal tubular reactor
Fence like
α-shaped tubular
Helical tubular
Helical tubular (bubble train)
Conical tubular
Flat plate
Vertical flat plate with bubbling
Vertical flat plate with recirculation
V-shaped flat
Flat plate with baffles
Tilted flat plate
Flat panel rocking motion
Fermentor type
Fermentor with internal illumination
Torus shaped
Triple jacketed reactor
Other types
Induce diffused reactor

Figure 2.4 Types of photobioreactors (Dasgupta *et al.* 2010)

Tubular reactors can be scaled-up by connecting a number of tubes to manifolds, but the length of the tubes is limited by the accumulation of gas (Akkerman *et al.* 2002). A disadvantage of these reactors is that they require large ground area. In comparing the hydrogen production performance of the panel and tubular reactors, Gebicki *et al.* (2010) reported that the ratio of the illuminated reactor surface to the installed ground area was 8:1 in the panel reactors, while in the tubular reactors it was 1:1.

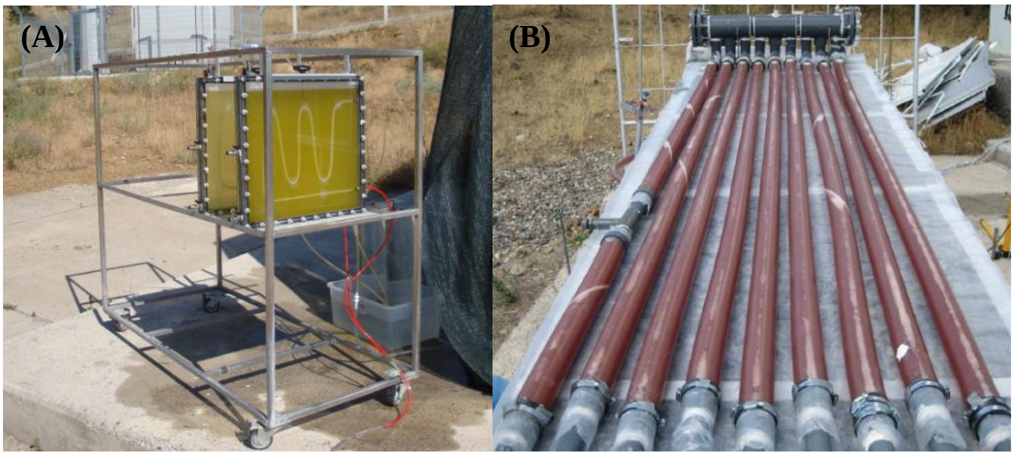

Figure 2.4 Operation of the (A) Flat panel photobioreactor and (B) Tubular photobioreactor in outdoor conditions (Androga *et al.* 2012).

A good reactor design that ensures proper mixing, easy gas collection and temperature control is targeted for sustainable hydrogen production. The optimized reactor should have the following properties: (i) a simply designed enclosed system that is impermeable to hydrogen, (ii) a transparent system that allows maximum light penetration, preferably at high visible light or near red-infrared transmissions, (iii) a system with high surface-to-volume ratio for a better distribution of light, (iv) a well-mixed system for uniform distribution of mineral and nutrients and (v) a system made from an inert material that is durable, easy to clean and sterilize (Akkerman *et al.* 2002, Dasgupta *et al.* 2010, Chen *et al.* 2011, Uyar *et al.* 2011).

2.3.2 Reactor Orientation, Mixing and Light Distribution

Investigations on the design of tubular reactors to improve hydrogen production have been reported in literature. Inclination (circa 10° to 30°) of the tubular reactors and circulation of the medium in the reactor using mechanical pumps were indicated to facilitate the separation of the evolved gas and assist in the homogenous distribution of cells, substrates and light within the tubular reactor (Tredici 2004, Gebicki *et al.* 2010, Boran *et al.* 2010). Turbulence caused by intense mixing in reactors improves light utilization (Troesch *et al.* 2003), but it may cause higher shear stress and inhibit cell growth (Hoekama *et al.* 2002).

Alias *et al.* (2004) investigated the effect of mechanical stress caused by pumping of fluids on biomass concentration in the reactor using centrifugal, diapraghm and peristaltic pumps. The highest mechanical stress was obtained using the centrifugal pumps and the peristaltic pump had the least damaging effect to biomass. Gebicki *et al.* (2010) investigated hydrogen production at different pumping rates ranging between 10 and 6000 Reynolds number (Re). They achieved maximum hydrogen production in the laminar flow at Re = 240, which corresponded to a circulation rate of 20 L/h in a 65 L tubular reactor.

The light intensity inside the reactor has been described to decay exponentially with the culture depth, following the Lambert-Beer law (Ogbonna *et al.* 2001). Boran (2011) studied the decay of light intensity using different light paths (1 to 6 cm) and reactor medium. Results showed that light penetration for each 1 cm of reactor depth was 89 % for modified Bieble and Pfennig (1981) medium, 70 % for thick juice dark fermenter effluent and 51 % for molasses dark fermenter effluent. It was concluded that a tubular reactor with a tube diameter less than 6 cm would be suitable for hydrogen production.

2.3.3 Material of Construction

Photobioreactors have been constructed using a wide variety of materials such as glass, low-density polyethylene film (LDPE), rigid acrylic or polymethyl methylacrylate (PMMA), polycarbonate and transparent polyvinylchloride (PVC). Glass is considered a very good construction material because it is transparent, has low hydrogen permeability and a long lifespan (circa. 20 years). Although it is brittle, rigid, heavy and not easily workable, the use of large scale reactor systems made of glass has been demonstrated to be feasible (Hai *et al.* 2000, Carlozzi and Sacchi, 2001, Adessi *et al.* 2012).

2.3.4 Mode of Operation

In designing reactors for hydrogen production, the choice of the mode of operation is important as it affects the capacity of the system to generate the gas, hence operating costs and the capital investment (Uyar *et al.* 2011). Continuous and fed-batch operated systems are suitable for biohydrogen production as they allow long-term operations through regular feeding of the bacteria at certain dilution rates. However, repeated fed-batch operation was described to be the most favorable mode of operation. The system can operate under high cell densities and permits the control of the reaction rates by adjustment of feed flow rates and compositions, therefore preventing substrate and product inhibitions (Soletto *et al.* 2008, Argun and Kargi, 2011).

2.3.5 Temperature Control

Photosynthetic bacteria that carry out anoxygenic hydrogen production grow and produce hydrogen optimally between 30°C and 35°C (Sasikala *et al.* 1993). They cannot grow or produce hydrogen above 38°C (Sevinç et al. 2012), except for a few such as the *Rhodospirilum centenum*, which was able to grow optimally between 40 and 42° C, but hydrogen production was limited by the inability of the cells to use substrates at high concentrations (Favinger *et al.* 1989). Very high or low temperatures negatively affect hydrogen production. During summer, daytime temperatures may rise up to 40°C, therefore reactor cooling becomes necessary and at night it falls below 20°C. In winter, temperatures generally remain below 10 °C therefore heating is required to prevent the bacteria from freezing (Androga *et al.* 2011b). Özgür *et al.* (2010) reported lower substrate conversion efficiencies, yields and hydrogen production rates after exposing batch cultures of *R. capsulatus* to fluctuating temperatures.

The major strategies often used to control temperatures and avoid overheating of the reactors are external cooling by water spraying and shading (Özgür *et al.* 2010), immersion of the reactors in a water bath or basin (Otsuki *et al.* 1998, Carlozzi and Sacchi 2001, Adessi *et al.* 2012) and the use of heat exchangers – water jackets (Degen *et al.* 2001, Camacho *et al.* 2011) and heat exchangers (Eroglu *et al.* 2008, Androga *et al.* 2011a, Avcıoğlu *et al.* 2011, Boran *et al.* 2012).

The temperature of an outdoor operated reactor containing *R. capsulatus* YO3 culture was maintained at 33°C by water spraying and partial shading (60%). Maximum hydrogen production rate of 0.32 mol $H_2/m^3/h$ and hydrogen yield of 0.045 g $H_2/g_{substrate}$ was achieved (Özgür *et al.* 2010). Otsuki *et al.* (1998) successfully controlled the temperature of a 0.8 L floating-type bioreactor by immersing it in seawater. The temperatratures of the reactor kept at 28 °C when the ambient air temperatures rose to 36°C and the sea water temperature increased to 25 °C. Carlozzi and Sacchi (2001) operated a tubular reactor for 6 months in outdoor conditions to produce *Rhodopseudomonas palustris* strain 42OL biomass. The reactor was submerged underwater to control the temperature. An average biomass productivity of 0.7 gram dry weight per gram acetic acid was achieved. Hydrogen production in an outdoor operated 50 L tubular reactor was investigated using *Rhodopseudomonas palustris* cultures. The reactor temperature was controlled by submerging it in a thermostated stainless steel water basin containing demineralized water set at 28±0.5°C. Maximum hydrogen production rate of 1.21 mol $H_2/m^3/h$ and substrate conversion efficiency of 49.7% was obtained. An internal cooling coil heat exchanger system was used to control temperatures in an outdoor operated 6.5 L flat panel reactor containing *Rhodobacter sphaeroides* O.U.001 cells. The maximum hydrogen production rate of 0.45 mol $H_2/m^3/h$ and maximum hydrogen yield of 4.6 mol $H_2/mol_{substrate}$ was obtained using medium with 15 mM acetate and 2 mM glutamate (Eroglu *et al.* 2008). In outdoor experiments carried out during the summer, flexible polyvinylchloride (PVC) cooling coils were integrated into flat panel reactors and cooling water (5 to 10°C) was circulated through them. The culture temperatures were successfully maintained below 35°C (Androga *et al.* 2011, Avcioglu *et al.* 2011). The temperature of *Rhodobacter capsulatus* YO3 (hup^-) culture grown in a 90 L manifold tubular reactor was kept below 40°C by passing cooling water through PVC tubing inserted in the reactor. Maximum hydrogen production rate of 0.40 mol $H_2/m^3/h$ and hydrogen yield of 0.35 mol H_2/mol acetate was obtained using medium with 15 mM acetate and 2 mM glutamate (Boran *et al.* 2012).

Water-spray systems have limited cooling capacity and their application is not suitable in humid areas (Sierra *et al.* 2008), while water basins are susceptible to substantial water loss through evaporation and attenuate light. Water is a good absorber of electromagnetic radiation, especially in the infrared region (Haltrin, 2006). The bacteria require infrared light for hydrogen production (Uyar *et al.* 2007); therefore its absorption by water molecules would hinder the hydrogen production process. Moreover, the energy absorbed by water increases the cooling duty and incurs extra operating costs. In contrast, the use of heat exchangers offers better heat transfer and saves on operating costs. The circulated water absorbs energy from the reactor during the day when temperatures are high and provides energy that can be used to warm the reactors at night when temperatures drop. This heat accumulation scheme greatly improves the energetic yield of the reactor system (Sierra *et al.* 2008).

2.4 Modeling of the Reactor Systems

Modeling of the bioreactor system requires an understanding of the interaction between the complex mechanisms that affect the photosynthetic bacterial growth and hydrogen production. These parameters can be divided into three major categories: (i) the reactor flow dynamics (flow regime, pressure drop, heat transfer), (ii) light energy distribution and (iii) kinetics (mass transfer, microbial growth, substrate consumption and product formation). A scheme of the interactions of the parameters is shown in Figure 2.5.

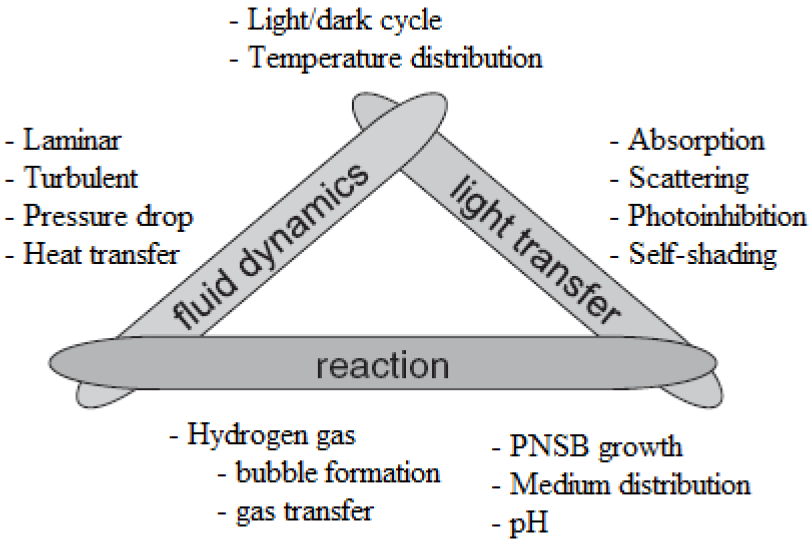
- Light/dark cycle
- Temperature distribution
- Laminar
- Turbulent
- Pressure drop
- Heat transfer
- Absorption
- Scattering
- Photoinhibition
- Self-shading
fluid dynamics
light transfer
reaction
- Hydrogen gas
- bubble formation
- gas transfer
- PNSB growth
- Medium distribution
- pH

Figure 2.5 The convoluted relationships between fluid dynamics, light energy and reaction kinetics in the photobioreactor (Adapted from Posten, 2009).

2.4.1 Computational Fluid Dynamics Modeling

Today, as the capability of computers to solve complicated mathematical relations and geometries improve, application of computational fluid dynamics (CFD) to model reactors is becoming more common. CFD utilizes numerical techniques to solve problems involving fluid flow, therefore enable detailed analysis of the reactor chacteristics (Bitog *et al.*, 2011).

Two main approaches are usually applied in modeling transport and bioreaction processes in bioreactors: (i) Eulerian and (ii) Lagrangian approach (Schugerl and Bellgardt, 2000). Both techniques involve solving species transport models using conservation equations describing reaction, convection and diffusion for each component species.

The Eulerian approach generally averages Navier-Stokes equations over a volume and so includes the species and a continuous phase. It leads to the development of partial differential equations (PDE) which describe the transport and reaction systems and is good for modeling two-phase systems such as the gas-liquid or liquid-liquid (Bitog *et al.*, 2011, Papácek *et al.*, 2011). The method uses a single pressure field for all phases (continuous or dispersed) and allows modeling of the interaction between the mean flows of phases including drag forces, virtual mass effects, acceleration of secondary phase relative to the primary and additional lift forces. For example, droplets or bubbles (secondary phase) dispersed in the fluid (primary or continuous phase) can be modeled by applying mass and momentum balances for each phase (Bertola *et al.*, 2003). The Eulerian model is used to model flow in separators, evaporators and aeration boilers (Bitog *et al.*, 2011).

In the Lagrangian approach, the fluid is treated as a continuum while the species (bacterial cell) is treated as a single particle where its trajectories can be calculated as a result of forces acting on it. Usually, this approach results in stochastic ordinary differential equations (ODE) for individual microbial cells (Papácek *et al.*, 2011). Because particles or cells are considered individually, an important number of particles or cells have to be simulated to be representative of the overall population. This requires high computational memory, speed and takes more time, explaining why the Eulerian approach is more attractive for modeling (Pruvost *et al.*, 2008).

A major advantage of CFD modeling is that it automatically accounts for the reactor geometry and scale effects (Baten *et al*., 2003). However, the success of the CFD simulation is dependent on many factors such as the type of model and the grid resolution (Gimbun, 2009). Most CFD studies in literature have been carried out using column bioreactors (Bitog *et al*., 2011), but there are a few studies on manifold tubular reactors. Powerful and flexible CFD packages such as ANSYS-FLUENT, OpenFoam and COMSOL have been used these studies.

Bajura and Jones (1976) examined the effects of several parameters such as the length to diameter ratio of the header, the diameter ratio of the header to the channel, flow resistance in the channel and friction factor on the flow distribution within manifolds with turbulent flow. Their analytical and experimental flow distribution characterization provided a wide range of design rules for manifolds operated at high Reynolds number flows. Ahn *et al.* (1998) investigated the effect of flow distribution in manifolds with laminar flow (low Reynolds) using CFD. They reported that flow distribution in the manifold was dependent on the ratio of the header (combining manifold) diameter to its length (α_c), the ratio of the footer (dividing manifold) diameter to its length (α_d) and the circulation rate (Reynolds number). Studying different α_c, α_d and Reynolds numbers (Re), they proposed a correlation; $\alpha_d \times Re^{0.64}=1.97$ at $\alpha_c \geq 0.25$ for optimal flow distribution. Tompiks *et al.* (2002) reported that the flow regime in the header manifold greatly controls flow within the microchannels. In investigations done on the two-phase refrigerant flow in microchannels, the high flow rates formed annular flow that caused non-uniform distribution of liquid and vapor in the header and the microchannels. In contrast, low mass flow rates formed stratified flow and uniform flow distribution. Lee *et al.* (2012) investigated the flow rate distribution and changes in the discharge angle between the outlets (orifices) in a multi-perforated tube using CFD analysis and experiments. The effect blockage ratio (caused by changes in the spacing and number of orifices) and the thickness of the tube at different Reynolds numbers were examined. Increase in the blockage ratio and tube thickness resulted in more uniform flow distribution between the orifices. Gebicki *et al.* (2010) applied CFD analysis to investigate hydrogen production in a tubular reactor. They studied the effects of flow between 10 and 6000 Reynolds (Re) number and obtained maximum hydrogen production at Re = 240.

Photosynthetic cells can be considered as fluid elements without slip velocities, therefore can be assumed to be part of the medium. This reduces the three-phase multiphase system assumption in the reactor to a two-phase system, whereby the liquid phase (cells and medium) are considered as the continuous phase and gas phase (hydrogen and carbondioxide gas bubbles) as the dispersed phase. The two-phase system can further be reduced to a single-phase system since the amount of liquid in the reactors is much higher than that of the gas. This simplifies calculations of the pressure drop and velocity distribution in the reactor geometries. Within the scope of this thesis, the flow distribution in tubular reactors operated at steady state conditions was analyzed using computational fluid dynamics. Single-phase steady state flow was solved using the COMSOL program. The theory behind the calculations used by the program is given in Appendix A.

2.4.2 Modeling Heat Transfer in the Solar Bioreactors

In literature, there are several reports of models that estimate solar irradiance and temperature changes, and relate their effects on the growth of the photosynthetic microorganisms. Most of these studies are on the growth of microalgae (Fernandez *et al.* 1997, Fernandez *et al.* 1998, Ribeiro *et al.* 2008, Bechet *et al.* 2010, Maor and Appelbaum, 2011, Goetz *et al.* 2011, Pereira *et al.* 2013).

Ribeiro *et al.* (2008) developed a mathematical model to simulate growth of the microalgae *Phaeodactylum tricornutum* and its dependency on medium temperature and light intensity. Numerical solutions of the model were performed with temperatures ranging from 274 K to 300 K, and the maximum biomass production was achieved at 294 K. Bechet *et al.* (2010) developed a mechanistic model that described the variation in culture temperature in a column photobioreactor operated outdoors. The model considered parameters such as the geographical location, the dimensions of the reactor, the solar radiation, ambient air temperature, the ground temperature and the veolicity of wind. They found that the radiative heat transfer (i.e. ambient air radiation, ground radiation, solar radiation and radiation from the reactor) and convective heat transfer controlled the reactor temperature. Goetz *et al.* (2011) developed a simplified thermal model to forecast the temperature change in a flat panel photobioreactor with time. They carried out the experiments in indoor conditions under controlled artificial illumination and in outdoor conditions under solar radiation during summer. The model predicted the temperature change in the reactors and was beneficial in investigating parameters influencing thermal behavior.

2.5 Outdoor Photofermentative Hydrogen Production

Over the years, as advances in hydrogen production studies are made, more laboratory- and pilot scale studies using photosynthetic microorganisms grown in outdoor conditions are carried out. Parameters such as the hydrogen production rates, hydrogen yields (substrate conversion efficiencies) and light conversion efficiencies are assessed to determine the performances of these outdoor reactors.

Listed in Tables 2.1 to 2.3 are the comparisons of hydrogen production in outdoor reactors. Differences in performances are due to variances in: geometry of the reactors, mode of operation of the reactors, type of microorganisms used, the nature of the feed, the composition of the feed medium, outdoor conditions (seasons) and geographical location of the reactor operation, just to name but a few.

Examining Tables 2.1, 2.2 and 2.3, it is observed that the highest hydrogen production rate of 1.21 mol/m^3/h was achieved using the tubular reactor studies by Adessi *et al.* 2012. Generally, substrate conversion efficiencies in the range of 50 to 78% were reported in the outdoor experiments, except for some instances (Boran *et al.* 2010, Boran *et al.* 2012 and Özgür *et al.* 2010) that were below 50 %, due to the difference in weather conditions. Also, comparing the performance of the artificial media to the convential crop products, it is seen that the use of agro-industrial by-products such thick juice and molasses offer a great potential in photofermentative hydrogen production (Avcıoglu *et al.* 2011, Özkan *et al.* 2012, Keskin and Hallenbeck, 2012, Emrah, 2012) - they resulted in better hydrogen production compared to the artificial feed media. This could be because they are complex media with multiple nutrients and elements that could enhance hydrogen production and yield.

Generally, low light conversion efficiencies of 0.5 to 6% for solar and tungsten lamps, are reported in literature (Hoekama *et al.* 2006). Higher light conversion efficiencies are obtained with decreasing light intensities. In outdoor experiments using cultures of *R. sphaeroides* 8703, the solar light conversion efficiency was observed to decrease from 7% at low sunlight intensities of 100 W/m^2 to 2% at high light intensities of 1000 W/m^2.

Table 2.1 Comparison of photofermentative hydrogen production performances in flat panel photobioreactors operated in outdoor conditions.

Reactor/ volume	**Micro organism**	**Feed**	**H_2 production Rate**	**Yield or substrate conversion efficiency**	**Ref.**
33 L, batch	*R.sphaeroides* B5/A	53 mM lactate, 5 mM glutamate	0.13 mol $H_2/m^3/h$	70 %	Kim *et al.* 1982
	R.sphaeroides B5/B		0.18 mol $H_2/m^3/h$	78 %	
6 L	*R.sphaeroides* B6	60 mM lactate, 6 mM glutamate and 150 mM lactate, 30 mM glutamate	0.84 mol $H_2/m^3/h$	63 %	Kim *et al.* 1987
4.4 L	*R.sphaeroides* RV	Lactate	0.56 mol $H_2/m^3/h$	-	Arai *et al.* 1998
6.5 L, batch	*R.sphaeroides* O.U.001 (DSM 5864)	15 mM acetate, 2 mM glutamate	0.45 mol $H_2/\ m^3/h$	4.6 mol $H_2/mol_{subs.}$	Eroglu *et al.* 2008
		30 mM malate, 2 mM glutamate	0.01 mol $H_2/\ m^3/h$	0.6 mol $H_2/mol_{subs.}$	
		30 mM acetate, 2 mM glutamate	0.36 mol $H_2/\ m^3/h$	1.2 mol $H_2/mol_{subs.}$	
		20 mM lactate, 2 mM glutamate	0.09 mol $H_2/\ m^3/h$	0.8 mol $H_2/mol_{subs.}$	
		Olive mill waste water	0.13 mol $H_2/\ m^3/h$	-	

Table 2.1 (continued)

Reactor/ volume	**Micro organism**	**Feed**	**H_2 production Rate**	**Yield or substrate conversion efficiency**	**Ref.**
4×25 L, fed-batch	*Rhodobacter capsulatus* DSM 155	Acetate, lactate, glutamate	0.94 mol $H_2/m^3/h$	-	Gebicki *et al.* 2010
4 L, fed-batch	*R.capsulatusus* DSM 1710	Molasses dark fer menter effluent	0.50mol $H_2/m^3/h$	50 %	Avcioglu *et al.* 2011
4 L, fed-batch	*R.capsulatus* YO3	Molasses dark fer menter effluent	0.67 mol $H_2/m^3/h$	78 %	Avcıoglu *et al.* 2011
4 L, fed-batch	*R.capsulatus* YO3	40 mM acetate, 4 mM glutamate	0.51 mol $H_2/m^3/h$	53 %	Androga *et al.* 2011
4 L, fed-batch	*R.capsulatusus* YO3	Thick juice dark fermenter effluent	1.12 mol $H_2/m^3/h$	77 %	Özkan *et al.* 2012

Table 2.2 Comparison of photofermentative hydrogen production performances in tubular photobioreactors operated in outdoor conditions.

Reactor/ volume	**Micro organism**	**Feed**	**H_2 production Rate**	**Yield or substrate conversion efficiency**	**Ref.**
65 L, fed-batch	*Rhodobacter capsulatus* DSM 155	Acetate, lactate, glutamate	0.74 mol $H_2/m^3/h$	51 %	Gebicki *et al.* 2010
80 L, fed-batch	*Rhodobacter capsulatus* DSM 1710	40 mM acetate, 2 mM glutamate	0.40 mol $H_2/m^3/h$	12 %	Boran *et al.* 2010
90 L, fed-batch	*Rhodobacter capsulatus* YO3 (hup$^-$)	20 mM acetate, 2 mM glutamate	0.37 mol $H_2/m^3/h$	16 %	Boran *et al.* 2012
50 L	*Rhodopseudomonas palustris* strain 42OL	malate, glutamate	1.21 mol $H_2/\ m^3/h$	50 %	Adessi *et al.* 2012

Table 2.3 Comparison of photofermentative hydrogen production performances in other types of photobioreactors operated in outdoor conditions.

Reactor/ volume	**Micro-organism**	**Feed**	**H_2 production Rate**	**Yield or substrate conversion efficiency**	**Ref.**
Column, 1.4 L	*R.sphaeroides* DSM 9483	Lactate	0.16 mol $H_2/\ m^3/h$	-	Rechenberg, 1998
Roux flask 0.7 L, batch	*Rhodobacter sphaeroides* RV	50 mM lactate,10 mM glutamate	0.13 mol $H_2/m^2/h$	-	Miyake *et al.* 1999
Glass bottle 0.55 L, batch	*Rhodobacter capsulatus* DSM 1710	30mM acetate, 7.5mM of lactate,2 mM glutamate	0.14 mol $H_2/\ m^3/h$	19 %	Özgür *et al.* 2010
	R.capsulatus YO3		0.32 mol $H_2/\ m^3/h$	33 %	

2.6 Aim of the Thesis

The main objectives of the studies performed in this thesis were:

(a) To optimize temperature and light intensity, the critical factors affecting photofermentative hydrogen production using response surface methodology. Optimization of these parameters is necessary to achieve maximum hydrogen production.

(b) To understand factors affecting hydrogen production in an outdoor operated tubular photobioreactor. The goal was to improve hydrogen production in the tubular reactors through modeling. Modeling of the photobioreactors will facilitate proper design considerations during scale up.

Most light intensity and temperature optimization studies have been carried out using the one-factor-at-a-time optimization technique, whereby a single factor is varied while the others are kept constant. This approach is time-consuming and costly due to the large number of experiments that might be needed and it neglects the interactive effects between factors, therefore the obtained optima may differ from genuine multi-variate values. Statistical modeling design of experiments (DOE) techniques such as response surface methodology, which accounts for interactions between factors, can be utilized. In this work, the influence of temperature and light intensity on photofermentative hydrogen production using *R. capsulatus* DSM 1710 was investigated using the 3^k general full factorial design.

In a previous study, Boran (2011) investigated hydrogen production using a 90 L pilot-scale tubular (manifold type) reactor that consisted of a PVC manifold header (25 L) and manifold footer (2.75 L) connected by 9 LDPE tubes with 6 cm inner diameter. Although the temperatures in the reactor were successfully kept below 40 °C during operation using cold water that was circulated through internal cooling tubes integrated in the system, low hydrogen productivities and yields were obtained. The low hydrogen productivities and yields were attributed to the high hydrogen permeability of the reactor’s material of construction, poor light penetration in the reactor and lack of proper mixing. The reactor material of construction (LDPE) had high hydrogen permeability (5.83×10^{-15} mole/m/s/Pa (Orme, 2003)), a short life-span of less than 3 years (Burgess et al. 2007)) and was susceptible to the weather conditions outdoors and unforeseen prevalences such as pecking and scratching by birds. The use of a more durable material was required. Also, light penetration measurements showed that for each 1 cm of depth of the reactor, there was 10 % decrease of light penetration using artificial medium (Boran *et al.* 2012). The tubular reactor used in the previous study had a large tube diameter (6 cm); therefore a smaller diameter that has a shorter light path length is needed to improve light penetraton in the reactor. In this study, glass tubes with inner diameters of 3 cm and 1.4 mm thickness were used to construct tubular reactors operated outdoors. Glass has less hydrogen permeability (2.00E-16 (Souers *et al*., 1978)) compared to LDPE.

Continuous circulation was reported to improve hydrogen productivity and yield (Boran, 2011). However, for proper reactor design, it is necessary to examine the flow distribution in the reactors since it greatly influences the distribution of velocity, pressure drop, mixing of nutrients and residence time of bacteria. Computational fluid dynamics (CFD) can be applied to investigate the flow distribution in various reactor geometries. In this study, the flow distribution in different tubular reactors is analyzed.

During photofermentative hydrogen production, the temperatures of the medium in the solar reactors change with the varying solar radiation and ambient temperatures during the day. Cooling is necessary on summer days when the solar radiation and ambient temperatures are high and heating of the reactor is needed in winter to prevent the culture from freezing. Understanding the temperature distribution within the reactor is essential to determine cooling duty or heating duty, which affects the reactor operating cost. It is vital in projecting the cost-effectiveness of producing hydrogen in large-scale. There are very few studies that report energy gained or lost during the daytime in outdoor operated reactors; specifically how to control temperatures in solar reactors used to grow the photosynthetic microorganisms. Even the ones that do report usually neglect aspects such as the heat required for biomass growth, heat of hydrogen production and pump work. In this dissertation, a dynamic thermal model that simulates the change in temperature inside an outdoor operated reactor is developed. The model included the effects of heat transfer mechanisms such as convection and radiation on the bulk temperature of the solar reactor, and was validated using experimental data. It describes the dependency of hydrogen production on the natural parameters (temperature and sunlight energy) in outdoor conditions, therefore is valuable in estimating the cost-effectiveness of producing hydrogen in large-scale.

CHAPTER 3

MATERIALS AND METHODS

3. 1 The Microorganisms

Two strains of photosynthetic bacteria were used in the present study. The *Rhodobacter capsulatus* (DSM 1710) obtained from DSMZ (Deutsche Sammlung von Mikroorganismen und Zellkulturen GmbH – German Collection of Microorganisms and Cell Cultures) was used in the indoor experiments, while *Rhodobacter capsulatus* YO3, a mutant strain of *Rhodobacter capsulatus* MT1131 that lacked the uptake hydrogenase enzyme (hup^-) was used in the outdoor experiments (Öztürk *et al.* 2006).

3. 2 Growth and Hydrogen Production Media

The bacteria were photoheterotrophically grown in modified Biebl and Pfennig (1981) medium. Different concentrations of organic acids as carbon source, sodium glutamate as nitrogen source, vitamins, trace elements and iron-citrate were added to the basal medium. Shown in Appendix B, Table B1, B2 and B3 are the components of the basal medium and trace elements.

In the indoor experiments, the inoculum growth medium was composed of 20 mM acetic acid, 7.5 mM lactic acid and 10 mM sodium glutamate, while the hydrogen production medium consisted of a mixture of 40 mM acetic acid, 7.5 mM lactic acid and 2 mM sodium glutamate.

In the outdoor experiments, the inoculum growth medium contained 20 mM acetic acid and 10 mM sodium glutamate and the hydrogen production medium consisted of 40 mM acetic acid and 4 sodium glutamate. All the media were sterilized by autoclaving and the vitamin, trace elements and iron-citrate added. The pH of the medium was adjusted to pH 6.4 by the addition of NaOH.

3. 3 The Experimental Procedure

3.3.1 Preparation of the Inoculum

Bacteria from active culture (10% v/v) was injected into 50 mL and 1 L photobioreactors and the mixture sparged with argon gas at a flow a rate of 100 – 150 ml/min in order to obtain anaerobic conditions. After sparging with argon gas for 3 to 5 minutes, the reactors were placed in the incubator set at 30 to 33 ºC and illumination of about 2500 lux (172 W/m^2) was provided using 100 W tungsten lamps. The bacteria inoculum was ready when it reached the mid-logarithmic phase (OD 1.0), after one or two days.

3.3.2 Cleaning, Sterilization and Leakage Tests of the Photobioreactors

The indoor photobioreactors were sterilized by autoclaving and the outdoor reactors were sterilized using 3% H_2O_2 solution. They were thoroughly rinsed with distilled water and completely filled to test for leakages.

3.3.3 Inoculation of the Photobioreactor

In the indoor experiments, 10% v/v of inoculum was introduced into the 50 mL photobioreactors. The mixture containing 5 mL bacteria and 45 mL hydrogen production medium was spurged with argon gas to create anaerobic atmosphere and the reactors were placed in the incubator and illumination at 2500 lux (172 W/m^2) was provided using 100 W tungsten lamps.

In the outdoor experiments, 25% v/v of inoculum was introduced into the tubular reactor. The reactors were completely filled and so no argon sparging was necessary. The reactors were operated in outdoor conditions.

3.3.4 Sampling

Samples (2.5 mL) were periodically taken from the reactors using 2.5 ml sterile syringes. In the indoor experiments samples were collected at 24 hour intervals, while in the outdoor experiments they were taken every 2 hours.

3.3.5 Shut-down of the Photobioreactors

At the end of the experiments, the photobiorecators were emptied and the effluent was sterilized chemically using hydrogen peroxide and discarded. The reactors were washed to remove remnants of cells, rinsed and stored.

3. 4 The Indoor Experiments

The batch experiments were carried out in 55 mL glass bottle photobioreactors. The hydrogen production medium was inoculated with 10% (v/v) bacteria to add up to a total working volume of 50 mL. The bottles were fitted with rubber stoppers, flushed with oxygen-free argon for 5 min to establish anaerobic conditions and then placed in a cooling incubator (Nüve ES250) to keep the temperature constant. Illumination was provided by a tungsten lamp (100 W) and

the initial pH was 6.4. Each temperature-illumination condition was run in duplicate and the samples were collected at 24 hour intervals for the analysis. The total time of the runs was 12 days. For a detailed description of the experimental setup, the reader is referred to Sevinç *et al.* 2012.

3. 5 The Outdoor Experiments

3.5.1 The Experiments Performed with Variable Flowrates

A U-tube tubular reactor made of glass measuring 1.4 m in thickness, 0.03 m in outer diameter and total length of 5 m was constructed. It was connected to a gas-liquid separator (0.5 L) using polyvinyl chloride (PVC) tubing and the medium (distilled water) was re-circulated using a pump (SEBO 3500). A PVC cooling coil with an outer diameter of 7 mm and thickness of 1 mm was inserted in the U-shaped glass tube (Figure 3.1). Detailed dimensions of the reactor and cooling tube dimensions are given in Appendix C. Cold water from a chiller (PNÖSO PSS 6 D) was passed through the coils so as to maintain the reactor temperature below 38°C. The glass tube had a working volume of 2.8 L.

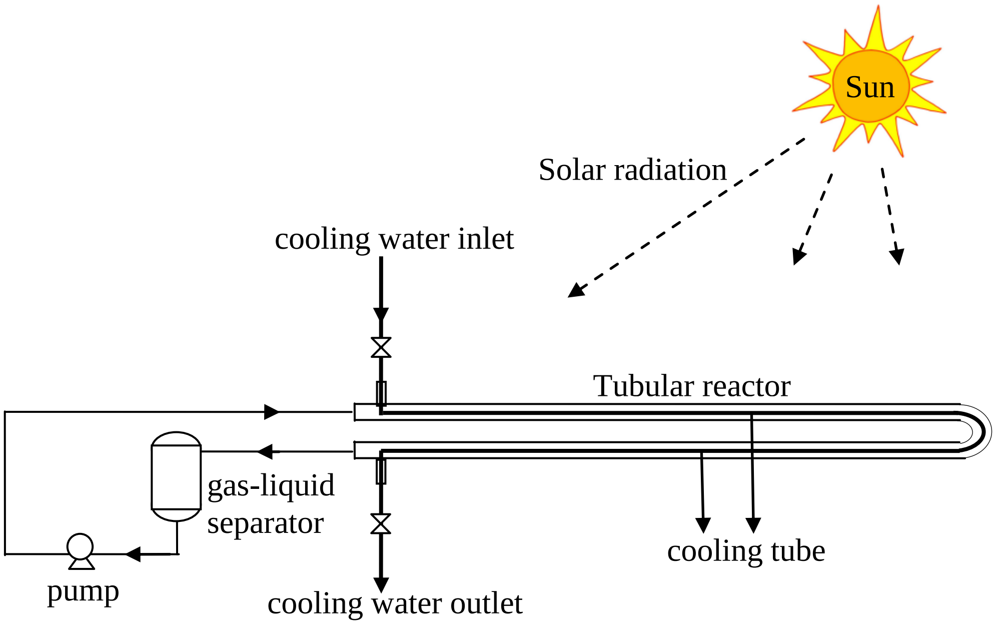
Sun
Solar radiation
cooling water inlet
Tubular reactor
gas-liquid
separator
cooling tube
pump
cooling water outlet

Figure 3.1 Flow chart of the outdoor reactor system.

The experiments were performed in the summer of 2012 and spring of 2013 at the Hydrogen Research Laboratory in the Chemical Engineering Department at the Middle East Technical University, Ankara, Turkey. Distilled water was continuously circulated at different flow rates circulation rates as shown in the Table 3.1 and data was collected for 12 hours (7 a.m. to 7 p.m.). Two sets of experiments were perfomed. In the first set, the change in temperature inside the reactors operated at different flow rates and cooled with water flowing in co-current and counter-current mode to the medium in the reactor was studied. In the second set of experiment, the radial variation of temperature within the reactor was investigated. Temperature probes (8 thermocouples) were inserted at different radial positions of the reactor (Figure 3.2). The cooling coils were removed while

carrying out these experiments. The radial temperature measurements were performed on the 5th of May, 2013 using flow rates of 100 ml/min (*Re* = 120) and 3240 ml/min (*Re* = 4200).

Table 3.1 Summary of the experiments to determine the change temperature in the tubular photobioreactors circulated at different flow rates.

Operation	**Date**	**Circulation rate (kg/s)**	**Reynolds Number (Re)**
Co-current flow[a]	29.08.2012	3.5×10^{-3}	160
	02.09.2012	4.0×10^{-2}	1860
	01.09.2012	5.8×10^{-2}	2700
Counter-current flow[a]	19.09.2012	3.5×10^{-3}	160
	17.09.2012	4.0×10^{-2}	1860
	18.09.2012	5.8×10^{-2}	2700
Radial temperature variation[b]	05.05.2013	2.7×10^{-3}	120
		9.0×10^{-2}	4200
Cooling water		1.1×10^{-2}	2710
Duration: 7 a.m. to 7 p.m.			

[a] The experiments investigated the change in temperature of medium in the reactors. [b] The experiments investigated the reactor radial temperature change.

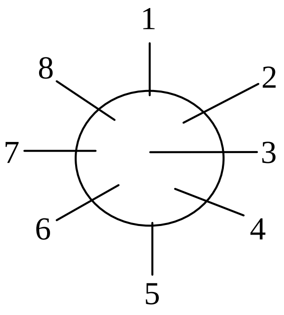

Figure 3.2 Radial measurements of temperature inside the reactors.

3.5.2 The Experiments Performed at Constant Flowrates

Four identical tubular photobioreactors were constructed and operated in parallel (Figure 3.3). Each tubular reactor was made of two horizontal glass tubes measuring 2.4 m in length, 0.03 m in outer diameter and 1.4 mm in thickness. It was connected to a 1 liter gas-liquid separator using polyvinylchloride (PVC) tubing. A PVC cooling tube that measured 7 mm in outer diameter and 1 mm in thickness was inserted in the glass tube, making a total working volume of 3.20 L for the annular reactor. Shown in Figure 3.4 is the process flow diagram of the experimental setup.

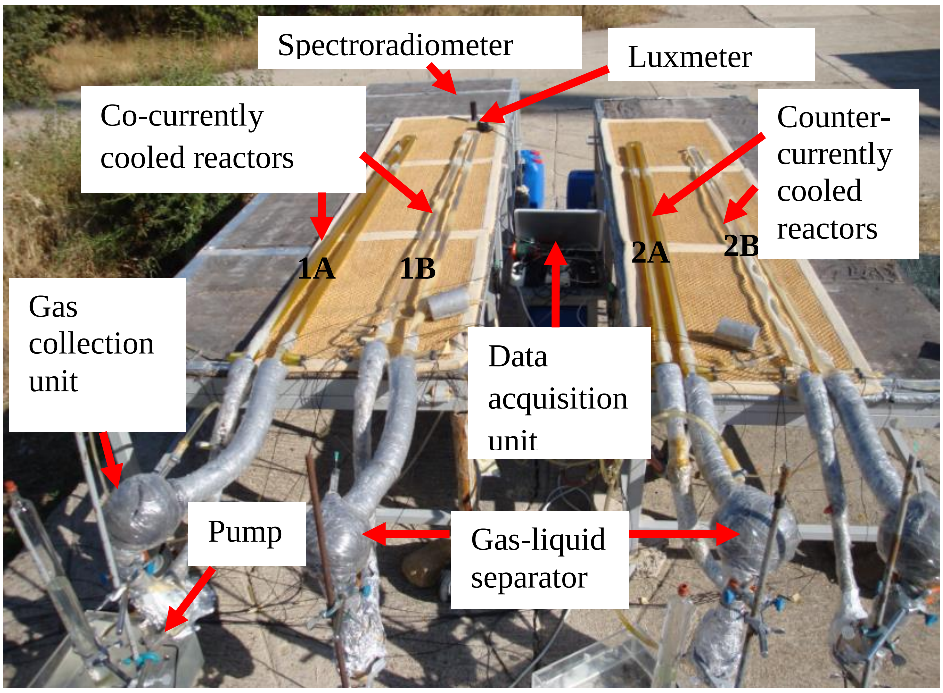
Spectroradiometer
Luxmeter
Co-currently cooled reactors
Counter-currently cooled reactors
1A
1B
2A
2B
Gas collection unit
Data acquisition unit
Pump
Gas-liquid separator

Figure 3.3 Photograph of the experimental set-up for the outdoor operated reactors. (1A – 1B) Co-currently cooled tubular reactor and (2A – 2B) Counter-currently cooled tubular reactor. Reactors 1A and 2A contain bacteria while 1B and 2B contain medium without bacteria.

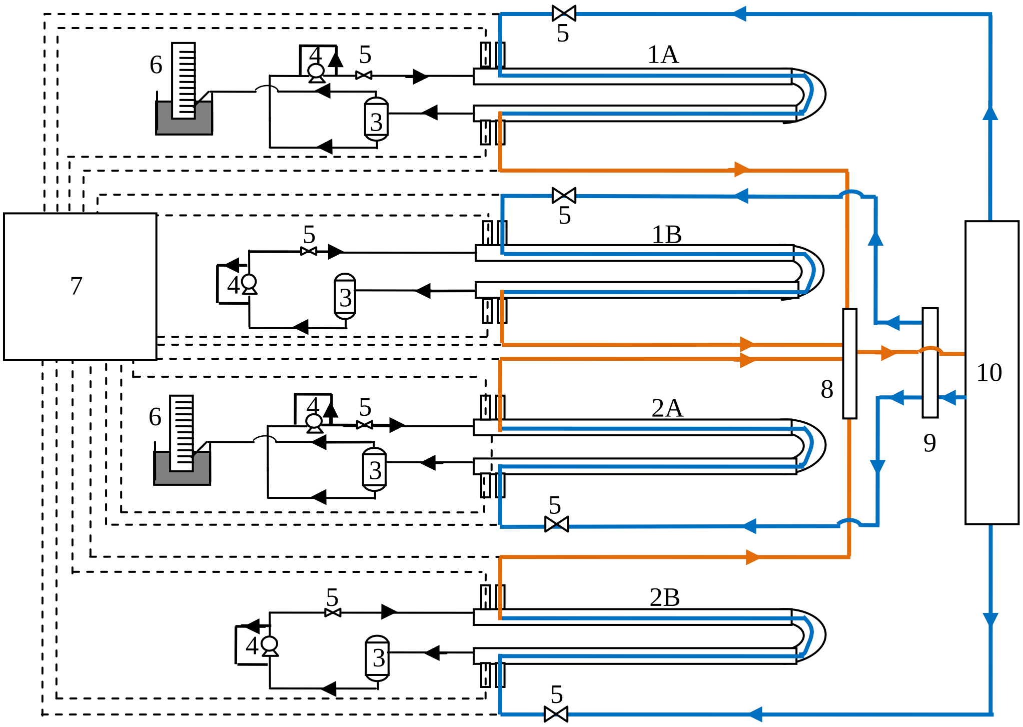

Figure 3.4 Flow chart of the reactor system. (1A – 1B) Co-currently cooled tubular reactor and (2A – 2B) Counter-currently cooled tubular reactor. Reactors 1A and 2A contain bacteria whereas 1B and 2B contain medium without bacteria. (3) Gas-liquid separators, (4) Reactor circulating pumps, (5) Valves, (6) Gas collection units, (7) Data acquisition unit, (8) Outflow cooling water manifold, (9) Inflow cooling water manifold and (10) Chilled water unit.

The experiments were performed on the 5th, 7th and 8th of August, 2013, at the Middle East Technical University's Hydrogen Research Laboratory, Ankara, Turkey. Medium with and without bacteria was continuously circulated in the reactors at a rate of 3.5×10^{-3} kg/s using aquarium pumps (Venus Aqua E3302). Cooling water was passed through internal cooling pipes in co-current and counter-current mode at flow rates of $3.5 - 5.0 \times10^{-3}$ kg/s in the reactors with and without reactors, respectively. A cooling protocol that aimed to maintain temperatures below 38.0 °C was applied during the experiments. Operation of the chiller began at 9 a.m. when the reactor temperature rose above 30.0 °C and stopped at 6 p.m. when the temperatures dropped to below 25.0 °C. In the reactors containing bacteria, an initial cell concentration of OD 1.0 corresponding to 0.465 gDCW/L was used. The hydrogen gas evolved was collected in water filled graduated glass columns and data were recorded for 14 hours (6 a.m. to 8 p.m.). Shown in Table 3.2 is a summary of the experiments performed.

Table 3.2 Summary of the experiments to determine the change temperature in the tubular photobioreactors circulated at constant flow rate. The experimements were performed in the summer of 2013.

Experiments	**Circulation rate (kg/s)**	**Reynolds number (Re)**
Co-current with bacteria	3.5×10^{-3}	160
Co-current without bacteria	3.5×10^{-3}	160
Counter-current with bacteria	3.5×10^{-3}	160
Counter-current without bacteria	3.5×10^{-3}	160
Cooling water	$3.5 - 5.0\times10^{-3}$	1120 – 1600
Initial bacteria concentration: 0.465 gDCW/L (OD 1.0)		
Dates: 5th, 7th and 8th of August, 2013		
Duration: 6 a.m. to 8 p.m.		

3.6 Analytical Methods

3.6.1 Cell Concentration

The bacterial cell concentration was determined by a spectrophotometer Shimadzu UV-1201) at 660 nm. An OD660 of 1.0 corresponded to 0.540 gDCW/L for *R.capsulatus* DSM 1710 (Uyar, 2008) and 0.465 for gDCW/L *R.capsulatus* YO3 (Öztürk, 2005). Distilled water was used as a blank solution.

3.6.2 pH

The pH of the liquid solution in the reactors was measured using a pH meter (Mettler Toledo 3311).

3.6.3 Temperature

The temperatures at the inlet and outlet of the outdoor operated reactors and the inlet and outlet of the cooling water were measured using thermocouples (Fe-const J type) connected to an online data logger (Ordel UDL100). The surface temperature of the reactor was manually measured using an infrared thermometer (Testo T1). A temperature sensor (HOBO-S-TMB-M002) connected to an online weather station (HOBO® U30 ETH) was used to monitor the variations in the air temperatures.

3.6.4 Light Intensity

In the indoor experiments, light intensity was measured using a luxmeter (Lutron LX-105 Light Meter) and in the outdoor experiments, solar radiation was measured using a pyranometer (HOBO-S-LIB-M003) that was connected to an online weather station (HOBO® U30 ETH).

3.6.5 Organic Acid Analysis

High Performance Liquid Chromatography (HPLC) (Shimadzu 20A series) was used to analyze organic acids concentrations in the samples. The liquid samples were filtered using 45µm nylon or cellulose filters (Millipore, 13 mm) and analyzed by an Alltech IOA-1000 (300 mm x 7.8 mm) HPLC column. 0.085 M H_2SO_4 was used as the mobile phase and the oven temperature was mainatained at 66 °C. A low gradient pump (Shimadzu LC-20AT) with a degasser (Shimadzu DGU-14A) was used to keep the mobile phase flow rate at 0.4 mL/min. 10µl sample was injected into the system and a UV detector (Shimadzu FCV-10AT) with absorbance set at 210 nm was used to determine the component separation. The organic acids measured were lactic acid, formic acid, acetic acid, propionic acid and butyric acid.

3.6.6 Gas Analysis

Gas chromatography (GC) equipment (Agilent Technologies 6890N) was used to measure the composition of gas samples collected using gas-tight syringes (Hamilton, 22 GA 500µL). The gas was sampled from the gas collection column. The GC had a thermal conductivity detector and a Supelco Carboxen 1010 column. Argon at a flow rate of 26 mL/min was used as a carrier gas and the oven, injector and detector temperatures were 140 ºC, 160 ºC and 170 ºC, respectively.

CHAPTER 4

MODELING AND SIMULATION OF PHOTOBIOREACTORS

4.1 Response Surface Methodology

A 3^2 general full factorial DOE was implemented to optimize temperature and light intensity for maximum hydrogen production by batch cultures of *R. capsulatus* DSM1710. Regression models that related hydrogen production rate (R_{H2}) and hydrogen yield (Y_{H2}) to temperature (20, 30, 38°C) and light intensity (100, 200, 340 W/m^2) and their interactions were developed. The levels of the experimental design consisted of 18 runs. For the regression, the variables were coded by Equation (4.1).

$$x = \frac{\left[X - \left(\frac{X_{\max} + X_{\min}}{2} \right) \right]}{\frac{X_{\max} + X_{\min}}{2}} \tag{4.1}$$

where x is the coded factor, X is the original factor, X_{max} is the maximum factor and X_{min} is the minimum factor. Coding normalizes units of measure, thereby reducing errors that could occur due to different measurement scales.

A regression analysis was performed to estimate the response function of Equation (4.2).

$$Y = \beta_0 + \beta_1 x_1 + \beta_2 x_2 + \beta_{12} x_1 x_2 + \beta_{11} x_1^2 + \beta_{22} x_2^2 \tag{4.2}$$

where β_0 is the offset term, β_1 and β_2 are the linear coefficients, β_{11} and β_{22} are the quadratic coefficients, β_{12} is the interactive coefficient and x_1 and x_2 are the temperature and light intensity input variables, respectively.

The regression equations obtained were analyzed using the analysis of variance methodology (ANOVA). Briefly, ANOVA is a statistical method in which the means of treatment groups are compared to each other, taking into account the magnitude of the contributions to the overall variation of the data (Daniel, 2009). Measures for the significance and fit of the experimental data to the model equations were obtained from this analysis.

The hydrogen production performance of the cultures in the photobioreactors was quantified by hydrogen production rates and yields. The maximum hydrogen production rate (calculated from the linear hydrogen production phase during exponential bacterial growth) was determined as the amount of hydrogen gas produced divided by the time taken to generate the gas per working volume of the photobioreactor (Equation 4.4).

$$\text{H}_2 \text{ production rate (mol/m}^3\text{/h)} = \frac{\text{Amount of H}_2 \text{ produced (mol)}}{\text{Reactor working volume (m}^3\text{)}\times\text{time (h)}} \tag{4.4}$$

The hydrogen yield estimates how effectively the substrates (carbon sources) fed to the culture were utilized for hydrogen production. Acetate and lactate were used as carbon sources during the experiments and their conversion to hydrogen is represented by Equations (4.5) and (4.6). The hydrogen yield was calculated as the ratio of the actual amount of hydrogen produced to the theoretical amount of hydrogen that would have been produced from the substrate consumed, as shown in Equation (4.7).

$$\text{Acetate: } C_2H_4O_2 + 2H_2O \rightarrow 4H_2 + 2CO_2 \tag{4.5}$$

$$\text{Lactate: } C_3H_6O_3 + 3H_2O \rightarrow 6H_2 + 3CO_2 \tag{4.6}$$

$$\text{H}_2 \text{ yield} \left(\frac{\text{mol H}_2}{\text{mol substrate}}\right) = \frac{\text{H}_2 \text{ produced (mol)}}{4 \times \text{acetate (mol)} + 6 \times \text{lactate (mol)}} \tag{4.7}$$

4.2 Dynamic Heat Transfer Model for the Outdoor Operated Tubular Bioreactors

4.2.1 Thermal Balance on the Reacting System

An energy balance was made on the liquid medium in the reactor. The thermal balance included radiative heat transfer, convective heat transfer, the heat absorbed by the cooling water, pump work and the metabolic heat exchanged in the system (Figure 4.1). Shown in Equation 4.8 is the one-dimensional energy balance.

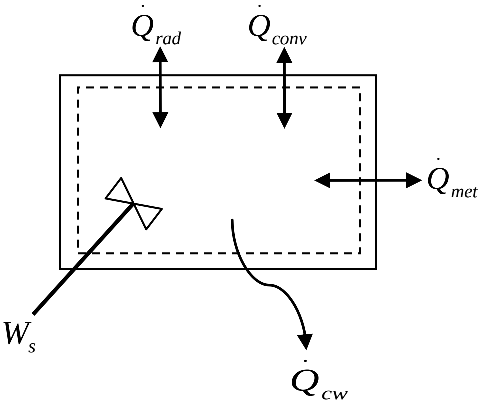

Figure 4.1 Schematic of the energy transfer in the reactor system.

$$\dot{Q}_{rad} + \dot{Q}_{conv} + \dot{Q}_{met} - \dot{Q}_{cw} + W_s = \rho_r V_r Cp_r \frac{dT}{dt} \qquad (4.8)$$

where $\dot{Q}_{rad}$ is the net radiative heat transferred (W), $\dot{Q}_{conv}$ is the convective heat transferred (W), $\dot{Q}_{met}$ is the heat required (W) for the metabolic activities of the bacteria, $\dot{Q}_{cw}$ is amount of heat (W) absorbed by the cooling water, W_s is the pump work (W), ρ_r is the density (kg/m^3) of the reactor medium, V_r is the working volume (liquid) (m^3) of the reactor, Cp_r is the specific heat capacity (J/kg/K) of the reactor medium and T_r is the temperature (K) of the reactor medium.

4.2.1.1 Radiative Heat Transfer

The net heat transferred by radiation ($\dot{Q}_{rad}$) to the reactor system can be presented as

$$\dot{Q}_{rad} = \dot{Q}_{rad,D} + \dot{Q}_{rad,d} + \dot{Q}_{rad,a} + \dot{Q}_{rad,g} + \dot{Q}_{re,a} + \dot{Q}_{re,g} + \dot{Q}_{rad,r} \qquad (4.9)$$

where $\dot{Q}_{rad}$ is the net radiative heat transferred (W), $\dot{Q}_{rad,D}$ is the direct solar radiation (W), $\dot{Q}_{rad,d}$ is the diffuse solar radiation (W), $\dot{Q}_{rad,a}$ is radiation from the air surrounding the reactor (W), $\dot{Q}_{rad,g}$ is the ground radiation (W), $\dot{Q}_{re,a}$ is the reflected air radiation (W), $\dot{Q}_{re,g}$ is the reflected radiation from the ground (W) and $\dot{Q}_{rad,r}$ is the radiation energy emitted by the reactor (W).

Solar Radiation

As solar radiation enters the atmosphere, part of it is absorbed and scattered by clouds and dust particles. The amount of solar radiation (G_s) measured at the ground is the total of the direct (G_D) and diffuse (G_d) solar radiation. The direct and diffuse solar radiation can be represented as functions of the total radiation reaching the horizontal surface (G_s) and the fraction of diffuse radiation impacting the ground (K_d) (Fernandez *et al.* 1997).

$$G_d / G_s = K_d \qquad (4.10)$$

$$G_D = (1 - K_d) G_s \qquad (4.11)$$

The fraction of diffuse radiation (K_d) reaching the ground was estimated using the correlation given by Liu and Jordan (1960) (Equation. 4.12).

$$K_d = 1.39 - 4.027\, K_h + 5.530\, K_h^2 - 3.108\, K_h^3 \qquad (4.12)$$

where K_h, the clearness index, is the ratio of the global solar radiation measured at the ground level to the total solar radiation on the atmosphere surface (extraterrestrial radiation).

Direct Solar Radiation

The direct solar radiation on the surface of the reactor is estimated as

$$\dot{Q}_{rad,D} = \tau \varepsilon_r G_D Cos\theta_z A_{ro} f_A f(t) \tag{4.13}$$

where τ is the wall transmittance of the reactor, ε_r is the emissivity of the reactor medium, G_D is the intensity of the direct solar radiation (W/m^2) reaching the ground surface in the vertical direction, θ_z is the angle of incidence (rad), A_{ro} is the outer surface area (m^2) of the reactor that is exposed to atmosphere, f_A is the form factor between the reactor surface and the atmosphere and *f(t)* is the shading function. θ_z is the angle between a vector normal to the ground surface and the sun direction. It is a function of the latitude φ (rad), the solar declination δ (rad) and the solar hour angle (Equation 4.14) (Duffie and Beckman, 2006, Bechet *et al.* 2010).

$$Cos(\theta_z) = Sin\ \varphi\ Sin\ \delta + Cos\ \varphi\ \mathrm{Cos}\ \delta\ \mathrm{Cos}\ \omega \tag{4.14}$$

The latitude (φ) of Ankara, where the experiments were performed is 39° 55' 38 N.

Solar declination (δ) is calculated as a function of the day of the year, *N*.

$$\delta = 23.35\left(\frac{2\pi}{360} Sin\left(2\pi\left(\frac{284+N}{365}\right)\right)\right) \tag{4.15}$$

The solar hour angle (ω) is the angular displacement of the sun east or west of the local meridian due to rotation of the earth on its axis at 15° per hour (Duffie and Beckman, 2006). It is calculated as a function of the solar hour (*hs*) and is usually negative before noon and positive in the afternoon.

$$\omega = 15(12 - hs) \tag{4.16}$$

f(t), the shading function is equal to 1 when the reactor is exposed to the sun, else equal to zero (Bechet *et al.* 2010). The form factor (f_A) for the reactor is 0.5 therefore Equation (4.13) was reduced to,

$$\dot{Q}_{rad,D} = \tau \varepsilon_r G_D Cos\theta_z \pi R_o L \tag{4.17}$$

where R_o is the outer radius (m) and L is the length (m) of the reactor.

Diffuse Solar Radiation

Diffuse radiation is the radiation resulting from the scattering of solar beams by molecules or suspensions in the atmosphere. It is not dependent on the angle of incidence (θ_z) and is evenly radiated in all directions. Applying the form factor theory, it could be expressed as

$$\dot{Q}_{rad,d} = \tau \varepsilon_r G_d \pi R_o L \tag{4.18}$$

Radiation from the Air Surrounding the Reactor

The air surrounding the reactor is heated up by the solar radiation and it emits radiation to the surface of the reactor. The amount of air radiation was calculated using Stefan-Boltzman's power law. Applying the form factor theory yields,

$$\dot{Q}_{rad,a} = \tau \varepsilon_r \varepsilon_a \sigma T_a{}^4 \pi R_o L \tag{4.19}$$

where $\mathcal{E}_a$ is the emissivity of air.

Radiation from the Ground

During the day, the ground heats up because of the solar and air radiation it receives. It emits part of the radiation back to the environment and reactor surface. In the experiments, the reactors were placed on a table covered with sisal mats. Applying Stefan-Boltzman's power law and the form factor theory, the amount of ground radiation emitted to the surface of the reactor was estimated as,

$$\dot{Q}_{rad,g} = \tau \varepsilon_r \varepsilon_g \sigma T_g{}^4 \pi R_o L \tag{4.20}$$

where $\mathcal{E}_g$ is the emissivity of the ground and T_g is the ground temperature (K).

Reflected Solar and Air Radiation from the Ground Surface

Solar radiation reaching the ground is reflected on the surface of the reactor. Since the ground was assumed to be diffuse (incoming radiation is evenly reflected in all directions) and opaque (emissivity equals absorptivity), the ground reflectivity (r_g) could be written as,

$$r_g = 1 - \mathcal{E}_g \tag{4.21}$$

Then amount of radiative energy that reaches the reactor after being reflected from the ground is,

$$\dot{Q}_{re,g} = \tau\varepsilon_r r_g G_s \pi R_o L \tag{4.22}$$

Similarly, the fraction of air radiation hitting the ground surface that is reflected onto the surface of the reactor is expressed as,

$$\dot{Q}_{re,a} = \tau\varepsilon_r\varepsilon_a r_g \sigma T_a^4 \pi R_o L \tag{4.23}$$

Radiation from the Reactor

The reactor medium gains heat energy as it is exposed to solar radiation during the day. It radiates the absorbed energy to the surroundings, in this case the surrounding air and the cooling water. The rate of radiation energy emitted by the medium was determined as,

$$\dot{Q}_{rad,r} = -\sigma\tau\varepsilon_r T_r^{\,4} 2\pi(R_i + r_o)L \tag{4.24}$$

where r_o is the outer diameter (m) of the cooling tube. The length of the cooling tube is equal to the length of the reactor (L).

4.2.1.2 Convective Heat Transfer

The tubular section of the reactor in which the cooling pipe is inserted forms an annulus (Figure 4.2). It was assumed that the cooling pipe was positioned at the center of the horizontal reactor tubes and because the medium in the reactor was continuously circulated using a pump, heat transfer in the annular section was mainly through forced convection.

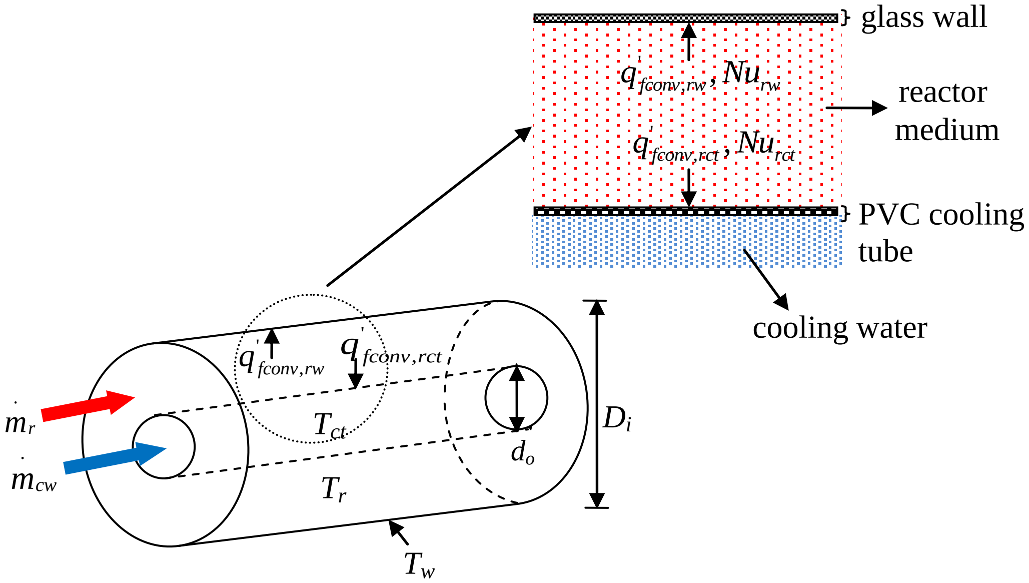
glass wall
$q'_{fconv,rw}$, Nu_{rw}
reactor medium
$q'_{fconv,rct}$, Nu_{rct}
PVC cooling tube
cooling water
$q'_{fconv,rw}$
$q'_{fconv,rct}$
$\dot{m}_r$
$\dot{m}_{cw}$
T_{ct}
T_r
D_i
d_o
T_w

Figure 4.2 Schematic of the annular section of the reactor system.

where $\dot{m}_r$ is the reactor medium mass flow rate (kg/s), $\dot{m}_{cw}$ is the cooling water mass flow rate (kg/s), q'_{rw} is the heat flux (W) from the bulk reactor to the reactor wall, q'_{rct} is the heat flux from the bulk reactor to the cooling tube outer surface, T_r is the reactor bulk temperature (K), T_{ct} is the cooling water temperature (K), T_w is the reactor wall temperature (K), D_i is the inner diameter (m) of the reactor tube, d_o is the outer diameter (m) of the cooling tube, Nu_{rw} is the Nusselt number for the reactor inner tube surface and Nu_{rct} is the Nusselt number for the outer surface of the cooling tube.

The flow in the reactors is ranged from lamiar to turbulent (*Re* = 160 to 4200). In order to determine convective heat transfer coefficient, it is important to ascertain whether the flows were developing or fully developed. This was done by estimating the hydrodynamic and thermal entry lengths with details given in Appendix D. For the low Reynolds number (*Re* = 120,160 and 260), the flow was found to be fully developed as the hydrodynamic and thermal lengths were small compared to the reactor length, while at higher flow rates, it was developing. In the experiments at low flow rates (*Re* = 160), the convective heat fluxes (q'_{rw} and q'_{rct}) were determined using the heat transfer coefficients derived from the Nusselt numbers (Nu_{rw} and Nu_{rct}) associated with the annular system. The convective heat transfer coefficients (h_{co} and h_{rw}) were calculated by solving the equations for the heat fluxes and coefficients for a fully developed laminar flow in a circular tube annulus with uniform heat flux given by Lunderberg *et al.* (1963). The equations 4.25 – 4.30 were solved simultaneously to estimate h_{co} and h_{rw}. The heat lost or gained by the reactor system and the cold water through forced convection were estimated using Equations 4.31 and 4.32.

$$Nu_{rw} = Nu_{oo} / \left(1 - \left(q'_{fconv,rct} / q'_{fconv,rw}\right)\theta_o^*\right) \tag{4.25}$$

$$Nu_{rct} = Nu_{ii} / \left(1 - \left(q'_{fconv,rw} / q'_{fconv,rct}\right)\theta_i^*\right) \tag{4.26}$$

$$Nu_{rw} = h_{rw} D_H / k_r \tag{4.27}$$

$$Nu_{rct} = h_{co} D_H / k_c \tag{4.28}$$

$$q'_{rw} = h_{rw}\left(T_w - T_r\right) \tag{4.29}$$

$$q'_{rct} = h_{co}\left(T_{ct} - T_r\right) \tag{4.30}$$

$$\dot{Q}_{fconv,rw} = A_{rw} q'_{fconv,rw} = A_{rw} h_{rw}\left(T_w - T_r\right) \tag{4.31}$$

$$\dot{Q}_{fconv,rct} = A_{co} q'_{fconv,rct} = A_{co} h_{co}\left(T_{ct} - T_r\right) \tag{4.32}$$

where h_{rw} is the convective heat transfer coefficient (W/m^2/K) on the reactor wall side, h_{co} is the convective heat transfer coefficient (W/m^2/K) on the cooling tube, Nu_{ii}, Nu_{oo}, θ_i^* and θ_o^* are coefficients for fully developed laminar flow in the circular tube annulus with uniform heat flux, D_H is the hydraulic diameter (m) of the reactor, k_r is the thermal conductivity (W/m^2/K) of the reactor bulk fluid, k_c is the thermal conductivity (W/m^2/K) of cooling water, T_{ct} is the wall temperature (K) of the cooling tube, $\dot{Q}_{fconv,rw}$ is the convective heat transferred (W) from the reactor medium to the inner wall of the reactor and $\dot{Q}_{fconv,rct}$ is the total convective heat transferred (W) from the reactor medium to the cooling tube surface.

The convective heat transfer in the transition and turbulent flow (Re ≥2300) were determined from the average Nusselt numbers calculated using the relation given by Gnielinski (Gnielinski, 1976).

$$\overline{Nu}_D = \frac{\bar{h}_r D}{k} = 3.66 + \frac{\left(f/8\right)\left(\mathrm{N}_{\mathrm{Re}_D} - 1000\right)\mathrm{Pr}}{1 + 12.7\left(f/8\right)^{1/2}\left(\mathrm{Pr}^{2/3} - 1\right)} \left[1 + \left(\mathrm{D}/\mathrm{L}\right)^{2/3}\right] \tag{4.33}$$

which is valid for developing or fully developed turbulent flow, 2300 ≤ Re ≤ 5.0×10^6 and 0.5 ≤ Pr ≤ 2000. D/L accounts for the entrance effects and is zero for the fully developed flow. f is the Darcy friction factor and for the smooth pipe, it can be estimated using the Petukov equation (Petukov, 1970).

$$f = (0.79 \ln Re - 1.64)^{-2} \tag{4.34}$$

4.2.1.3 Heat Removed by the Cooling Water

The amount of heat removed by the cooling water was calculated as,

$$\dot{Q}_{cw} = \dot{m}_{cw} Cp_c \left(T_{co} - T_{ci}\right) \tag{4.35}$$

where $\dot{Q}_{cw}$ is the rate of heat (W) removed by the cooling water, $\dot{m}_{cw}$ is the mass flow rate of the cooling water (kg/s), Cp_c (J/kg^{-1}/K) is the heat capacity of the cooling water, T_{ci} is the inlet temperature (K) of the cooling water and T_{co} is the inlet and outlet temperature (K) of the cooling water.

4.2.1.4 Work Done by the Pump

An energy balance is made around the pump to determine the minimum pump work (W_s). The pressure before and after the pump were measured using a barometer during the reactor operation. It was assumed that the flow was steady, incompressible and ideal with no irreversibilities or frictional losses. The elevations between the inlet and outlet of the pump were negligible ($z_1 = z_2$) and the kinetic correction factors for the fully developed laminar flow in the system are constant ($\alpha_1 = \alpha_2$).

$$\dot{m}_r\left(\frac{P_1}{\rho}+\alpha_1\frac{u_1^2}{2}+gz_1\right)+W_s=\dot{m}_r\left(\frac{P_2}{\rho}+\alpha_2\frac{u_2^2}{2}+gz_2\right) \tag{4.36}$$

where $\dot{m}_r$ is the mass flow rate (kg/s) of fluid in the reactor, P_1 and P_2 are the pressure (bars) values at the inlet and outlet of the pump, α_1 and α_2 are the kinetic correction factors for the fully developed laminar flow before and after the pump, u_1 and u_2 are the velocity (m/s) of the fluid at the pump inlet and outlet, g is gravity acceleration (m/s^2) and z_1 and z_2 are the elevation (m) at the inlet and outlet of the pump.

4.2.1.5 Metabolic Heat of the Reacting System

The system was considered to be a semi-batch reactor in which two independent reactions occurred.

Reaction 1: Hydrogen production

$$\underset{\substack{\text{Acetic acid}\\(A)}}{CH_3COOH(aq)}+2H_2O(l)\rightarrow 4H_2(g)+2CO_2(g) \tag{4.37}$$

Reaction 2: Biomass formation

$$\begin{aligned}0.602\underset{\substack{\text{Glutamic acid}\\(Glu)}}{C_5H_9NO_4(aq)}+\underset{\substack{\text{Acetic acid}\\(A)}}{CH_3COOH(aq)} &\rightarrow 0.710CO_2(g)+1.054H_2O(l)\\ &\quad +4.303\underset{\substack{\text{Biomass}\\(X)}}{CH_{1.7}O_{0.45}N_{0.14}(s)}\end{aligned} \tag{4.38}$$

An elementary balance was made to determine the stoichiometric coefficients in Equation (4.38). Calculations are shown in Appendix E. The biomass formula given by Hoekama *et al.* (2006) was used in the estimation.

The energy required by the bacteria for its metabolic activities was designated as $\dot{Q}_{met}$. It included the heat needed for hydrogen production and for growth (biomass formation).

$$\dot{Q}_{met} = \dot{Q}_{met.1} + \dot{Q}_{met.2} \tag{4.39}$$

where $\dot{Q}_{met.1}$ is the heat (W) required for hydrogen production and $Q_{met.2}$ is the heat (W) required for the growth of biomass.

$$\dot{Q}_{met.1} = V_R r_{A_1} \Delta H_{Rxn1} \tag{4.40}$$

$$-r_{A_1} = r_{H_2} Y'_{A/H_2} \tag{4.41}$$

$$r_{A1} = k_A C_A \tag{4.42}$$

$$r_{H_2} = Y'_{H_2/A}(k_A C_A) \tag{4.43}$$

$$\dot{Q}_{met.2} = V_R r_{A_2} \Delta H_{Rxn2} \tag{4.44}$$

$$-r_{A_2} = Y'_{A/X} r_X \tag{4.45}$$

$$r_X = Y'_{X/A}(k_A C_A) \tag{4.46}$$

where $\dot{Q}_{met.1}$ is the heat consumed (W) during hydrogen production, $-r_{A_1}$ is the acetic acid consumption rate for hydrogen production (mol/L/h), Y'_{A/H_2} is the yield coefficient that relates the amount of acetic acid consumed (mol) to the amount of hydrogen formed (mol), r_{H_2} is the hydrogen production rate (mol/L/h), k_A is the acetic acid consumption rate constant (h^{-1}), C_A is the concentration (mol/m^3) of acetic acid, $\dot{Q}_{met.2}$ is the heat required for biomass formation, $-r_{A_2}$ is the acetic acid consumption rate for biomass formation (mol/L/h), $Y'_{A/X}$ is the yield coefficient that relates the amount of acetic acid consumed to the amount of cells formed and r_X is the rate of biomass formation (mol/L/h). A polymath code was written to calculate $\dot{Q}_{met}$. It is shown in Appendix F.

The heats of reactions (ΔH_{Rxn1} and ΔH_{Rxn2}) in Equations (4.40) and (4.44) were determined using the standard heats of combustions and heat capacities of the reactants and products of the reactions for hydrogen production (Equation 4.37) and biomass formation (Equation 4.38) (Doran, 2000). The equations used are shown in Equations (4.47) to (4.49).

$$\Delta H_{Rxni} = \Delta H^{o}_{c,i} + \int_{T_{Ref}}^{T} Cp_i dT \tag{4.47}$$

$$\begin{aligned}\Delta H_{Rxn1} = {} & \left(H^{o}_{A} + 2H^{o}_{H_2O} - 4H^{o}_{H_2} - 2H^{o}_{CO_2}\right) + Cp_A\left(T - T_{Ref}\right) + 2Cp_{H_2O}\left(T - T_{Ref}\right) \\ & - 4Cp_{H_2}\left(T - T_{Ref}\right) - 2Cp_{CO_2}\left(T - T_{Ref}\right)\end{aligned} \tag{4.48}$$

$$\begin{aligned}\Delta H^{o}_{Rxn2} = {} & \left(H^{o}_{A} + 0.602H^{o}_{Glu} - 4.303H^{o}_{Biomass} - 0.710H^{o}_{CO_2} - 1.054H^{o}_{H_2O}\right) \\ & + Cp_A\left(T - T_{Ref}\right) + 0.602Cp_{Glu}\left(T - T_{Ref}\right) - 4.303Cp_{Biomass}\left(T - T_{Ref}\right) \\ & - 0.710Cp_{CO_2}\left(T - T_{Ref}\right) - 1.054Cp_{H_2O}\left(T - T_{Ref}\right)\end{aligned} \tag{4.49}$$

4.3 The Model Assumptions

The following assumptions were made during the derivation of the model equation.

- The reactor is well mixed and therefore longitudinal variations in the concentration of chemical species are neglected.
- The change of kinetic energy and potential energy are negligible.
- The bacteria dried weight and nutrient concentrations are very low compared to the amount of water in the reactor, therefore the intrinsic

properties of the culture (e.g. Cp, k, ρ, μ) are taken to be that of water.

- The radiating bodies are considered as diffuse gray bodies. Their irradiative properties do not depend on the wavelength or angle of radiation, but only on temperature.
- The reactor medium and ground surface are opaque – emissivity is equal to absorptivity.
- Part of the radiation that hits the surface of the reactor is transmitted and absorbed by the medium in the reactor while the remaining fraction is reflected.
- The gas evolved during the experiment is an ideal gas.

4.4 The Model Algorithm

The algorithm used to develop the thermal model is shown in Figure 4.3. The input data to the model included the dimensions of the reactor and the cooling tube (tube length and radius), the latitude of the reactor, day of the year and the changes in global solar radiation, temperatures (the reactor surface, the ground, the ambient air and cooling water inlet and outlet) after every 10 min. In addition to those, the concentrations of biomass, acetic acid and glutamate and the amount of hydrogen produced were input as data every half an hour. These data were used to calculate the energy contributions of radiative heat transfer, convective heat transfer, pump work and metabolic activities of the bacteria. The contributions were added or subtracted and the outcome divided by the product of the total mass of the medium in the reactor and its heat capacity. The inlet temperature of the reactor that was measured at the beginning of the experiment was assigned as the initial condition $\left(T_r\big|_{t=0}\right)$. The algorithm presented in Figure 4.3 was applied to each reactor operated next to each other. The constants used in the model were listed in Table 4.1. For the reactors operated without bacteria, the metabolic heat was excluded in the thermal balance, thus resulting in Equation 4.50. The fluid temperature (T_r) was predicted from the model using MATLAB (MathWorks, Inc.) software that applied a 60 second fixed step ode1 (Euler) solver.

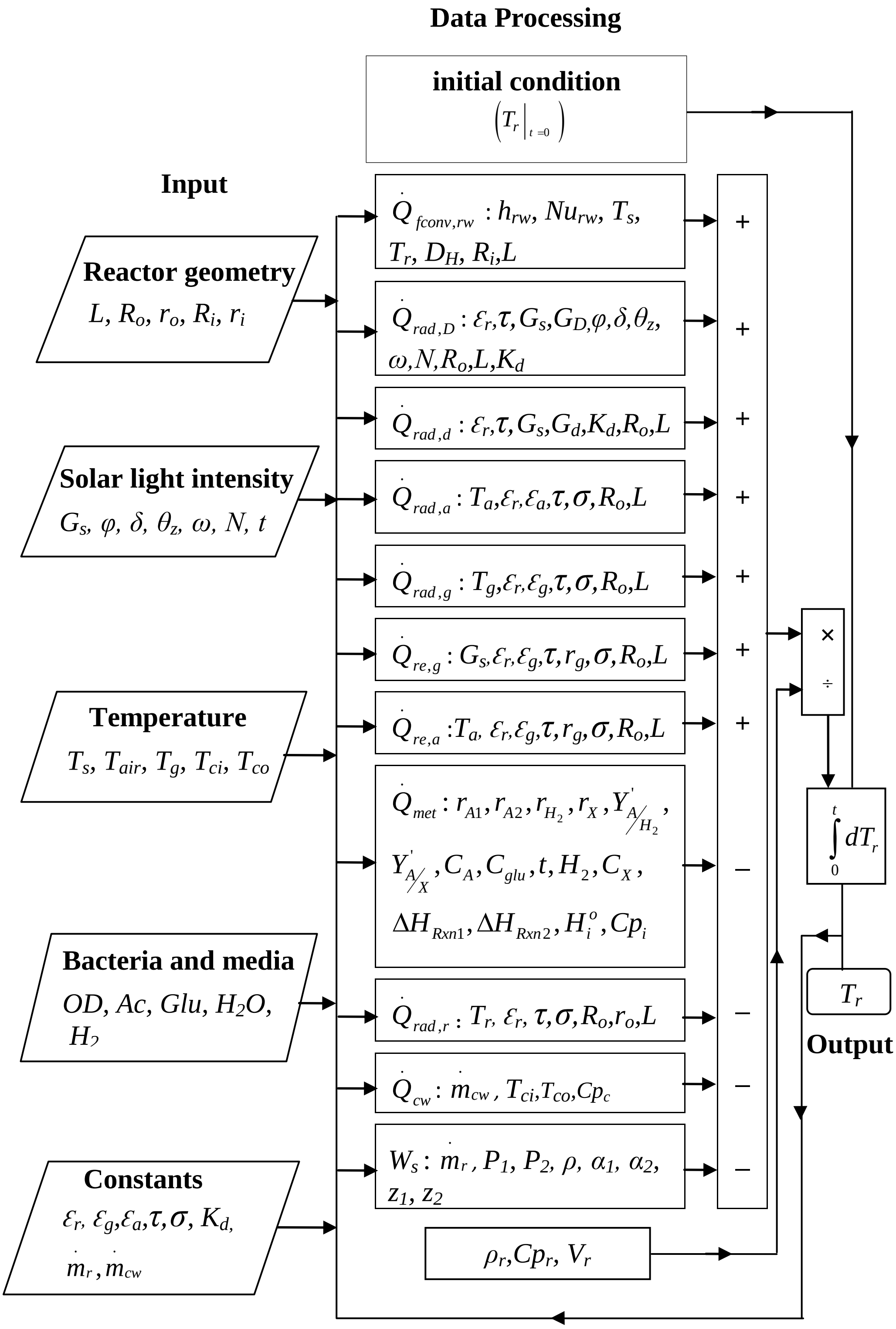
Data Processing
initial condition
$\left(T_r\big|_{t=0}\right)$
Input
Reactor geometry
L, R_o, r_o, R_i, r_i
Solar light intensity
$G_s, \varphi, \delta, \theta_z, \omega, N, t$
Temperature
$T_s, T_{air}, T_g, T_{ci}, T_{co}$
Bacteria and media
OD, Ac, Glu, H_2O, H_2
Constants
$\varepsilon_r, \varepsilon_g, \varepsilon_a, \tau, \sigma, K_d, \dot{m}_r, \dot{m}_{cw}$
$\dot{Q}_{fconv,rw}: h_{rw}, Nu_{rw}, T_s, T_r, D_H, R_i, L$
$\dot{Q}_{rad,D}: \varepsilon_r, \tau, G_s, G_D, \varphi, \delta, \theta_z, \omega, N, R_o, L, K_d$
$\dot{Q}_{rad,d}: \varepsilon_r, \tau, G_s, G_d, K_d, R_o, L$
$\dot{Q}_{rad,a}: T_a, \varepsilon_r, \varepsilon_a, \tau, \sigma, R_o, L$
$\dot{Q}_{rad,g}: T_g, \varepsilon_r, \varepsilon_g, \tau, \sigma, R_o, L$
$\dot{Q}_{re,g}: G_s, \varepsilon_r, \varepsilon_g, \tau, r_g, \sigma, R_o, L$
$\dot{Q}_{re,a}: T_a, \varepsilon_r, \varepsilon_g, \tau, r_g, \sigma, R_o, L$
$\dot{Q}_{met}: r_{A1}, r_{A2}, r_{H_2}, r_X, Y'_{A/H_2}, Y'_{A/X}, C_A, C_{glu}, t, H_2, C_X, \Delta H_{Rxn1}, \Delta H_{Rxn2}, H_i^o, Cp_i$
$\dot{Q}_{rad,r}: T_r, \varepsilon_r, \tau, \sigma, R_o, r_o, L$
$\dot{Q}_{cw}: \dot{m}_{cw}, T_{ci}, T_{co}, Cp_c$
$W_s: \dot{m}_r, P_1, P_2, \rho, \alpha_1, \alpha_2, z_1, z_2$
+
+
+
+
+
+
+
−
−
−
−
ρ_r, Cp_r, V_r
×
÷
$\int_0^t dT_r$
T_r
Output

Figure 4.3 Solution algorithm of the thermal model.

Table 4.1 Constants used in developing the transient thermal model.

Symbol	**Parameter**	**Value**
α_1 and α_1	kinetic correction factors	2.0
ε_a	emissivity of air	1.0
ε_r	emissivity of the reactor medium	0.97
ε_g	emissivity of the ground	0.90
σ	Stefan-Boltzman constant	5.67×10^{-8} W/m/K^4
φ	Latitude	39° 55’ 38 N
Nu_{ii}	coefficients for forced convection in annular tube with uniform flux at both surfaces (Lunderberg *et al.* (1963)	7.95
Nu_{oo}		4.88
θ_i^*		0.82
θ_o^*		0.13
τ	transmissivity of the reactor glass wall	0.92
K_d	fraction of diffuse radiation reaching the ground	0.18
m	maintenance coefficient of the bacteria	0.05 h^{-1}
$\dot{m}_{cw}$	mass flow rate of the cooling water	$3.0 - 5.0\times10^{-3}$ kg/s
$\dot{m}_r$	reactor medium mass flow rate	3.5×10^{-3} kg/s
P_1	pressure at the inlet of the pump	0.05 bars
P_2	pressure at the outlet of the pump	0.26 bars
R_o	outer radius of the reactor tube	0.03 m
R_i	inner radius of the reactor tube	0.027 m
R_{ct}	outer radius of the cooling tube	0.007 m
u_1	velocity at the inlet of the pump	0.015 m/s
u_2	velocity at the outlet of the pump	0.031 m/s
V_r	volume of the reactor	0.0032 m^3

$$\dot{Q}_{rad} + \dot{Q}_{conv} - \dot{Q}_{cw} + W_s = \rho_r V_r Cp_r \frac{dT}{dt} \tag{4.50}$$

4.5 Heat Transfer at the Auxilliary Section of the Reactor System

The reactor system can be divided into two parts, the U-tube section where the cooling coil is inserted and the auxiliary part, which includes the gas-liquid separator (reservoir), the connecting pipes between the inlet and outlet of the reactors and the circulation pump (Figure 4.4).

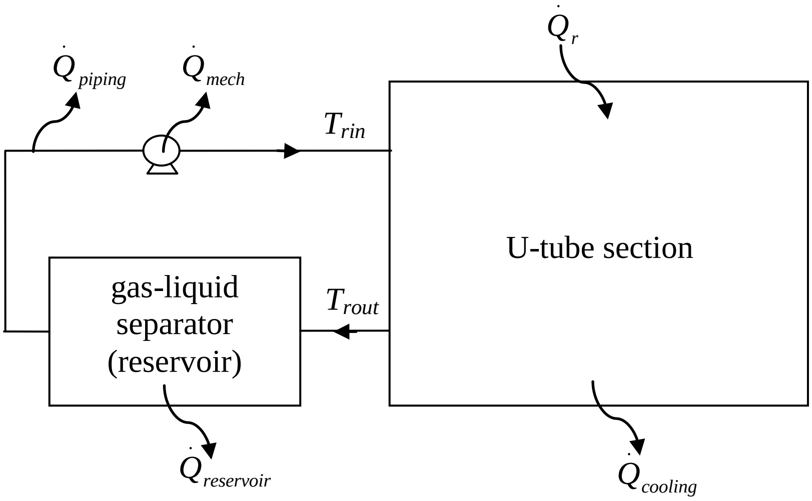
$\dot{Q}_r$
$\dot{Q}_{piping}$
$\dot{Q}_{mech}$
T_{rin}
U-tube section
gas-liquid separator (reservoir)
T_{rout}
$\dot{Q}_{reservoir}$
$\dot{Q}_{cooling}$

Figure 4.4 A schematic of the heat transfer in the reactor system.

The total amount of heat transferred at the auxiliary was calculated as the sum of heat exchanged at the reservoir ($\dot{Q}_{reservoir}$), connecting pipes ($\dot{Q}_{piping}$) and thermal energy generated by frictional effects of the pump ($\dot{Q}_{pump}$) as shown in Equation (4.51).

$$\dot{Q}_{auxiliary} = \dot{Q}_{reservoir} + \dot{Q}_{piping} + \dot{Q}_{mech} \tag{4.51}$$

4.6 The Overall Heat Transfer Coefficient

The overall heat transfer coefficients that represented the thermal resistance between the cooling water and medium in the reactor (U_{co}) were calculated from the following heat balances.

For the co-current system,

$$\dot{m}_{\mathrm{cw}}\, Cp_{\mathrm{cw}}\left(T_{ci} - T_{co}\right) = U_{co} A_{co} \frac{\left(T_{ri} - T_{ci}\right) - \left(T_{ro} - T_{co}\right)}{\ln\left(\dfrac{T_{ri} - T_{ci}}{T_{ro} - T_{co}}\right)} \tag{4.52}$$

For the counter-current system,

$$\dot{m}_{\mathrm{cw}}\, Cp_{\mathrm{cw}}\left(T_{ci} - T_{co}\right) = U_{co} A_{co} \frac{\left(T_{ri} - T_{co}\right) - \left(T_{ro} - T_{ci}\right)}{\ln\left(\dfrac{T_{ri} - T_{co}}{T_{ro} - T_{ci}}\right)} \tag{4.53}$$

where $\dot{m}_{cw}$ is the mass flow rate of the cooling water (kg/s), Cp_{cw} is the heat capacity (J/kg/K) of the cooling water, T_{ci} are the inlet temperature (°C) of the cooling water and T_{co} is the outlet temperature (°C) of the cooling water.

The total thermal resistance in the reactors was estimated as,

$$R_{\mathrm{total}} = R_{\mathrm{o}} + R_{\mathrm{wall}} + R_{\mathrm{i}} = \frac{1}{h_{co} A_{co}} + \frac{\ln\left(d_o / d_i\right)}{2\pi k_{pvc} L_{ct}} + \frac{1}{h_{ci} A_{ci}} \tag{4.54}$$

where R_o is thermal resistance between the reactor medium and the outer surface of the cooling tube, R_{wall} is thermal resistance of the cooling tube, R_i is thermal resistance between the cooling water and the inner outer surface of the cooling tube, h_{co} is the convective heat transfer coefficient (W/m^2/K) between the medium in the reactor and the outer surface of the cooling tube, A_{co} is the outer surface area of the cooling tube, d_o is the outer diameter (m) of the cooling tube, d_i is the inner diameter (m) of the cooling tube, k_{pvc} is the thermal conductivity of the cooling tube, L_{ct} is the length (m) of the cooling tube, h_{ci} is the convective heat transfer coefficient (W/m^2/K) between the cooling water and the inner surface of the cooling tube and A_{ci} is the inner surface area of the cooling tube.

4.7 Modeling of Growth and Hydrogen Production by *Rhodobacter capsulatus*

The growth of *Rhodobacter capsulatus* YO3 cells in the outdoor operated photobioreactors was modeled using the logistic model (Sevinç *et al.* 2012).

$$X = \frac{X_{\max}}{\left(1+\exp\left(-k_c t\right)\left(\frac{X_{\max}}{X_o-1}\right)\right)} \tag{4.56}$$

where X is the cell concentration (gDCW/L) at time t (h), X_o is the initial cell concentration (gDCW/L), k_c is the apparent specific growth rate (1/h) and X_{max} is the maximum cell concentration (gDCW/L).

The cumulative hydrogen production in the reactors was modeled using the modified Gompertz model (Sevinç *et al.* 2012).

$$H = H_{\max}\exp\left[-\exp\left(\frac{R_{\max}}{H_{\max}}e\left(\lambda-t\right)+1\right)\right] \tag{4.57}$$

where H is the hydrogen cumulative hydrogen (mmol/L) produced at time t (h), H_{max} is the maximum cumulative hydrogen (mmol/L), R_{max} is the maximum hydrogen production rate (mol/L$^/$h), e is the euler number (2.718) and λ is the lag time (h).

The constants in Equations (4.56 and 4.57) were determined using the curve fitting tool in the Matlab (MathWorks Inc.)program.

CHAPTER 5

OPTIMIZATION OF TEMPERATURE AND LIGHT INTENSITY FOR IMPROVED PHOTOFERMENTATIVE HYDROGEN PRODUCTION

A 3^2 general full factorial DOE was implemented to optimize temperature and light intensity for maximum hydrogen production by batch cultures of *R. capsulatus* DSM1710. Regression models that related hydrogen production rate (R_{H2}) and hydrogen yield (Y_{H2}) to temperature (20, 30, 38°C) and light intensity (100, 200, 340 W/m^2) and their interactions were developed. The levels of the experimental design for the complete set of 18 runs are displayed in Table 5.1.

5.1 Hydrogen Production Rate

Equations (5.1) and (5.2) display the coded and uncoded (actual) regression models, obtained using Minitab® 16.0, which relate the rate of hydrogen production by *R. capsulatus* DSM 1710 to temperature and light intensity.

$$\mathrm{y}_{\mathrm{coded}} = -\,1.90 + 0.147x_1 + 3.05\times10^{-3}x_2 - 2.54\times10^{-3}x_1^2 - 4.10\times10^{-6}x_2^2 - 3.00\times10^{-5}x_1x_2 \tag{5.1}$$

$$\mathrm{Y}_{\mathrm{uncoded}} = -\,2.40 + 1.82\times10^{-2}X_1 + 2.67\times10^{-5}X_2 - 3.14\times10^{-5}X_1^2 - 2.93\times10^{-10}X_2^2 - 2.44\times10^{-8}X_1X_2 \tag{5.2}$$

An ANOVA analysis was performed to test the significance of the fit of the second-order polynomial equations to the experimental data. Table 5.2 shows the results of the analysis of variance (ANOVA) for the regression model.

Table 5.1 Experimental design table for the optimization of hydrogen production rate and yield.

Run	Temperature (°C)		Light intensity (W/m^2)		Hydrogen production rate (mmol/L/h)	Hydrogen Yield (mol H_2/mol substrate)
	x_1^a	X_1^b	x_2^a	X_2^b		
1	3	30	2	100	0.430	0.263
2	3	38	1	340	0.220	0.157
3	2	38	1	340	0.260	0.159
4	3	20	3	340	0.400	0.284
5	2	20	3	200	0.360	0.234
6	1	20	2	340	0.440	0.280
7	2	30	1	340	0.500	0.288
8	1	38	3	200	0.300	0.157
9	1	38	1	200	0.340	0.199
10	3	20	2	100	0.270	0.151
11	2	30	2	100	0.440	0.222
12	1	20	3	200	0.380	0.214
13	3	38	3	100	0.140	0.122
14	3	38	1	100	0.210	0.100
15	1	30	2	200	0.470	0.302
16	1	30	1	340	0.610	0.283
17	2	30	2	200	0.510	0.312
18	2	20	3	100	0.230	0.180

[a] coded factor values and [b] uncoded (actual) factor values.

The F-value of 27.1 obtained for this analysis indicated that the model was significant, with a p<0.01%. The p-values are a measure of the statistical significance of each variable; low p-values correspond to a high statistical significance of the variables within the model (Liu *et al.* 2003). In the present work, p-values less than 0.05 were accepted to be significant.

Table 5.2. ANOVA for the rate of hydrogen production by *Rhodobacter capsulatus* DSM1710.

Factors	Sum of Squares	DF	Mean Square	F-value	p-value
Model	0.244	5	0.049	**27.1**	<0.0001
X_1	0.0230	1	0.159	88.1	<0.0001
X_2	0.0390	1	0.026	14.2	0.00300
X_1^2	0.164	1	0.164	91.3	<0.0001
X_2^2	0.0120	1	0.012	6.90	0.0220
X_1X_2	0.00600	1	0.006	3.42	0.0890
Residual Error	0.0220	12	0.002		
Lack-of-Fit	0.00900	3	0.003	**2.09**	0.172
Pure Error	0.0130	9	0.001		
Total	0.266	17			

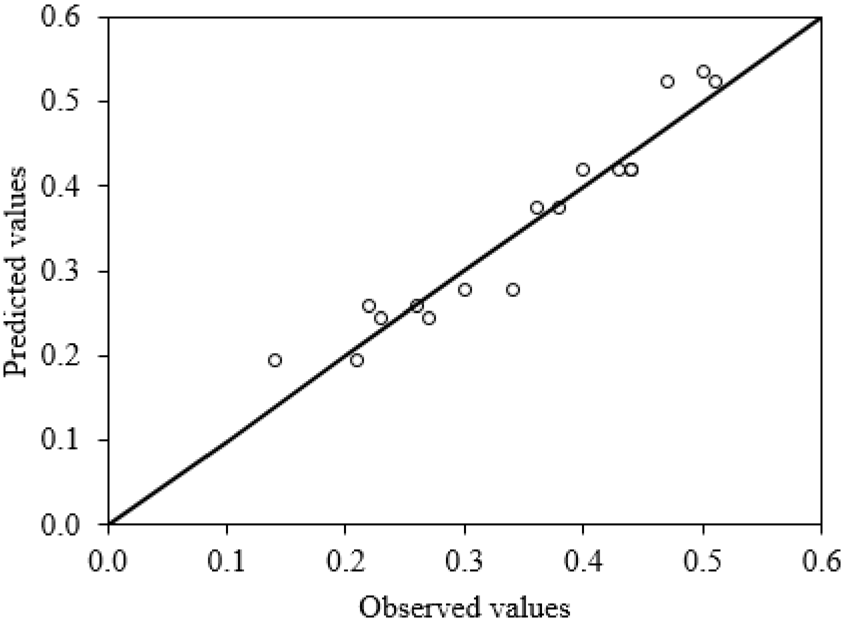

Figure 5.1 Correlation between the predicted and observed values for hydrogen production rate using batch cultures of *Rhodobacter capsulatus* DSM1710.

The lack-of-fit F-value compares the variance caused by the discrepancy of the model with the data, to variance due to random (or pure) error. If this lack-of-fit F-value is significant, it means that the model does not fit the data well. The lack-of-fit of F-value calculated was 2.09, which corresponds to a p-value of 0.172. This indicates that the lack-of-fit is not significant, confirming that the model fits the experimental hydrogen production data well. The linear (X_1 and X_2) and quadratic (X_1^2 and X_2^2) effects of temperature and light intensity on the model were found to be significant ($p<0.005$), while the interaction effects (X_1X_2) were insignificant as p value was 0.089 ($p>0.005$). The measure of the goodness of fit (R^2, 0.919) was close to 1, showing a good agreement between predicted and observed values (Figure 5.1). In other words, the model could be used to describe the effects of temperature and light intensity on the rate of hydrogen production. The value of adequate precision, which measures the ratio of signal to noise, was calculated as 34; values greater than 4 imply a good precision. Also, a low coefficient of variance (11.7%) was found, which demonstrates a good reliability of the experimental variables.

Figure 5.2 shows the three-dimensional response surface and contour plot for the rate of hydrogen production as a function of temperature and light intensity, as formulated by Equation (5.2). The response surface plot graphically represents the regression equation and can be used to predict the response for different values of the test variables. On the other hand, a contour plot generally helps to identify the type of interactions between the variables. A circular contour of response surface indicates that the interaction between the corresponding variables is negligible, while an elliptical one indicates that the interactions between the corresponding variables are significant (Muralidhar *et al.* 2001). From the response surface plot (Figure 5.2A), R_{H2} can be observed to increase as temperature and light intensity increase, until a peak, after which it decreases even when temperature and light intensity continue to increase.

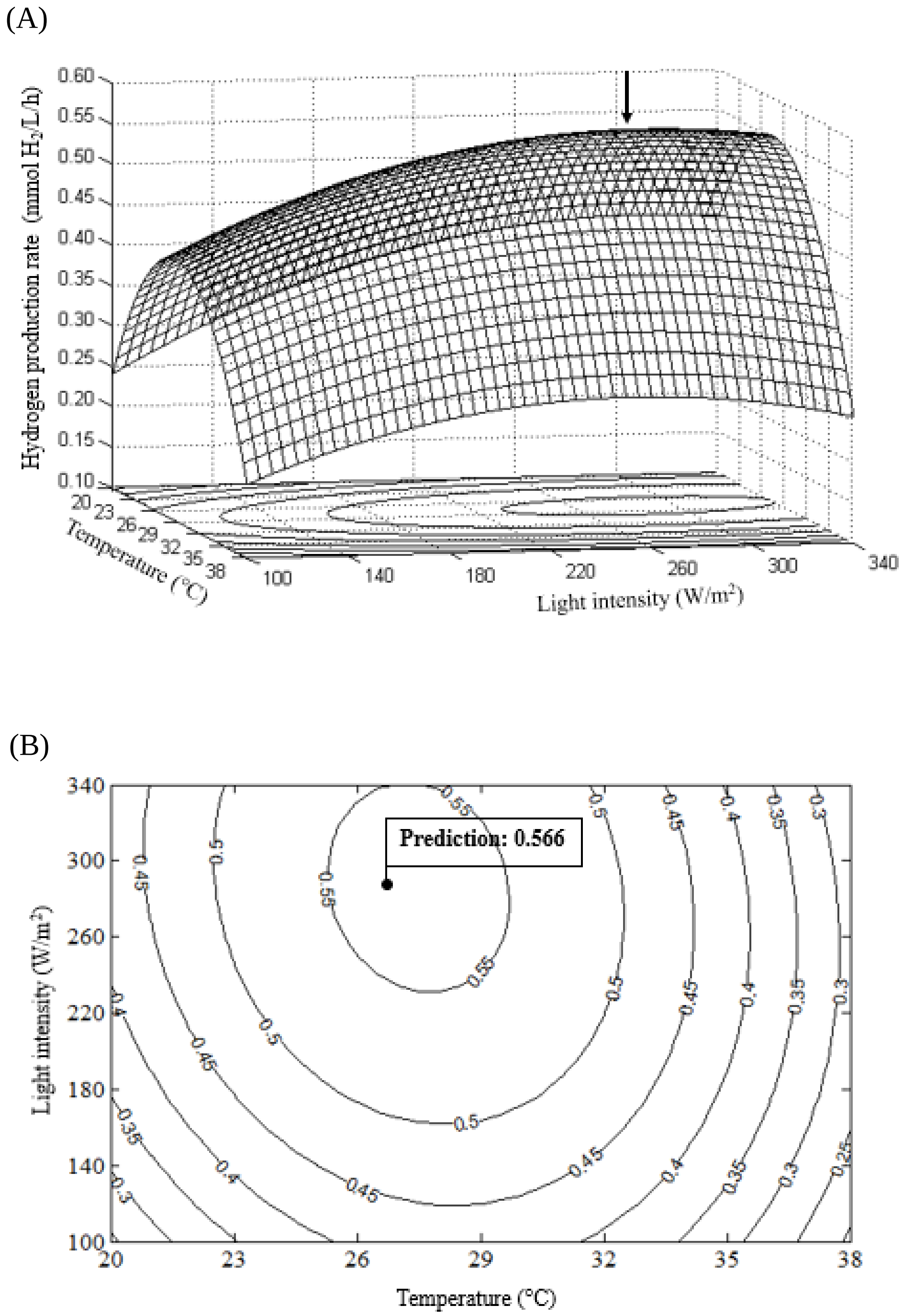

Figure 5.2 Plots for the hydrogen production rate model using batch cultures of *Rhodobacter capsulatus* DSM1710. (A) Three-dimensional response surface plot and (B) Two-dimensional contour plot. The arrow on the response surface plot indicates the position of the maximum hydrogen production rate.

At a low temperature (20°C), R_{H2} slightly increases with increasing light intensity, mostly remaining below 0.25 mol/m^3/h. The highest R_{H2} values were observed approximately at 27°C and 280 W/m^2. The surface plot in Figure 5.2A also reveals that the R_{H2} response was more sensitive to temperature change than to light intensity as it exhibited a steeper slope on the temperature axis compared to the light intensity axis. In Figure 5.2B the contour plots are circular in nature, implying that interactive effects are negligible.

The non-linear regression Equation (5.2) was solved using Mathcad 15 and a maximum R_{H2} of 0.566 mol/m^3/h was determined at 27.5°C and 286 W/m^2 (Figure 5.2B). To test the validity of the predicted maximum, experiments were conducted in duplicate under the determined optimum conditions, 27.5°C and 286 W/m^2, resulting in a maximum hydrogen production rate of 0.56±0.1 mol/m^3/h, thus confirming the estimates.

5.2 Hydrogen Yield

Shown in Equations (5.3) and (5.4) are the coded and uncoded (actual) regressions obtained (using Minitab® 16.0) when relating hydrogen yield (Y_{H2}) to temperature and light intensity.

$$y_{\text{coded}} = -0.888 + 7.01\times10^{-2}x_1 + 1.93\times10^{-3}x_2 - 1.22\times10^{-3}x_1^2 - 2.56\times10^{-6}x_2^2 - 1.77\times10^{-5}x_1x_2 \tag{5.3}$$

$$Y_{\text{uncoded}} = -1.13 + 8.66\times10^{-3}X_1 + 1.66\times10^{-5}X_2 - 1.50\times10^{-5}X_1^2 - 1.78\times10^{-10}X_2^2 - 1.64\times10^{-8}X_1X_2 \tag{5.4}$$

The results of the ANOVA for the regression model are shown in Table 5.3. The model was found to be significant (F-value 34.7, $p<0.005$). The lack-of-fit F-value (0.130) is not significant relative to pure error, indicating that the model fits the hydrogen yield data well. All variables and their interactions were found to be significant ($p<0.005$). Further, the high value of goodness of fit (R^2, 0.935) and the adequate precision of 37 showed that the model could correctly estimate the effects of temperature and light intensity on hydrogen yield. This was confirmed by the good agreement between predicted and observed values (Figure 5.3). Moreover, a low coefficient of variance (9.39%) further illustrates that there was little extent in variability, and thus good reliability of the experimental variables.

Table 5.3 ANOVA for hydrogen yield by *Rhodobacter capsulatus* DSM1710.

Factors	Sums of squares	DF	Mean squares	F-value	p-value
Model	0.0722	5	0.0144	**34.7**	<0.0001
X_1	0.0138	1	0.0361	86.6	<0.0001
X_2	0.0127	1	0.0106	25.3	<0.0001
X_1^2	0.0377	1	0.0377	90.4	<0.0001
X_2^2	0.00509	1	0.00509	12.2	0.0004
X_1 X_2	0.00295	1	0.00295	7.09	0.021
Residual error	0.00500	12	0.000417		
Lack of fit	0.00225	3	0.000749	**2.45**	0.13
Pure error	0.00275	9	0.000306		
Total	0.0772	17			

Figure 5.4 illustrates the response surface and contour plots of Equation (5.4). An optimum point was found to exist within the design boundary (Figure 5.4A). The hydrogen yield exhibits a peak within the ranges of 25 – 28°C and 260 – 320 W/m^2 (Figure 5.4B). Temperature and light intensity values beyond the higher end of these ranges result in decreased yields. At lower temperatures (20°C), the hydrogen yield was observed to increase from 0.14 to 0.26 mol H_2/mol substrate (acetate and lactate mixture) while light intensity increased from 100 to 250 W/m^2.

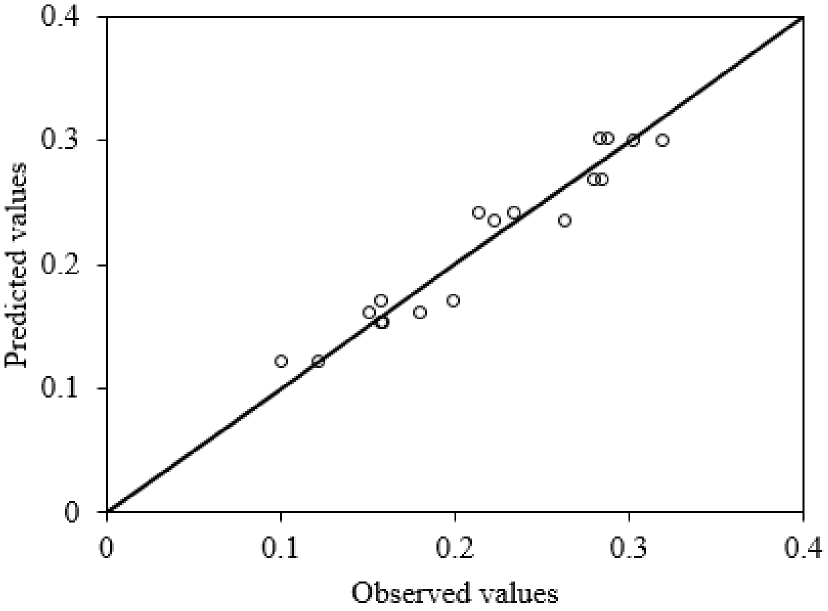

Figure 5.3 Correlation between the predicted and observed values of hydrogen yield (mol H_2/mol substrate) using batch cultures of *Rhodobacter capsulatus* DSM1710.

Similar to the hydrogen production rate, the highest hydrogen yield was observed around 27°C and under high light intensities (about 280 W/m^2) (Figure 5.4B). Hydrogen yield is on the whole more sensitive to temperature changes than light intensity and interactions between variables are significant as implied by the elliptical contour and non-planar surface plots (Figure 5.4). Solving the non-linear Equation (5.4) with Mathcad 15, a maximum hydrogen yield of 0.326 mol H_2/mol substrate was estimated at 26.7°C and 285 W/m^2. Validation of the experiments at the optimum conditions resulted in an average hydrogen yield of 0.32±0.3 mol H_2/mol substrate.

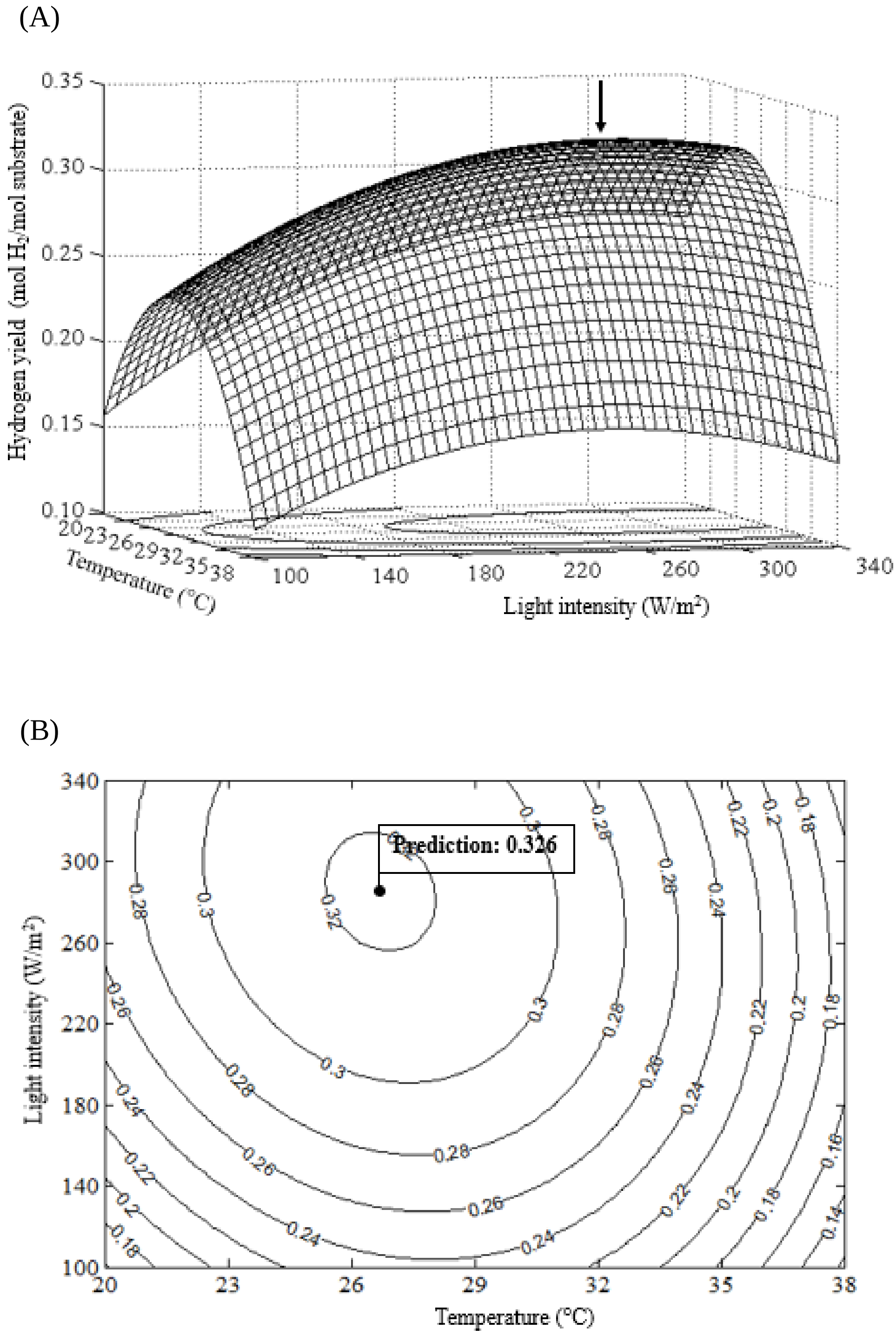

Figure 5.4 Effects of temperature and light intensity on hydrogen yield for batch cultures of *Rhodobacter capsulatus* DSM1710. (A) Three dimensional response surface plot and (B) Two dimensional contour plot. The arrow on the response surface plot indicates the position of the maximum yield.

5.3 Discussion

The hydrogen production rate and yield were found to be dependent on changes in temperature and light intensity. At fixed light intensities, hydrogen production rates and yields were seen to increase with increasing temperatures, reaching a maximum after which they decrease (Figure 5.2A and 5.4A). From the locus of the maxima, the global maximum of the light intensity-temperature surface was found to be 27 °C. This agrees, within experimental variation, with findings from previous literature which report an optimum around 30 °C (Özgür *et al.* 2010, Androga *et al.* 2011b, Sevinç *et al.* 2012).

The existence of such optima can be interpreted with respect to competing effects in the cellular metabolism. For temperatures below 30 °C, increasing the temperature is likely to enhance hydrogen production, while for temperatures above 30 °C, reversible inactivation of enzymes and heat stress effects can be expected to adversely affect hydrogen production (Muazzez, 2011). For bacterial cells in general, it is hypothesized that a decrease in temperature results in a reduction of the cell membrane fluidity and of protein folding efficiency, therefore hindering ribosome functions as well as transcription and translation (Phadtare, 2004). This, in turn, negatively affects cell growth and hydrogen production. Elevated temperatures, on the other hand endanger, the viability of the microorganism by denaturing cellular proteins. Heat shock proteins (Hsp) such as proteases and chaperones are induced to reduce the concentration of the damaged proteins (Ron, 2006). Thus the bacteria may cease producing hydrogen as they prioritize metabolic activities for survival instead. Furthermore, the optimum temperature for nitrogenase, which is the primary enzyme catalyzing hydrogen production, has been reported as 30 °C (Jouanneau *et al.* 1985), with temperatures above or below resulting in lower activities, leading to less hydrogen production.

Light is required by the PNSB for growth and hydrogen production. Similar to the temperature response at fixed temperatures, hydrogen production rates and yields were found to increase with increasing light intensities until a threshold as shown in Figures 5.2A and 5.4A. This could be attributed to the fact that light intensity controls the synthesis of the photosynthetic apparatus, which is responsible for converting light energy to ATP. Under low light intensities, the incident light energy is insufficient to meet the high ATP demand of nitrogenase for hydrogen production. At high light intensities on the other hand, the saturation of the photosynthetic apparatus prevents further gains in hydrogen production (Shi and Yu, 2005), and even stronger intensities may start to decrease the hydrogen production efficiency due to adverse effects such as self-shading that results from increased biomass concentrations. The slight decrease in the hydrogen production rates and yields at high light intensities range in Figures 5.2 and 5.4 can be attributed to such effects.

In this study, optimum light intensities of 285 W/m^2 (4220 lx) and 287 W/m^2 (4250 lx) were obtained for a maximum R_{H2} (0.566 mol/m^3/h and Y_{H2} (0.326 mol H_2/mol substrate). These intensities are in agreement with the reported optimal range of 4000 – 6000 lx in other studies (Shi and Yu, 2005, Castillo *et al.* 2012).

CHAPTER 6

COMPUTATIONAL FLUID DYNAMICS MODELING OF FLOW IN TUBULAR BIOREACTORS

A fundamental problem in bioreactor design is the achievement of uniform flow distribution. Uniform flow distribution in the reactor allows proper mixing of minerals and nutrients, dispersal of cells, good light distribution and easy separation of the evolved gas. In order to obtain optimal flow, proper consideration should be given to the behavior of flow according to the geometry and flow rates. Photobioreactors of different sizes and geometries are used for photofermentative hydrogen production (Dasgupta *et al.* 2010). In this section, Computational Fluid Dynamics (CFD) modeling was used to investigate flow in tubular reactors. The velocity distribution and pressure drop of single phase flow in tubular reactors operating at steady state conditions were modeled using the COMSOL 4.3 program. The following tubular reactors were studied.

i. U-tube modular reactor
ii. Serpentine reactor
iii. Manifold type reactor with single inlet and single outlet
iv. Manifold type reactor with multiple inlets and single outlet

The geometries of the reactors are described in Table 6.1.

Table 6.1 Geometry of the tubular reactors.

Photobioreactor	Property
U-tube modular reactor	
Diameter	0.0272 m
Length	4.0 m
Volume	2.2 L
Serpentine reactor	
Diameter	0.0272 m
Length	52 m
Volume	30 L
Manifold type reactor	
Header	
Diameter	0.10 m
Length	0.90 m
Volume	25 L
Footer	
Diameter	0.05 m
Length	0.90 m
Volume	2.75 L
Tubing	
Diameter	0.06 m
Length	2.4 m
No. of tubes	9
Inlet diameter	0.030 m
Outlet diameter	0.035 m
Total reactor volume	90 L

6.1 Meshing

The reactor geometries were meshed using tetrahedrals. The mesh element quality is an important aspect to consider when validating a model. It measures the regularity of the mesh elements' shapes. Low mesh qualities can result in inaccurate results and usually range between 0 and 1.0, where 0 represents a degenerated element and 1.0 a completely symmetric element. The average quality of elements in this study ranged between 0.6 and 0.9, therefore were reasonable.

Table 6.2 The number and quality of elements used in meshing the tubular reactors.

Tubular Photobioreactor	**No. of elements**	**Average element quality**
U-tube modular (2.2 L)	136519	0.6
Serpentine (30 L)	886102	0.6
Manifold reactor with single inlet and single outlet (90 L)	275244	0.8
Manifold type reactor with multiple inlets and single outlet (90 L)	115427	0.7

6.2 Velocity Distribution and Pressure Drop in the Tubular Photobioreactors

The velocity distribution and pressure drop in the tubular reactors operating at steady state conditions was modeled using COMSOL 4.3 program. All the reactors were operated at the constant flow rate of 255 mL/min. Figure 6.1 illustrates the velocity profile in the U-tube modular reactor. The flow in the reactor is laminar (Re = 250) and uniform. Generally, in laminar flow, the fluid velocity in a tube changes from zero at the walls (due to friction) to a maximum (V_{max}) at the tube centre. The maximum velocity (0.0124 m/s) was obtained at the centre of the reactor (shown by the red line in the centre of the pipe) and the lowest velocity (shown blue in color) was obtained at the walls of the reactor. The maximum velocity was approximately double the inlet velocity of 0.0073 m/s. For laminar flow of an incompressible fluid in a smooth circular tube with constant cross-sectional area, the maximum velocity occurs at the center and is twice the average velocity (Çengel, 1998). The yellow streamlines visualize the path taken by a particle as it is carried by the flow. The lines were uniformly distributed, suggesting uniform flow in the reactor. To confirm this, the change in velocity along the diameter of each tube was plotted in Figure 6.2. Equal V_{max} values were achieved in the U-tube modular reactor, indicating uniform flow distribution in the reactor.

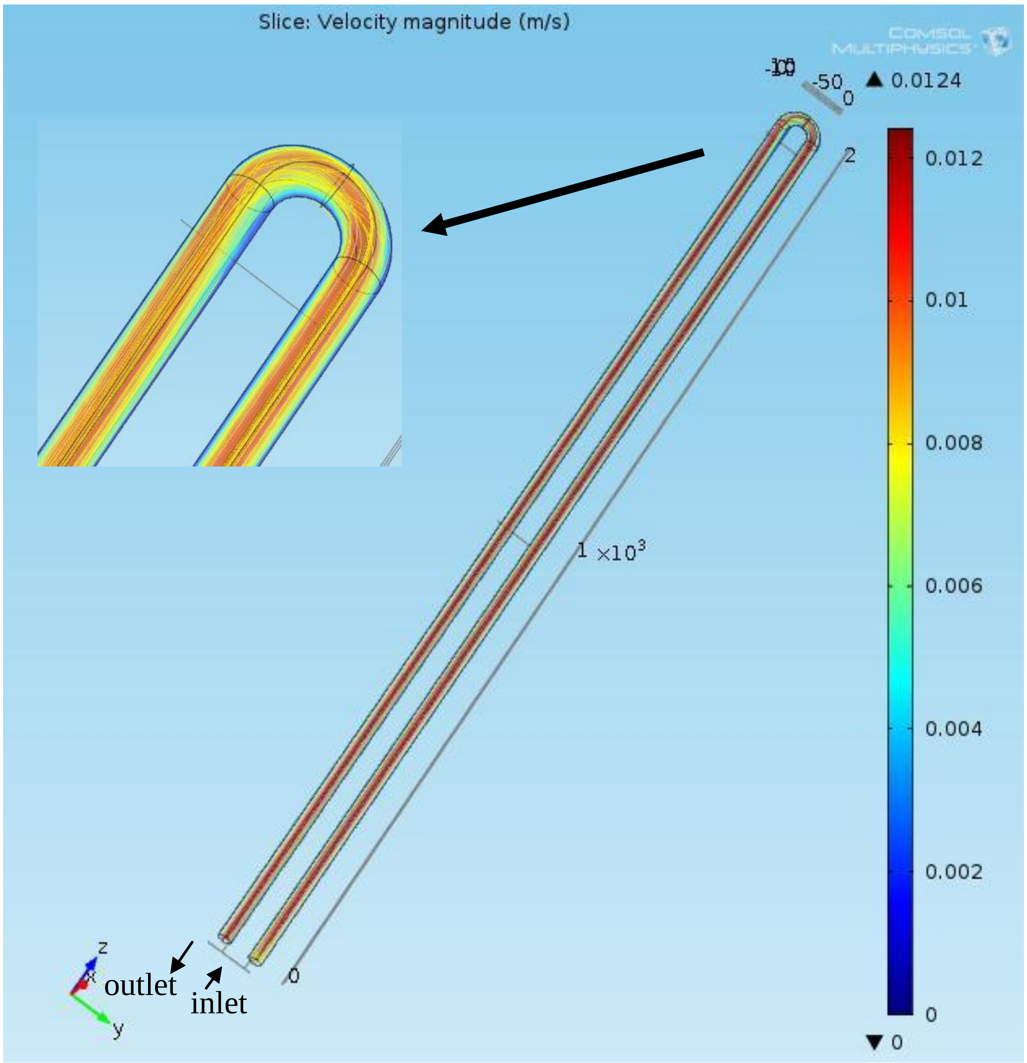
Slice: Velocity magnitude (m/s)
COMSOL MULTIPHYSICS
-100
-50
0
▲ 0.0124
2
0.012
0.01
0.008
0.006
0.004
0.002
0
▼ 0
1 ×10³
0
z
x
y
outlet
inlet

Figure 6.1 The velocity (m/s) distribution in the U-tube modular reactor. The inset shows the yellow streamlines, which are the paths taken by particles as they are carried by the flow.

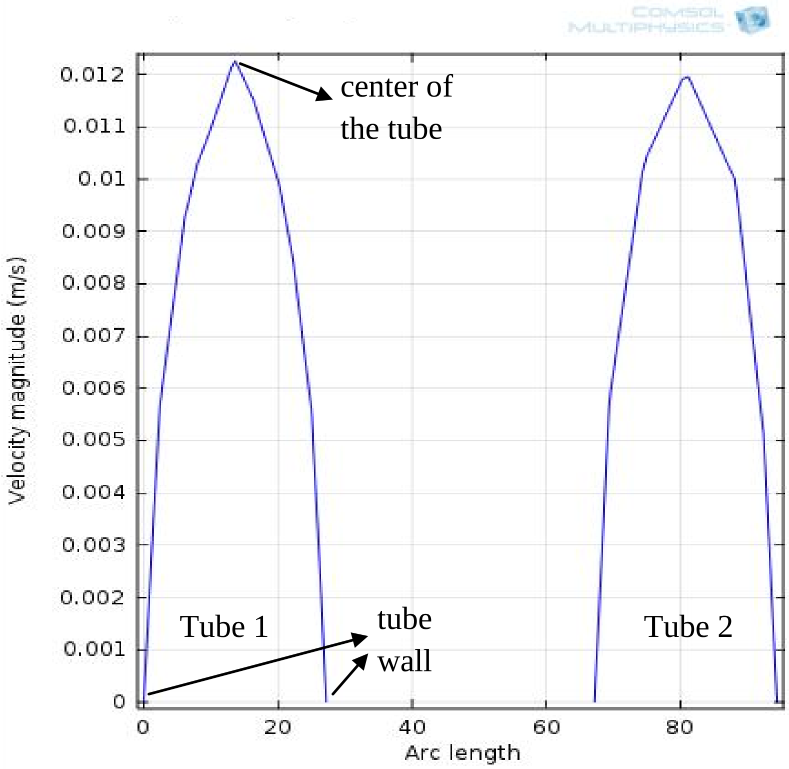

Figure 6.2 The change in velocity across the tube diameters of the U-tube modular reactor. The reactor consists of 2 tubes and the arc length (mm) is the horizontal distance between the tubes.

The change in the pressure inside the U-tube modular reactor is illustrated in Figure 6.3. The pressure at the inlet of the reactor was high (red in color) and decreased towards the outlet as it equalized with the atmospheric pressure (blue in color) (Figure 6.3). A small pressure drop (ΔP) of 1.2 Pa was obtained because of the low volumetric flow rate of 255 mL/min in the reactor. The ΔP obtained was small, < 0.1 % of the atmospheric pressure, hence, negligible.

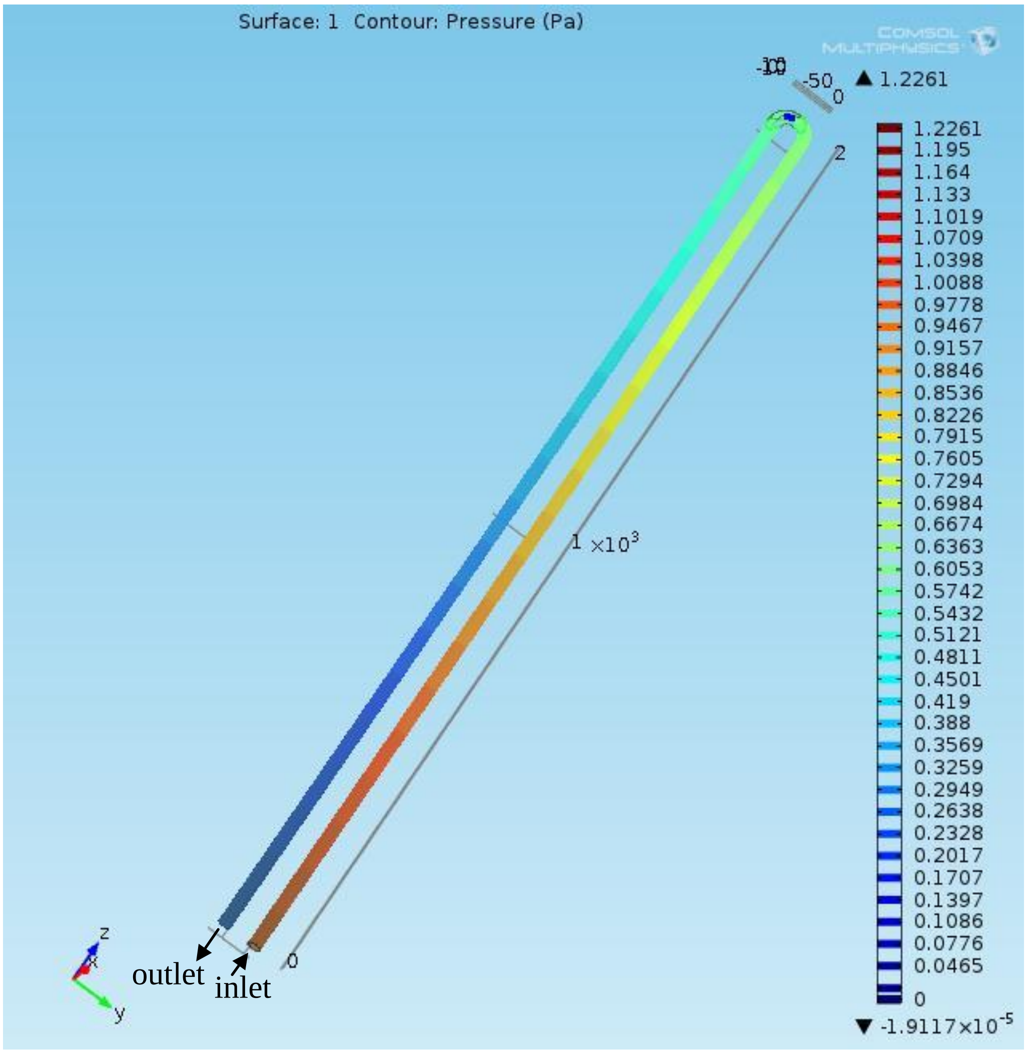

Figure 6.3 Pressure drop (Pa) in the U-tube modular reactor.

The velocity distribution in the serpentine reactor is illustrated in Figure 6.4. Similar to the U-tube modular reactor, maximum velocity of 0.0124 m/s was obtained at the center of the tube and the minimum velocity at the walls of the reactor. Evenly distributed streamlines (shown in Figure 6.4) and matching trends of velocities across the reactor tubes' diameters indicated that the flow in the reactor was uniform – equal V_{max} values were obtained in all the 25 tubes (Figure 6.5).

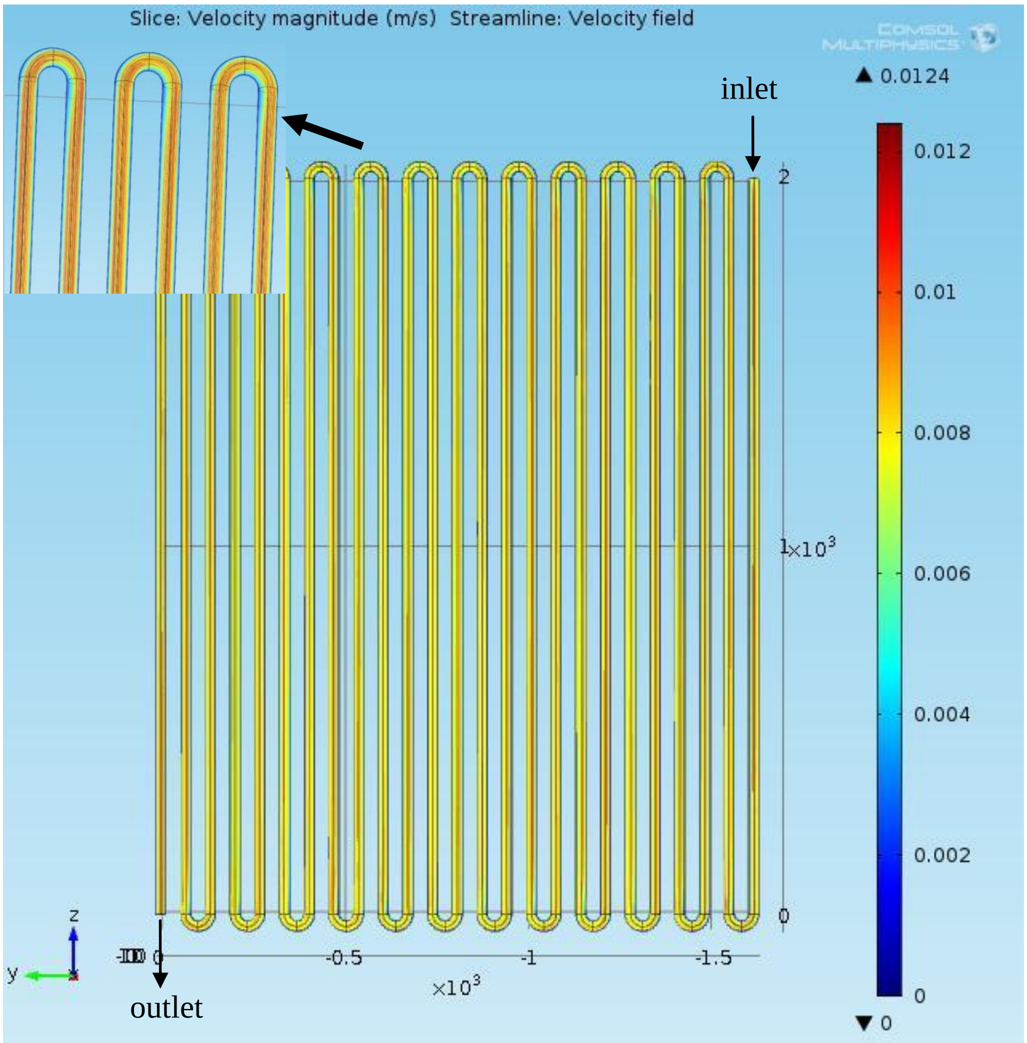

Figure 6.4 The velocity (m/s) distribution in the serpentine reactor. The yellow streamlines in the inset show the path taken by particles as they are carried by the flow.

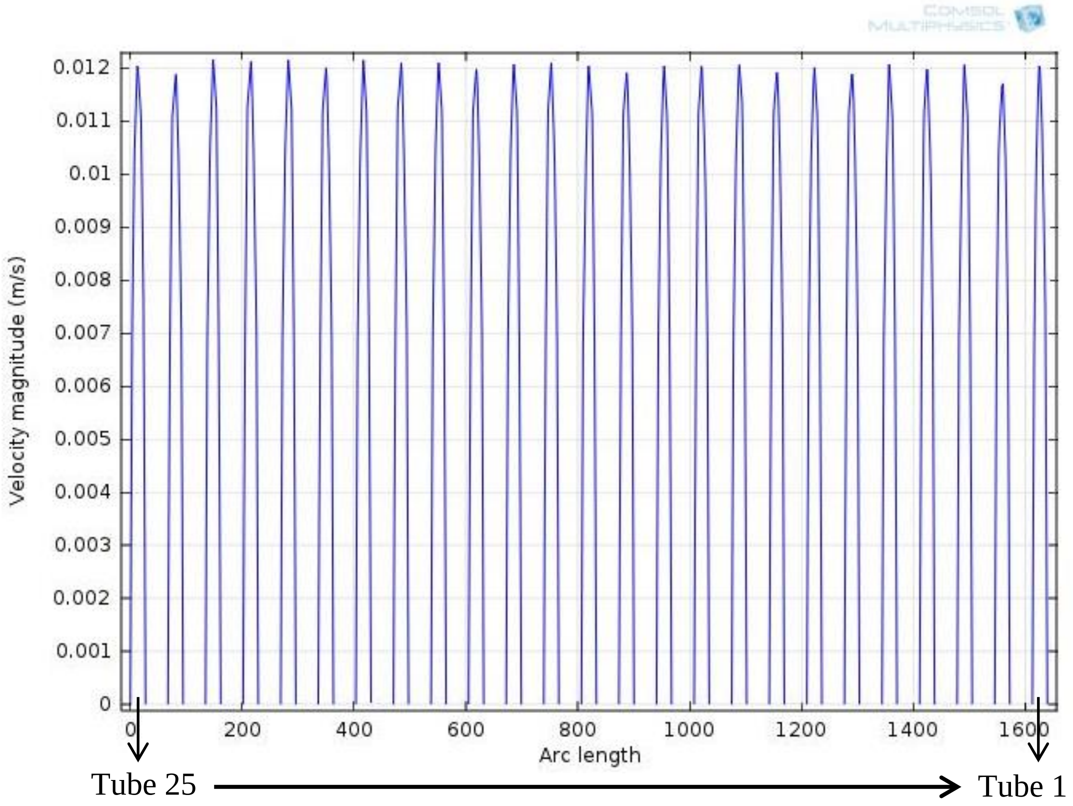

Figure 6.5 The change in velocity across the tube diameters of the serpentine reactor. The reactor consists of 25 tubes and the arc length (mm) is the horizontal distance between the tubes.

The change in the pressure inside the serpentine reactor is shown in Figure 6.6. High pressure at the inlet and low pressure at the outlet was observed – ΔP of about 15.8 Pa was obtained in the reactor. This value was higher than the ΔP in the U-tube modular reactor (ΔP = 1.2) because the fluid flowing in the reactor had to cover a longer distance (52 m) from the inlet to the outlet and overcome more wall resistance in the serpentine reactor compared to the U-tube modular reactor that had a total reactor length of 4 m. The ΔP in the reactors is 0.3 Pa/m.

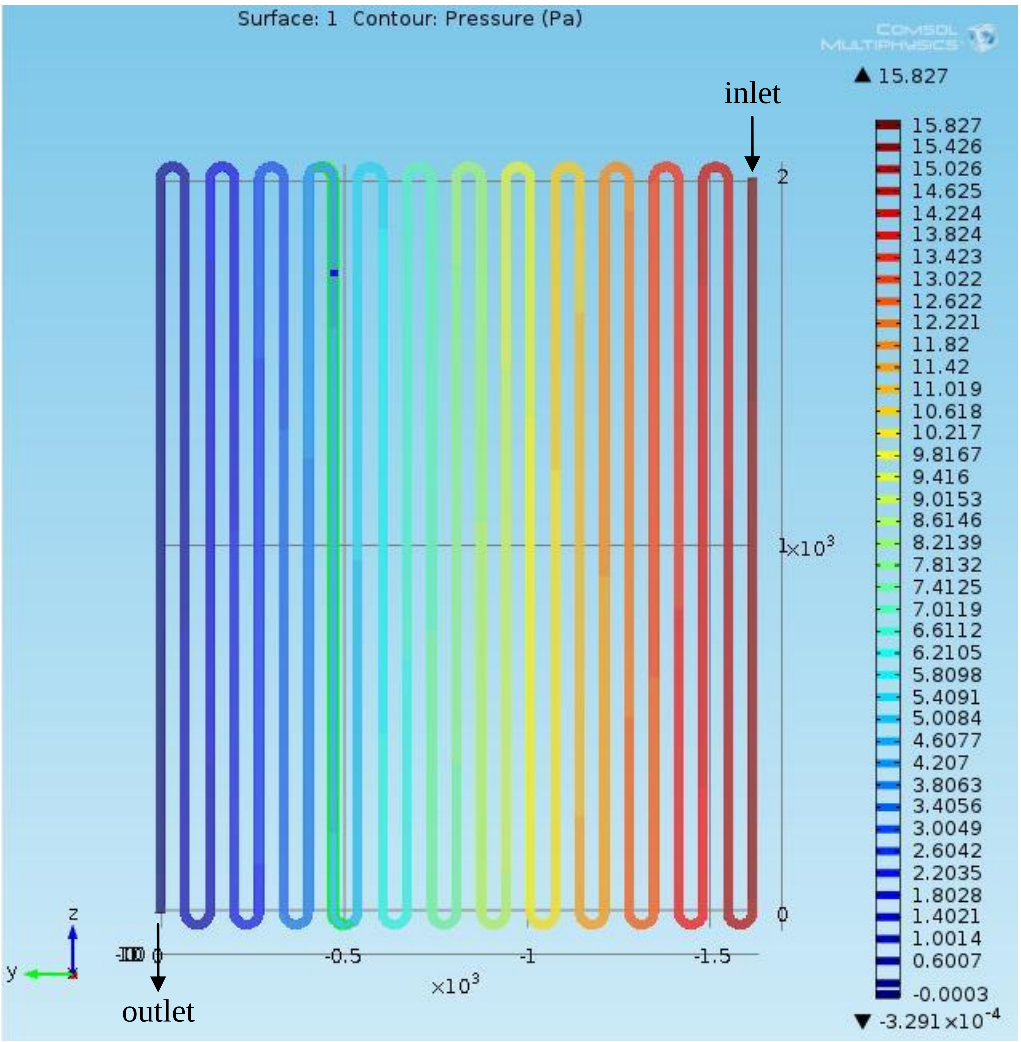

Figure 6.6 Pressure drop in the serpentine reactor.

The flow distribution in the manifold type reactor with a single inlet and a single outlet is shown in Figure 6.7. A maximum velocity of 0.0097 m/s was obtained in the reactor. The yellow streamlines showed that the paths followed by the particles in the reactor system were uneven – more streamlines were observed in the last (9th) tube compared to the other tubes. This indicated more flow rate in this tube and non-uniform flow in the reactor. It also demonstrates the possibilities of channeling, especially at higher flow rates. Figure 6.8 illustrates the change in velocity across each tube diameter in the reactor. Unequal values of V_{max} were

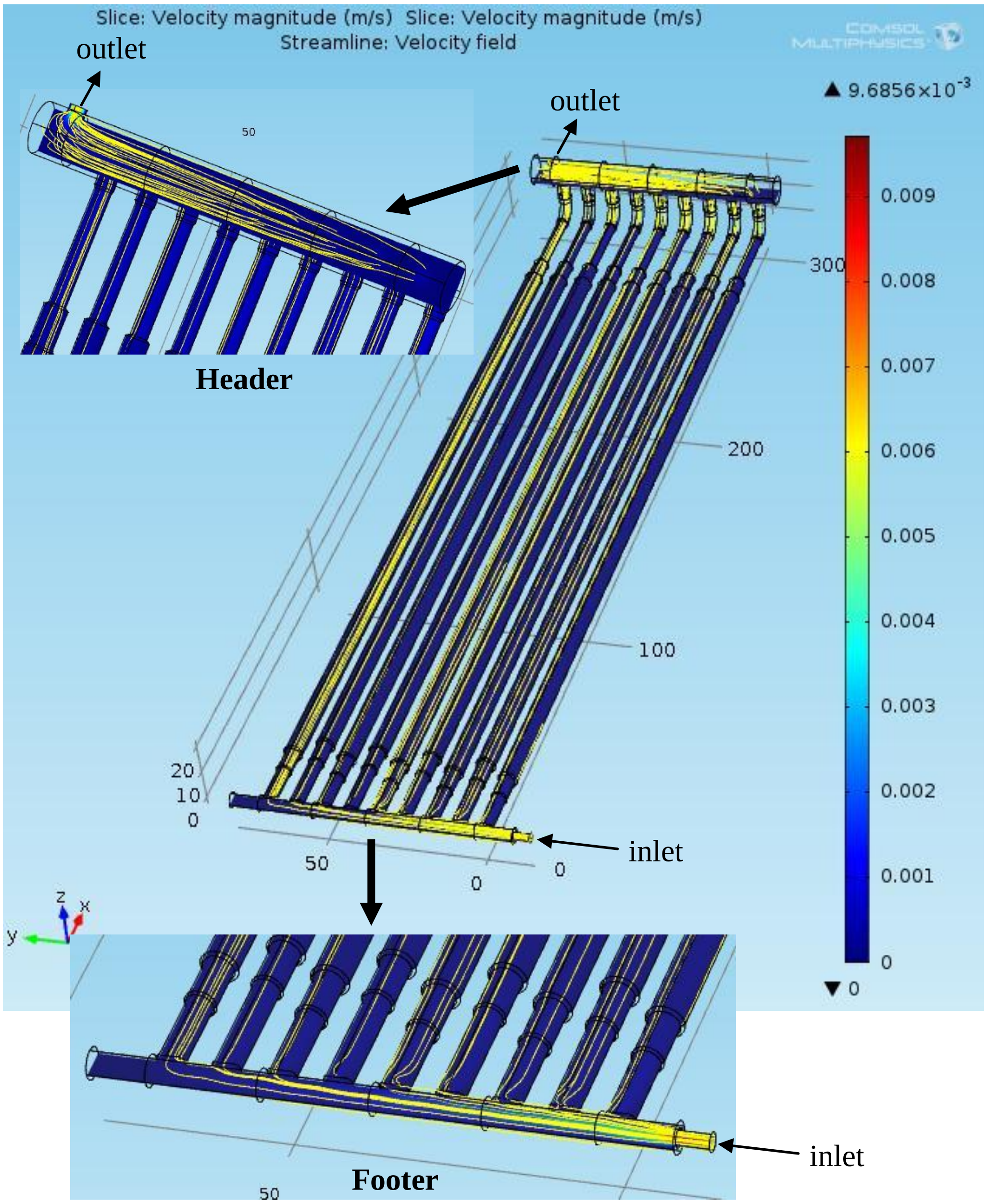

Figure 6.7 The velocity (m/s) distribution in the manifold reactor with a single inlet and a single outlet. The yellow streamlines in the inset show the path taken by a particle as it is carried by the flow.

obtained. V_{max} was about 0.34 $\times 10^{-3}$ m/s in the last tube (9), while it ranged between 0.31 $\times 10^{-3}$ m/s and 0.25 $\times 10^{-3}$ m/s in the remaining tubes (Figure 6.8). This showed that non-uniform flow existed in the manifold type reactor with a single inlet and a single outlet.

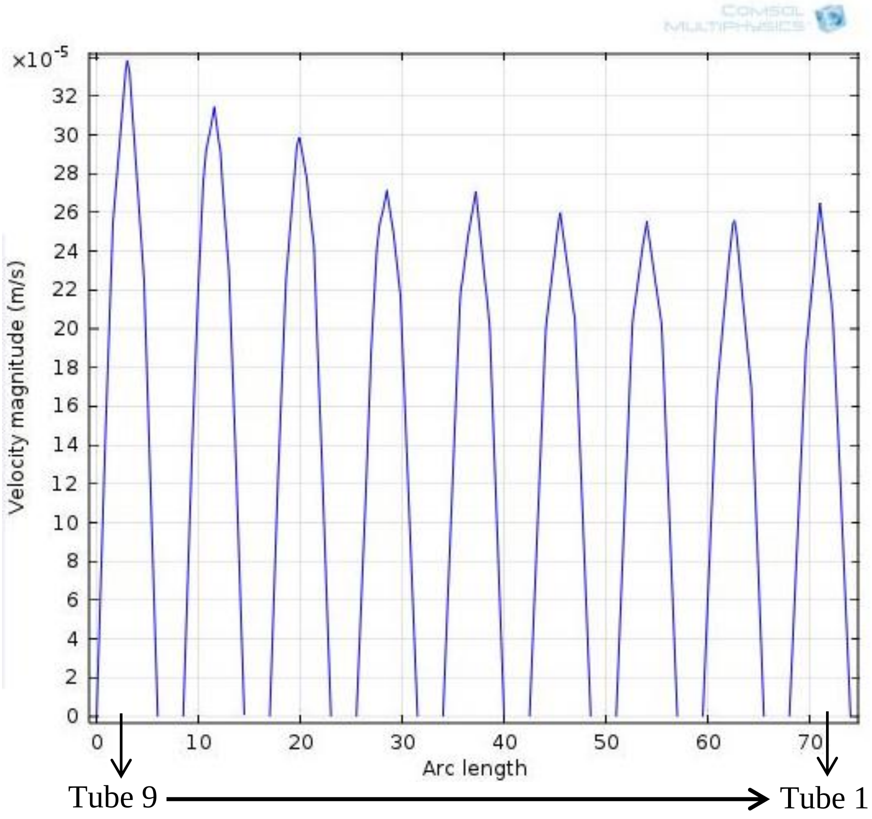

Figure 6.8 The change in the velocity across the tube diameters of the manifold type reactor with a single inlet and a single outlet. The reactor consists of 9 tubes and the arc length (mm) is the horizontal distance between the tubes.

A low pressure drop (0.0574 Pa) was obtained in the reactor system because of the small flow rate (255 mL/min). The highest pressure was observed at the inlet of the reactor (Figure 6.9) and the pressure remained between 0.01 and 0.03 Pa in the rest of the system.

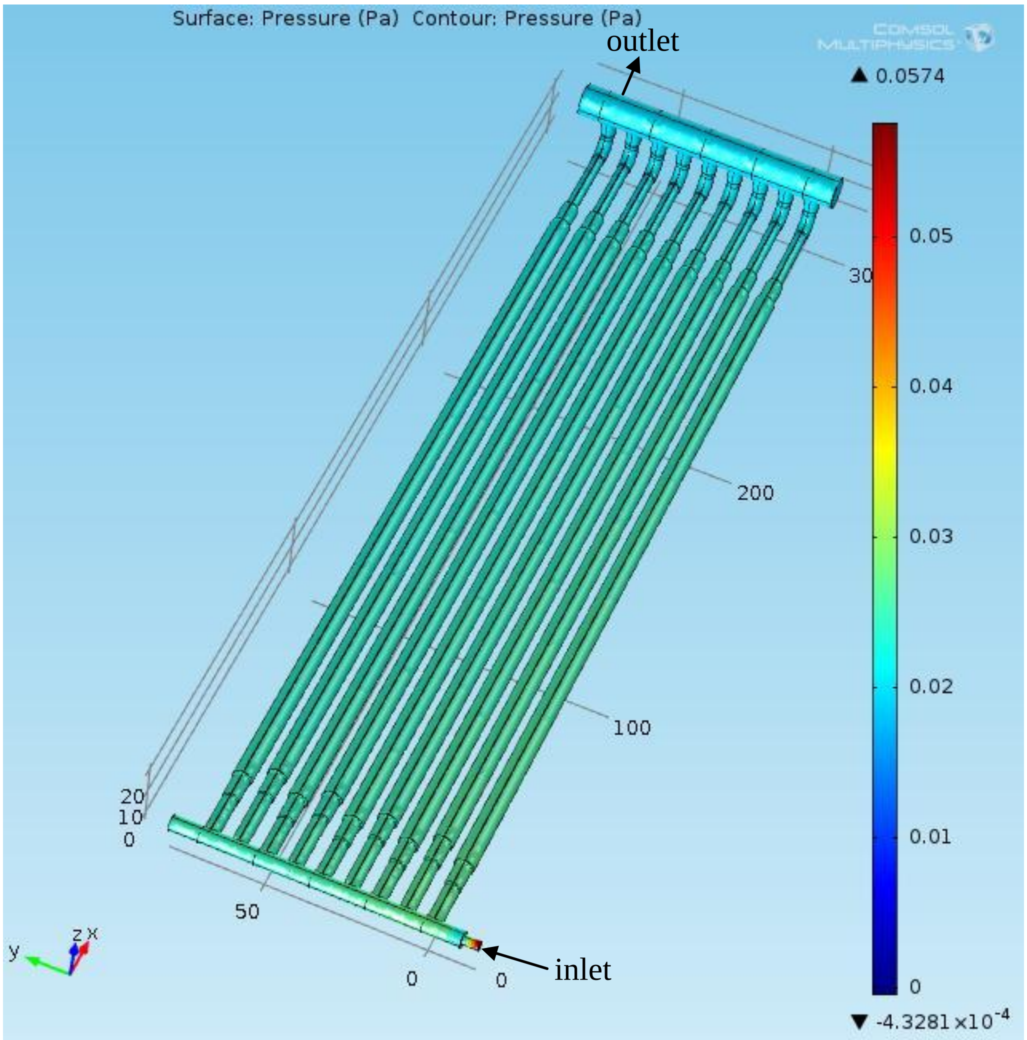
Surface: Pressure (Pa) Contour: Pressure (Pa)
outlet
COMSOL MULTIPHYSICS
▲ 0.0574
0.05
0.04
0.03
0.02
0.01
0
▼ -4.3281×10⁻⁴
30
200
100
20
10
0
50
0
0
inlet
y
z
x

Figure 6.9 Pressure drop in the manifold type reactor with a single inlet and a single outlet.

Figure 6.10 illustrates the velocity distribution in the manifold reactor with multiple inlets and a single outlet. The volumetric flow rate at the inlet of the manifold type reactor with a single inlet and single outlet was divided into the five inlets of the manifold type reactor with multiple inlets; for this reason lower V_{max} value of 1.8×10^{-3} m/s was achieved (Figure 6.10). However, more even streamlines and better flow distribution was attained in the multiple inlet reactor compared to the reactor a single inlet (Figure 6.11).

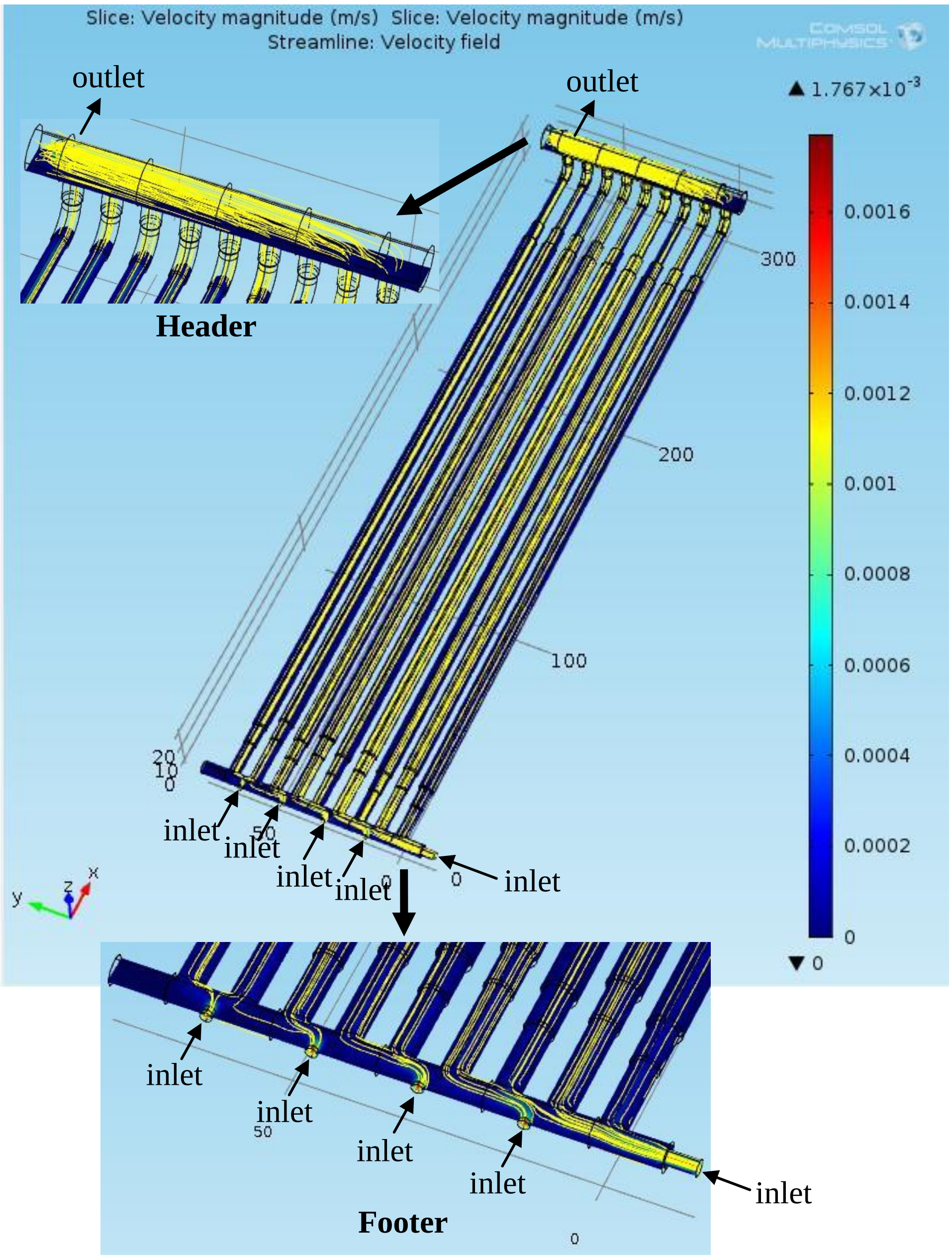
Slice: Velocity magnitude (m/s) Slice: Velocity magnitude (m/s)
Streamline: Velocity field
COMSOL MULTIPHYSICS
outlet
outlet
Header
▲ 1.767×10⁻³
0.0016
0.0014
0.0012
0.001
0.0008
0.0006
0.0004
0.0002
0
▼ 0
300
200
100
20
10
0
50
0
0
inlet
inlet
inlet
inlet
inlet
y
z
x
inlet
inlet
50
inlet
inlet
inlet
Footer
0

Figure 6.10 Velocity (m/s) distribution in the manifold type reactor with multiple inlets and a single outlet. The yellow streamlines in the inset show the path taken by a particle as it is carried by the flow.

Comparisons of velocities across the tube diameters revealed that the highest velocity of 1.8×10^{-3} m/s was obtained in the last tube (9), while V_{max} ranged between 1.2 – 1.4×10^{-3} m/s in the rest of the tubes – averaging 1.3×10^{-3} m/s. Therefore, the introduction of the multiple inlets improved flow in the reactor.

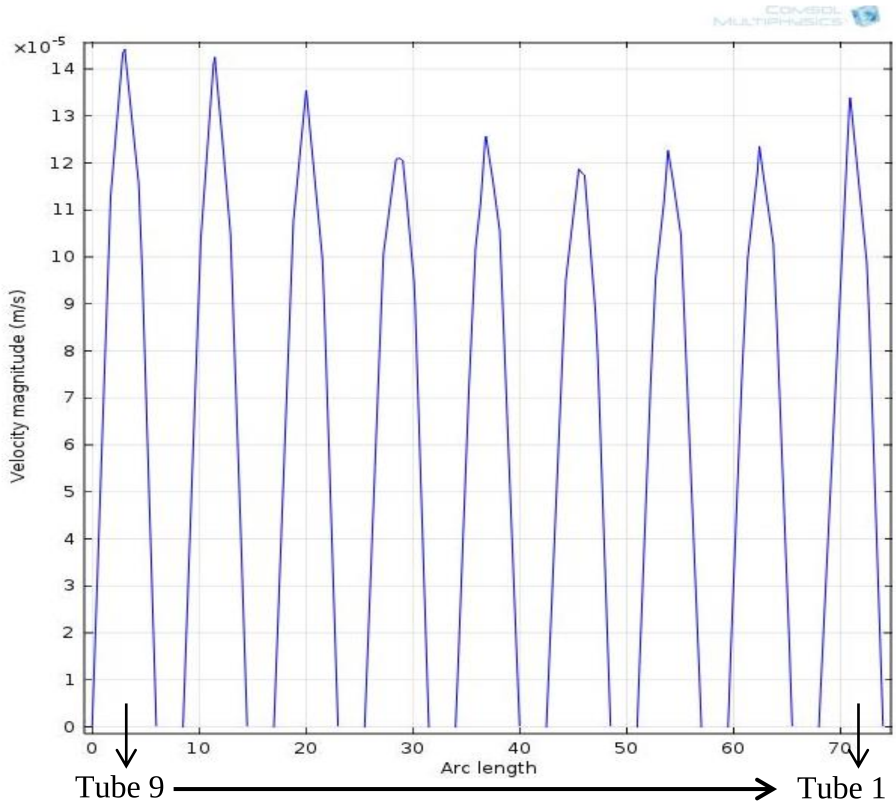

Figure 6.11 The flow distribution across reactor tubes in the manifold type reactor with multiple inlets and a single outlet. The arc length (mm) is the horizontal distance between the tubes. The reactor consists of 9 tubes.

Illustrated in Figure 6.12 is the pressure drop in the reactor system with multiple inlets and a single outlet. A low ΔP of 0.01 Pa was obtained in the reactor system compared to its counterpart with a single inlet and a single outlet that had ΔP of 0.05 Pa (Figure 6.9). The lower ΔP was because of lower flow rates at the inlet of the reactor.

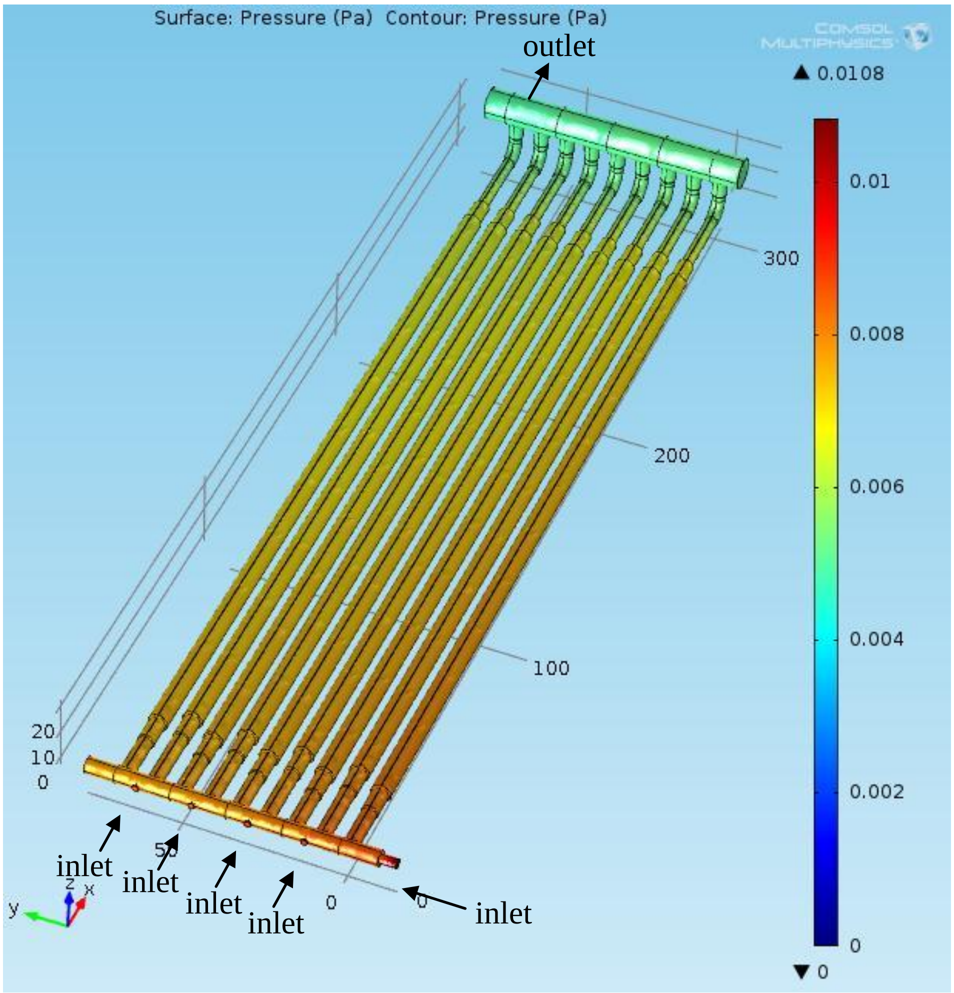
Surface: Pressure (Pa) Contour: Pressure (Pa)
outlet
▲ 0.0108
0.01
0.008
0.006
0.004
0.002
0
▼ 0
300
200
100
20
10
0
50
0
0
inlet
inlet
inlet
inlet
inlet
y
z
x

Figure 6.12 Pressure drop in the manifold type reactor with multiple inlets and single outlet.

6.3 Comparisons of the Volumetric Flow Rates in the Tubular Reactors

The average volumetric flow rate (m^3/h) in each pipe of the tubular reactors was calculated using V_{max} values and compared in Figures 6.13 and 6.14. A sample calculation of Q_{ave} is given in Appendix I.12. Q_{ave} in the U-tube and serpentine reactors ranged between 12.6×10^{-3} m^3/h and 12.8×10^{-3} m^3/h (about 1.6% difference), therefore indicating that the flow distribution in the reactors is uniform (Figure 6.13). In the manifold type reactor with a single inlet and a single outlet,

Q_{ave} increased from about 1.2×10^{-3} m^3/h in the tubes closer to the inlet, to 1.7×10^{-3} m^3/h in the tube farthest from the inlet. This revealed that there was channeling in the reactor system as Q_{ave} varied about 30% in the reactor system (Figure 6.14). The introduction of multiple inlets resulted in reduced flow rates but better flow distribution in the reactor as seen in Figure 6.14. Q_{ave} ranged between 0.6×10^{-3} m^3/h and 0.7×10^{-3} m^3/h, which corresponded to about 14% difference in the reactor system.

The CFD analyses perfomed compared the velocity distribution and pressure drop in tubular reactors. The results showed that the geometry of the reactor greatly influenced the flow distribution. The U-tube modular and serpentine reactors had uniform flow distribution compared to the manifold type tubular reactors. Higher pressure drops were obtained in the serpentine reactors because of the wall friction in the tube – the distance from the inlet of the reactor to the outlet was long. Low pressure drops were obtained in the manifold reactors and the velocity distribution was not uniform. Regions of low and high flow rates were observed in the reactor. The non-uniformity in flow could be due to the design of the manifold header and footer. The flow distribution in manifold reactors has been reported to be dependent in the design parameters such as the ratio of the header diameter to its length, spacing of the manifold and the flow rates (Bajura and Jones 1976, Ahn *et al.* 1998, Tompiks *et al.* 2002, Lee *et al.* 2012). Better flow rates can be achieved by redesigning the system and increasing the volumetric flow rates. The circulation rate is an important parameter to be considered in the design and operation of reactors. Low flow rates cause less shear stress and strain on the microorganisms in the reactor, but result in extended hydraulic retention time (HRT) which may reduce the performance of the systems. In the present study, HRT value of 10 minutes was estimated in the U-tube modular reactor, 120 minutes in the serpentine reactor and 350 minutes in the manifold type reactor. Shorter HRTs are targeted in photofermentative hydrogen production in order to prevent the uptake hydrogenase enzyme of the PNSB from converting the generated hydrogen gas to protons and electrons (Uyar *et al.* 2011, Androga *et al.* 2012).

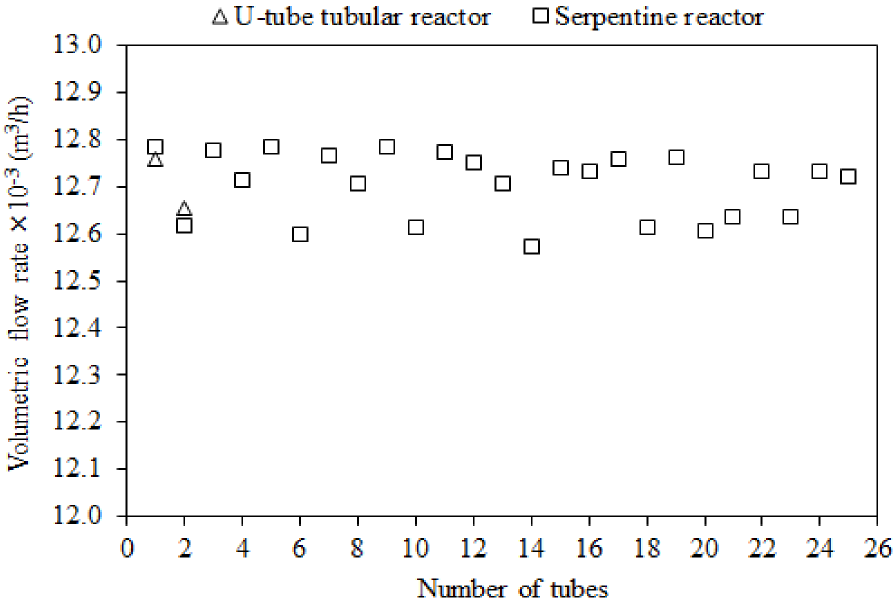

Figure 6.13 Comparison of the average volumetric flow rate in the U-tube modular reactor and the serpentine reactor.

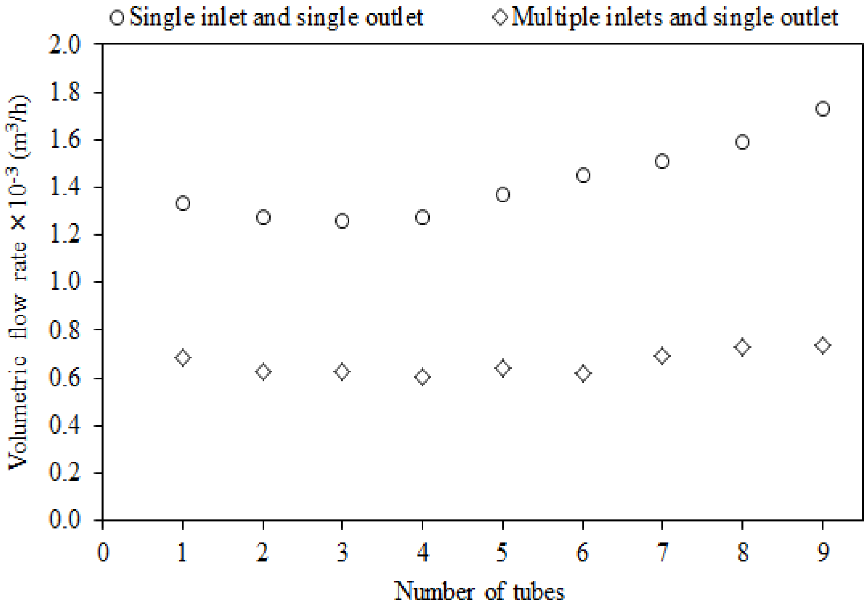

Figure 6.14 Comparison of the average volumetric flow rate in the manifold type tubular reactor with a single inlet and single outlet and multiple inlets and a single outlet.

On the other hand, high circulation rates provide better mixing in the reactors, which is convenient for gas-liquid separation and transport of the gas out of the reactor, however it results in a high pressure drop. More power is required for pumping, thus incurs extra operating costs. Also, the use of very high flow rates and vigorous mixing is discouraged as it may damage the bacteria cells and deter hydrogen production. The increased velocities obtained at the center of the tube could negatively affect microbial growth and hydrogen production. Investigations on the dispersion of microorganisms in a fluid flowing through the reactor tubes revealed that the cells were suspended mostly in the centre of the tubing (Poflee *et al.* 1997, Bees and Croze, 2010). The use of helical mixers was suggested to improve mixing in the tubular reactors (Sastre *et al.* 2007).

Photobioreactors used for hydrogen production are multiphase systems consisting of bacteria cells, media and the gas evolved. The fluid mechanics and heat transfer vary with the design and operating conditions of the photobioreactors, making scaling-up a difficult task. The thermo-fluid behavior (hydrodynamics), heat and mass transfer and light distribution affect growth of the photosynthetic microorganism. It is difficult to optimize the design and operating conditions for lab-scale systems and apply them to large scale systems. The use of CFD becomes invaluable. As in the present study, the flow in a 2.2 L U-tube modular tubular reactor was compared to a scaled-up 30 L serpentine reactor and a 90 L manifold type tubular reactor. The models developed are beneficial in the scale-up of reactor systems. Parameters affecting flow distribution - flow rate, inclination and geometry of the reactor, can be investigated and optimized using CFD and validated using experimental data.

CHAPTER 7

DYNAMIC MODELING OF TEMPERATURE CHANGE IN OUTDOOR OPERATED TUBULAR BIOREACTORS FOR HYDROGEN PRODUCTION

The temperature of the medium in photobioreactors operated outdoors is dependent on the amount of solar radiation received and the changes in ambient temperature. During summer, cooling of the photobioreactor is necessary to prevent damage to the culture and in winter, heating of the reactors might be necessary to avoid it freezing. An energy balance can be used to determine the change in temperature and the energy distribution inside the reactor system. The model developed can be used to estimate the amount of energy needed for cooling or heating.

In the present work, a dynamic thermal model that explores the effects of heat transfer mechanisms such as convection and radiation on the bulk temperature of an outdoor operated bioreactor is developed. For this purpose, tubular glass reactors with internal cooling tubes were designed, constructed and operated outdoors. Thermal balances on the liquid phase of the reactor systems were made (Equations 4.8 and 4.50) taking into account convection and radiation heat transfer, pump work and heat generated by metabolic activities of the photosynthetic bacteria. The values of the parameters that were used as input to the model changed with time and were measured during the experiments. They included: the global solar, dimensions of the reactor and cooling water tube, the ambient temperature, the ground temperature, the reactor inlet, outlet and surface temperatures, the cooling water inlet and outlet temperatures, the biomass growth, acetic acid concentration and the amount of hydrogen produced.

The energy balance was solved using MATLAB 2013-Simulink software that applied a 60 second fixed step ode1 (Euler) solver. A schematic of the program solution is shown in Appendix I.

Three sets of experiments were performed using the 2.8 L U-tube photobioreactors. In the first set of experiments, temperature change in the reactors operated at different flow rates (Re = 160, 1860, 2700) was investigated. In the second set of experiments, the radial change of temperature in the outdoor reactors was investigated at different flow rates (Re = 120 and 4200), while in the third set of experiments, the temperature change in the outdoor operated reactors circulated at the constant flow rate (Re = 160) was investigated using reactors with or without *Rhodobacter capsulatus* YO3 grown on acetate and glutamate medium. Hydrogen production, biomass growth, air temperature, ground temperature and light intensity variations were recorded during the experiments.

7.1 Dynamic Modeling of Temperature Change in Bioreactors Operated at Different Flow Rates in Outdoor Conditions

In these experiments, pure water was used as the working fluid in the photobioreactors.

7.1.1 Temperature Variation in Bioreactors Operated at Different Flow Rates in Outdoor Conditions

The change of the solar light intensity (H_g), air temperature (T_{air}) and ground temperature (T_g) with time for the experiment performed on the 29th of August, 2012, is shown in Figure 7.1. T_{air} and T_g increased with increasing solar radiation. A similar trend was observed on the days the other experiments were performed as shown in Appendix J, Figure J.1 and J.2. A summary of the maximum temperature values recorded on the different days of the experiments is shown in Table 7.1. The high insolation, elevated T_{air} and T_g experienced during the experiments resulted in the increase of the reactor temperature. The ground (table top surface) on which the reactors were placed absorbed solar radiation and heated up, resulting in higher ground temperatures as observed in Figure 7.1, Figures J.1 and J.2 in Appendix J.

Table 7.1 Summary of the maximum air temperatures, ground temperatures and solar radiation recorded during the outdoor experiments.

Operation	**Date**	***Re***	**Air temperature (°C)**	**Ground temperature (°C)**	**Solar radiation (W/m^2)**
Co-current flow	29.08.2012	160	27.0	63.4	1179
	02.09.2012	1860	29.5	64.7	1151
	01.09.2012	2700	28.0	65.5	1136
Counter-current flow	19.09.2012	160	31.0	66.0	1044
	17.09.2012	1860	33.0	67.3	1071
	18.09.2012	2700	34.0	68.6	1078

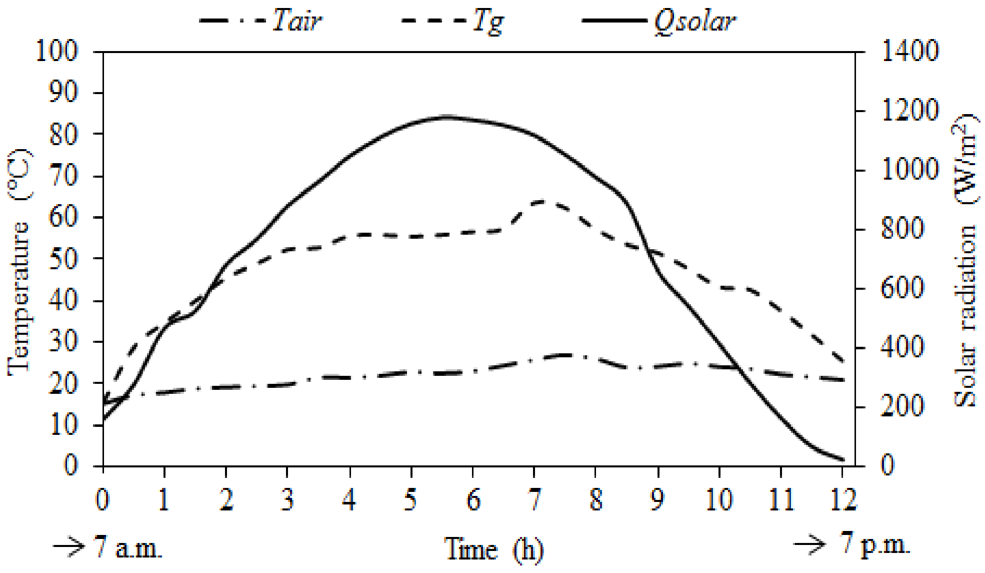

Figure 7.1 The change in the air temperature (— · —), the ground temperature (– –) and solar radiation (———) with time. The reactor contained water circulated at Reynolds number 160, in co-current flow to the cooling water. The experiment was performed on the 28th of August, 2008. The start of the experiment (0th hour) corresponds to 7 a.m. and the end of the experiment (12th hour) corresponds to 7 p.m.

The change of temperatures at the inlets and outlets of the reactor and cooling water are shown in Figures 7.2 and 7.3. The temperatures rose with the increasing solar radiation, air temperatures and ground temperature and cooling was started when they exceeded 25.0 °C. The temperatures in the reactors were successfully maintained between 30.0 and 37.0 °C during the day by cooling - average maximum temperatures of about 36.0 °C was obtained in the reactors operated on different days at different flow rates.

At low circulation rate ($Re = 160$), the difference between the reactor inlet and outlet temperatures ($\Delta T_r = T_{ri} - T_{ro}$) were higher compared to that in the reactors with greater circulation rates (Re = 1860 and 2700) whose inlet and outlet temperatures values were close to each other (Figures 7.2 and 7.3). ΔT_r was higher in the counter-currently cooled reactors compared to the co-currently cooled reactors. During co-current operation, a maximum ΔT_r of 3.0 °C was attained in the reactors with $Re = 160$ while the reactors with Re = 1860 and 2700 had maxima of 1.0 °C. In counter-current operation, maximum ΔT_r in the reactor with $Re = 160$ was 7.0 °C while in the reactors with Re = 1860 and 2700, it was 2.0 °C. The differences in ΔT_r could be due to the high turbulence and better mixing achieved at higher flow rates.

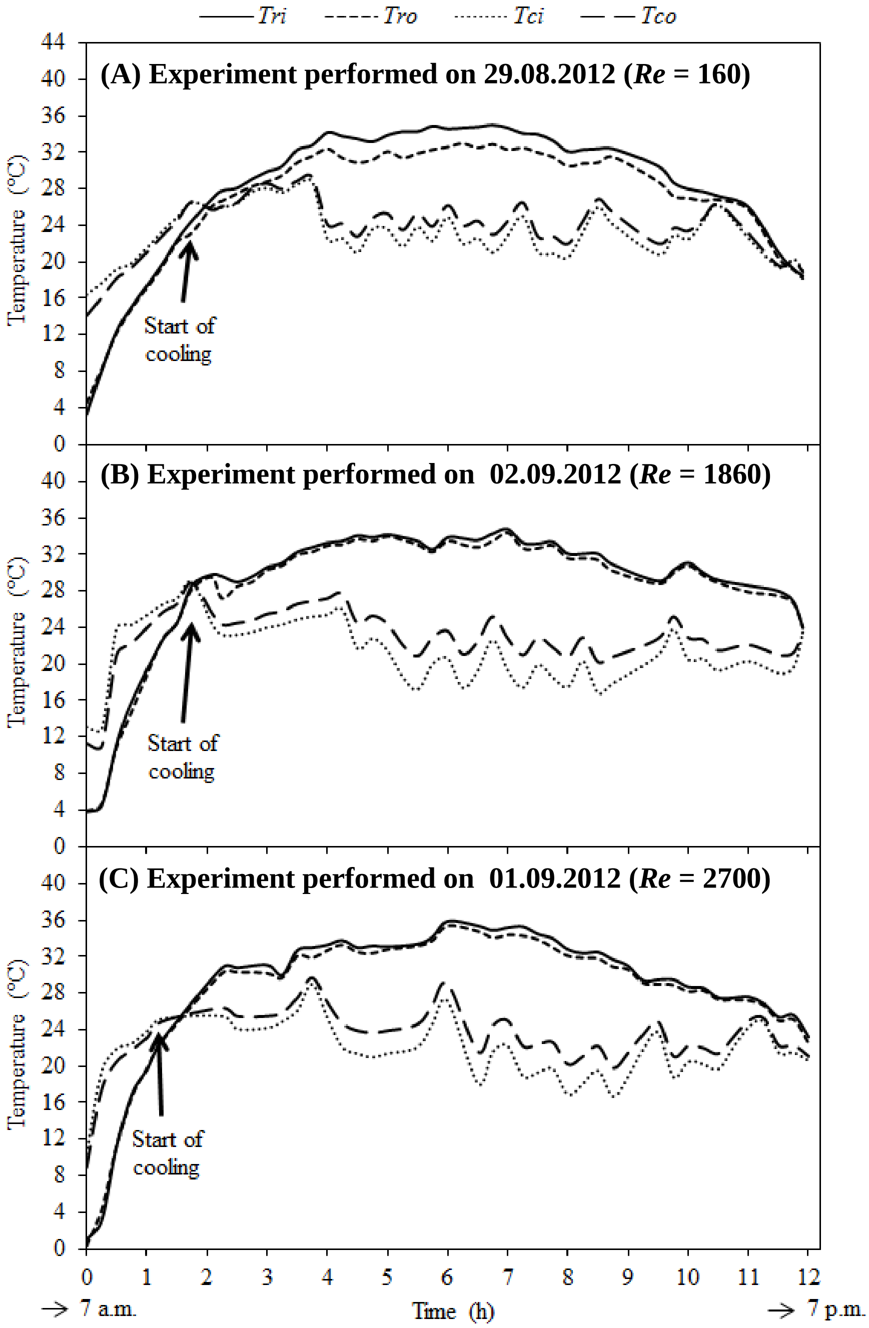

Figure 7.2 Comparisons of the changes in the reactor inlet temperatures (T_{ri}, —), the reactor outlet temperatures (T_{ro}, – –), the cooling water inlet temperatures (T_{ci}, ·······) and the cooling water outlet temperatures (T_{co}, — —) with time. The reactors contained water circulated at Reynolds number 160, 1860 and 2700 in co-current flow to the cooling water.

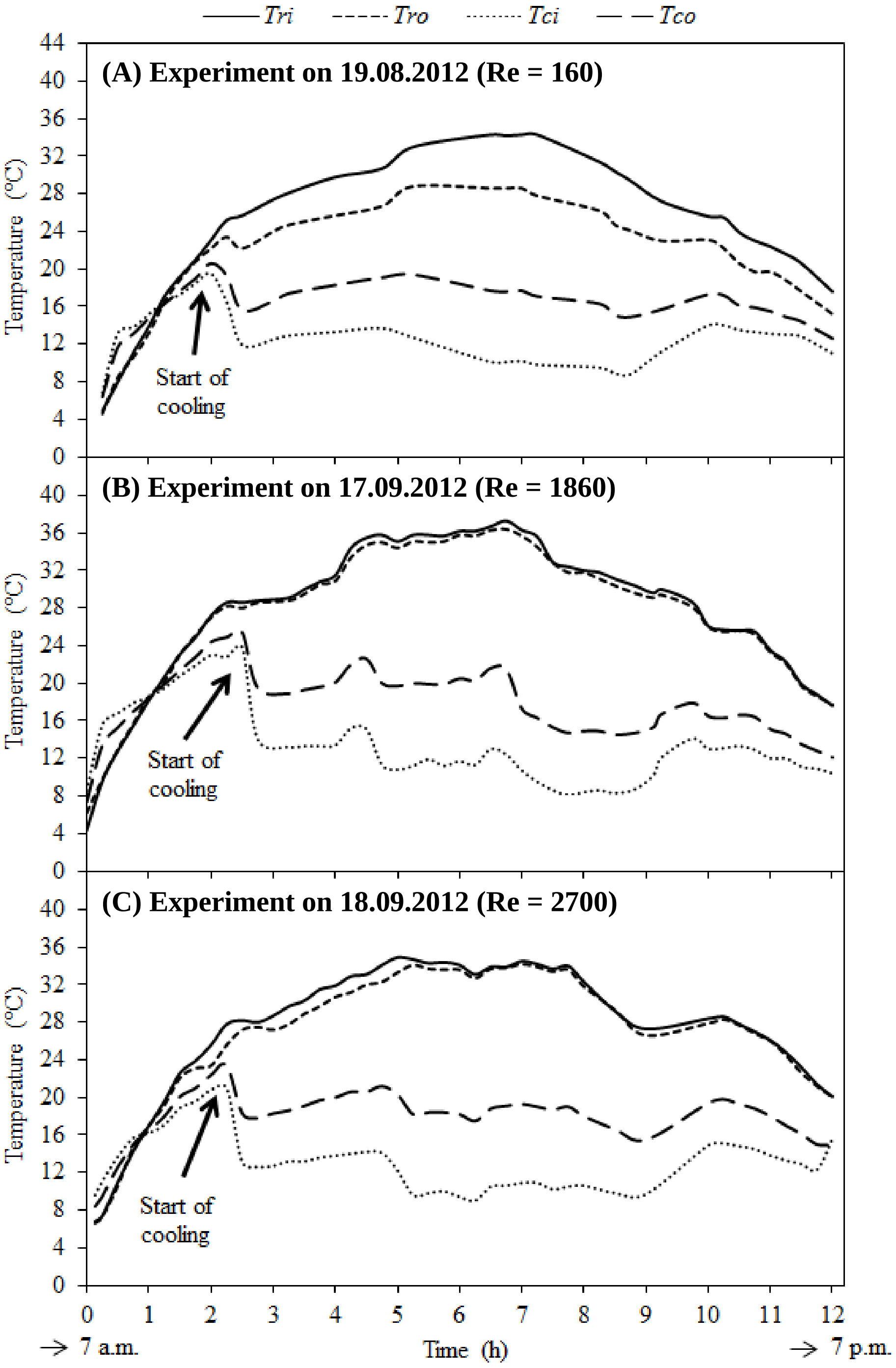

Figure 7.3 Comparisons of the changes in the reactor inlet temperatures (T_{ri}, —), the reactor outlet temperatures (T_{ro}, - -), the cooling water inlet temperatures (T_{ci}, ······) and the cooling water outlet temperatures (T_{co}, — —) with time. The reactors contained water circulated at Reynolds number 160, 1860 and 2700 in counter-current flow to the cooling water.

Comparing the differences between the cooling water inlet and outlet ($\Delta T_c = T_{cout} - T_{cin}$) of the outdoor reactors, higher ΔT_c was obtained in the counter-currently cooled reactor than the co-currently cooled ones. During co-current operation, maximum ΔT_c of 2.0 °C was obtained in the reactors with Re = 160, while in the reactors with high flow rates (Re = 1860 and 2700), it was about 4.0 °C (Figure 7.2). The counter-currently cooled reactors had maximum ΔT_c of 7 to 9 °C. The results indicated that more heat was removed during counter-current operation. No significant changes in ΔT_c were observed with increasing flow rates in both modes of operation (Figures 7.2 and 7.3).

7.1.2 Temperature Change Along the Bioreactors Operated at Different Flow Rates in Outdoor Conditions

The temperatures at the surface of the reactors were measured at four different points during different times of the days. The temperatures did not to vary with the reactor length, but were a function time. Maximum temperature differences of 0.5 °C were recorded, showing that the reactor wall surface could be considered isothermal. The highest surface temperatures were recorded between the 7th and 9th hours of the experiments (1 p.m. to 3 p.m.), which corresponded to the time the maximum solar radiation was received (Figure 7.1). A sample of the longitudinal variation of temperature is shown in Figure 7.4.

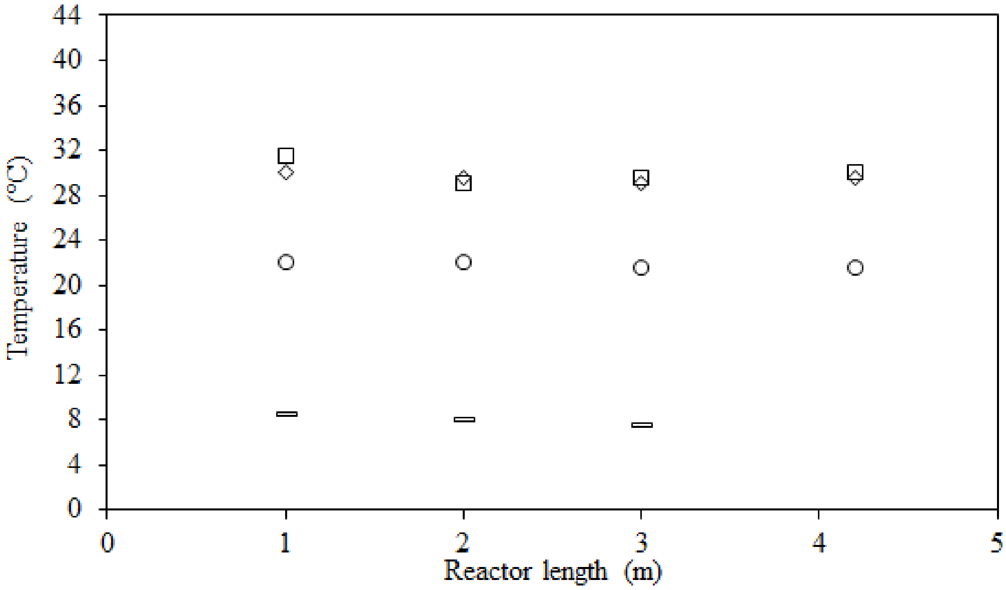

Figure 7.4 The change in the surface temperature along the reactor tube at different times of the day. The experiment were performed on the 1st of September, 2012 using reactor with medium circulated at 5.8×10^{-2} kg/s (*Re* = 2700) and the reactor co-currently cooled. (▭) 07:00, (□) 11:00, (◇) 15:00 and (○) 19:00.

7.1.3 Dynamic Modeling of Temperature Change in Bioreactors Operated at Different Flow Rates in Outdoor Conditions

Models describing the change in temperature within the reactors were developed for the three different cases: *Re* = 160, 1860 and 2700 in co-current and counter-current flow. The comparisons of the reactor average temperatures (T_{ave}), the reactor surface temperatures (T_s) and the predicted (model) temperatures (T_m) revealed that the change of T_m with time corresponded well with the changes of T_{ave} and T_s. (Figure 7.5, Appendix J, Figures J.3 and J.4). The reactor temperature was predicted within a 10% error margin at an accuracy of ±2°C. The results indicated that the assumptions made in developing the model were reasonable.

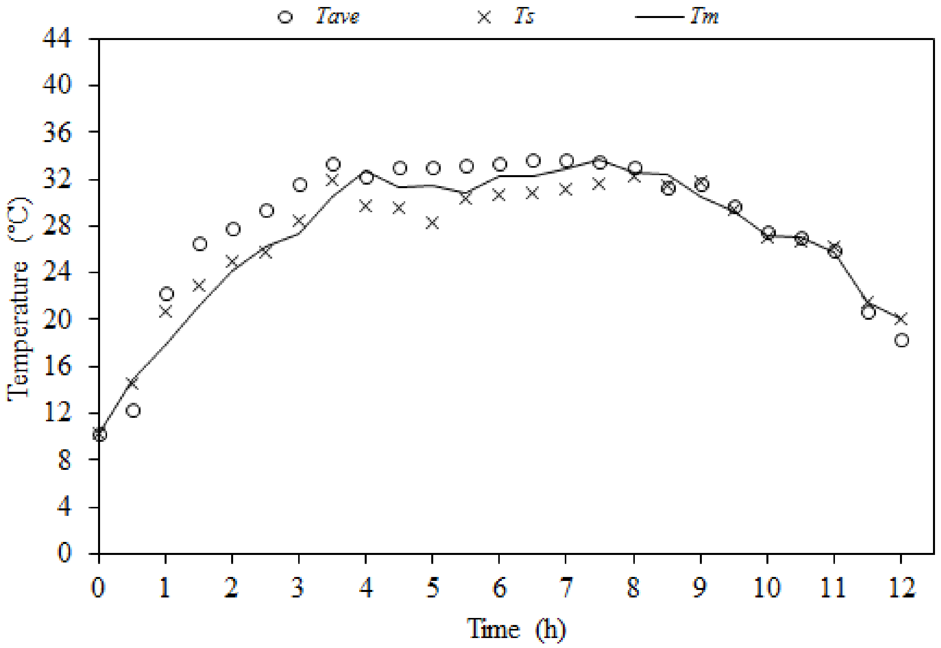

Figure 7.5 Comparison of the changes in the reactor average temperatures T_{ave} (o), the reactor surface temperatures T_s (x) and the predicted (model) temperatures T_m (–) with time. The experiment was performed on the 29th of August, 2012.

7.1.4 Energy Transfer in the Bioreactors Operated at Different Flow Rates in Outdoor Conditions

The energy gained or lost through the different heat transfer mechanisms in the models for the reactors operated at different flow rates in outdoor conditions are shown in Figures 7.6 and 7.7. The values correspond to the total energy transferred in the 12 hour duration of the experiment.

Energy was gained by the systems mainly through radiation. The degree of radiative energy received by the reactors was in the order $\dot{Q}_{rad,r} > \dot{Q}_{rad,g} > \dot{Q}_{rad,a} > \dot{Q}_{rad,D} > \dot{Q}_{rad,d} > \dot{Q}_{re,g} > \dot{Q}_{re,a}$. In developing the model, $\dot{Q}_{rad,r}$ represented the amount of radiative energy emitted by the medium in the reactor. In this study, $\dot{Q}_{rad,r}$ was found to be positive - it was a major heat source to the system and varied between 200.1 and 201.9 W in the co-current systems and between 196 and 202.7 W in the counter-current systems (Figures 7.6 and 7.7). $\dot{Q}_{rad,r}$ being positive indicates that the system absorbed more energy than it emitted.

Heat was also gained through radiation from the ground ($\dot{Q}_{rad,g}$). The temperatures of the ground (table surfaces) on which the reactors were put increased to as high as 68 °C (Table 7.1). This in turn heated the reactor surface. Since the contact area between the reactor and the table surface was small (0.02 m^2), conduction was neglected in the calculations. $\dot{Q}_{rad,g}$ ranged between 105.3 and 108.9 W in the co-current cooled reactors and between 107.3 and 112 W in counter-currently system (Figures 7.6 and 7.7). The values were different because the experiments were performed on different dates under varying solar radiation and air temperatures.

Radiation energy from the air surrounding the reactors ($\dot{Q}_{rad,a}$) was also another heat source to the reactors. It varied between 75.6 and 82.5 W in the outdoor reactors (Figures 7.6 and 7.7). The amount of energy received from direct sunlight ($\dot{Q}_{rad,D}$) was greater than the diffuse radiative energy ($\dot{Q}_{rad,d}$), while the reflected ground ($\dot{Q}_{re,g}$) and air radiation ($\dot{Q}_{re,a}$) were negligible as they accounted for less than 1% of the total radiative energy gained (Figures 7.6 and 7.7).

The heat loss from the reactors was mainly through the heat removed by the cooling water ($\dot{Q}_{cw}$) and heat energy lost through forced convection ($\dot{Q}_{fconv,rw}$). $\dot{Q}_{cw}$ was higher in the counter-currently cooled reactors compared to the co-currently cooled reactors and increased with the increasing flow rates of the medium in the reactor. $\dot{Q}_{cw}$ ranged between -32.7 and -72 W in the co-current systems and between -181.7 and -227.4 W in the counter-current systems (Figures 7.6 and 7.7). These results indicate that counter-current cooling was more effective in controlling the reactor temperatures. Energy loss by forced convection also displayed a similar trend as $\dot{Q}_{cw}$. $\dot{Q}_{fconv,rw}$ ranged increased from -6.4 W to -50.2 W as the Reynolds number in the reactors was increased from *Re* = 60 to *Re* = 2700 in the co-currently cooled systems. In the counter-currently cooled systems it increased from -120.6 W to -162.2 W as the circulation rates of the medium in the reactors increased from *Re* = 160 to *Re* = 2700. This implied that better heat transfer was achieved in the counter-current system and with increasing flow rates.

There was a net energy gain by the systems as the amount of energy obtained was more than the amount of heat lost (Figures 7.6 and 7.7). The co-current cooled systems had a higher net heat gain of 356.5 W to 444.6 W compared to the counter-currently cooled systems that ranged between 86.4 W and 155 W. This indicated that the counter-current systems were better in controlling temperatures in the reactor systems.

Low cooling duty ($\dot{Q}_{cw}$) values were observed in the co- and counter-currently cooled reactors at *Re* = 160 (Figure 7.6 and 7.7) compared to operation at *Re* = 1860 and 2700; for this reason this *Re* = 160 was selected to be the circulation rate to be used in the experiments with bacteria culture.

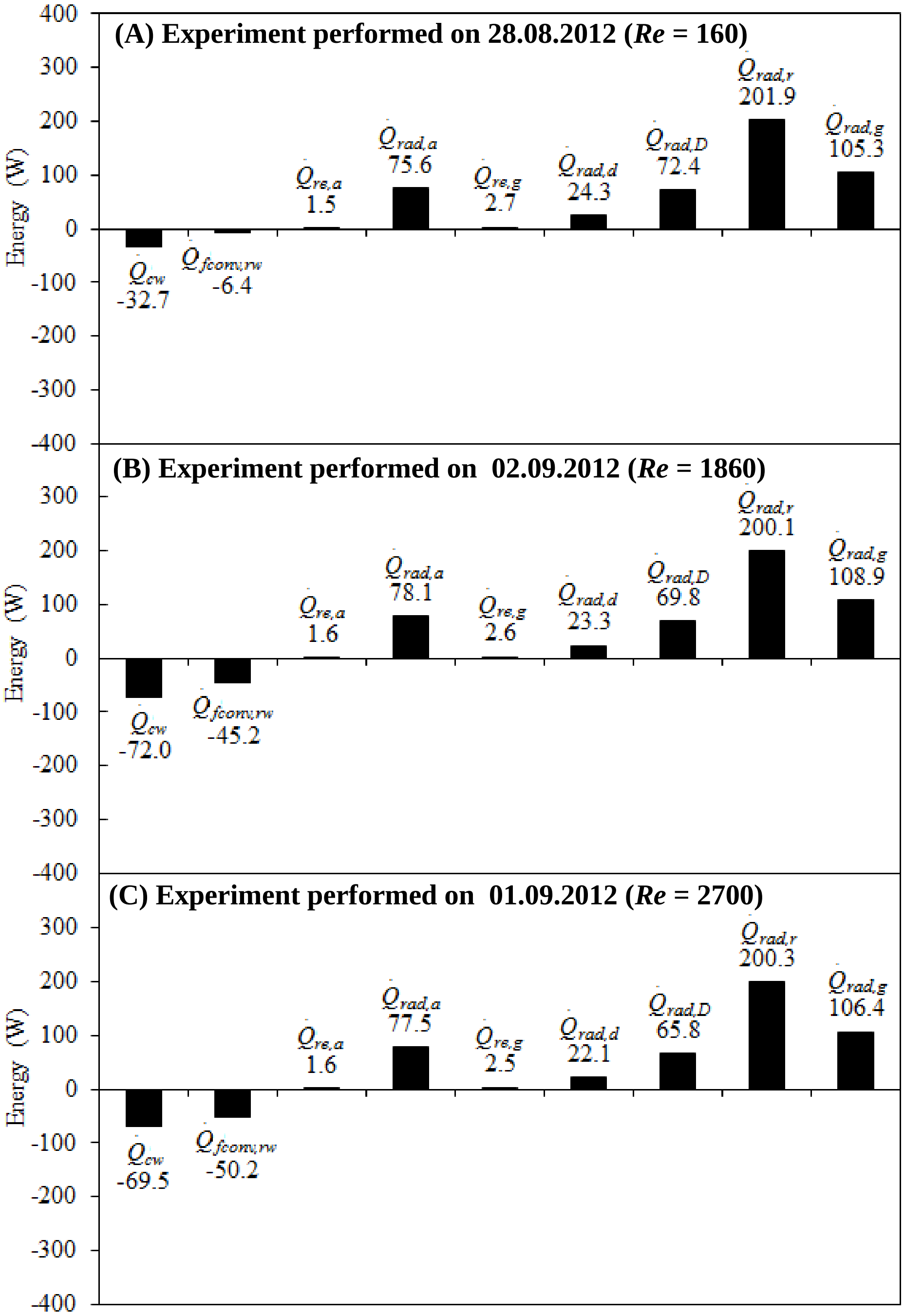

Figure 7.6 Comparison of the energy gained or lost during the day time in the co-currently cooled reactors operated in outdoor conditions.

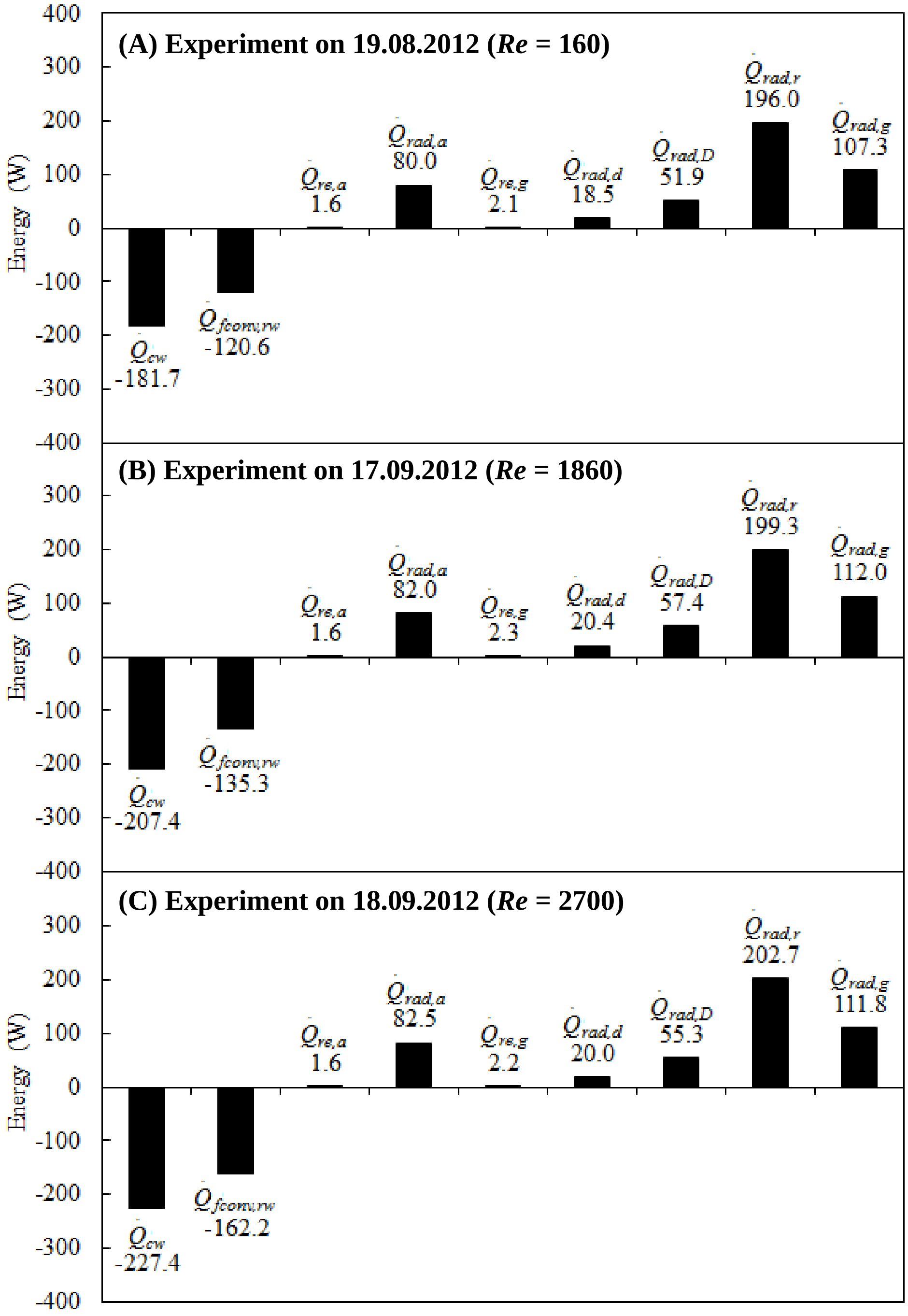

Figure 7.7 Comparison of the energy gained or lost during the day time in the counter-currently cooled reactors operated in outdoor conditions.

7.2 Radial Variation of Temperature in Bioreactors Operated Outdoors at Different Flow Rates

The temperature variations in radial direction inside tubular reactors were measured using thermocouple probes (T1 to T8) as described in Section 3.5.1 and shown in Figure 7.8. Figures 7.8 and 7.9 illustrate the radial change in the temperatures for the reactors circulated at low flow rate (*Re* = 120) and high flow rate (*Re* = 4200). It is observed that the temperatures increased during the day but there was no significant radial variation either in the reactor with low flow rate or higher flow rate.

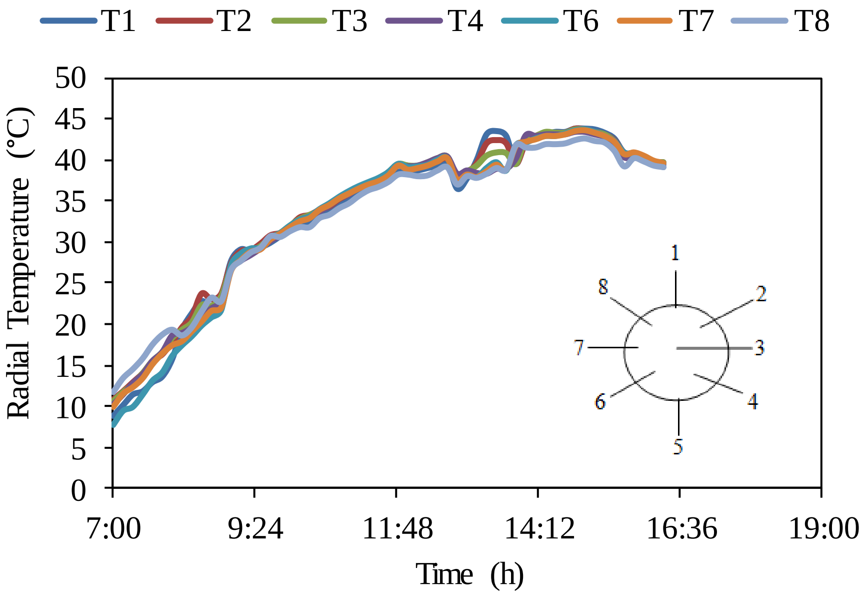

Figure 7.8 Temperature variation in radial direction for the reactor circulated at low flow rate (*Re* = 120).

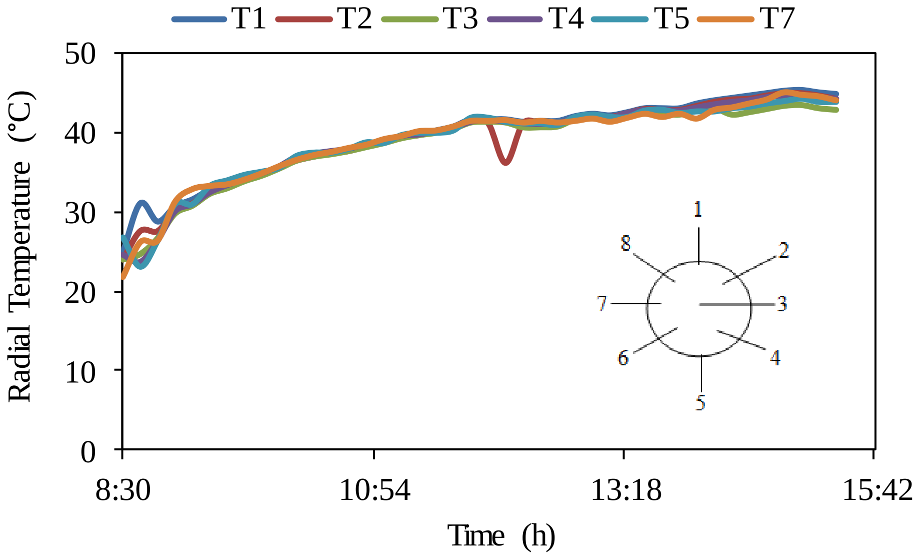

Figure 7.9 Temperature variation in radial direction for the reactor circulated at high flow rate (Re = 4200).

7.3 Dynamic Modeling of Temperature Change in Bioreactors Operated Outdoors With or Without *Rhodobacter capsulatus* YO3

In these experiments, 2.8 L U-tube reactors with or without *Rhodobacter capsulatus* YO3 cultures were operated in outdoor conditions. The reactors were co-current and counter-currently cooled and medium circulated at constant *Re* of 160.

7.3.1 Temperature Variation in the Outdoor Operated Reactors

The variation of light intensity, air temperature and ground temperature are shown in Figure 7.10. During the day, the air temperatures (T_{air}) and ground temperatures (T_g) increased with increasing solar radiation. T_{air} ranged between 25.0 and 31.6 °C and T_g of the co-current and counter-currently cooled reactors varied between rose to as high as 56 °C. The maximum solar radiation of about 820 W/m^2 was observed between the 6th (12 p.m.) and 8th hour (2 p.m) of the experiments. The experiments were performed on three consecutive days, the 5th, 7th and 8th of August, 2013 and similar extent of solar radiation was received (Figure 7.10, Appendix J, Figures J.5 and J.6).

Shown in Table 7.2 is a summary of the maximum air temperatures, maximum ground temperatures and the maximum solar radiation recorded during the experiments.

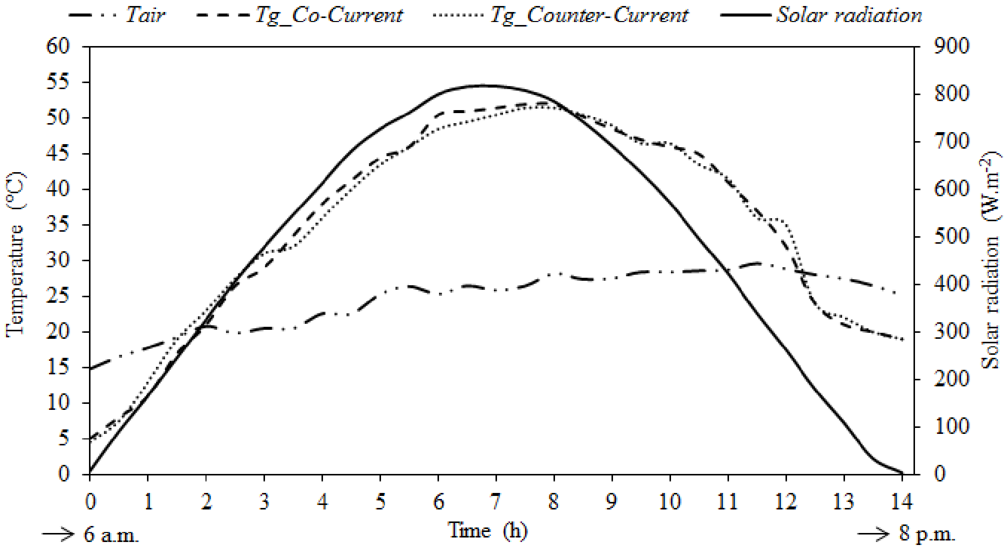

Figure 7.10 The change in the air temperature (— · ·), the co-currently cooled reactor ground temperature (– – –), the counter-currently cooled reactor ground temperature (·······) and the solar radiation (——) with time. The experiments were carried out on the 5th of August, 2013. The start of the experiment (0th hour) corresponds to 6 a.m. and the end of the experiment (14th hour) corresponds to 8 p.m.

Table 7.2 Summary of the maximum air temperatures, ground temperatures and solar radiation recorded during the outdoor experiments.

Date	**Maximum Air Temperature (°C)**	**Maximum Ground Temperature (°C)**	**Maximum Solar Radiation (W/m^2)**
05.08.2013	29.6	52.0	820
07.08.2013	29.7	54.5	806
08.08.2013	31.6	56.0	830

The experiments in this study were performed on a summer day when high insolation was received. The high sunlight energy (maximum 806 W/m^2, 820 W/m^2 and 830 W/m^2) received during the three days of the experiments elevated the ground and air temperatures, which heated the reactor surface and the bulk fluid, mainly through radiation. The ground (table covered with sisal mat) on which the reactors were placed absorbed solar radiation and heated up, resulting in higher ground temperatures as observed in Figure 7.10.

The change of temperature with time at the reactor inlets (T_{ri}), reactor outlets (T_{ro}), cooling water inlets (T_{ci}) and cooling water outlets (T_{co}) is shown in Figure 7.11 for the co-currently cooled reactors and in Figure 7.12 for the counter-currently cooled reactors. The reactor inlet and outlet temperatures increased with increasing solar radiation and ambient air temperatures, until the start of cooling at the 3rd hour. Temperatures in the reactors were succesfully maintained below 38 °C during the experiments. The temperature values at the reactor inlets and outlets did not vary greatly; the maximum difference ($\Delta T_r = T_{ri} - T_{ro}$) ranged between 0 and 3.2 °C. The outlet temperatures were lower than the inlet temperatures since cooling was provided at the U-tube section of the reactor, however, the increase in temperature from the outlet of the reactor to the inlet of the reactor implied that there was a heat gain in the auxiliary part of the system. Although the gas-liquid separator (reservoir) and connecting pipes were insulated using a Styrofoam cover, the insulation might not have been sufficient or thermal energy due to frictional effects of the pump could result in a temperature. The heat effects on the external pumping and piping units were found to significantly increase the heating duty 10 to 40%. Better insulation and/or external cooling might be required.

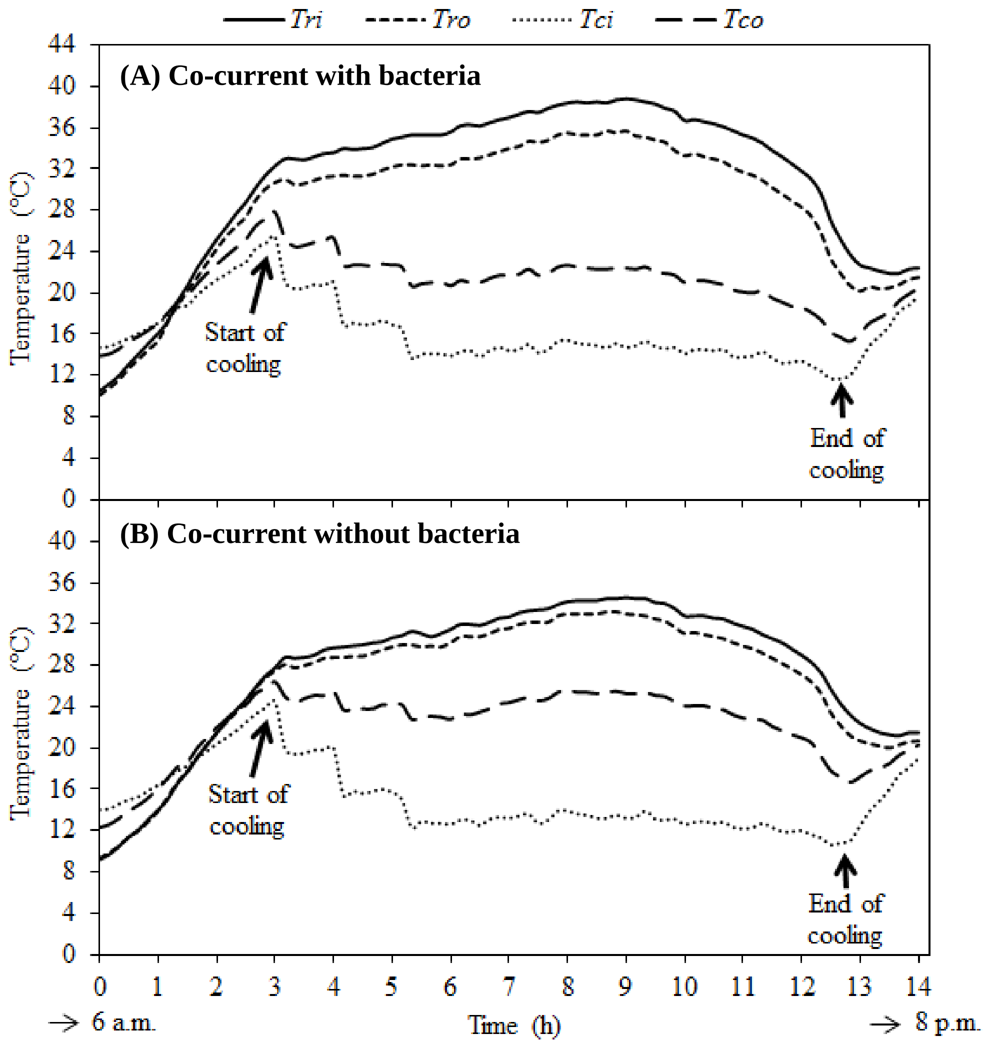

Figure 7.11 Comparisons of the changes in the reactor inlet temperatures (T_{ri}, —), the reactor outlet temperatures (T_{ro}, – –), the cooling water inlet temperatures (T_{ci}, — —) and the cooling water outlet temperatures (T_{co}, ·······) with time. The experiments were performed on the 5th of August, 2013 using co-currently cooled reactors with and without *Rhodobacter capsulatus* YO3 cultures operated in outdoor conditions.

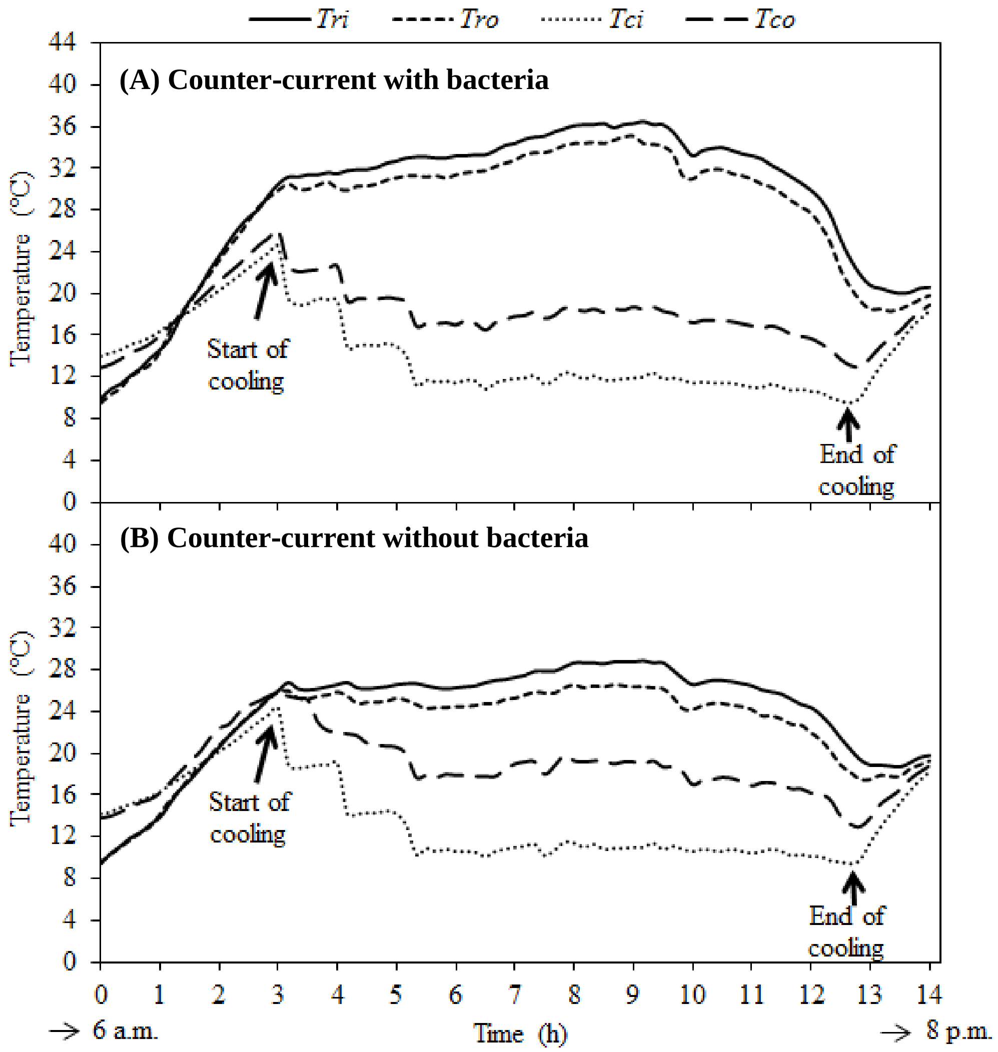

Figure 7.11 Comparisons of the changes in the reactor inlet temperatures (T_{ri}, —), the reactor outlet temperatures (T_{ro}, – –), the cooling water inlet temperatures (T_{ci}, — —) and the cooling water outlet temperatures (T_{co}, ·······) with time. The experiments were performed on the 5th of August, 2013 using counter-currently cooled reactors with and without *Rhodobacter capsulatus* YO3 cultures operated in outdoor conditions.

At the start-up of the experiment, the cooling water heated up as the medium in the reactor warmed with increasing insolation, but after the start of cooling (at the 3rd hour), the cooling water temperatures dropped and the difference between the cooling water inlet and outlet ($\Delta T_c = T_{cout} - T_{cin}$) rose. Maximum temperature difference of 8.5 °C was obtained in the reactors with bacteria and 12.8 °C in the reactors without bacteria (Figures 7.11 and 7.12). ΔT_c in the co-currently cooled reactors with bacteria varied between 6.7 and 8.5 °C, while it ranged between 8.2 and 12.2 °C in the co-currently cooled reactors without bacteria. The counter-currently cooled reactors with bacteria had ΔT_c in the range of 5.4 and 6.8 °C and between 8.5 and 12.8 °C in the reactors without bacteria. Figures 7.11 and 7.12 demonstrated that temperatures in the reactors increased with increasing solar radiation but were successfully kept between 30 and 38.0 °C by cooling. This temperature range was reported to be optimum for growth and hydrogen production by *R.capsulatus* (Sevinç *et al.* 2012). The results indicate that the internal cooling heat exchange system used was efficient in controlling the reactor temperatures. Sierra *et al.* (2008) reported that cooling by heat exchange systems are superior to other temperature control methods such as water-spraying as they have a higher cooling capacity and can be used to cool the reactor systems during the day and heat them at night, therefore improving energy yields.

Temperatures in the reactors with bacteria were higher than those without bacteria (Figures 7.11 and 7.12). This could be attributed to the light absorbing properties of the microorganisms in the reactor. The PNSB such as *R.capsulatus* YO3 contain pigments, namely bacteriochlorophyll *a* and carotenoids that absorb light at certain wavelengths. The bacteriochlorophyll *a* of living cells of *R.capsulatus* has absorption maxima values at 376-378, 450 to 455, 478 to 480, 508 to 513, 590 to 592, 802 to 805 and 860 to 863 nm (Imhoff, 1984). Divisions of the solar spectrum show that about 48 % is visible light (380 to 780 nm), 45.6 % is infrared light (above 780 nm) and the remaining 6.4% is ultraviolet light (< 380 nm) (Tiwari, 2002). The light energy absorbed by the bacteria is used for biomass growth, maintenance, hydrogen production and the excess dissipated as heat (Hoekama *et al.* 2006), therefore could influence temperature within the reactor. A measurement of the absorbance spectrum of *R.capsulatus* YO3 at different cell concentrations revealed that absorbance increased with increasing biomass concentration (Appendix G, Figure G.1).

In this study, the counter-current systems used exhibited lower temperatures compared to their co-current counterparts (Figures 7.11 and 7.12), indicating that better temperature control was achieved in the counter-current system compared to the co-current system under the same operating conditions. Similar results were observed in the experiments performed on the 7th and 8th of August, 2013 as shown in Appendix J, Figures J.6 to J.9. Incropera (1996) explains that the configuration of the counter-flow systems allow heat exchange at both the hotter and colder ends of the reactors, while in co-current (parallel) flow there is a large temperature difference at the entrance ($\Delta T = T_{rin} - T_{ci}$), which rapidly reduces with increasing distance. Unlike in parallel flow, ΔT does not change much with distance hence the counter-flow provides better heat transfer.

7.3.2 Temperature Change Along the Reactor Surface

Figures 7.13 and 7.14 illustrate the longitudinal change of the temperatures in the reactor at different times of the days. The measurements were taken at six different points along the reactor surface. The temperature did not vary with the reactor length, but was a function time. Maximum temperature differences of 0.5 °C were recorded, showing that the reactor wall surface could be considered isothermal. The highest surface temperatures were recorded at the 9th hour of the experiment (15:00), which corresponded to the time the maximum solar radiation was received (Figure 7.10). The surface temperatures did not vary along the reactor length in the experiments carried out on the 7th and 8th of August, 2013 (Appendix J, Figures J.10 to J.13.).

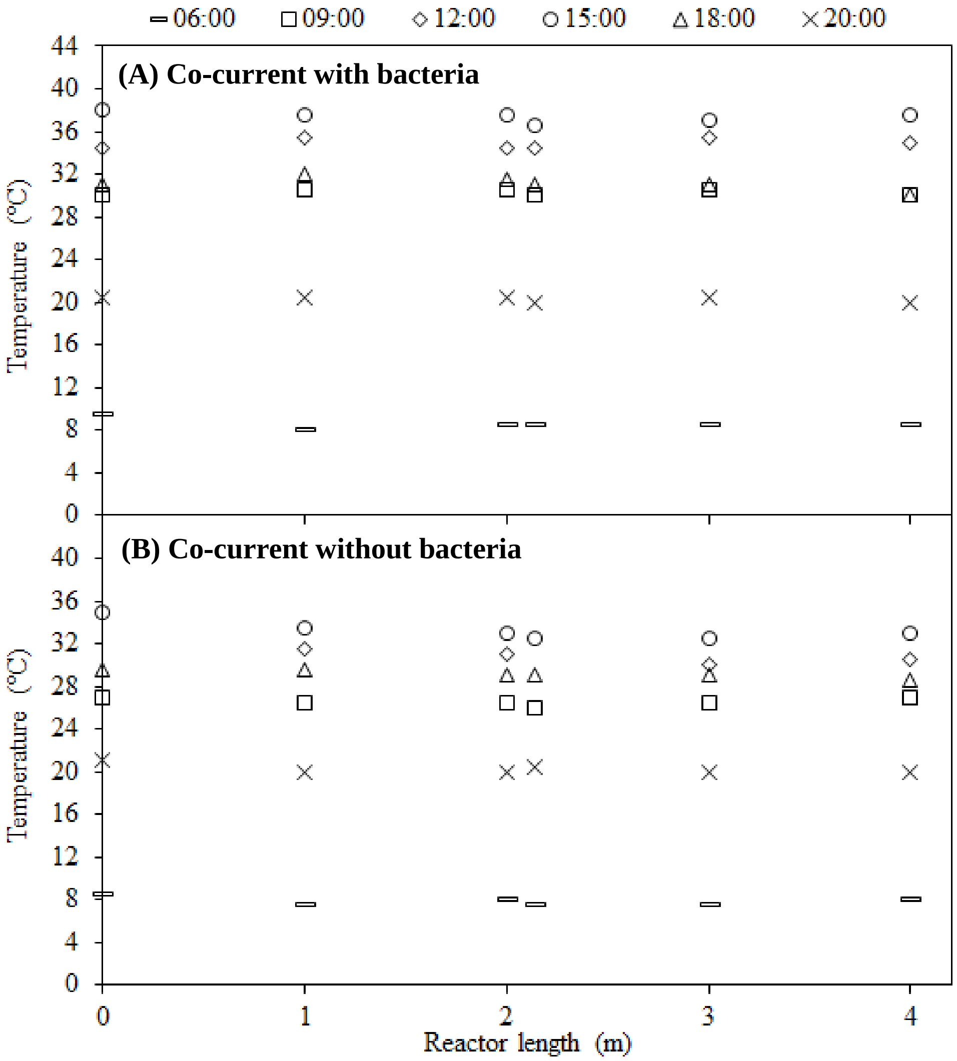

Figure 7.13 The change in the surface temperature along the reactor tube at different times of the day. The experiments were performed on the 5th of August, 2013 using co-currently cooled reactors with and without *Rhodobacter capsulatus* YO3 cultures operated in outdoor conditions. (▭) 06:00, (□) 09:00, (◇) 12:00 p.m., (○) 15:00, (△) 18:00 and (×) 20:00.

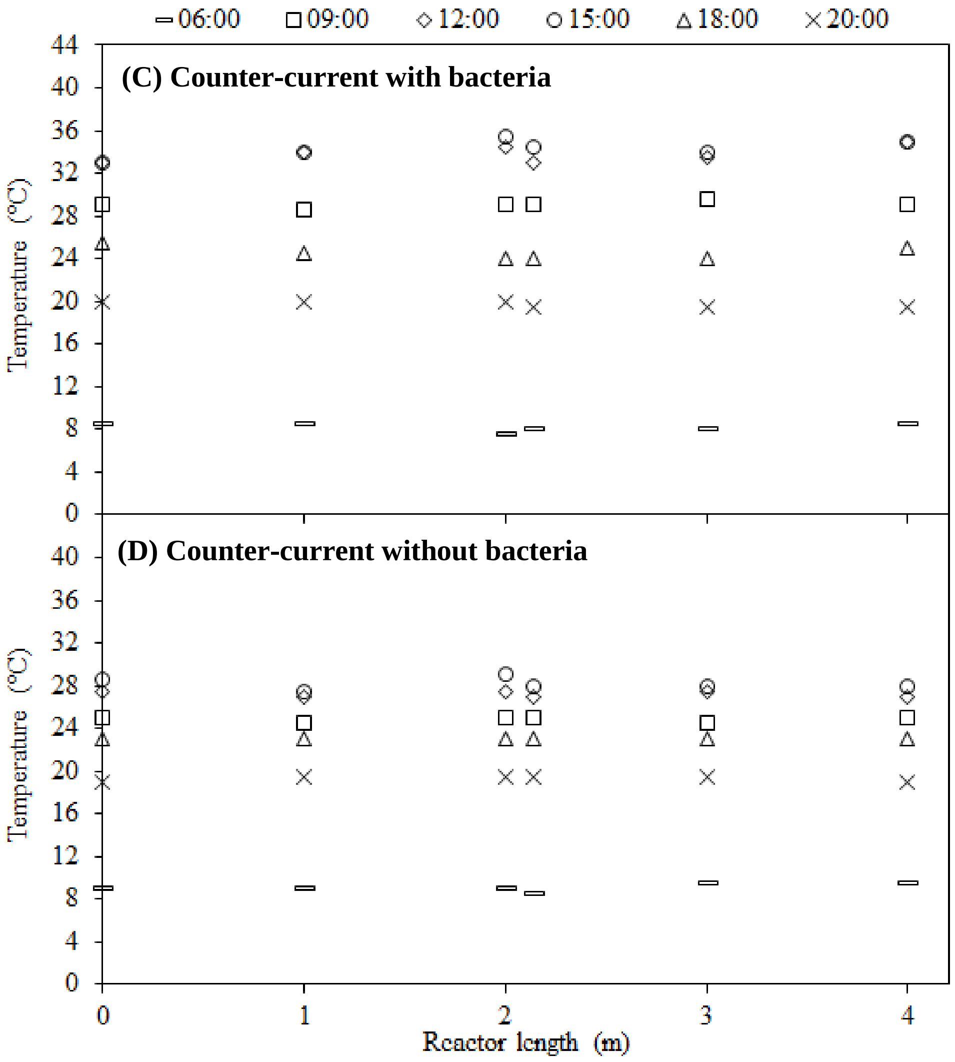

Figure 7.14 The change in the surface temperature along the reactor tube at different times of the day. The experiments were performed on the 5th of August, 2013 using counter-currently cooled reactors with and without *Rhodobacter capsulatus* YO3 cultures operated in outdoor conditions. (▭) 06:00, (□) 09:00, (◇) 12:00 p.m., (○) 15:00, (△) 18:00 and (×) 20:00.

7.3.3 Dynamic Modeling of Temperature Change in the Outdoor Operated Bioreactors

Shown in Figures 7.15 and 7.16 are the comparisons of the variations in the predicted reactor temperatures (T_m), the average reactor temperatures (T_{ave}) and the reactor surface temperatures (T_s) with time. T_{ave} was estimated as the average of the measured reactor inlet and outlet temperatures. T_{ave} and T_s increased up to 30.0 °C within 3 hours after sunrise and then they were kept within 30.0 to 38.0 °C as cooling water ran from the 3rd hour (9 a.m) to the 12th hour (6 p.m) of the experiment. Temperature peaks were observed between the 6th hour (12 p.m.) and the 8th hour (2 p.m.) when the highest solar irradiance (820 W/m^2) was measured.

In Figures 7.15 and 7.16, the reactors with bacteria showed higher $T_{m,}$ T_s and T_{ave} values compared to those without bacteria. The co-currently cooled reactors with bacteria reached a maximum of 38.0 °C (Figures 7.15A), while the co-currently cooled reactor without bacteria had a maximum of 35.5 °C (Figure 7.15B). Maximum temperatures of 36.5 °C were attained in the counter-currently cooled reactor with bacteria (Figure 7.16A) compared the highest value of 30.5 °C in the counter-currently cooled reactor without bacteria (Figure 7.16B).

Also in the experiments performed on the 7th and 8th, $T_{m,}$ T_s and T_{ave} values were higher in the reactors with bacteria than those without and the co-currently cooled reactors exhibited higher temperature value than the counter-currently cooled ones (Appendix J, Figures J.14 to J.17).

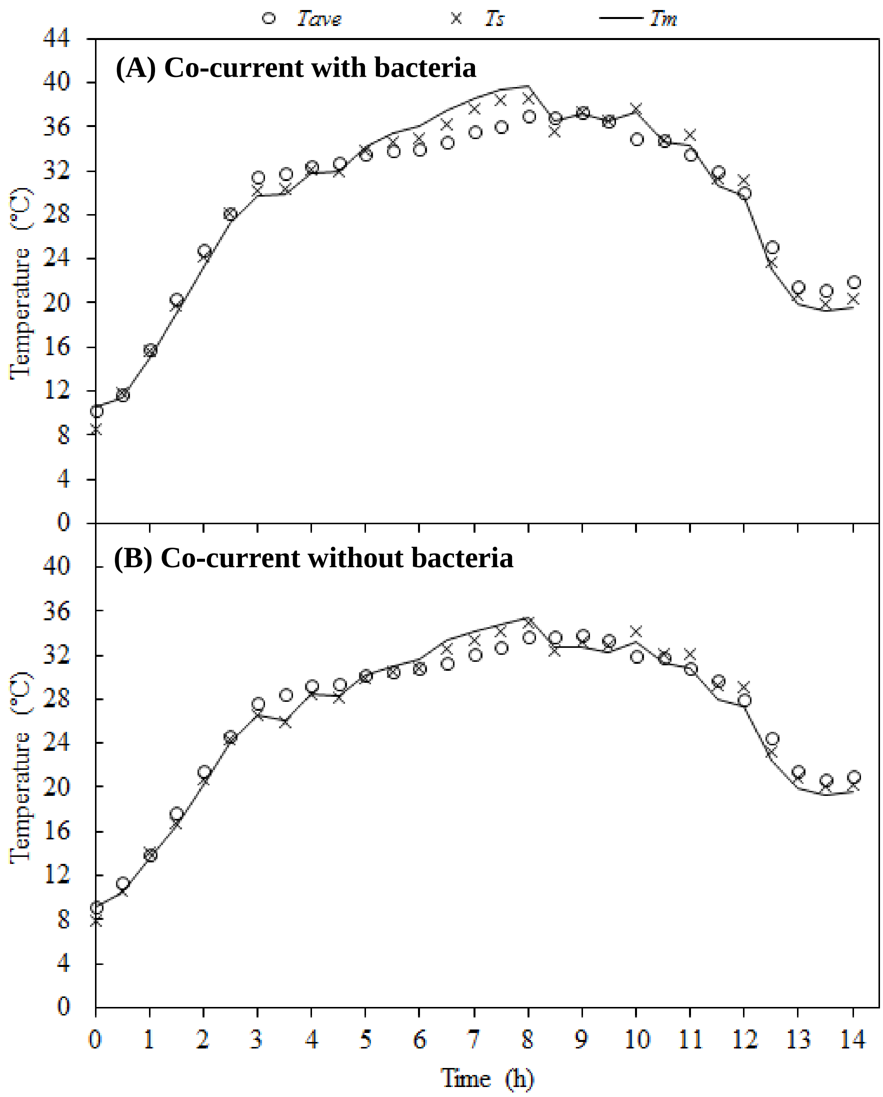

Figure 7.15 Comparison of the changes in the reactor average temperatures T_{ave} (o), the reactor surface temperatures T_s (x) and the predicted (model) temperatures T_m (–) with time. The experiments were performed on the 5th of August, 2013 using co-currently cooled reactors with and without *Rhodobacter capsulatus* YO3 cultures operated in outdoor conditions.

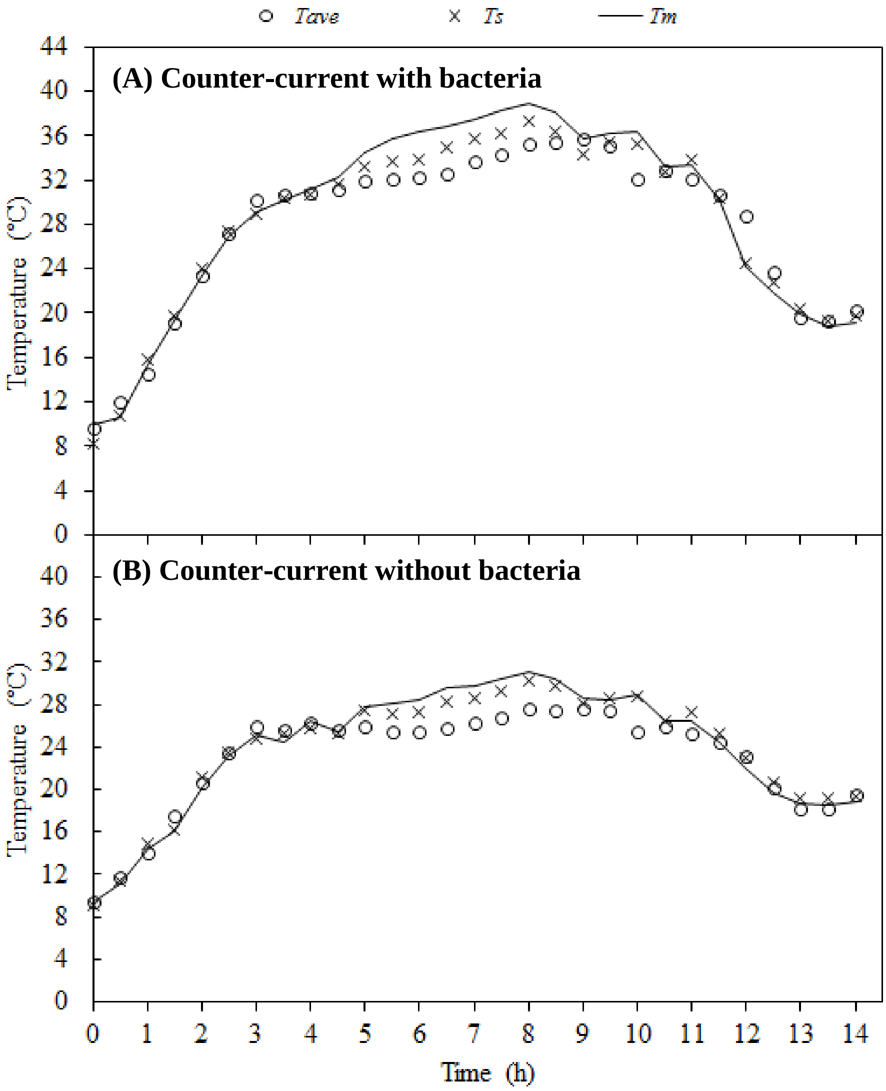

Figure 7.16 Comparison of the changes in the reactor average temperatures T_{ave} (o), the reactor surface temperatures T_s (x) and the predicted (model) temperatures T_m (–) with time. The experiments were performed on the 5th of August, 2013 using counter-currently cooled reactors with and without *Rhodobacter capsulatus* YO3 cultures operated in outdoor conditions.

T_m, T_s and T_{ave} had similar trends during the outdoor experiments (Figures 7.15 and 7.16 and Appendix J, Figures J.14 to J.17). This was confirmed by the comparison of T_s and T_{ave} to T_m in Figures 7.17 and 7.18 (and Appendix J, Figures J.18 to J.21) which illustrate that T_m fit T_{ave} and T_s well within a 10 % error margin. The experimental results showed that T_m was equal to or greater than T_{ave} by 1.0 to 3.2 °C and equal to or greater than T_s by 0.5 to 1.0 °C. These results indicate that the model developed could correctly determine the bulk temperature of the outdoor operated bioreactor at different times of the day. Also, it showed that the assumptions made in simplifying the model were reasonable.

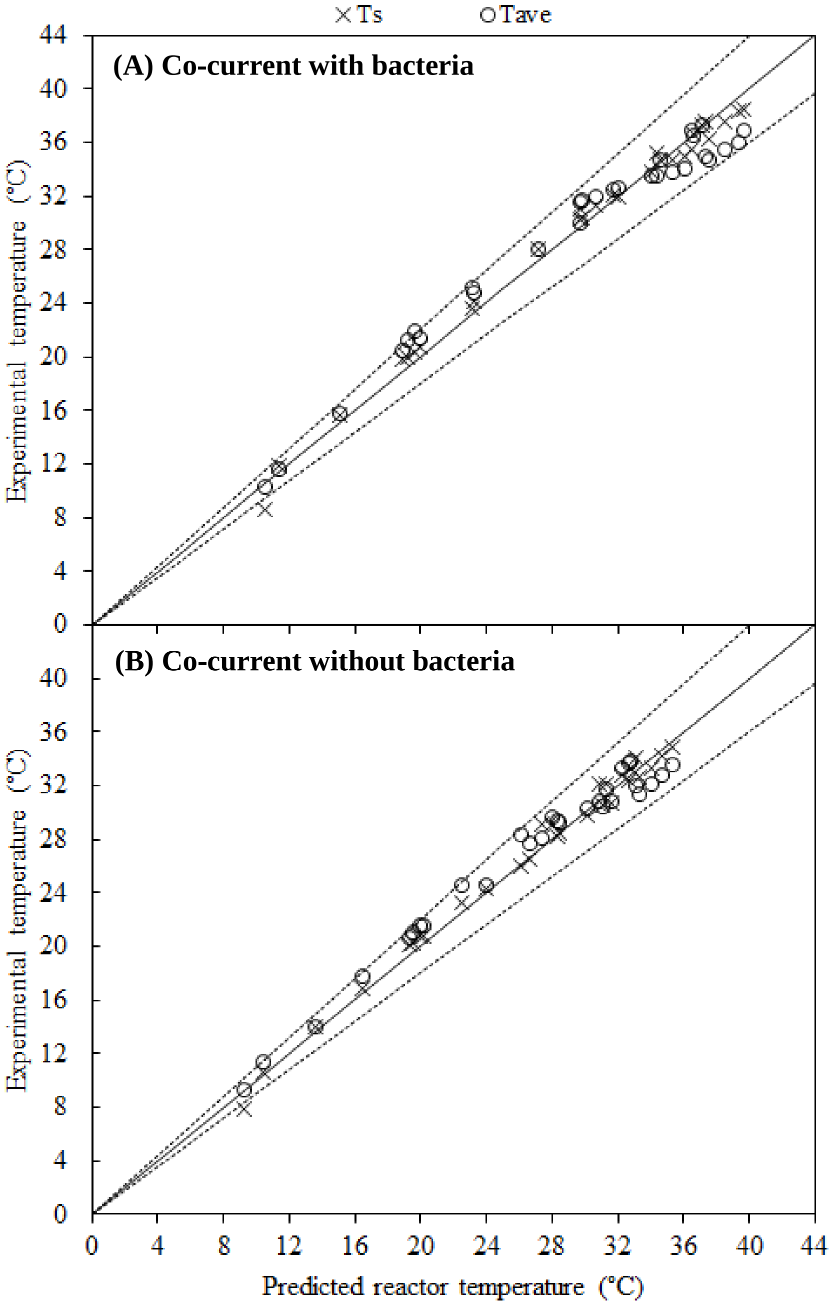

Figure 7.17 Comparisons of the experimental reactor surface temperatures T_s (x) and the average reactor temperatures T_{ave} (o) with the predicted reactor temperatures. The dashed lines (······) indicate the 10 % temperature error margin. The experiments were performed on the 5th of August, 2013 using co-currently cooled reactors with and without *Rhodobacter capsulatus* YO3 cultures operated in outdoor conditions.

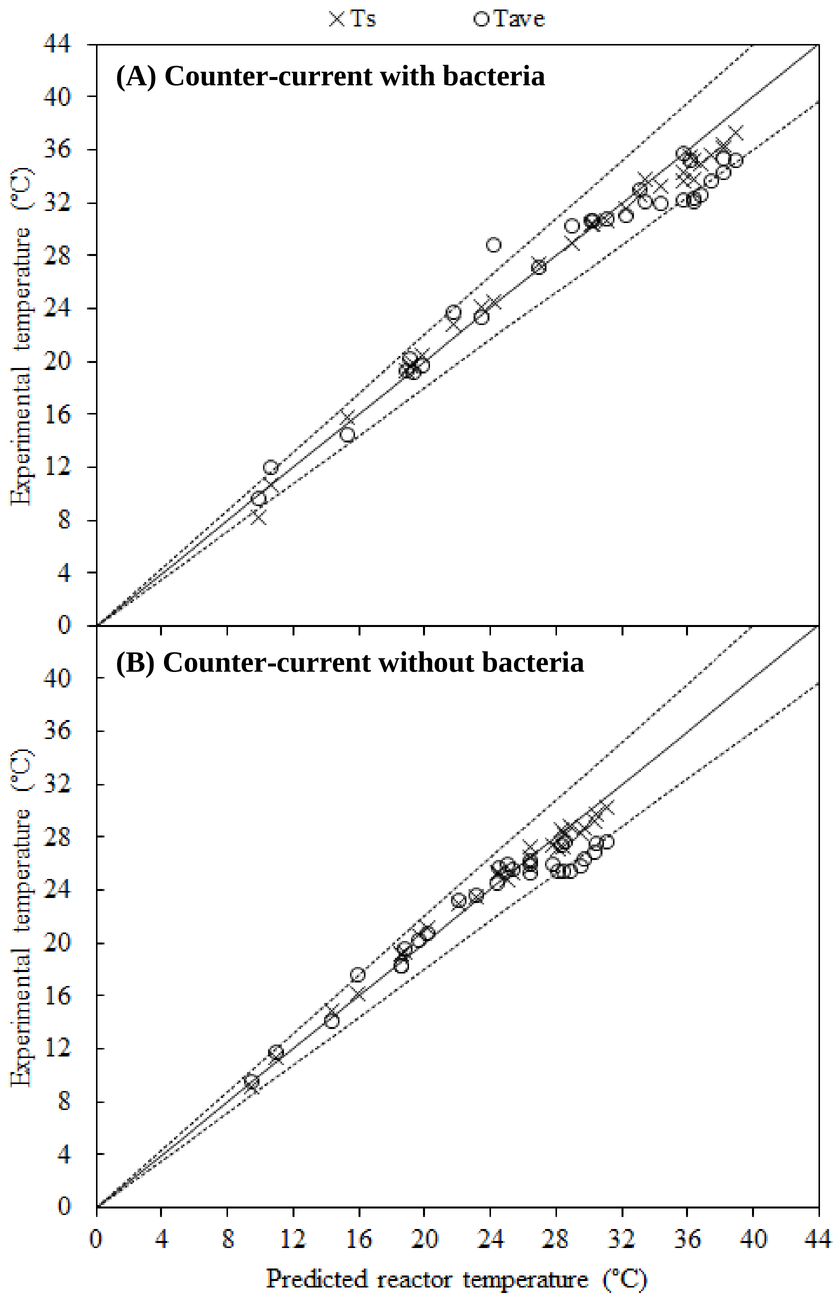

Figure 7.18 Comparisons of the experimental reactor surface temperatures T_s (x) and the average reactor temperatures T_{ave} (o) with the predicted reactor temperatures. The dashed lines (······) indicate the 10 % temperature error margin. The experiments were performed on the 5th of August, 2013 using counter-currently cooled reactors with and without *Rhodobacter capsulatus* YO3 cultures operated in outdoor conditions.

7.3.4 Energy Transfer in the Outdoor Operated Reactors

The energy gained or lost through the different heat transfer mechanisms included in the model is illustrated in Figures 7.19 and 7.20. The values correspond to the total energy transferred in the 14 hour duration of the experiment.

The heat gain to the reactors was mainly through radiative heat transfer from the ground, air, direct sunlight and the energy absorbed by the medium in the reactor. Since the experiments were performed on the same day, the energy transferred through radiation did not vary among the reactors (Figure 7.19 and 7.20). The ground radiation ($\dot{Q}_{rad,g}$) (82.1 – 82.7 W), air radiation ($\dot{Q}_{rad,a}$) (79.0 W), direct solar radiation ($\dot{Q}_{rad,D}$) (50.1 W), diffuse solar radiation ($\dot{Q}_{rad,d}$) (15.4 W), reflected ground radiation ($\dot{Q}_{re,g}$) (8.5 W) and reflected air radiation ($\dot{Q}_{re,a}$) (7.9 W) were identical in all the reactors. The highest heat gain was through $\dot{Q}_{rad,r}$, which varied between 178.7 and 193 W, indicating that not all the energy absorbed by the medium in the reactors was emitted to the surroundings. This showed that the assumption that the medium in the reactor was opaque (emissivity equals absorptivity) was not precise. The degree of radiative energy received by the reactors was in the order $\dot{Q}_{rad,r} > \dot{Q}_{rad,r} > \dot{Q}_{rad,a} > \dot{Q}_{rad,D} > \dot{Q}_{rad,d} > \dot{Q}_{re,g} > \dot{Q}_{re,a}$.

During the day, the temperatures of the air and ground were shown to increase with increasing solar irradiance (Figure 7.10). This resulted in the air and ground warming up and imparting radiative energy to the surface of the reactors. Considering that air has poor thermal conductivity (about 0.0268 W/m/K at 37.0 °C) and the contact area between the ground and reactor was small (0.02 m^2), heat transfer from the ground by conduction was negligible. Total energy of about 79.0 W was gained by air radiation and 82.1 – 82.7 W by ground radiation (Figure 7.19 and 7.20).

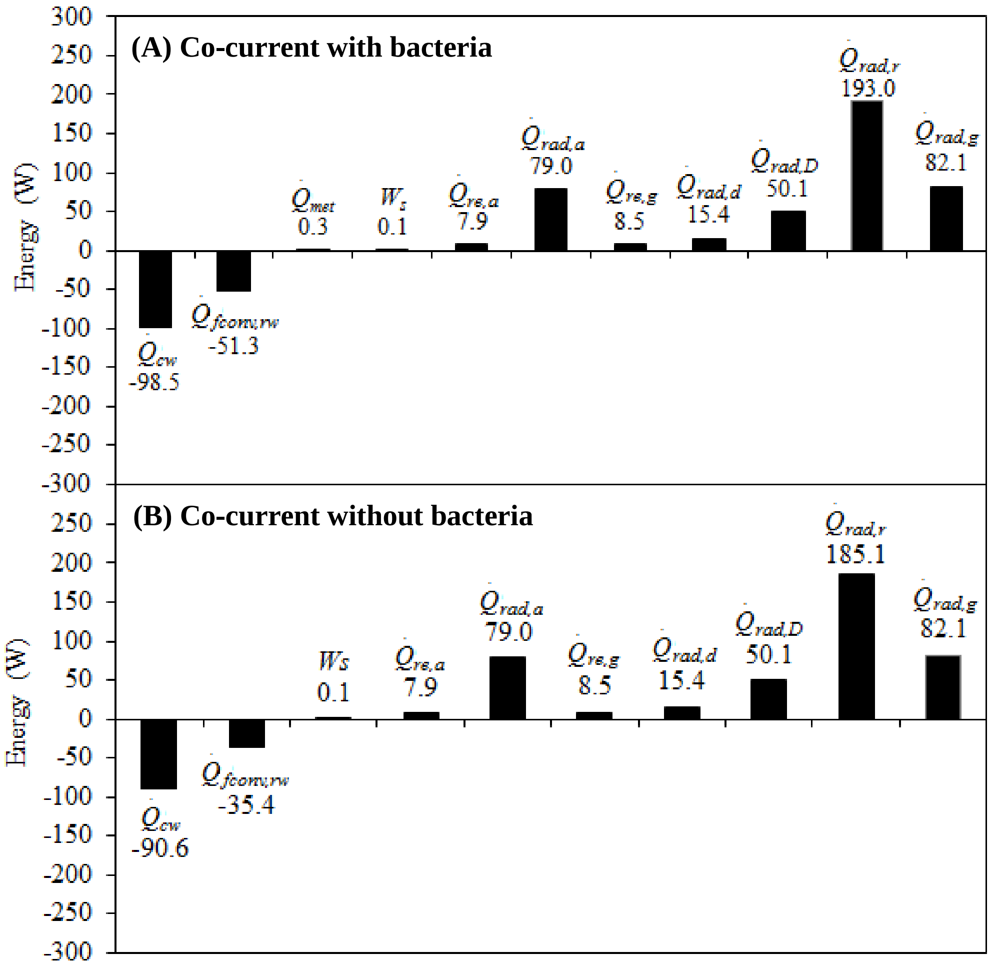

Figure 7.19 Comparison of the energy gained or lost during the day time in the outdoor operated reactors. The experiments were performed on the 5th of August, 2013 using co-currently cooled reactors operated outdoors with and without *Rhodobacter capsulatus* YO3 cultures.

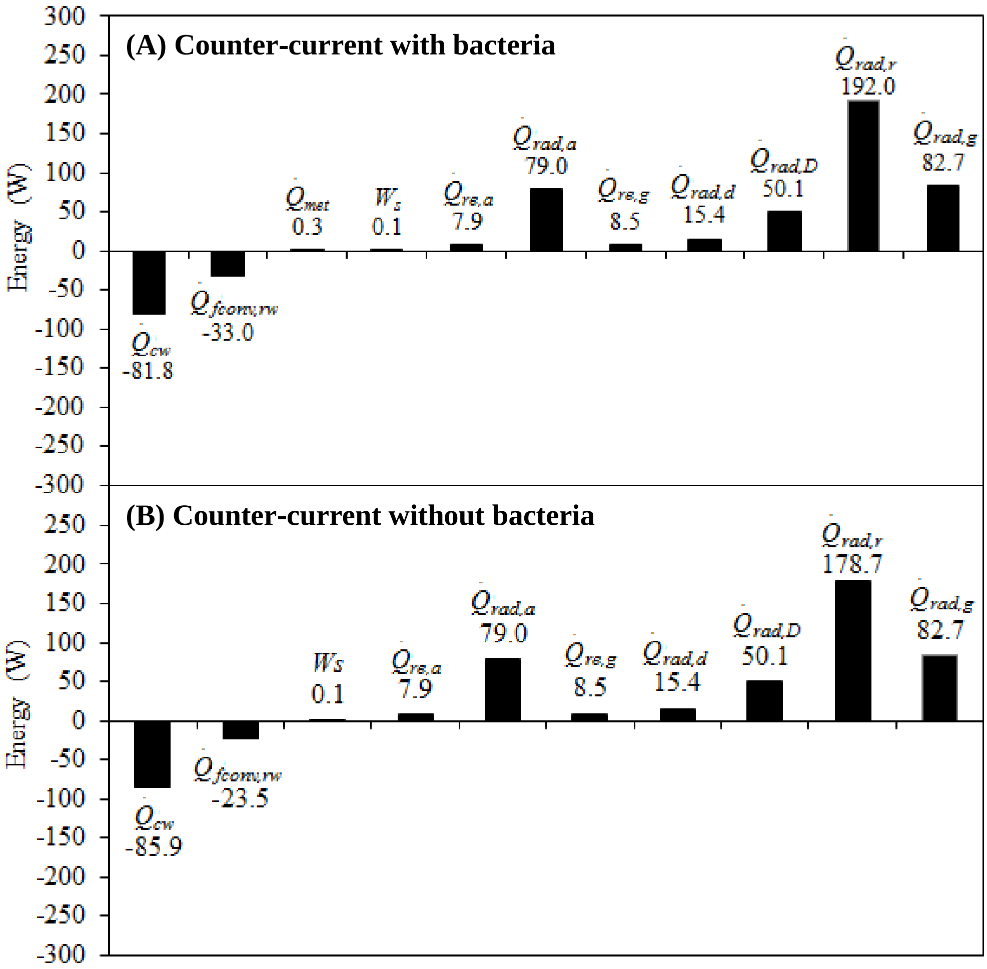

Figure 7.20 Comparison of the energy gained or lost during the day time in the outdoor operated reactors. The experiments were performed on the 5th of August, 2013 using counter-currently cooled reactors operated outdoors with and without *Rhodobacter capsulatus* YO3 cultures.

The experiments were carried out on a clear sky day and so most of the solar energy received was from direct solar radiation ($\dot{Q}_{rad,D}$) as opposed to diffuse solar radiation ($\dot{Q}_{rad,d}$) as seen in Figures 7.19 and 7.20. In calculating the amount of diffuse radiation, the clearness index for Ankara that was reported to be 0.74 (Çağlar *et al.* 2013) was used to estimate the fraction of diffuse radiation (K_d)

reaching the ground. K_d was estimated to be 0.18 using the relation given by Liu and Jordan (1960) (Equation 4.12), therefore resulting in less diffuse solar radiation (15.4 W) compared to the direct solar radiation (50.1 W). Generally, K_d ranges between 0.1 and 0.3 (Liu *et al.* 1960, Bechet *et al.* 2010).

The heat lost from the reactors was mainly through the cooling water ($\dot{Q}_{cw}$) and through forced convection ($\dot{Q}_{fconv,rw}$). $\dot{Q}_{cw}$ ranged between -81.8 W and -98.5 W and $\dot{Q}_{fconv,rw}$ varied between -23.5 W and -51.3 W. The co-currently cooled reactor had the higher cooling duties compared to the counter-current reactors reactor temperature (Figure 7.19 and 7.20). The cooling duties in the reactors with bacteria were more than in those without bacteria because of the energy absorption by the microorganisms.

The reflected air radiation $\dot{Q}_{re,a}$ (8.5W), reflected ground radiation ($\dot{Q}_{re,g}$) (7.9 W), the rate of shaft work (W_s) (0.1 W) and the amount heat required by the bacteria for its metabolic activities ($\dot{Q}_{met}$) (0.3 W) were the same in all the reactors (Figures 7.10 and 7.20). They were negligible as they accounted for less than 1.5% of the heat gained by the systems. Most of $\dot{Q}_{met}$ was used for hydrogen production (59% and 50% in the co-current and counter-currently cooled reactors, respectively) and the remainder was utilized for other cellular activities such as growth, maintenance and by-product formation. Hydrogen production is an energy demanding process – 4 ATPs are required for formation of hydrogen by the nitrogenase enzyme (Koku *et al.* 2002).

There was a net heat gain to the systems in Figures 7.19 and 7.20 - the amount of energy gained was more than the amount of heat lost. The net heat gain in each reactor during the daytime was 280 to 320 W. This heat might be lost to the surroundings during the night as the ambient temperatures decrease. The experiments performed on the 7th and 8th gave similar results as shown in Appendix J, Figures J.22 to J.25.

The results in the present study emphasize the necessity for thermal control, especially in areas with high solar radiation and air temperature. Excess sunlight energy could not only result in temperature increase of the reactor, but also photoinhibition. The use of light shade bands (Wakayama and Miyake, 2002, Adessi *et al.* 2012) and special mirrors that reflect or absorb near-infrared heat-generating wavelengths (Goetz *et al.* 2011) has been suggested to reduce excessive sunlight. On the other hand, the high amount of energy received by the reactor from ground radiation could be alleviated by placing the reactors in a stand (preferably with hooks to support the glass tubes) above the ground instead of placing them on a hard surface that is likely to heat up and conduct or emit energy to the reactor.

The model developed in this study was based on that of Bechet *et al.* 2013, but there are important differences to account for the metabolic heat generated by the bacteria, geometry and operation of the tubular reactor. Bechet *et al.* 2013 developed a mechanistic model for a column reactor used to grow the microalgae *Chlorella sorokiniana*. In their model, they considered evaporation, conduction and cooling by air bubbling and neglected the metabolic heat of the bacteria. In the present work, a tubular system was used to grow and produce hydrogen using the PNSB *R.capsulatus* YO3, and the metabolic heat and shaft work were considered, while conduction was neglected since the contact area between the reactor tubing and the ground was small. Also, the energy transfer in reactors with and without bacteria was compared. Similar to Bechet *et al.* 2013, radiation from the ground, radiation from the air, radiation from the reactor, solar radiation (diffuse and direct) and convection influenced the reactor temperature.

The accuracy of the model developed might be affected by several issues. For example, the assumption that the bodies are gray and diffuse surfaces (that is their emissivity is independent of direction and wavelength of radiation) could lead to calculation errors as radiation is a complex phenomenon. Actually the bodies are real surfaces and are characterized by emissivity that is not constant, but varies with temperature, wavelength and direction of radiation (Çengel, 1998). The gray and diffuse surface assumption is made to the simplify calculations. Also, the sensitivity of the measuring equipment such thermocouples and pyranometer are other sources of discrepancies in developing the model. Furthermore, since the experiments were performed in outdoor conditions, the reactor surface was exposed to dust, which could decrease light transmittance through the reactor glass surface.

7.3.5 Comparison of the Overall Heat Transfer Coefficients

A comparison of the overall heat transfer coefficients between the culture and cooling water (U_{co}) is shown in Figure 7.21. The average U_{co} varied between 60 and 145 W/m/K. The average values of the convective heat transfer coefficients between the medium in the reactor and the outer surface of the cooling tube (h_{co}) and the convective heat transfer coefficients between the cooling water and the inner surface of the cooling tube (h_{ci}) is shown in Table 7.3. The values of h_{co} are found to range between 54 and 118 W/m^2/K, while h_{ci} varied between 515 and 524 W/m^2/K.

Shown in Table 7.4 are the minimum and maximum resistances involved in calculating the overall heat transfer coefficients in the experiments. The values were calculated using Equation (4.54). The order of thermal resistances was $R_o < R_{wall} < R_i$. This indicated that U_{co} was dominated by the convective heat transfer between the medium in the reactors and the cooling tube outer surface, then the wall resistance and then resistance to the convective heat transfer from the inner surface of the cooling tube and the cooling water. These results were reasonable in that the medium in the reactor was circulated at lower velocity (Re =160) compared to the velocity of the cooling water (Re = 2700). Low flow rates increase film layer formation causing further resistance to heat transfer, while higher flow result in reduced film layer formation and less resistance to heat transfer as demonstrated in the results.

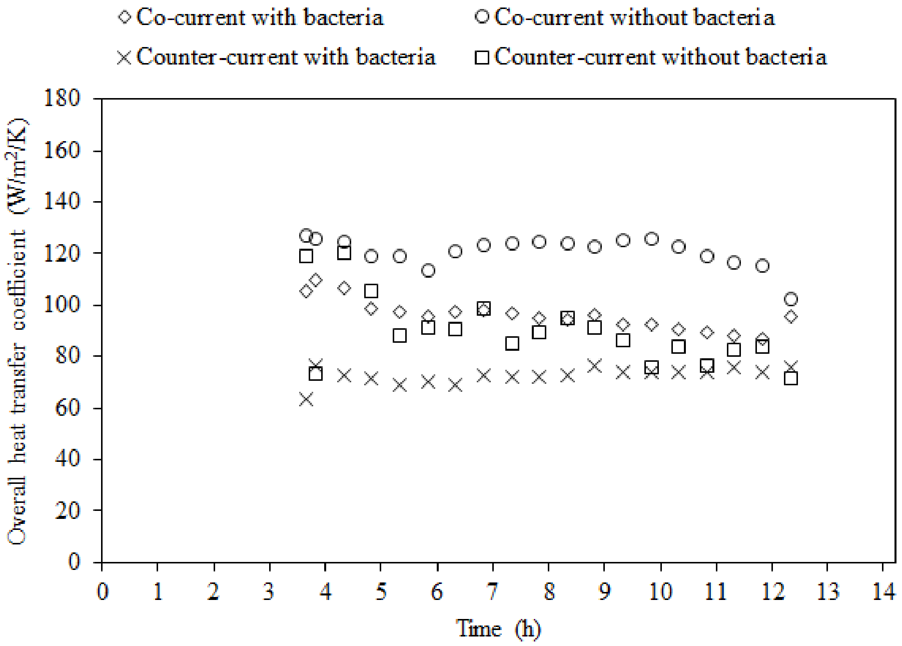

Figure 7.21 Comparison of the overall heat transfer coefficients between the medium in the reactors and the cooling water. The experiments were performed on the 5th of August, 2013, using reactors with and without *Rhodobacter capsulatus* YO3.

Table 7.3 The average values of the convective heat transfer coefficients between the reactor medium and the outer surface of the cooling tube (h_{co}) and the cooling water and the inner surface of the cooling tube (h_{ci}).

Date	**Reactor**	h_{co} **(W/m^2/K)**	h_{ci} **(W/m^2/K)**
05.08.2013	Co-current with bacteria	95	520
	Co-current without bacteria	65	520
	Counter-current with bacteria	108	516
	Counter-current without bacteria	72	516
07.08.2013	Co-current with bacteria	98	521
	Co-current with bacteria	74	518
	Counter-current with bacteria	118	516
	Counter-current without bacteria	54	524
08.08.2013	Co-current with bacteria	97	520
	Co-current with bacteria	72	520
	Counter-current with bacteria	109	515
	Counter-current without bacteria	66	517

Table 7.4 The minimum and maximum values of the thermal resistances between the reactor medium and the outer surface of the cooling tube (R_o), the cooling tube wall (R_{wall}) resistance and the thermal resistance between the cooling water and the inner surface of the cooling tube (R_i).

	R_o **(W/K)**	R_{wall} **(W/K)**	R_i **(W/K)**
Minimum	0.1	0.07	0.03
Maximum	0.2	0.07	0.03

CHAPTER 8

PHOTOFERMENTATIVE HYDROGEN PRODUCTION BY RHODOBACTER CAPSULATUS IN OUTDOOR OPERATED PHOTOBIOREACTORS

In this study photofermentative hydrogen production by *Rhodobacter capsulatus* YO3 cultures grown in bioreactors operated outdoors was investigated. The bioreactors were co-currently and counter-currently cooled and the biomass growth and hydrogen production modeled.

8.1 Growth and Hydrogen production by R.capsulatus YO3 in Outdoor Conditions

Shown in Figure 8.1 are the changes in the concentrations of biomass, the cumulative hydrogen produced and the concentrations of acetic acid in the outdoor operated reactors, with time. The biomass concentrations doubled during the 14 h experiment time (Figure 8.1A) – the initial biomass concentration of 0.55 gDCW/L increased to about 1.2 gDCW/L, irrespective of whether the system was co-current or counter-current. The rapid growth of the bacterial cells could be attributed to the presence of enough sunlight energy, controlled temperature and sufficient nutrients and optimum C/N ratio in the feed. The reactors were exposed to high light energy (maxima of 820 W/m^2) during the day (Table 7.2). Previous studies have shown that light intensities of about 300 W/m^2 to be optimum for growth of the photosynthetic bacteria (Uyar *et al.* 2007, Sevinç *et al.* 2012, Androga *et al.* 2013). The high cell proliferation could also be attributed to the use of optimum C/N of 25 (feed containing 40 mM acetic acid and 4 mM glutamate). Androga *et al.* (2011b) investigated the effects of changing the C/N ratio on the long-term stability of biomass growth and hydrogen production using feed containing different acetate (40 – 80 mM) and glutamate (2 – 4 mM) concentrations. They achieved stable

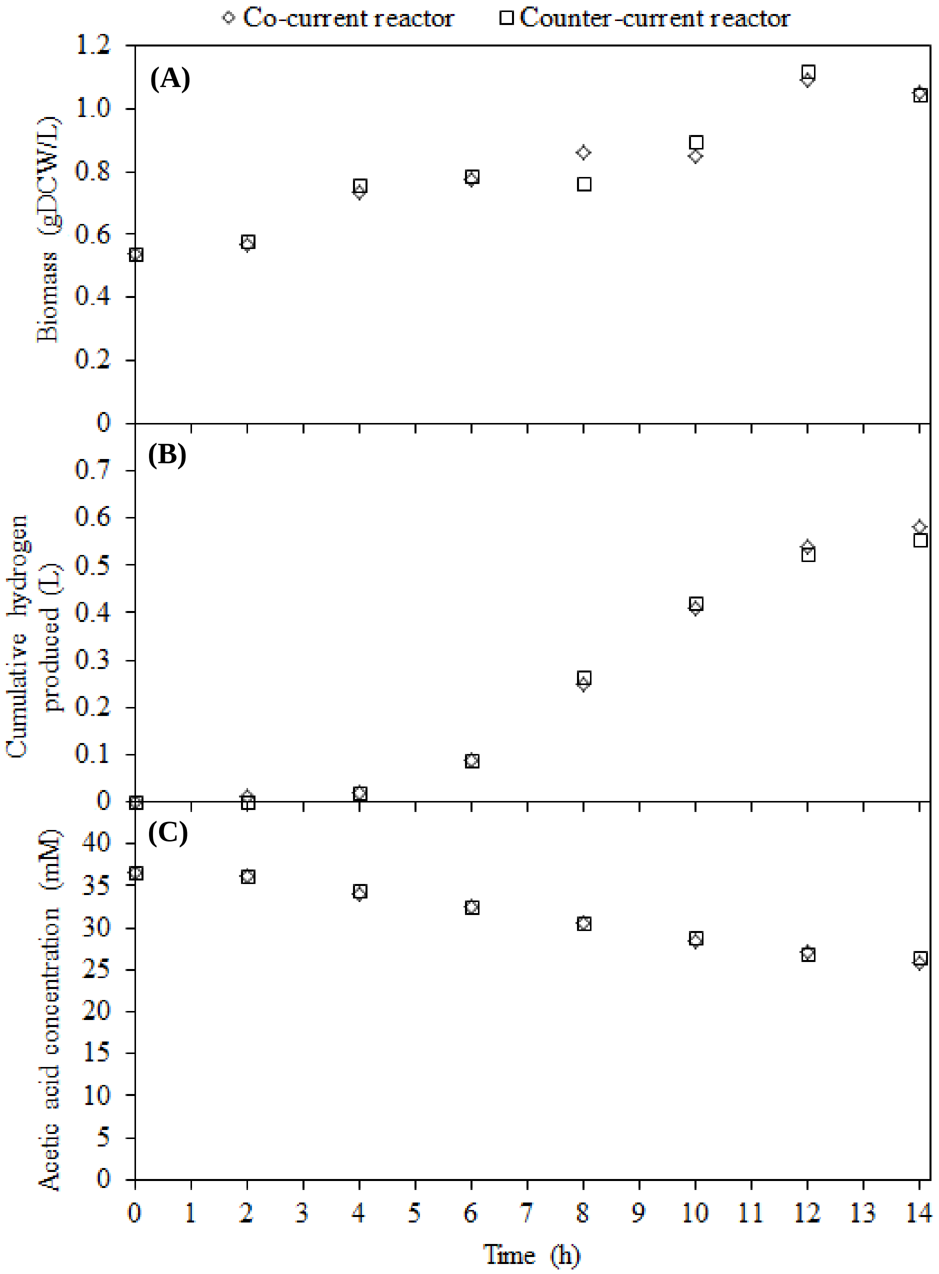

Figure 8.1 The change in the biomass concentration, the cumulative hydrogen production and acetic acid concentration in the outdoor reactors with time. The experiments were performed on the 5th of August, 2013 using reactors operated outdoors with and without *Rhodobacter capsulatus* YO3 cultures. (A) Biomass growth, (B) Cumulative hydrogen produced and (C) Acetic acid consumption. (◊) Co-currently cooled reactor and (□) Counter-currently cooled reactor.

biomass of 0.4 gDCW/L and maximum hydrogen production rate of 0.66 mol/m^3/h using medium containing 40 mM acetate and 4 mM glutamate (corresponding to C/N of 25) for over 20 days. During the experiments, the pH varied between 6.8 and 7.1, which is in the range specified for optimum biomass and hydrogen production (Nath and Das, 2009).

Shown in Figures 8.1B is the average cumulative hydrogen produced by the bacteria culture in the co-current and counter-current reactors. It is seen that similar amounts of hydrogen were producted in the co-current and counter-currently cooled reactors. The highest cumulative hydrogen of 0.58 L was produced in the co-currently cooled reactor and 0.55 L was produced in the counter-currently cooled reactor during the experiments performed (Figure 8.1B, Table 8.1).

Acetic acid consumption by *R.capsulatus* cultures in the reactors is shown in Figures 8.1C. It is seen that about 10 mM of acetic acid was consumed by the bacteria during the experiments. The acetic acid concentration was reduced from the initial 36 to about 26 mM in both reactors. The starting concentrations were not exactly 40 mM due to sampling errors. During the experiments, acetic acid was efficiently used for growth and hydrogen production by the PNSB. Being a central intermediate in the overall carbon cycle, it is a prime substrate for hydrogen production by the photofermentative bacteria (Segers *et al.*, 1981). It was consumed following the first order rate kinetics as confirmed by the high coefficient of determinations in Table 8.1 and Figures J.29 to J.31 in Appendix J. These results are in agreement with the findings of Özgür *et al.* (2010) who investigated acetic acid consumption rate using different initial concentrations and reported that below 40 mM initial concentration, the bacteria consumed the organic acid following the first order kinetics while above 40 mM it was consumed using second order kinetics. In studies using a mixture of lactic acid and acetic acid, Sevinç *et al.* (2012) reported that *R.capsulatus* DSM 1710 cells consumed acetic acid using zero order kinetics and shifted to first order kinetics when most of the lactic acid had been depleted.

Table 8.1 The rate constants for acetic acid consumption and the coefficient of determination values (R^2) for the *Rhodobacer capsulatus* YO3 cultures grown on media containing 40 mM acetic acid reactors as carbon source and 4 mM sodium glutamate as nitrogen source.

Date	**Reactor**	***k* (1/h)**	***R^2***
05.08.2013	Co-current	0.024	0.98
	Counter-current	0.023	0.97
07.08.2013	Co-current	0.021	0.97
	Counter-current	0.022	0.97
08.08.2013	Co-current	0.018	0.96
	Counter-current	0.022	0.99

Table 8.2 gives a summary of the distribution of acetic acid consumption for biomass formation and hydrogen production consumption and glutamate consumption during the experiments. Estimations were done based on the stoichiometric coefficients that were determined from elemental balances given in Appendix. The balance equations for hydrogen production (Equation 4.37) and biomass formation (Equation 4.38) were used in the calculations.

Analyzing the distribution of the acetic acid consumption given in the Tables 8.2, most of the acetic acid was used for growth (49 %), then for biosynthesis and maintenance (31 %) and the remaining for hydrogen production (20 %). Abundant light energy and optimal feed conditions during the experiments might have resulted in the high consumption of acetic acid for growth. This was confirmed by the doubling of initial biomass during the experiments (Figures 8.1A). The high biomass concentration meant higher demand of acetate for maintenance and other biosynthesis activities. Most of the glutamate fed was consumed for growth (86 %). This indicated that the assumption that the glutamate fed was only used for growth was reasonable. The remaining glutamate amount could have been utilized for cellular metabolic activities such as hydrogen production and by-product formation. *R.capsulatus* contains the Fe-Mo and Fe-Fe nitrogenase enzymes for nitrogen fixation and all the glycolytic genes (for both the Embden–Meyerhoff and Entner–Doudoroff pathways) necessary for carbohydrate metabolism (Haselkorn et al. 2001). The results found in this study were similar to those of Boran *et al.* (2012a), who reported that about 40% of acetic acid was utilized for biomass growth, 12 % for hydrogen production and the remaining 48% for biosynthesis and maintenance.

The repeated experiments performed on the 7th and 8th of August, 2013 had similar biomass growth trend as the observed in the experiments performed on the 5th of August, 2013. The initial biomass of about 0.55 gDCW/L doubled during the experiments (Figures J. 27A and J.28A, Appendix J). However, the experiments performed on the 7th and 8th of August had lower cumulative hydrogen production (0.35 L and 0.38 L), (Figure J. 27B and I.28B, Table J.1 and Table J.2) because of the varying outdoor conditions and differences such as the age of the inoculants used. About 10 mM of acetic acid was consumed by the bacteria during the experiments (Figures J.27 B and J.28B) - The organic acid concentration was reduced from the initial 37 to about 27 mM.

Table 8.2 Summary of the results showing the acetic acid and glutamate consumption for growth, maintenance and hydrogen production by *Rhodobacter capsulatus* YO3. The experiment was performed on the 5th of August, 2013.

	Co-currently cooled reactor	**Conversion (%)**	**Counter-currently cooled reactor**	**Conversion (%)**
Biomass formed (mol)	0.072	n/a	0.071	n/a
Hydrogen formed (mol)	0.027	n/a	0.026	n/a
Acetic acid consumed (mol)	0.034	n/a	0.032	n/a
• Hydrogen (mol)	0.007	20	0.006	20
• Growth (mol)	0.017	49	0.016	51
• Biosynthesis and maintenance (mol)	0.011	31	0.0096	30
Glutamate consumed (mol)	0.010	86	0.0099	84
Cumulative hydrogen produced (L)	0.58		0.55	n/a

n/a not applicable.

8.2 Modeling of Growth and Hydrogen Production by *Rhodobacter capsulatus* YO3

8.2.1 Modeling the Growth *Rhodobacter capsulatus* YO3

Shown in Table 8.3 are the constants obtained from fitting the biomass growth using the logistic model (Equation 4.52) with 95% confidence bounds. Since the biomass growth in the co-current and counter-current reactors were similar (Figure 8.1, Appendix J, Figures J.27 and J.28), their average values were used in modeling.

Table 8.3 Logistic model parameters and the coefficient of determination values (R^2) for the growth *Rhodobacter capsulatus* YO3 cultures grown on media containing 40 mM acetic acid reactors as carbon source and 4 mM sodium glutamate as nitrogen source in outdoor conditions.

Date	**Reactor**	X_o **(gDCW/L)**	X_{max} **(gDCW/L)**	k_c **(1/h)**	R^2
05.08.2013	Co-current	0.53	1.49	0.11	0.94
	Counter-current	0.54	1.74	0.09	0.90
07.08.2013	Co-current	0.45	1.10	0.17	0.98
	Counter-current	0.46	1.32	0.13	0.99
08.08.2013	Co-current	0.48	1.31	0.13	0.99
	Counter-current	0.51	1.27	0.13	0.99

The results showed that the model fit the experimental values with good accuracy as the goodness of fit (R^2) was high in all the reactors. This was confirmed by the plots in Figure 8.2.

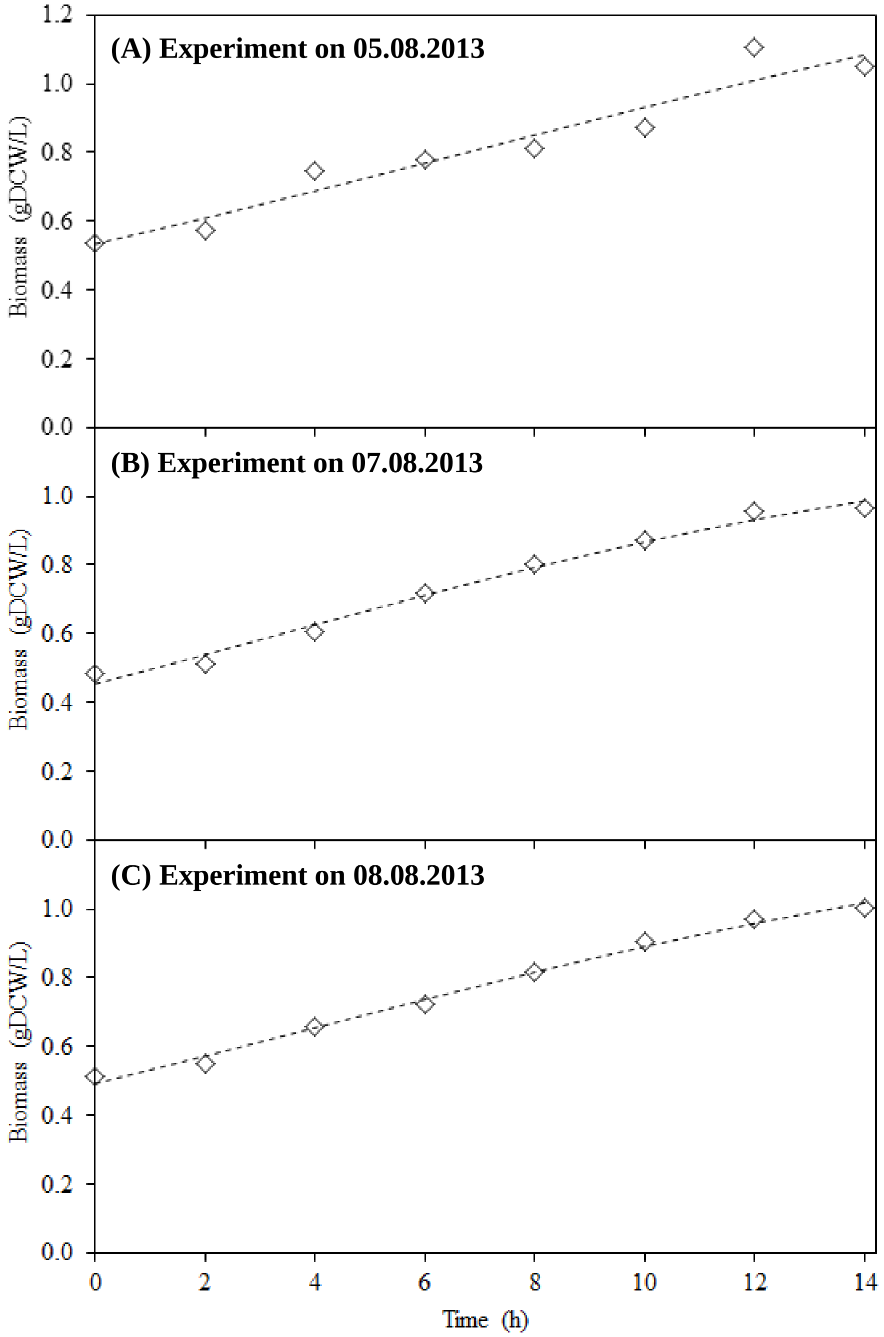

Figure 8.2 Comparison of the experimental and predicted biomass growth in the outdoor operated reactors. (◊) Experimental value and (----) predicted value using the logistic model.

High apparent growth rates (k_c) were observed, ranging between 0.09 – 0.17 h^{-1}. These values were higher than the 0.086 h^{-1} previously reported for outdoor experiments using *R.capsulatus* (Boran, 2011). Differences could be due to the type of feed, the reactor geometry and operating conditions. The experiments were also performed at different periods, so physical conditions like temperature and solar light energy received varied.

8.2.2 Modeling the Hydrogen Production by *Rhodobacter capsulatus* YO3

Shown in Table 8.4 are the constants obtained from fitting the cumulative hydrogen produced using the modified model (Equation 4.53) with 95% confidence bounds. Since the cumulative hydrogen produced in the co-current and counter-current reactors were similar (Figure 8.1 to 8.3), their average values were used in modeling.

Table 8.4 Modified Gompertz model parameters and the coefficient of determination values (R^2) for the cumulative hydrogen produced by *Rhodobacter capsulatus* YO3 cultures in outdoor conditions.

Date	**Reactor**	H_{2max} **(mol/m^3)**	R_{max} **(mol/m^3/h)**	λ **(h)**	R^2
05.08.2013	Co-current	9.2	1.2	5.2	0.99
	Counter-current	8.4	1.3	5.2	0.99
07.08.2013	Co-current	5.6	1.1	5.8	0.99
	Counter-current	5.5	1.1	5.8	0.99
08.08.2013	Co-current	5.1	0.9	5.9	0.99
	Counter-current	5.6	1.0	6.0	0.99

The results indicated that the model fit the experimental values with good accuracy as the goodness of fit (R^2) was high in all the reactors. This is confirmed by the plots Figure 8.3, which show sigmoidal shapes with lag phases and stationary phases for hydrogen production. The lag-phases occurred as the culture cells acclimated to the outdoor conditions. Long hydrogen production lag phases (5.2 to 6 h) were predicted by the model (Table 8.4). The extended lag phase durations are detrimental to hydrogen production as they reduce the period for hydrogen production. In this study, the problem of long lag phase could be alleviated by several options. Firstly, the inocula used could be taken from mid-exponential phase, where the cells are actively dividing, instead of the late-exponential or stationary phase. The age and past growth history of the culture has been reported to have a significant impact on hydrogen production rate. Inocula cells got from the exponential phase were found to produce hydrogen better than those taken from the stationary phase (Koku *et al.* 2003). In this study, inocula cells from either late-exponential or early-stationary phase were used. Secondly, using inocula acclimated to outdoor conditions would improve hydrogen production. The inocula cells were grown in indoor conditions under controlled temperature and light intensity, using growth medium containing 20 mM acetate and 4 mM glutamate. Despite having been acclimated to acetate and glutamate in the growth medium, they require time to adapt to the fluctuating temperature and light intensity in outdoor conditions. Fluctuating temperatures and light intensities in outdoors have been shown to greatly influence growth and hydrogen production (Özgür *et al.* 2010). Reduction of the lag phase by prior acclimation of inocula to outdoor conditions would increase the total amount of hydrogen produced during the day.

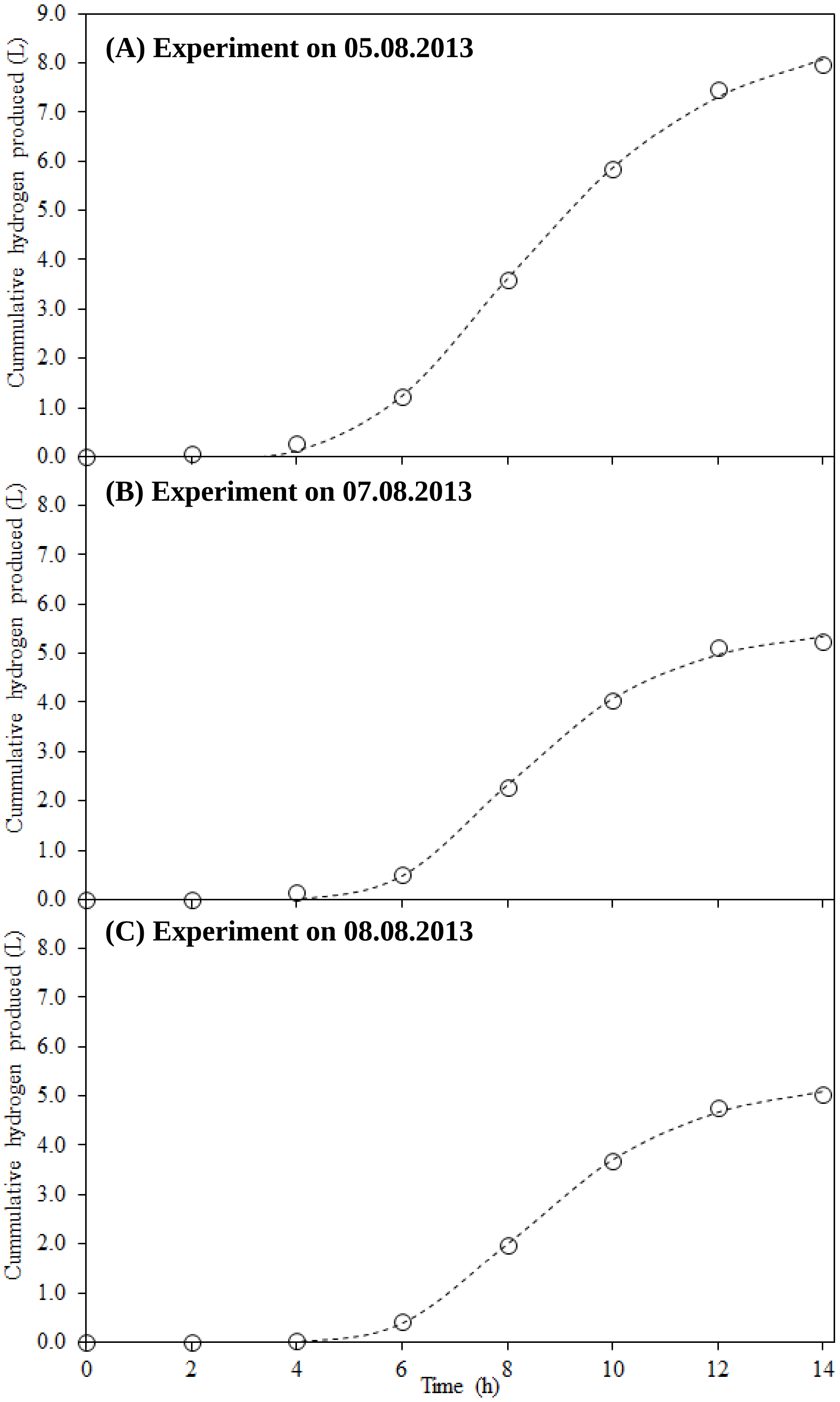

Figure 8.3 Comparison of the experimental and predicted biomass growth in the outdoor operated reactors. (○) Experimental value and (----) predicted value using the logistic model.

8.3 Comparison of Hydrogen Production Studies in Outdoor Conditions

Over the years, advances in photofermentative hydrogen production have been made using different microoganisms grown in various reactor geometries and feed media. The studies were mostly performed in semi-pilot scale reactors operated in outdoor conditions under the natural sunlight (Adessi and De Philippis, 2014). Figure 8.4 and 8.5 compares the hydrogen production rates obtained in this study to those reported in literature.

The overall hydrogen production rates in this study ranged between 0.4 and 0.6 mol/m^3/h while the maximum hydrogen production rate was between 0.9 and 1.3 mol/m^3/h (Table 8.4). These values were among the highest reported in literature (Figure 8.4 and 8.5). Differences could be due to the type of the microorganism, the feed composition, the reactor geometry and the operating conditions of the reactor.

In Figures 8.4 and 8.5 it is observed that the hydrogen production rate decreases as the volume of the reactors increase. Scale up of the reactor systems faces several challenges which affect hydrogen production rates. The first is related with the geometry of reactor. With scale up, larger volumes of the reactors increase the distance that the light and evolved gas travels. This raises the possibility of photolimitaion and hydrogen being used up by the microorganisms or hydrogen diffusion through the reactor. Scale up of the height and width of the flat panel reactors to 1 m was reported suitable to reduce light deflection by the plates and allows gas-tightness of the enclosed volume without excessive pressure build (Gebicki *et al.* 2010). Tubular reactors can be scaled-up by elongating the tubing connected to manifolds (Akkerman *et al.* 2002) – very long tubes result in longer residence times and increase chances of the produced hydrogen being consumed by the microorganism, thus reducing hydrogen productivity. Also, with longer pipes, more power will be required to mix the culture, hence increase operating costs.

Another problem of scale up is that self-shading of cells becomes more pronounced. The effect increases with increasing reactor size and cell concentration, negatively affecting cell growth and hydrogen production (Barbosa *et al.* 2001). Due to the lack of sufficient light energy, bacterial growth rate and hydrogen production is reduced as the PNSB switch to alternative modes of growth (Özgür *et al.* 2010). The problem of self-shading can be alleviated by use of reactors with larger illumination areas (Adessi and De Philippis 2014), use of optic fibers inside the reactors (Chen *et al.* 2008) or genetically tailoring the photosynthetic apparatus of the photosynthetic bacteria (Eroglu and Melis 2011). These solutions may lead to the requirement of larger ground area, increasing the system costs and bring about ethical issues of using genetically modified microorganisms at industrial scale.

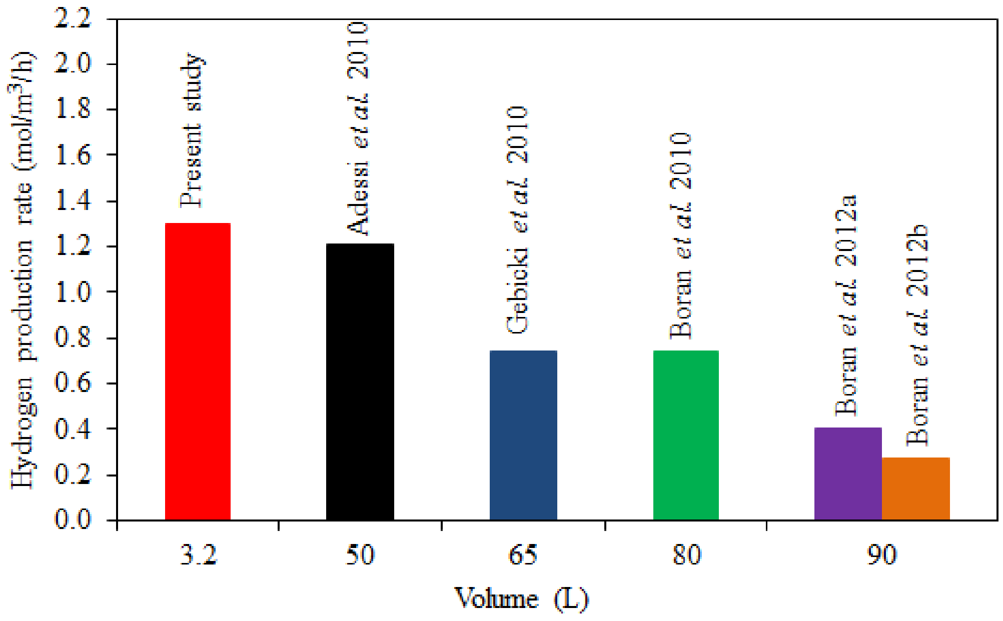

Figure 8.4 Comparison of the hydrogen production rates in outdoor operated tubular reactors.

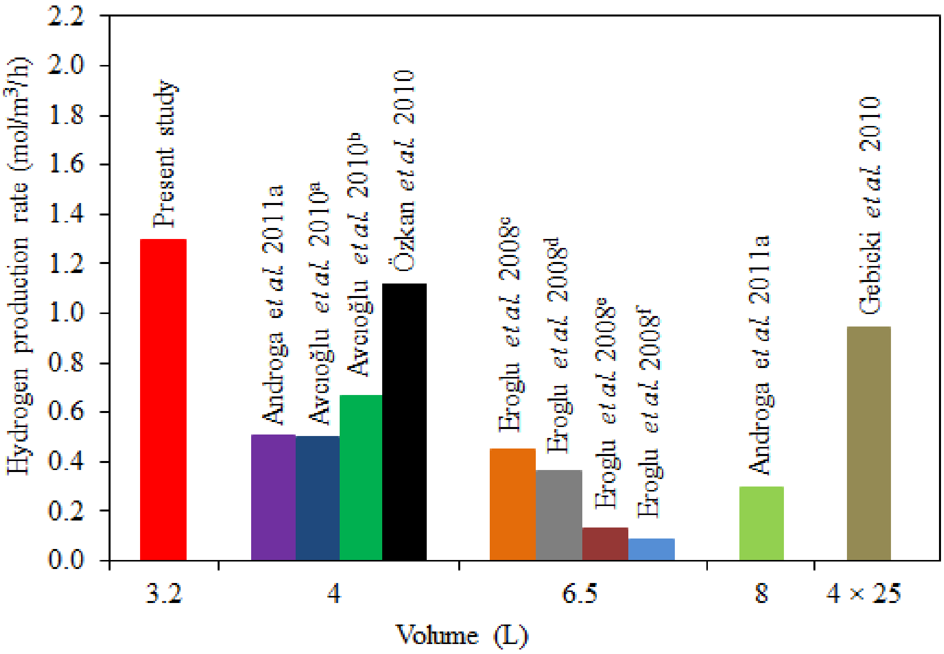

Figure 8.5 Comparison of the hydrogen production rates in outdoor operated panel reactors and the present study reactors.

[a] Experiment performed using *Rhodobacter capsulatus* DSM 1710.

[b] Experiment performed using *Rhodobacter capsulatus* YO3.

[c] Malate used as carbon source in the feed media.

[d] Acetate used as carbon source in the feed media.

[e] Olive mill waste water used as feed.

[f] Lactate used as carbon source in the feed media.

The composition of feed media greatly influences photofermentative hydrogen production. PNSB can use different carbon sources, preferably, volatile fatty acids such as acetic, butyric, lactic and malic acid for hydrogen production and nitrogen sources such as glutamate and ammonium for growth (Li *et al.* 2009). They can also use sugar containing wastes derived from various industries such as tofu industry wastewater (Zhu *et al.* 1999), olive mill wastewater (Eroglu *et al.* 2006), sugar refinery wastewater (Yetiş *et al.* 1999) dairy wastewater (Seifert *et al.* 2010) and ground wheat starch (Kapdan *et al.* 2009). The use of dark fermenter effluents of agricultural wastes such as molasses and sugar beet juice as feed media has also been shown to be viable in photofermentative hydrogen production (Avcıoğlu *et al.* 2011, Boran et al. 2012a, Özkan *et al.* 2012). In some cases it even led to better hydrogen production than the artificial feed media as observed in Figure 8.4 (Özkan *et al.* 2012). This could be attributed to its multi-component nature in which the presence of extra minerals, vitamins and nutrients that enhance hydrogen production and yield. However, pre-treatment of the medium might be required to remove inhibitory components in the media. Androga *et al.* (2012) removed ammonium ions from molasses dark fermenter effluent using a natural zeolite (clinoptilolite) and obtained maximumydrogen productivities of 1.16 mol/m^3/h. Eroglu *et al.* (2006) demonstrated the successful application of olive mill wastewater treatment using clay and zeolite for photofermentative hydrogen production.

CHAPTER 9

CONCLUSIONS AND RECOMMENDATIONS

9.1 Conclusions

The following conclusions were reached as a result of this thesis:

1. Temperature and light intensity are critical parameters affecting hydrogen production rate and yield. Response surface methodology was used to optimize temperature and light intensity to achieve maximum hydrogen production and hydrogen yield using batch cultures of *Rhodobacter capsulatus* DSM 1710. Regression models for a 3^2 design were developed and analyzed. ANOVA results showed that both parameters significantly affected hydrogen production rate and yield. Three-dimensional surface plots and two-dimensional contour plots revealed the existence of maxima at which the highest hydrogen production rate and yield could be achieved. Maximum hydrogen production rate of 0.566 mol $H_2/m^3/h$ was achieved at 27.5°C and 287 W/m^2, while maximum hydrogen yield of 0.326 mol H_2/mol substrate (acetate and lactate mixture) was achieved at 26.8°C and 285 W/m^2. Validation experiments at the optimized conditions resulted in similar values.

2. Computational fluid dynamics analysis was applied to investigate flow in tubular reactors of different geometries. Uniform velocity distribution was achieved in the serpentine reactors but high pressure drops were also obtained. Analysis of a previously used manifold reactor showed that non-uniform fluid distribution existed in the system. This problem could be alleviated by increasing the flow rate and/or modifying the design of the

reactor to include several inlets and outlets. This studies shows that CFD analysis can be effectively used to investigate the effect of changing parameters such as geometry and flow rates.

3. Temperature change in photobioreactors operated outdoors was investigated at different circulation rates (*Re* = 160 to 2700). The temperatures in the reactors were found to increase with the increasing solar radiation and ambient air temperatures. Cooling provided in co-current and counter-current mode to the reactor medium kept the reactor temperatures below 38.0 °C.

4. Measurements of the temperatures at different points along the reactor surface revealed that it did not change along the reactor length. The temperature differences observed at the inlet and outlet of the reactor could be attributed to the heat gain at the auxiliary part of the system, which consists of the gas-liquid separator (reservoir), connecting pipes and the circulating pump.

5. The radial variation of temperature in the reactors was not significant. The reactors were operated at high and low circulation rates (*Re* = 120 and 4200) no cooling was provided.

6. A one-dimensional transient model to analyze the temperature variation of the tubular reactors operated outdoors was developed and compared to experimental results obtained by the setup. The energy balance that was made on the solution in the reactor included the effects of convection and radiative heat exchange on the reactor temperature. It took into account the solar irradiance, ambient temperature, biomass growth and hydrogen production. The temperatures in the reactors increased with increasing solar radiation and ambient air temperatures during daytime. The developed

model predicted reactor temperatures well with 10% accuracy to the measured experimental values.

7. Energy transfer to the outdoor operated reactors was mainly through radiation absorbed by the reactor medium, ground radiation, air radiation and solar radiation (direct and diffuse radiation), while the major heat loss from the reactors was the energy absorbed by the cooling water and lost through forced convection. Reflected ground radiation, reflected air radiation, metabolic activities of the bacteria and pump work had negligible effects on the reactor temperature. There was a net gain of energy in the reactor systems during daytime. This energy might be lost at night when ambient temperatures decrease.

8. Counter-current cooling performed better in controlling the reactor temperature than the co-current cooling since lower temperature values were achieved and less cooling duty was required during operation. The reactors with bacteria exhibited higher temperatures compared to those without bacteria because of the light absorbing properties of the microorganism.

9. Growth and hydrogen production by the photosynthetic bacteria *Rhodobacter capsulatus* YO3 was modeled. The change in biomass was fitted using logistic model while the cumulative hydrogen production was fitted using the modified Gompertz equation. The photosynthetic bacteria consumed acetic acid with initial concentrations of 40 mM using the first order kinetics and utilized most of it for growth.

Photofermentative hydrogen production in outdoor conditions was shown to be highly dependent on the amount of sunshine received and ambient temperature - uncontrolled environmental factors. The model developed identifies the major heat transfer mechanisms and assisted in approximating the temperature profiles in reactors. It associates the kinetic model (based on growth and hydrogen production) of photosynthetic bacteria to temperature change in the reactors. This is useful for thermal management since it gives insight into thermal control strategies. The model can be utilized to estimate parameters such as the cooling duty by providing the transient variables such as the solar radiation and ambient air temperature and the fixed variables such as the reactor dimensions. Being able to describe the dependency of hydrogen production on the natural parameters is valuable in estimating the cost-effectiveness of producing hydrogen in large-scale.

9.2 Recommendations

Several recommendations are made from the work done in this dissertation.

1. The reactor is a two-phase system - it consists of the gas evolved by the photosynthetic bacteria and the liquid medium (culture). CFD analyses for two-phase (gas-liquid) flows can be carried out to determine the velocity distribution and pressure drop in the different reactor geometries.
2. Improvement of the reactor design to ensure uniform flow distribution can be investigated using multiple inlets, introducing inclination to the reactor for easier gas-liquid separation and operating the reactor at different flow rates.
3. Further studies can be done to find a more suitable material for the cooling system that is inert, has high thermal conductivity, is malleable and durable.
4. Better cooling and insulation strategies for the reactor system can be investigated.
5. Studies in which the reactors are operated away from the ground can be performed to reduce the effects of ground radiation.

REFERENCES

Ahn, H., Lee, S., Shin, S., 1998, “Flow Distribution in Manifolds for Low Reynolds Number Flow”, KSME International Journal, 12:87 – 95.

Adessi, A., Torzillo, G., Baccetti, E., De Philippis, R., 2012, “Sustained Outdoor H_2 Production with *Rhodopseudomonas palustris* Cultures in a 50 L Tubular Photobioreactor”, International Journal of Hydrogen Energy, 37: 8840 – 8849.

Adessi, A., De Philippis, R., 2014, “Photobioreactor design and illumination systems for H_2 production with anoxygenic photosynthetic bacteria: A review”, International Journal of Hydrogen Energy, 39: 3127 – 3141.

Akkerman, I., Janssen, M., Rocha, J., Wijffels, R.H., 2002, “Photobiological hydrogen Production: Photochemical Efficiency and Bioreactor Design”, International Journal of Hydrogen Energy, 27: 1195 – 1208.

Alias, C. B., Lopez, M. G.M., Fernandez, F.A., Sevilla, J.F., Sanchez, J.G., Grima, E.M., 2004, “Influence of Power supply in the Feasibility of *Phaeodactylum tricornutum* Cultures”, Biotechnology and Bioengineering, 87: 723 – 733.

Androga, D.D., Özgür, E., Eroglu, I., Gündüz, U., Yücel, M., 2011a, ‘‘Significance of carbon to nitrogen ratio on the long-term stability of continuous photofermentative hydrogen production’’, International Journal of Hydrogen Energy, 36: 15583 – 15594.

Androga, D.D, Özgür, E., Gündüz, U., Yücel, M., Eroglu, I., 2011b, ‘‘Factors affecting the long-term stability of biomass and hydrogen productivity in outdoor photofermentation’’, International Journal of Hydrogen Energy, 36: 11369 – 11378.

Androga, D.D, Özgür, E., Gündüz, U., Yücel, M., Eroglu, I., 2012, “Amelioration of Photofermentative Hydrogen Production from Molasses Dark Fermenter Effluent by Zeolite-Based Removal of Ammonium Ion”, International Journal of Hydrogen Energy, 37:16421 – 16429.

Androga, D.D, Özgür, E., Gündüz, U., Yücel, M., Eroglu, I., 2012, “Photofermentative hydrogen production in outdoor conditions”, In: Hydrogen Energy - Challenges and Perspectives. Editors: Minic, D., InTech, Rijeka, Croatia, 77 – 120.

Androga, D.D., Sevinç, P, Koku, H., Yücel, M., Gündüz, U., Eroglu, I, 2014, “Optimization of temperature and light intensity for improved photofermentative hydrogen production using *Rhodobacter capsulatus* DSM 1710”, International Journal of Hydrogen Energy, 39:2472 – 2480.

Arai, T, Wakayama, T., Okana, S., Kitamura, H., 1998, “Open air hydrogen production by photosynthetic bacteria used solar energy during winter seasons in central Japan”, presented in Int. Conference on Biological Hydrogen Production, Hawaii, USA.

Argun, H., Kargi, F., 2011, “Bio-Hydrogen Production by Different Operational Modes of Dark and Photofermentation: An Overview”, International Journal of Hydrogen Energy, 36:7443 – 7459.

Avcioglu, S.G., Özgür, E., Eroglu, I., Yücel, M., Gündüz, U., 2011, “Biohydrogen Production in an Outdoor Panel Photobioreactor on Dark Fermentation Effluent of Molasses”, International Journal of Hydrogen Energy, 36:11360 – 11368.

Barbosa, M.J., Rocha, J.M.S., Tramper J., Wijffels, R.H., 2001, ‘‘Acetate as a Carbon Source for Hydrogen Production by Photosynthetic Bacteria’’, Journal of Biotechnology, 85:25–33.

Bechet, Q., Shilton, A., Fringer, B.O., Munoz, R., Guiyesse, A.B., 2010, “Mechanistic Modeling of Broth Temperature in Outdoor Photobioreactors”, Environmental Science and Technology, 44:2197 – 2203.

Bees, M.A., Croze, O. A., 2010, “Dispersion of Biased Swimming Micro-organisms in a Fluid Flowing Through a Tube”, *Proceedings of the Royal Society*, 2057 – 2077.

Bernard, O., 2011, “Hurdles and Challenges for Modelling and Control of Microalgae for CO_2 Mitigation and Biofuel Production”, Journal of Process Control, 21:1378 – 1389.

Bertola, F., Vanni, M., Baldi, G., 2003, “Application of Computational Fluid Dynamics to Multiphase flow in Bubble Columns”. International Journal of Chemical Engineering 1, Article A3.

Biebl, H., Pfennig, N., 1981, “Isolation of Members of the Family *Rhodosprillaceae*”, In: The prokaryotes. Editors: Starr, M.P., Stolp, H., Trüper, H.G., Balows, A., Schlegel, H.G., New York: Springer-Verlag, 267 – 273.

Bitog, J. P., Lee, I.B., Kim, K.S., Hwang, H.S., Hong, S.W., Seo, I.H., Mostafa, E. 2011, “Application of Computational Fluid Dynamics for Modeling and Designing Photobioreactors for Microalgae Production: A Review”, Computers and Electronics in Agriculture, 131 – 147.

Boran, E., Özgür, E., van der Burg, J., Yücel, M., Gündüz, U., Eroglu, I., 2010, “Biological Hydrogen Production by *Rhodobacter capsulatus* in Solar Tubular Photo Bioreactor. Journal of Cleaner Production”, 18:S29 – S35.

Boran, E., 2011, “Process Development for Continuous Photofermentative Hydrogen Production”, M.Sc. Thesis in Chemical Engineering, Middle East Technical University, Ankara, Turkey.

Boran, E., Özgür, E., Yücel, M., Gündüz, U., Eroglu, I., 2012a, “Biohydrogen Production by *Rhodobacter capsulatus* Hup$^-$ Mutant in Pilot Solar Tubular Photobioreactor”, International Journal of Hydrogen Energy, 37:16437-45.

Boran, E., Özgür, E., Yücel, M., Gündüz, U., Eroglu, I., 2012b, “Biohydrogen Production by *Rhodobacter capsulatus* in Solar Tubular photobioreactor on Thick Juice Dark fermenter Effluent, 31:150 – 157.

Box, G.E.P., Behnken, D.W., 1960, “Three Level Design for the Study of Quantitative Variables”, Technometrics, 2:455 – 475.

Burgess, G., Fernández-Velasco J.G., 2007, “Materials, Operational Energy Inputs and Net Energy Ratio for Photobiological Hydrogen Production”, International Journal of Hydrogen Energy, 32:1225 – 1234.

Çağlar, A., Yamalı, C., Baker, D.K., Kaftanoğlu, B., 2013, “Measurement of Solar Radiation in Ankara, Turkey”, Journal of Thermal Science and Technology, 33:135 – 142.

Carlozzi, P., Sacchi, A., 2001, “Biomass Production and Studies on *Rhodopseudomonas palustris* grown in an Outdoor, Temperature Controlled, Underwater Tubular Photobioreactor,” Journal of Biotechnology, 88:239 – 249.

Carlozzi, P., Lambardi, M., 2009, “Fed-batch operation for Bio-H_2 production by *Rhodopseudomonas palustris* (strain 42OL)”, Renewable Energy 2009;34:2577 – 2584.

Castillo, P., Magnin, J.P., Velasquez, M., Willison, J., 2012, ‘‘Modeling and optimization of hydrogen production by the photosynthetic bacterium *Rhodobacter capsulatus* by the methodology of design of experiments (DOE): Interaction between lactate concentration and light luminosity’’, Energy Procedia. 29: 357 – 366.

Chen, C.Y., Saratale, G.D., Lee, C.M., Chen, P.C., Chang, J.S., 2008, “Phototrophic Hydrogen Production in Photobioreactors Coupled with Solar-Energy-Excited Optical Fibers”, International Journal of Hydrogen Energy, 33:6886 – 6895.

Chen, C.H., Lu, W.B., Wu, J.F., Chang, J.S., 2007, “Enhancing Phototrophic Hydrogen Production of *Rhodopseudomonas palustris* via Statistical Experimental Design” International Journal of Hydrogen Energy, 32:940 – 949.

Churchill, S.W., Bernstein, M., A., 1977, “Correlating Equation for Forced Convection from Gases and Liquids to a Circular Cylinder in Cross Flow”, Journal of Heat Transfer ,99:300 – 306.

Çengel, Y., “Heat transfer: A Practical Approach”, McGraw-Hill, New Jersey, 1998.

Claassen, P.A.M., de Vrije, T., Koukios, E.G., van Niel, E.W.J., Özgür, E., Eroglu, I., et al. 2010, “Non-thermal Production of Pure Hydrogen from Biomass: HYVOLUTION”, In: Stolten Detlef, Weinheim: WILEY-VCH Verlag GmbH & Co. KGaA.

Daniel, W.W., “Biostatistics: A foundation for Analysis in the Health Sciences”, 9th Ed. New Jersey: John Wiley & Sons, Inc. 2009.

Das, D., Veziroğlu, T.N., 2001, "Hydrogen Production by Biological Processes: A Survey of Literature", International Journal of Hydrogen Energy, 26:13 – 28.

Das, D. and N. Basak, 2007 "The Prospect of Purple Non-sulfur (PNS) Photosynthetic Bacteria for Hydrogen Production: the Present State of Art" World Journal of Microbology and Biotechnology, 23: 31-42.

Dasgupta, C.N., Gilbert, J.J., Lindblad, P., Heidorn, T., Borgvang, S.A., Skjanes, K., Das, D., 2010, "Recent Trends on the Development of Photobiological Processes and Photobioreactors for the Improvement of Hydrogen Production", International Journal of Hydrogen Energy, 35:10218 – 10238.

Degen J., Uebele A., Retze A., Schmid-Staiger U., Trösch W., 2001 " A novel airlift photobioreactor with baffles for improved light utilization through the flashing light effect" Journal of Biotechnology, 92: 89-94.

Doran, P.M., "Bioprocess Engineering Principles", 5th Ed. San Diego: Academic Press Limited. 2000.

Dubbs, J.M., Tabita, F.R., 2004, "Regulators of Non Sulfur Purple Phototrophic Bacteria and the Interactive Control of CO_2 Assimilation, Nitrogen Fixation, Hydrogen Metabolism and Energy Generation", FEMS Microbiology Reviews, 28:353 – 376.

Duffie, J.A., Beckman, W.A., "Solar Engineering of Thermal Processes", 3rd Ed., John Wiley and Sons Inc., 2006.

Eroglu, E., Eroglu, I., Gündüz, U., Türker, L., Yücel, M., 2006, "Biological Hydrogen Production from Olive Mill Wastewater with Two-Stage Processes", International Journal of Hydrogen Energy, 31:1527 – 1535.

Eroglu, E., Melis, A., 2011, “Photobiological hydrogen production: Recent Advances and State of the Art”, Bioresource Technology, 102: 8403 – 8413.

Eroğlu, I., Aslan, K., Gündüz, U., Yücel, M., Türker, L., 1999, ‘‘Substrate Consumption Rates for Hydrogen Production by *Rhodobacter sphaeroides* in a Column Photobioreactor’’, Journal of Biotechnol. 70: 103–113.

Eroglu I., Tabanoglu A., Gunduz U., Eroglu E., Yucel M., 2008, “Hydrogen Production by *Rhodobacter sphaeroides* O.U. 001 in a Flat-Plate Solar Bioreactor” International Journal of Hydrogen Energy, 33: 531-541.

Hallenbeck, P., Ghosh, D., 2009, “Advances in Fermnentatuive Biohydrogen Production: The Way Forward?”, Trends in Biotechnology, 27: 287 – 297.

Favinger, J., Stadtwald, R., Gest, H., 1989, “*Rhodospirillum centenum, sp. nov*., a Thermotolerant Cyst-Forming Anoxygenic Photosynthetic Bacterium”, Antonie Van Leeuwenhoek, 55:291 – 296.

Fedorov, A.S., Tsygankov, A.A., Rao, K.K., Hall, D.O., 1998, “Hydrogen Photoproduction by *Rhodobacter sphaeroides* Immobilised on Polyurethane Foam”, Biotechnology Letters, 20:1007 – 1009.

Fedorov, A.S, Tsygankov, A.A., Rao, K.K., Hall, D.O., 2001, “Production of Hydrogen by an *Anabaena variabilis* Mutant in a Photobioreactor Under Aerobic Outdoor Conditions. In: Miyake, J., Matsunaga, T., San Pietro, A., (Editors), Biohydrogen II. New York: Pergamon, 223 – 228.

Fernandez, F.G., Camacho, F.G., Perez, J.A., Sevilla, J.M., Grima, E.M., 1997, “A Model for Light Distribution and Average Solar Irradiance Inside Outdoor Tubular Photobioreactors for the Microalgal Mass Culture”, Biotechnolgy and Bioengineering, 55:701 – 714.

Fernandez, F.G., Camacho, F.G., Perez, J.A., Sevilla, J.M., Grima, E.M., 1998, Modeling of Biomass Productivity in Tubular Photobioreactors for Microalgal Cultures: Effects of Dilution Rate, Tube Diameter, and Solar Irradiance", Biotechnolgy and Bioengineering, 58:605 – 616.

Firsow, N.N., Drews, G., 1977, "Differentiation of the Intracytoplasmic Membrane of *Rhodopseudomonas palustris* Induced by Variations of Oxygen Partial Pressure or Light Intensity", Archives of Microbiology,115:299 – 306.

Gebicki, J., Modigell, M., Schumacher, M., van der Burg, J., Roebroeck, E., 2010, "Comparison of Two Reactor Concepts for Anoxygenic H_2 Production by *Rhodobacter capsulatus*", Journal of Cleaner Production, 18:S36 – S42.

Ghosh, D., Sobro, I.F., Hallenbeck, P.C., 2012a, "Optimization of the Hydrogen Yield from Single-Stage Photofermentation of Glucose by *Rhodobacter capsulatus* JP91 Using Response Surface Methodology", Bioresource Technology, 123:199 – 206.

Ghosh, D., Sobro, I.F., Hallenbeck, P.C., 2012b, "Stoichiometric Conversion of Biodiesel Derived Crude Glycerol to Hydrogen: Response Surface Methodology Study of the Effects of Light Intensity and Crude Glycerol and Glutamate Concentration", Bioresource Technology, 106:154 – 160.

Gimbun, J., 2009, "Assessment of the Turbulence Models for Modeling of Bubble Column", The Institution of Engineers Journal Malaysia, 70: 53 – 67.

Gnielinski, V., 1976, "New Equations for Heat and Mass Transfer in Turbulent Pipe Flow and Channel Flow", International Chemical engineering, 16:359 – 368.

Goetz, V., Le Borgne, F., Pruvost, J., Plantard, G., Legrand, J., 2011, “A Generic Temperature Model for Solar Photobioreactors”, Chemical Engineering Journal, 175:443 – 449.

Goldstein, R.J., Sparrow, E.M., Jones, D.C., 1973, “Natural Convection Mass Transfer Adjacent to Horizontal Plates”, International Journal of Heat and Mass Transfer, 16:1025 – 1035.

Hai, T., Ahlers, H., Gorenflo, V., Steinbüchel, A., 2000, “Axenic Cultivation of Anoxygenic Phototrophic Bacteria, Cyanobacteria and Microalgae in a New Closed Tubular Glass Photobioreactor”, Applied Microbiology and Biotechnology 2000,53:383 – 389.

Haselkorn, R., Lapidus, A., Kogan, Y., Vlcek, C., Paces, J., Paces, V., Ulbrich, P., Pecenkova, T., Rebrekov, D., Milgram, A., Mazur, M., Cox, R., Kyrpides, N., Ivanova, N., Kapatral, V., Los, T., Lykidis, A., Mikhailova, N., Reznik, G., Vasieva, O., Fonstein, M., 2001, “The *Rhodobacter capsulatus* genome”, Photosynthesis Research, 70: 43 – 52.

He, D., Bultel, Y., Magnin, J.P., Willison, J.C., 2006, “Kinetic Analysis of Photosynthetic Growth and Photohydrogen Production of Strains of *Rhodobacter capsulatus*”, Enzyme Microbial Technology, 38:253 – 259.

Hoekema, S., Douma R. D, Janssen M, Tramper J, Wijffels RH., 2006 “Controlling Light-Use by *Rhodobacter capsulatus* Continuous Cultures in a Flat-Panel Photobioreactor” Biotechnology and Bioengineering, 95: 613-626.

Imhoff, J.F., Truper H.G., Pfennig, N., 1984, ‘‘Rearrangement of the Species and Genera of the Phototrophic Purple Non-Sulfur Bacteria’’, International Journal of Systematic Bacteriology, 34: 340–343.

Incropera FP, Dewitt DP, Bergman TL, Lavine AS. Fundamentals of Heat and Mass Transfer. 6th Edition, John Wiley & Sons, Inc. 2007, New Jersey;5:260–62.

Infantes, D., Gonzalez del Campo, A., Villasenor, J., Fernandez, F.J., 2011, “Influence of pH, Temperature and Volatile Fatty Acids on Hydrogen Production by Acidogenic Fermentation. International Journal of Hydrogen Energy, 36:15595 – 16601.

Jamil, Z., Mohamad A.M.S., Ibrahim, S., Vikineswary, S., 2009, “Optimization of Phototrophic Hydrogen Production by *Rhodopseudomonas palustris* PBUM001 via Statistical Experimental Design”, International Journal of Hydrogen Energy, 34:7502 – 7512.

Jo, J.H., Lee, D.S., Park, J.M., 2006, “Modeling and Optimization of Photosynthetic Hydrogen Gas Production by Green Alga *Chlamydomonas reinhardtii* in Sulfur-Deprived Circumstance”, Biotechnoly Progress, 22:431 – 437.

Kapdan, I.K., Kargi, F., Oztekin, R., Argun, H., 2009, “Bio-hydrogen Production from Acid Hydrolyzed Wheat Starch by Photofermentation using Different *Rhodobacter sp*.”, International Journal of Hydrogen Energy, 34:2201 – 2207.

Kars, G., Gunduz, U., Yucel, M., Rakhley, G., Kovacs, K., Eroglu, I., 2009, “Evaluation of Hydrogen Production by *Rhodobacter sphaeroides* O.U.001 and its hupSL Deficient Mutant Using Acetate and Malate as Carbon Sources”, International Journal of Hydrogen Energy, 34:2184 – 2190.

Kars, G. & Gündüz, U., 2010, “Towards a super H2 producer: Improvements in photofermentative biohydrogen production by genetic manipulations. International Journal of Hydrogen Energy, 35:6646 – 6656.

Katsuda, T., Arimoto, T., Igarashi, K., Azuma, M., Kato, J., Takakuwa, S., Ooshima, H., 2000, "Light Intensity Distribution in the Externally Illuminated Cylindrical Photo-bioreactor and its Application to Hydrogen Production by *Rhodobacter capsulatus*", Biochemal Engineering Journal, 5: 157 – 64.

Kays, W.M., and Crawford, M.E., "Convection Heat and Mass transfer", 3rd Ed., McGraw Hill, New York, 1993.

Keskin, T., Hallenbeck, P., 2012, "Hydrogen Production from Sugar Industry Wastes Using Single-Stage Photofermentation", Bioresource Technology, 112: 131 *– 136.*

Kim J. S., Ito K., Takahashi H., 1982, "Production of Molecular Hydrogen in Outdoor Batch Culture of *Rhodopsedomonas sphaeroides*" Agricultural Biology and Chemistry 46: 937-941.

Kim J. S., Ito K., Izaki K., Takahashi H., 1987 "Production of Molecular Hydrogen by a Semi-continuous Outdoor Culture of *Rhodopseudomonas sphaeroides*" Agricultural and Biological Chemistry, 51: 1173 – 1174.

Koku, H., Eroğlu, I., Gunduz, U., Yucel, M., Turker, L., 2002, "Aspects of the Metabolism of Hydrogen Production by *Rhodobacter sphaeroides*'', International Journal of Hydrogen Energy, **2**:1315-29.

Kondo, T., Arakawa, M., Hirai, T., Wakayama, T.G., Hara, M., Miyake, J., 2002, "Enhancement of Hydrogen Production by a Photosynthetic Bacterium Mutant with Reduced Pigments", Journal of Bioscience and Bioengineering, 93:145 – 150.

Lee, S., Moon N., Lee, J., 2012, "A study on the Exit Flow Characteristics Determined by the Orifice Configuration of Multi-Perforated Tubes", Journal of Mechanical Science and Technology, 26:2751 – 2758.

Lee, C.M., Hung, G.J., Yang, C.F., 2011, "Hydrogen Production by *Rhodopseudomonas palustris* WP 3-5 in a Serial Photobioreactor Fed with Hydrogen Fermentation Effluent. Bioresource Technology,102:8350 – 8356.

Levin, D., Azbar, N., 2011, "Biohydrogen in Perspective", In: Levin, D., Azbar, N., (Editors), State of the Art and Progress in Production of Biohydrogen. Danvers MA: Bentham Science Publishers, 3 – 7.

Li, R.Y., Fang, H.H.P., 2009, "Heterotrophic Photofermentative Hydrogen Production", Critical Reviews in Environmental Science and Technology, 39:1081 – 1108.

Liu, B.Y., Jordan, R.C., 1960, "The Interrelationship and Characteristic Distribution of Direct, Diffuse and Total Solar Radiation", Solar Energy, 4:1–19.

Ljunggren, M., Wallberg, O., Zachhi, G., 2011, "Techno-economic Comparison of a Biological Hydrogen Process and a 2nd Generation Ethanol Process Using Barley Straw as Feedstock, Bioresource Technology, 102:9524 – 9531.

Lunberg, R.E., McCuen, P.A., Reynolds, W.C., 1963, "Heat Transfer in Annular Passages: Hydrodynamically Developed Laminar Flow with Arbitrarily Prescribed Wall Temperature or Heat Fluxes", International Journal of Heat and Mass Transfer, 6:495 – 592.

Maor, T., Appelbaum, J., 2011, "Solar Radiation on Horizontal Ttubular Microalgae Photobioreactor: Direct Beam Radiation", Journal of Solar Energy Engineering, 133, 024502: 1 – 5.

McCabe, W.L. Smith J.C., Harriot, P. " Unit Operations of Chemical Engineering", 5th Ed. McGraw-Hill Inc., New York, 1993.

Merchant and Captive Report, ‘‘Global Hydrogen Generation Market by Merchant and Captive Type, Distributed and Centralized Generation, Application and Technology - Trends and Forecasts (2011 – 2016)’’, Energy and Power Report. (2011).

Miyake, J., Wakayama T., Schnackenberg J., Takaaki A., Asada Y., 1999, “Simulation of the Daily Sunlight Illumination Pattern for Bacterial Photo-Hydrogen Production” Journal of Bioscience and Bioengineering, 88: 659-663.

Montgomery, D,C., “Design and Analysis of Experiments”, 7th Ed. New Jersey: Wiley Hoboken, 2009.

Mu, Y., Zheng, X.J., Yu, H.Q., 2009, “Determining Optimum Conditions for Hydrogen Production from Glucose by an Anaerobic Culture Using Response Surface Methodology”, International Journal of Hydrogen Energy, 34:7959 – 7963.

Muazzez, G.D., 2011 “Microarray Analysis of the Effects of Heat and Cold Stress on Hydrogen Production Metabolism of *Rhodobacter capsulatus*”, M.Sc. Thesis in Biological Sciences, Middle East Technical University. Ankara, Turkey.

Obeid, J., Magnin, J.P., Flaus, J.M., Adrot, O., Willison, J.C., Zlatev R. 2009, “Modelling of Hydrogen Production in Batch Cultures of the Photosynthetic Bacterium *Rhodobacter capsulatus*. International Journal of Hydrogen Energy, 34:180 – 185.

Ogbonna, J.C., Toshihiko, S., Tanaka, H., 1998, “Development of Efficient Large Scale Photobioreactors: A Key Factor for Practical Production of Biohydrogen”, In: Zaborsky, O.R., (Editor), Biohydrogen. London: Plenum Press, 329-343.

Ogbanna, J.C., Tanaka, H., 2001, “Photobioreactor Design for Photobiological Production of Hydrogen”, In: Miyake, J., Matsunaga, T., Pietro, A.S., (Editors), BIOHYDROGEN II. London: Elsevier Science: 245 – 261.

Orme C. J., Stone M. L., Benson M. T., Peterson E. S., 2003 “Testing of Polymer Membranes for the Selective Permeability of Hydrogen” Separation Science and Technology 38: 12, 3225-3238.

Otsuki, T., Uchiyama, S., Fujiki, K., Fukunaga, S., 1998, “Hydrogen Production by a Floating-type Photobioreactor”, In: Zaborsky, O.R., (Editor), Biohydrogen. London: Plenum Press; 1998. 369 – 374.

Özgür, E., Uyar, B., Öztürk, Y., Yücel, M., Gündüz, U., Eroglu, I., 2010, “Biohydrogen Production by *Rhodobacter capsulatus* on Acetate at Fluctuating Temperatures”, Resource Conservation and Recycling, 54:31.

Özkan, E., Uyar, B., Ozgur, E., Yucel, M., Eroglu, I., Gunduz, U., 2012, “Photofermentative Hydrogen Production Using Dark Fermentation Effluent of Sugar Beet Thick Juice in Outdoor Conditions” International Journal of Hydrogen Energy, 37:2044 – 2049.

Öztürk, Y., 2005, “Characterisation of the Genetically Modified Cytochrome Systems and Their Application to Biohydrogen Production in *Rhodobacter capsulatus*”, Ph.D. Thesis in Biotechnology, Middle East Technical University, Ankara.

Öztürk, Y., Yücel, M., Daldal, F., Mandaci, S., Gündüz, U., Türker, L., Eroglu, I., 2006, “Hydrogen Production by Using *Rhodobacter capsulatus* Mutants with Genetically Modified Electron Transfer Chains”, International Journal of Hydrogen Energy, 31:1545 – 1552.

Papácek, S., Matonoha C., Stumbauer, V., Stys D., 2011, “Modelling and Simulation of Photosynthetic Microorganism Growth: Random Walk vs. Finite Difference Method”, Mathematics and Computers in Simulation, 54:1791 – 1795.

Pandey, A., Pandey, A., 2008, “Reverse Micelles as Suitable Microreactor for Increased Biohydrogen Production. International Journal of Hydrogen Energy”, 33:273 – 278.

Pemberton, J.M., Horne, I.M., McEwan, A.G., 1998, “Regulation of Photosynthetic Gene Expression in Purple Bacteria”, Microbiology, 144: 267 – 278.

Pereira, D.A., Rodrigues, V.O., Gómez, S.V., Sales, E.A., Jorquera, O., 2013, “Parametric Sensitivity Analysis for Temperature Control in Outdoor Photobioreactors”, Bioresource Technology, 144: 548– 553.

Petukov, B.S., 1970, “Heat Transfer in Turbulent Pipe Flow with Variable Physical Properties”, In: Irvine, T.F., and Hartnett, J.P., (Editors), Advances in Heat Transfer. New York; Academic, 504 – 564.

Phadtare, S., 2004, “Recent developments in Bacterial Cold-shock Response”, Current Issues in Molecular Biology, 6: 125-136.

Poflee, N.M., Rakow, A.L., Dandy, D.S., Chappell, M.L., Pons, M.N., 1997, “Inertial Migration Based Concentration Factors for Suspensions of *Chlorella* Micro-Algae in Branched Tubes”, Biorheology, 34: 405 – 421.

Posten, C., 2009, “Design principles of Photo-bioreactors for Cultivation of Microalgae”, Engineering and Life Sciences, 9:165 – 177.

Pruvost, J., Cornet, J.F., Legrand, J., 2008, “Hydrodynamics Influence on Light Conversion in Photobioreactors: An Energetically Consistent Analysis”, Chemical Engineering Science, 63:3679 – 3694.

Rechenberg, I., 1998, “Artificial Bacterial Algal Symbiosis (Project ArBAS): Sahara experiments”, In: Zaborsky, O.R., (Editor), Biohydrogen. London: Plenum Press, 281 – 294.

Ribeiro, R.L.L., Mariano, A.B., Souza, J.A., Vargas, J.V.C., 2008, “Transient Modeling and Simulation of Compact Photobioreactors”, Thermal Engineering, 7:66 – 71.

Ron, E.Z., 2006, “Bacterial Stress Response”, In: Rosenberg, E., Stackerbrandt, E., Thompson, F., Lory, S., Delong, E., (Editors), The Prokaryotes: A Handbook on the Biology of Bacteria, Ecophysiology and Biochemistry, Vol. 2. Springer: 1012 – 1027.

Sastre, R.R., Csogor, Z., Perner-Nochta, I., Fleck-Schneider, P., Posten, C., 2007, “Scale-down of Microalgae Cultivations in Tubular Photo-bioreactors - A Conceptual Approach”, *Journal of Biotechnology,* 127 – 133.

Sasikala, K., Ramana, C.V., Rao, PR.., Kovacs, K.L., 1993, ‘‘Anoygenic Phototropic Bacteria: Physiology and Advances in Hydrogen Production Technology,’’ Advanced Applied Microbiology, 38:211-295

Sakurai, H., Masukawa, H., Kitashima, M., Inoue, K., 2013, “Photobiological Hydrogen Production: Bioenergetics and Challenges for its Practical Application”, Journal of Photochemistry and Photobiology C, 17: 1 – 25.

Sarı, S., 2007, “Development of helical tubular reactor for hydrogen producing photosynthetic bacteria”, M.Sc. Thesis in Biotechnology, Middle East Technical University, Ankara, Turkey.

Schugerl, K., Bellgardt K.H., “Bioreaction Engineering: Modeling and Control”, Springer-Verlag, Berlin, Heidelberg, 2000.

Segers, L., Verstraete, W., 1983, “Conversion of Organic Acids to Hydrogen by *Rhodospirillaceae* Grown with Glutamate or Dinitrogen as Nitrogen Source”, Biotechnology and Bioengineering, 25:2843 – 2853.

Seifert, K., Waligorska, M., Laniecki, M., 2010, “Hydrogen Generation in Photobiological Process from Dairy Wastewater”, International Journal of Hydrogen Energy, 35:9624 – 9629.

Sevinç, P., Gündüz, U., Eroglu, I., Yücel, M., 2012, “Kinetic Analysis of Photosynthetic Growth, Hydrogen Production and Dual Substrate Utilization by *Rhodobacter capsulatus*”, International Journal of Hydrogen Energy, 2012, 37:16430 – 16436.

Shi, X.Y., Yu, H.Q., 2005a, “Optimization of Glutamate Concentration and pH for H_2 Production from Volatile Fatty Acids by *Rhodopseudomonas capsulata*”, Letters in Applied Microbiology, 40:401 – 406.

Shi, X.Y., Yu H.Q., 2005b, ‘‘Response Surface Analysis on the Effect of Cell Concentration and Light Intensity on Hydrogen Production by *Rhodopseudomonas capsulata*’’, Process Biochemistry, 40: 2475 –2481.

Show, K, Lee, D., Chang, J., 2011, “Bioreactor and Process Design for Biohydrogen Production”, Bioresource Technology, 102: 8524 – 8533.

Sierra E., Acien F. G., Fernandez J. M., Garcia J. L., Gonzalez C., Molina E., 2008, “Characterization of a Flat Plate Photobioreactor for the Production of Microalgae”, Chemical Engineering Journal, 138: 136 – 147.

Parthasarathy, P., Narayanan K.S., 2014, “Hydrogen Production from Steam Gasification of Biomass: Influence of Process Parameters on Hydrogen Yield - A Review”, Renewable Energy, 66: 570 – 579.

Soletto, D., Binaghi, L., Ferrari, L., Lodi, A., Carvalho, J.C.M., Zilli, M., 2008, “ Effects of Carbon dioxide Feeding Rate and Light Intensity on the Fed-Batch Pulse-Feeding Cultivation of *Spirulina platensis* in Helical Photo-Bioreactor”, Biochemical Engineering Journal, 39:369 – 375.

Sözen, A., Arcalioğluö E., Ozalp, M., Kani, E.G., 2005, “Solar Energy Potential in Turkey”, Applied Energy, 80:367 – 381.

Sun, Q., Xiao, W., Xi, D., Shi, J., Yan, X., Zhou, Z., 2010, “Statistical Optimization of Biohydrogen Production from Sucrose by a Co-culture of *Clostridium acidisoli* and *Rhodobacter sphaeroides*”, International Journal of Hydrogen Energy, 35:4076 – 4084.

Tandori, J., Hideg, E., Nagy, L., Maroti, P., Vass, I., 2001, “Photoinhibition of Carotenoidless Reaction Centers from *Rhodobacter sphaeroides* by Visible Light. Effects on Protein structure and Electron Transport”, Photosynthesis Research, 70:175 – 184.

Tredici, M.R., 1999, ‘‘Bioreactors’’, In: Flickinger, M.C., Drew, S.W. (Eds.), Encyclopedia of Bioprocess Technology: Fermentation, Biocatalysis and Bioseparation, vol. 1. Wiley, New York, pp. 395–419.

Tredici, M.R., 2004, “Mass Production of Microalgae: Photobioreactors”. In: Handbook of Microalgal Culture, Biotechnology and Applied Phycology”, A. Richmond, Blackwell Scientific, 178-214.

Tompkins, D.M., Yoo, T., Hrnjak, P., Newell, T., Cho, K., 2002, "Flow Distribution and Pressure Drop in Micro-channel Manifolds", International Refrigeration and Air Conditioning Conference, Paper 554.

Tsygankov, A.A., 2001' "Hydrogen Photoproduction by Purple Bacteria: Immobilized vs Suspension Culture", In: Miyake, J., Matsunaga, T., San Pietro, A., (Editors), Biohydrogen II. New York:Pergamon, 229 – 243.

Tsygankov, A.A., Fedorov, A.S., Kosourov, S.N., Rao, K.K., 2002, "Hydrogen Production by Cyanobacteria in an Automated Outdoor Photobioreactor Under Aerobic conditions. Biotechnology and Bioengineering", 80:777 – 783.

Uyar, B., Gündüz, U., Yücel, M., Türker, L., Eroglu, I., 2007, "Effect of Light Intensity, Wavelength and Illumination Protocol on Hydrogen Production in Photobioreactors", International Journal of Hydrogen Energy, 32: 4670– 4677.

Uyar, B., 2008, "Hydrogen production by microorganisms in solar bioreactor", Ph.D. Thesis in Biotechnology Department, Middle East Technical University, Ankara, Turkey.

Uyar, B., Kars, G., Yücel, M., Gündüz, U., Eroglu, I., 2011, "Hydrogen Production via Photofermentation", In: Levin, D., Azbar, N., (Editors), State of the Art and Progress in Production of Biohydrogen. Danvers MA: Bentham Science Publishers, 54 – 77.

Verméglio, A., Joliot, P., 1999, "The Photosynthetic Apparatus of *Rhodobacter sphaeroides*", Trends in Microbiology, 7:435 – 440.

Vignais, P.M., Colbeau, A., Willison, J.C., Jouanneau, Y., 1985, "Hydrogenase, Nitrogenase, and Hydrogen Metabolism in Photosynthetic Bacteria", Advanced Microbial Physiology. Microbial Phys., 26: 154-234.

Wang, J., Wan, W., 2009, “Experimental Design Methods for Fermentative Hydrogen Production: A Review”, International Journal of Hydrogen Energy, 34:235 – 244.

Wakayama, T., Miyake, J., 2002, “Light shade bands for the improvement of solar hydrogen production efficiency by *Rhodobacter sphaeroides* RV”, International Journal of Hydrogen Energy,27:1495 – 1500.

Wild, G., Li, H.Z., Poncin, S., Olmos, E., 2003, “Some Aspects of the Hydrodynamics of Bubble Column”, International Journal of Chemical Reactor Engineering, 1: 1 – 36.

World Energy Outlook Special Report Report. ‘‘Chp 6 – Renewables, Renewable Energy Outlook Basking in the Sun?’’, International Energy Agency (2013).

Yetiş, M., Gündüz, U., Eroglu, I., Yücel, M., Türker, L., 2000, “Photoproduction of Hydrogen from Sugar Refinery Wastewater by *Rhodobacter sphaeroides* O.U.001”, International Journal of Hydrogen Energy, 25:1035 – 1041.

Zabut, B., Kahlout, K.E., Yücel, M., 2006, “Hydrogen Gas Production by Combined Systems of *Rhodobacter sphaeroides* O.U. 001 and *Halobacterium salinarum* in a Photobioreactor. International Journal of Hydrogen Energy, 31:1553 – 1562.

Zhang, K., Kurano, N., Miyachi, S., 2002, “Optimized Aeration by Carbon dioxide Gas for Microagal Production and Mass Transfer Characterization in a Vertical Flat-plate Photobioreactor”, Bioprocess and Biosystems Engineering, 25:97 – 101.

Zhu, H., Suzuki, T., Tsygankov, A.A., Asada, Y., Miyake, J., 1999, “Hydrogen Production from Tofu Wastewater by *Rhodobacter sphaeroides* Immobilized in Agar Gels”, International Journal of Hydrogen Energy, 24:305 – 310.

Zhu, Y,S., Hearst, J.E., 1986, “Regulation of Expression of Genes for Light-Harvesting Antenna Proteins LH-I and LH-II; Reaction Center Polypeptides RC-L, RC-M, and RC-H; and Enzymes of Bacteriochlorophyll and Carotenoid Biosynthesis in *Rhodobacter capsulatus* by Light and Oxygen”, Proceedings of NationaI Academy of Science, USA, 83:7613 – 7617.

APPENDIX A: FLOW THEORY

A.1 COMSOL: GENERAL SINGLE PHASE FLOW THEORY

The single-phase fluid-flow model solved using COMSOL are based on the Navier-Stokes equations of fluid motion. The general form of the equation is shown in Equation A.1.

$$\rho\frac{\partial u}{\partial t}+\rho(u.\nabla)u=\nabla.\left[-pI+\tau\right]+F \qquad \text{(A.1)}$$

where ρ is the density (kg/m^3), u is the velocity vector (m/s), p is pressure (Pa), τ is the viscous stress tensor (Pa), F is the volume force vector (N/m^3)

Equations A.1 is solved assuming that the fluid is Newtonian and so the viscous stress tensor is estimated as;

$$\tau = 2\mu \mathrm{S} - \frac{2}{3}\mu\left(\nabla.\mathrm{u}\right)\mathrm{I} \qquad \text{(A.2)}$$

where μ is the dynamic viscosity (Pa.s).

The reactors were plotted, meshed and the velocity and pressure drop solved (assuming steady state flow) using the COMSOL 4.3 program.

A.2 ANALYTICAL SOLUTION OF PRESSURE DROP

A mechanical energy balance (Equation A.3) was used to determine the pressure drop in the U-tube reactor. It was assumed that the total mechanical power loss was only due to frictional losses along the tubing (h_L).

$$\frac{P_a}{\rho}+\frac{gZ_a}{g_c}+\frac{\alpha_a\overline{V}_a^2}{2g_c}=\frac{P_b}{\rho}+\frac{gZ_b}{g_c}+\frac{\alpha_b\overline{V}_b^2}{2g_c}+h_L \qquad \text{(A.3)}$$

where P_a and P_b are the pressure (Pa) values at the inlet and outlet of the reactor, g is the gravity acceleration (m/s^2), Z_a and Z_b are the elevation (m) at the inlet and outlet of the reactor, g_c is Newton's law proportionality factor (1 kg.m/N/s^2), α_a and α_b are the kinetic correction factors for the fully developed laminar flow at the inlet and outlet of the reactor, $\overline{V}_a$ and $\overline{V}_b$ are the average velocities (m/s) of the fluid at the reactor inlet and outlet and h_L is the frictional loss along the reactor tube (m.s^2/kg/N).

It was assumed that;

i. The flow in the reactor is steady and incompressible. Velocity at the reactor inlet and outlet are the same ($\overline{V}_a = \overline{V}_b$).
ii. The reactor is placed horizontally. i.e. $Z_a = Z_b$
iii. The correction factors for the fully developed laminar flow at the entrance and exit of the reactor are equal i.e. $\alpha_a = \alpha_b = 2.0$.

Equation A.3 simplifies to

$$\Delta P = P_a - P_b = h_L\rho \qquad \text{(A.4)}$$

$$\Delta P = \left(4f\frac{L}{D}+K_f\right)\frac{\overline{V}}{2g_c}\rho \qquad \text{(A.5)}$$

where ΔP is the pressure drop (Pa) in the reactor, f is the fanning friction factor, L is the length (m) of the reactor, D is the diameter (m) of the reactor tube, K_f is the return bend loss coefficient, ρ is the density (kg/m^3) of the fluid in the reactor and $\overline{V}$ is the average fluid velocity (m/s). For the return bend, K_f is estimated as 2.2 (McCabe *et al.* 1993).

APPENDIX B

THE COMPOSITION OF THE FEED MEDIUM

Table B.1 The composition of the standard basal (modified Biebl and Pfennig media), growth and hydrogen production medium per litre of solution.

Component	Amount
Standard Basal Medium	
KH_2PO_4 (22 mM)	0.5g
$MgSO_4.7H_20$	0.5g
$CaCl_2.2H_2O$	0.5g
Vitamin Solution	1 ml
Fe-Citrate[a]	0.1 ml
Trace Elements	0.1 ml
Growth Medium[b]	
Acetic acid	20 mM
Lactic acid[c]	7.5 mM
Sodium glutamate	10 mM
Hydrogen Production Medium[b]	
Acetate	40 mM
Lactic acid[c]	7.5 mM
Sodium glutamate	2 – 4 mM

[a] 0.5 g Fe-citrate was dissolved in 100 ml distilled water and sterilized by autoclaving.

[b] A mixture of the standard basal medium, acetatic acid, lactic acid and sodium glutamate.

[c] Used as carbon source in the indoor experiments.

Table B.2 The composition of trace element solution.

Composition Amount	**Amount**
HCl (25% v/v)	1 ml
$ZnCl_2$	70 mg
$MnCl_2 \times 4H_2O$	100 mg
H_3BO_3	60 mg
$CoCl_2 \times 6\ H_2O$	200 mg
$CuCl_2 \times 2\ H_2O$	20 mg
$NiCl_2 \times 6\ H_2O$	20 mg
$NaMoO_4 \times 2\ H_2O$	40 mg
H_2O	Complete to 1 L

Table B.3 The composition of the vitamin solution.

Composition	**Amount**
Thiamine	500 mg
Niacin (Nicotinate)	500 mg
Biotin	15 mg
H_2O	Complete to 1 L

APPENDIX C

THE DIMENSIONS OF THE PHOTOBIOREACTOR

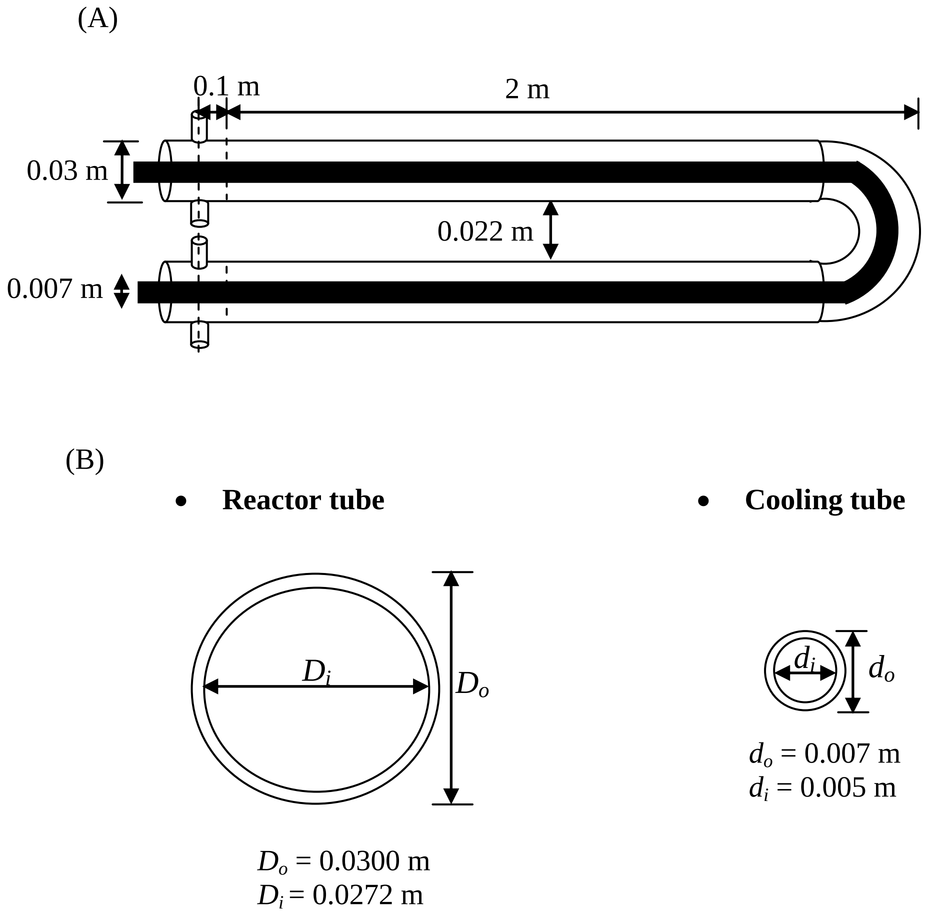
(A)
0.1 m
2 m
0.03 m
0.022 m
0.007 m
(B)
Reactor tube
Cooling tube
D_i
D_o
d_i
d_o
d_o = 0.007 m
d_i = 0.005 m
D_o = 0.0300 m
D_i = 0.0272 m

Figure C.1 Dimensions of the (A) photobioreactor and (B) reactor tube and the cooling tube.

APPENDIX D

HYDRODYNAMIC AND THERMAL ENTRY LENGTH IN THE TUBULAR PHOTOBIOREACTORS

As fluid enters the reactor with uniform velocity, a boundary layer develops with increasing distance along the tube. An inviscid boundary layer develops near the wall of the reactor due to friction between the fluid and the wall, and it merges at the center of the tube after which the velocity profile does not change with increasing distance along the tube. At this point, the flow is said to be fully developed and the distance from the entrance at which the fully developed condition is achieved is termed the hydrodynamic entry length, L_h (Incropera, 1996). A thermal boundary layer also develops as fluid enters the tube and a point of thermally fully developed condition is reached in the tubes. In laminar flow, the velocity profile developed is parabolic while in turbulent flow it is flatter because of radial turbulent mixing (Incropera, 1996).

The hydrodynamic entry length is calculated as (Latif, 2006),

For laminar flow ($\mathrm{Re}_D \le 2300$), by,

$$\frac{L_h}{D_i} \approx 0.056\,\mathrm{Re}_D \qquad \text{(D.1)}$$

For turbulent flow ($\mathrm{Re}_D \ge 4000$),

$$10 \le \left(\frac{L_h}{D_i}\right)_{turblent} \le 60 \qquad \text{(D.2)}$$

The thermal entry length is calculated as (Latif, 2006),

For laminar flow ($\mathrm{Re}_D \leq 2300$), by,

$$\left(\frac{L_t}{D_i}\right)_{laminar} \approx 0.043\,\mathrm{Re}_D\,\mathrm{Pr} \tag{D.3}$$

For turbulent flow ($\mathrm{Re}_D \geq 4000$),

$$\frac{L_{t_{turblent}}}{D_i} \approx 10 \tag{D.4}$$

It is important to know the lengths of the thermal and hydrodynamic regions to see whether fully developed flow assumption for the reactors can be made or not. Shown in Table D1 is a summary of the hydrothermal entry lengths and thermal entry lengths of the flow rates used in this study.

Table D.1 Summary of the hydrothermal entry lengths and thermal entry lengths of the different flow rates used in the outdoor experiments.

Reynolds Number (Re)	**Hydrothermal entry lengths (m)**	**Thermal entry lengths (m)**
120	0.2	0.8
160	0.2	0.8
230	0.3	1.1
1860	2.1	8.8
2700	$10 \leq 0.2 - 1.2 \leq 60$	0.2
4200	$10 \leq 0.3 - 1.6 \leq 60$	0.3

At low flow rates (*Re* = 120, 160 and 230), L_h and L_t are small compared to the reactor length (4.192 m), therefore the flow can be assumed to be fully develoloped, while at Re = 1860 the flow is developing since the values of L_h and L_t are large compared to the reactor length.

APPENDIX E

ELEMENTARY BALANCE TO DETERMINE STOICHIOMETRIC COEFFICIENTS FOR BIOMASS FORMATION

An elemental balance was made to determine the stoichiometric coefficients for biomass formation of *Rhobacter capsulatus*. The glutamate fed was assumed to be solely used for growth and the formula of *Rhobacter capsulatus* given by Hoekama *et al.* (2006) was used in the calculations.

$$\underset{\text{Glutamic acid }(Glu)}{aC_5H_9NO_{4(aq)}} + \underset{\text{Acetic acid }(A)}{bCH_3COOH_{(aq)}} \rightarrow \underset{\text{Biomass (X)}}{cCH_{1.7}O_{0.45}N_{0.14(s)}} + dCO_{2(g)} + eH_2O_{(l)} \qquad \text{(E.1)}$$

C balance: 5a + 2b = c + d (E.2)

H balance: 9a + 4b = 1.7c+2e (E.3)

N balance: a = 0.14c (E.4)

O balance: 4a + 2b = 0.45c + 2d + e (E.5)

Unknowns: a, b, c, d, e

Equations: 4

Assuming a = 0.14;

- $c = \frac{0.14}{0.14} = 1$ (E.6)
- 5(0.14) + 2b = 1 + d (E.7)

  0.7 + 2b = 1 + d (E.8)

  2b – d = 0.3 (E.9)

- 9(0.14) + 4b = 1.7(1) + 2e (E.10)

$$1.26 + 4b = 1.7 + 2e \tag{E.11}$$

$$4b - 2e = 0.44 \tag{E.12}$$

$$e = 2b - 0.22 \tag{E.13}$$

- $$4(0.14) + 2b = 0.45(1) + 2d + e \tag{E.14}$$

$$0.56 + 2b = 0.45 + 2d + e \tag{E.15}$$

$$0.11 = 2d + e - 2b \tag{E.16}$$

Substituting (E.13) into (E.16)

$$0.11 = 2d + 2b - 0.22 - 2b \tag{E.17}$$

$$0.33 = 2d \tag{E.18}$$

$$d = 0.165 \tag{E.19}$$

Substituting (E.19) into (E.9)

$$2b - 0.165 = 0.3 \tag{E.20}$$

$$b = 0.233 \tag{E.21}$$

Substituting (E.21) into (E.13)

$$e = 2(0.233) - 0.22 \tag{E.22}$$

$$e = 0.245 \tag{E.23}$$

Substituting the stoichiometric coefficients calculated from the elementary balance into the reaction equation yields,

$$\begin{aligned} 0.602C_5H_9NO_4(aq) + CH_3COOH(aq) \rightarrow 4.303CH_{1.7}O_{0.45}N_{0.14}(s) + 0.710CO_2(g) \\ +1.054H_2O(l) \end{aligned} \tag{E.24}$$

APPENDIX F

POLYMATH PROGRAM FOR CALCULATING THE METABOLIC HEAT

```
# Kinetic model for hydrogen production in the outdoor reactors
# Experiment date: 05.08.2013_Co-currently cooled reactor
 # Scheme for a semi-batch reactor operated outdoors
# Assumptions:
# 1. Properties of variables calculated at 35 0C.
# 2. The reference temperature is 25 0C.
# 3. Medium in the reactor is assumed to have similar properties to that of water.
# 4. Henry's law is used to detemine the mole fractions of hydrogen in the liquid.
#    but the mole fraction of carbon dioxide was not determined because it is held
#    in the liquid by bacteria.
# 5. The amount of hydrogen in the liquid phase is constant.

# The subscripts: a=acetic acid, x=cells, h2=hydrogen, glu=Glutamate

# Experiment time range
t(0)=0.00001                # start of the experiment (h)
t(f)=13                     # end of the experiment (h)

V=32*10^-4                  # reactor volume (m^3)
rhow=994                    # density of water (kg/m^3)

#Properties of the gas evolved
P=1                         # pressure of the gas evolved (atm)
Qh2=4.6236*10^-5           # volumetric flow rate of hydrogen (m^3/h)



Qco2 =3.2942*10^-6         # volumetric flow rate of carbon dioxide (m^3/h)
```

```
Vgas=(Qh2+Qco2)*t           # volume of the gas evolved (m^3)
yh2v=9335*10^-4             # volume fraction of hydrogen in the total gas (%)
yco2v = 665*10^-4       # volume fraction of carbon dioxide in the total gas (%)

yh2m=(yh2v*899*10^-4/2)/(yco2v*1997*10^-3/44+yh2v*899*10^-4/2)
                              # mole fraction of hydrogen in the total gas
yco2m=(yco2v*1997*10^-3/44)/(yco2v*1997*10^-3/44+yh2v*899*10^-4/2)
                              # mole fraction of carbon dioxide in the total gas

Vh2gas=yh2v*Vgas*10^3              # volume of hydrogen evolved (m^3)
Vco2gas=yco2v*Vgas*10^3            # volume of carbondioxide evolved (m^3)

#Properties of the gas in the liquid phase
Hh2=74*10^3           # Henry's gas constant for hydrogen (atm/mole fraction)
Hco2 = 2095           # Henry's gas constant for hydrogen (atm/mole fraction)

xh2m=P*yh2m/Hh2        # mole fraction of hydrogen in the liquid phase
xco2m=P*yco2m/Hco2    # mole fraction of carbon dioxide in the liquid phase

# The yield factors (determined experimentally)
Yh2a=764*10^-3        # yield coefficient = moles biomass formed/moles of
                         acetic acid consumed to form new cells
Yxa=2418*10^-3        # yield coefficient = moles H2 formed/moles of acetic
                        acid consumed
m=5*10^-2             # maintenance coefficient (1/h)

# Acetic acid consumption
d(Ca) / d(t) = -ka*Ca
ka=24*10^-3           # acetic acid consumption rate constant (1/h)



Ca(0) = 36.326464     # initial concentration of acetic acid (mol/m^3) or (mM)
```

```
# Sodium glutamate consumption
d(Cglu) / d(t)= -kglu*Cglu
kglu=245*10^-2                # glutamate rate constant (1/mol/h)
Cglu(0)=4                     # initial concentraion of glutamic acid (1/mol/h)

# Biomass formation
d(Cx) / d(t) = ka*Ca*Yxa
Cx(0) =24.84829               # initial cell concentration-average cell conc in the
outdoor experiment
Xx=Cx*2.286*10^-4             # cell concentration (g/L)

# Hydrogen
d(Ch2gas) / d(t) = (V/Vgas)*(ka*Ca*Yh2a)-Ch2gas/t
Ch2gas(0) = 0.00467

Nw=V*rhow*1000/18             # amount of water in the reactor (mol)
Nh2liq=Nw*xh2m                # amount of hydrogen in the liquid phase (mol)
Ch2liq = Nh2liq/V
Nh2 = Ch2gas*Vgas+Ch2liq*V
Nh2gas=Nh2-Nh2liq

# Carbon dioxide
Nco2=Nh2/2                # total amount of carbon dioxide produced (mol)
Nco2gas=Nh2gas*yco2m/yh2m # amount of carbon dioxide in the gas phase (mol)
Nco2liq=Nco2-Nco2gas      # amount of carbon dioxide in the liquid phase (mol)

# Gas produced
Ngas=Nh2gas+Nco2gas  # total amount of gas produced (moles)
```

```
# Heat of reaction
# Two reactions are considered;
#     (i) hydrogen production: CH3COOH + 2H2O = 4H2 + 2CO2
#     (ii) biomass formation: CH3COOH + 0.60 C5H9NO4 = 4.30
                                              CH1.76O0.38N0.14 + 0.71 CO2 + 1.05 H2O

deltahrxn1= 269  # Heat of reaction for hydrogen production (kJ/mol)
deltahrxn2= 156  # Heat of reaction for hydrogen production (kJ/mol)

Qrxn1  =  V*deltahrxn1*(1/Yh2a)*(ka*Ca)*(1/3600)*1000   #  Heat  evolved  from hydrogen production (reaction 1) (W)
Qrxn2  =  V*deltahrxn2*(1/Yxa)*ka*Ca*(1/3600)*1000    #  Heat  evolved  from biomass formation (reaction 2) (W)
Qmet = Qrxn1+Qrxn2     # Metabolic heat of reaction (W)

# End of file
```

APPENDIX G

ABSORBANCE SPECTRUM OF RHODOBACTER CAPSULATUS AT DIFFERENT CELL CONCENTRATIONS

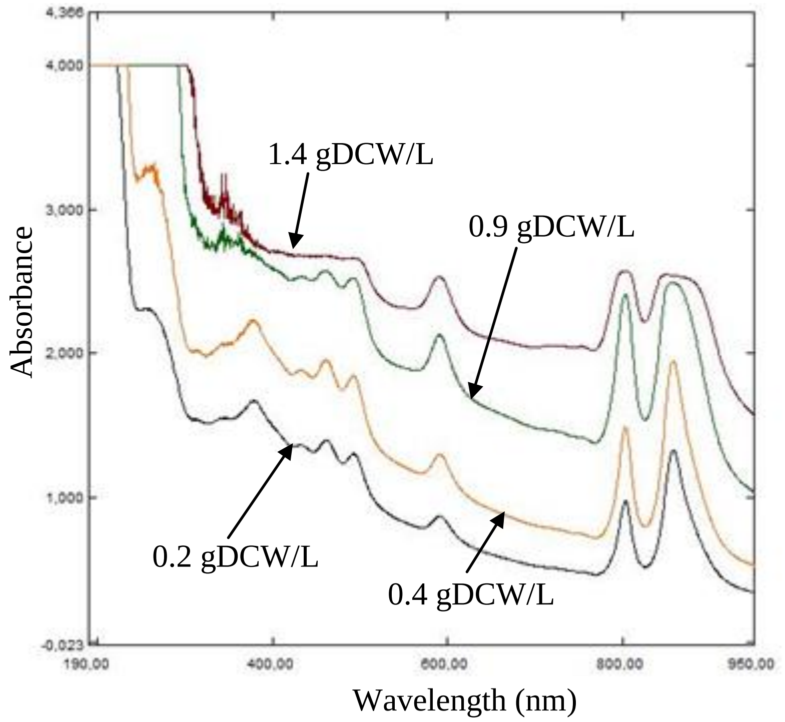

Figure G.1 Absorbance spectrum of *Rhodobacter capsulatus YO3* at different cell concentrations.

APPENDIX H

UNSTEADY STATE ONE_DIMENSIONAL THERMAL MODEL

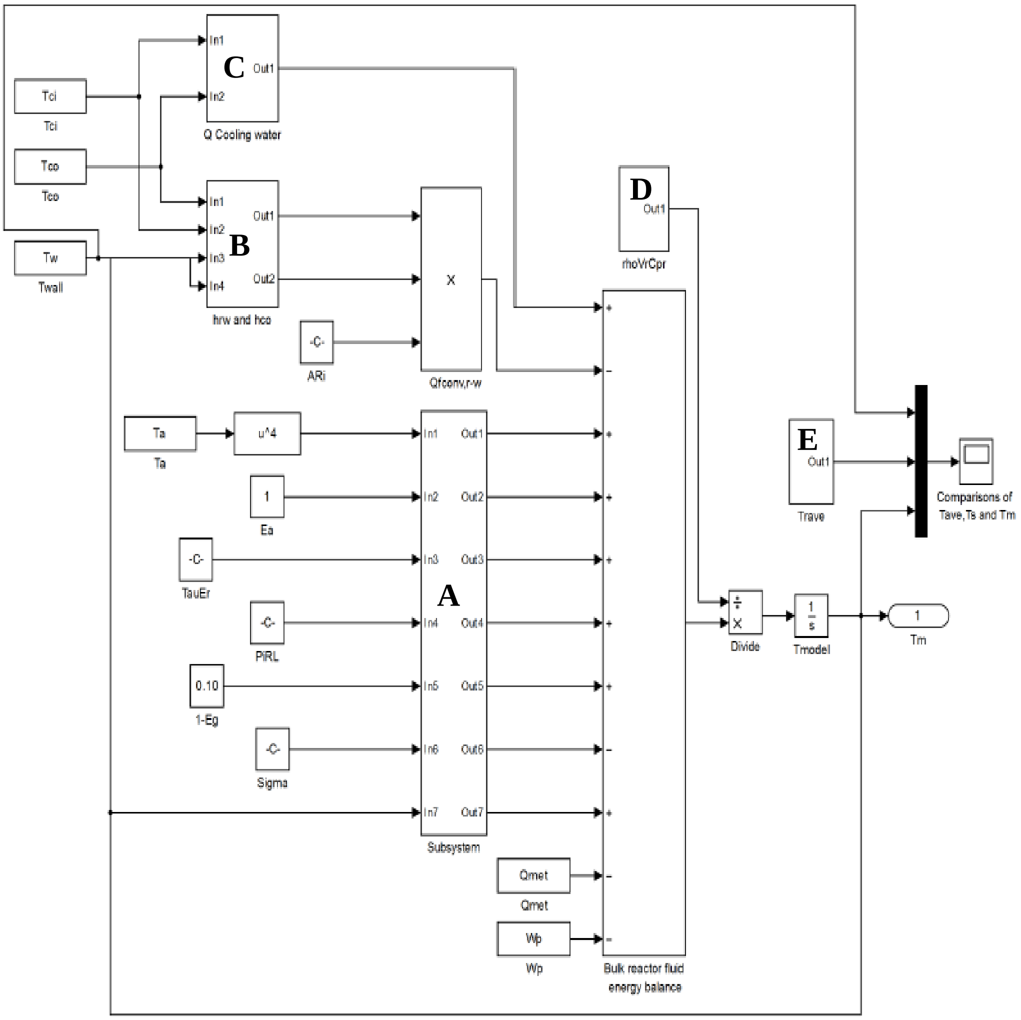
C
In1
In2
Out1
Q Cooling water
Tci
Tci
Tco
Tco
Tw
Twall
B
In1
In2
In3
In4
Out1
Out2
hrw and hco
X
-C-
ARi
Qfconv,r-w
D
Out1
rhoVrCpr
Ta
Ta
u^4
1
Ea
-C-
TauEr
-C-
PiRL
0.10
1-Eg
-C-
Sigma
A
In1
In2
In3
In4
In5
In6
In7
Out1
Out2
Out3
Out4
Out5
Out6
Out7
Subsystem
Qmet
Qmet
Wp
Wp
+
-
Bulk reactor fluid energy balance
E
Out1
Trave
Comparisons of Tave,Ts and Tm
÷
X
Divide
1/s
Tmodel
1
Tm

Figure H.1 The dynamic thermal model solved using Matlab 2013_Simulink.

Subsystem A: Calculation of the Total Radiative Heat Transferred

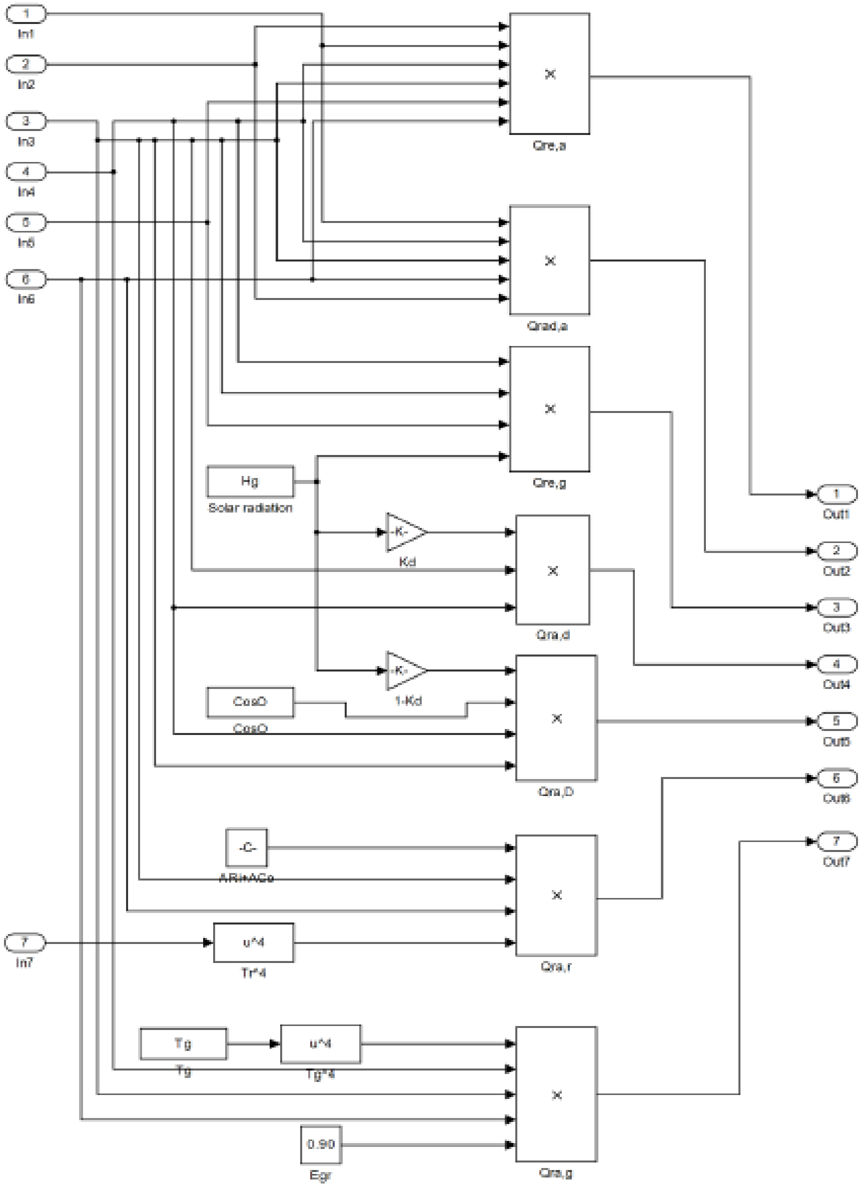
1
In1
2
In2
3
In3
4
In4
5
In5
6
In6
×
Qre,a
×
Qrad,a
×
Qre,g
Hg
Solar radiation
-K-
Kd
×
Qra,d
-K-
1-Kd
CosO
CosO
×
Qra,D
-C-
ARi+ACo
×
Qra,r
7
In7
u^4
Tr^4
Tg
Tg
u^4
Tg^4
×
0.90
Egr
Qra,g
1
Out1
2
Out2
3
Out3
4
Out4
5
Out5
6
Out6
7
Out7

Figure H.2 The total radiative heat transferred in the dynamic thermal model.

Subsystem B: Calculation of the Convective Heat transfer Coefficients in the Reactor

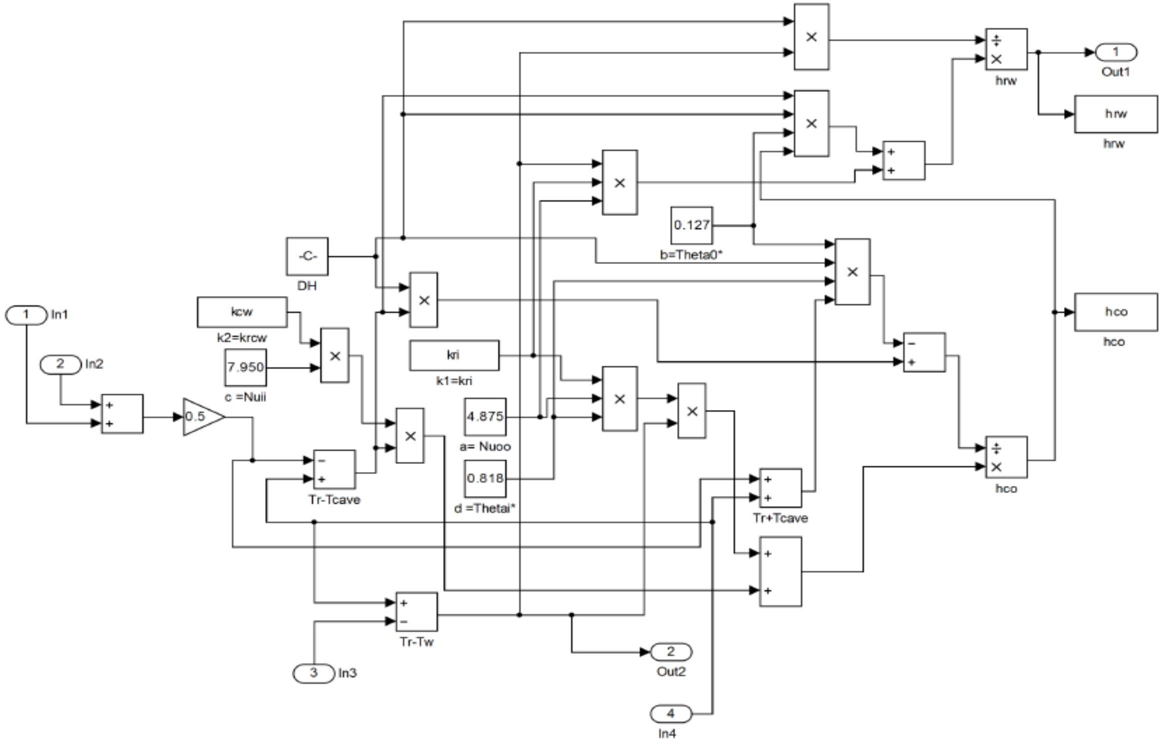
1
Out1
hrw
hrw
hrw
0.127
b=Theta0*
-C-
DH
1
In1
kcw
k2=krcw
2
In2
7.950
c =Nuii
kri
k1=kri
hco
hco
0.5
4.875
a= Nuoo
hco
0.818
d =Thetai*
Tr-Tcave
Tr+Tcave
Tr-Tw
2
Out2
3
In3
4
In4

Figure H.3. Calculation of the convective heat transfer coefficients in the reactor.

Subsystem C: Calculation of the Cooling Duty

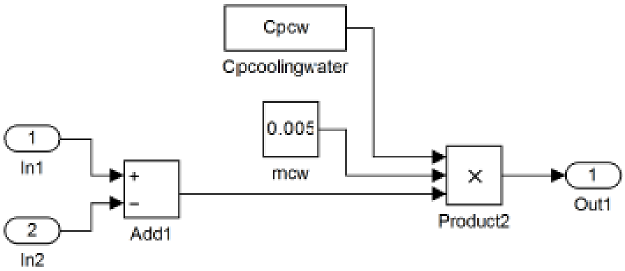
Cpcw
Cpcoolingwater
0.005
mcw
1
In1
2
In2
+
-
Add1
×
Product2
1
Out1

Figure H.4 calculations of the amount of heat removed by the cooling water.

Subsystem D: Calculation of the Amount of Energy in the Reactor

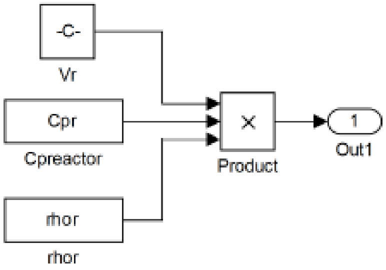
-C-
Vr
Cpr
Cpreactor
rhor
rhor
×
Product
1
Out1

Figure H.5 Calculation of the amount of heat in the reactor.

Subsystem E: Calculation of the Average Reactor Temperature

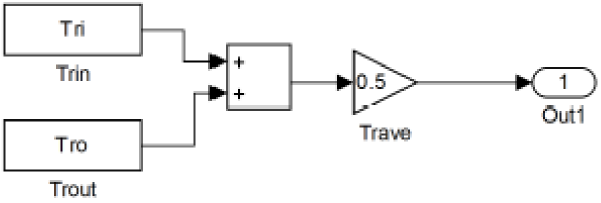
Tri
Trin
Tro
Trout
+
+
0.5
Trave
1
Out1

Figure H.6 Calculations of the average reactor temperature.

APPENDIX I

SAMPLE CALCULATIONS

I.1 Volume of the Outdoor Photobioreactor

$$V_r = V_{reactor\ cylinder} - V_{cooling\ tube} \tag{I.1}$$

$$V_{reactor\ cylinder} = \pi \times \left(0.0136m\right)^2 \times 4.192m = 2.44 \times 10^{-3} m^3 \tag{I.2}$$

$$V_{cooling\ tube} = \pi \times \left(0.0035m\right)^2 \times 4.192m = 1.61 \times 10^{-4} m^3 \tag{I.3}$$

$$V_r = 2.44 \times 10^{-3} m^3 - 1.61 \times 10^{-4} m^3 = 2.28 \times 10^{-3} m^3 \tag{I.4}$$

I.2 Surface Area of the Photobioreactor and the Cooling Tube

- Photobioreactor outer glass tube surface area

$$SA_{RO} = \pi D_o L \tag{I.5}$$

$$= \pi\ (0.03\ \mathrm{m})\ (4.192\mathrm{m}) = 0.396\ \mathrm{m}^2$$

- Photobioreactor inner glass tube surface area

$$SA_{RI} = \pi D_i L \tag{I.6}$$

$$= \pi\ (0.0272\ \mathrm{m})\ (4.192\mathrm{m}) = 0.358\ \mathrm{m}^2$$

- Cooling tube outer surface area

$$SA_{CTO} = \pi d_o L \tag{I.7}$$

$$= \pi\ (0.007\ \mathrm{m})\ (4.192\ \mathrm{m}) = 0.092\ \mathrm{m}^2$$

- Cooling tube inner surface area

$$SA_{CTI} = \pi d_i L \tag{I.8}$$

$$= \pi\,(0.005\text{ m})\,(4.192\text{ m}) = 0.066\text{ m}^2$$

I.3 Determination of the Hydraulic Diameter

The hydraulic diameter is defined as the cross-sectional area perpendicular to flow divided by the wetted perimeter.

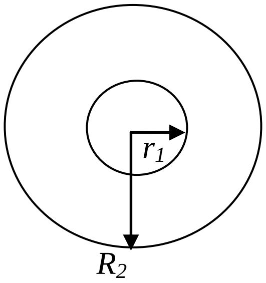

Figure I.1 Determination of the hydraulic diameter.

$$D_H = \frac{4\left(\pi R_2^{\,2} - \pi r_1^{\,2}\right)}{2\pi R_2 + 2\pi r_1} = 2\left(R_2 - r_1\right) = 2\left(0.0136 - 0.0035\right)m \tag{I.9}$$

$$= 0.0202\ m$$

I.4 Reactor Medium Mass Flow Rate

$$Q = 210\frac{ml}{\min}\times 10^{-6}\frac{m^3}{\mathrm{m}l}\times 1\frac{\min}{60s} = 3.5\times 10^{-6}\frac{m^3}{s} \tag{I.10}$$

$$velocity\ (u) = \frac{Q}{A}$$

$$= \frac{3.5\times 10^{-6}\,\frac{m^3}{s}}{\pi\left(0.0136\right)^2 m^2 - \pi\left(0.0035\right)^2 m^2} = 6.45\times 10^{-3}\,\frac{m}{s}$$

$$\dot{m}_r = Q \times \rho_w$$

$$= 3.5\times10^{-6}\,\frac{m^3}{s}\times\ 996\,\frac{kg}{m^3} \qquad \text{(I.11)}$$

$$= 3.486\times10^{-3}\,\frac{kg}{s}$$

I.5 Cooling Water Mass Flow Rate

$$\dot{m}_{cw} = F_{cw}\times\rho_w$$

$$= 640\,\frac{\text{ml}}{\text{min}}\times\frac{\text{min}}{60\text{s}}\times10^{-6}\,\frac{m^3}{\text{ml}}\times996\,\frac{kg}{\text{m}^3} \qquad \text{(I.12)}$$

$$= 0.01064\,\frac{kg}{s}$$

I.6 Reynolds Number

$$\text{Re} = \frac{\rho u D_H}{\mu}$$

$$= \frac{996\,\dfrac{kg}{m^3}\times6.451\times10^{-3}\,\dfrac{m}{s}\times0.0202m}{0.798\times10^{-3}\,\dfrac{kg}{m.s}} = 160 \qquad \text{(I.13)}$$

I.7 Prandtl Number

$$\text{Pr} = \frac{Cp_w\mu}{k_w}$$

$$= \frac{4178\,\dfrac{J}{kg.K}\times0.798\times10^{-3}\,\dfrac{kg}{m.s}}{0.615\,\dfrac{J}{m..s.K}} = 5.42 \qquad \text{(I.14)}$$

I.8 Peclet Number

$Pe = RePr$

= 163 × 5.42 = 882 (Since Pe > 100, the assumption that axial conduction is negligible is valid)

(I.15)

I.9 Hydrodynamic and Thermal Entry Length

For laminar flow (Re < 2300); (Latif, 2006) (I.16)

$$L_{\mathrm{h}} \approx 0.056 \,\mathrm{Re}\, D_H \quad (1.17)$$

$$L_{\mathrm{t}} \approx 0.043 N_{\mathrm{Re}} \,\mathrm{Pr}\, D_H \quad (\mathrm{I.18})$$

where L_h and L_t are the hydrodynamic and thermal entry lengths, respectively.

- Re = 160

$$L_{\mathrm{h}} = 0.056 \times 160 \times 0.0202 m = 0.18\ m \quad (\mathrm{I.19})$$

$$L_{\mathrm{t}} = 0.043 \times 160 \times 5.66 \times 0.0202 m = 0.787\ m \quad (\mathrm{I.20})$$

Since L_h and L_t are small compared to the reactor length (4.192 m), the flow in the system can be considered to be fully developed.

I.10 Pressure Drop Calculation

Assuming flow in the water at 35 °C is continuously circulated in the U-tube reactor at 255 ml/min reactor.

$$Q = uA \quad (\mathrm{I.21})$$

$$u = \frac{Q}{A} = \frac{255 \dfrac{ml}{\min} \times \dfrac{1\min}{60s} \times \dfrac{10^{-6} m^3}{ml}}{\pi \left(\dfrac{0.0272^2}{4} \right) m^2} = 0.0073\, {}^{m}\!/\!_{s} \quad (\mathrm{I.22})$$

$$\mathrm{Re} = \frac{\rho u D_H}{\mu} \quad (\mathrm{I.23})$$

$$= \frac{994\frac{kg}{m^3}\times 0.0073\frac{m}{s}\times 0.0202m}{0.720\times 10^{-3}\frac{kg}{m.s}} = 275 \qquad \text{(I.24)}$$

$$\Delta P = \left(4f\frac{L}{D}+K_f\right)\frac{\overline{V}}{2g_c}\rho \qquad \text{(I.25)}$$

$$\Delta P = \left(4\left(\frac{16}{275}\right)\frac{4m}{0.0272m}+2.2\right)\frac{0.0073^2\frac{m}{s}}{2\left(1\frac{kg.m}{N.s^2}\right)}\left(994\frac{kg}{m^3}\right)$$

$$= 0.97\frac{kg.m}{s^2} = 0.97\text{Pa} \qquad \text{(I.26)}$$

I.11 Hydrualic Retention Time Calculation

$$\text{Hydraulic Retention Time (HRT)} = \frac{\text{Volume of the photobioreactor (m}^3\text{)}}{\text{Volumetric flow rate (m}^3\text{/s)}} \qquad \text{(I.27)}$$

i. U-tube reactor

$$\text{Residence time (RT)} = \frac{2.8\times 10^{-3}m^3}{255\frac{ml}{\min}\times\frac{10^{-6}m^3}{ml}} = 10\min \qquad \text{(I.28)}$$

ii. Serpentine reactor

$$\text{Residence time (RT)} = \frac{30\times 10^{-3}m^3}{255\frac{ml}{\min}\times\frac{10^{-6}m^3}{ml}} = 120\min \qquad \text{(I.29)}$$

iii. Manifold reactor

$$\text{Residence time (RT)} = \frac{90\times 10^{-3}m^3}{255\frac{ml}{\min}\times\frac{10^{-6}m^3}{ml}} = 350\min \qquad \text{(I.30)}$$

I.12 Average Volumetric Flow Rate

$$\text{Average Volumetric Flow Rate } (Q_{ave}) \ (\text{m}^3/\text{s}) = \text{Velocity of the fuid (m/s)} \times \text{Cross-sectional area } (\text{m}^2) \quad \text{(I.31)}$$

I.13 Latitude (φ) of Ankara

Ankara: 39° 55’ 38 N

$$\sim 39.93° \text{ x } \pi/180 \ = 0.697 \text{ rad} \quad \text{(I.32)}$$

I.14 Solar Declination (δ)

For the experiment carried out on the 7th of August, 2012,

N = 219

$$\delta = 23.35 \frac{2\pi}{360} Sin\left(2\pi \frac{284+219}{365}\right) = \ 0.283 \text{ rad} \quad \text{(I.33)}$$

I.15 Solar Hour Angle (ω)

$$\omega = (\text{Time} - 12.00) \text{ x } (15°) \text{ x } \pi/180 \text{ (rad)} \quad \text{(I.34)}$$

e.g. At 7 a.m

$$\omega = (06.00 - 12.00) \text{ x } (15°) \text{ x } \pi/180 = 1.571 \text{ rad} \quad \text{(I.35)}$$

I.16 Angle of incidence (θ_z)

$$Cos(\theta_z) = Sin\ \varphi\ Sin\ \delta + Cos\ \varphi\ \text{Cos}\ \delta\ \text{Cos}\ \omega \quad \text{(I.36)}$$

For example, the experiment carried out on the 7th of August, 2013 in Ankara, Turkey, at 6 a.m.

$$Cos(\theta_z) = \left(\begin{array}{l} \left(Sin\ (0.697) \times Sin\ (0.283)\right) + \\ \left(\begin{array}{l} Cos\ \ (0.697) \times Cos\ (0.283) \\ \times Cos\ (1.571) \end{array} \right) \end{array} \right) \quad \text{(I.37)}$$

$$= \ 0.179$$

I.17 Work Done by the Pump

$$\dot{m}_r\left(\frac{P_1}{\rho}+\alpha_1\frac{u_1^2}{2}+gz_1\right)+\dot{W}_s=\dot{m}_r\left(\frac{P_2}{\rho}+\alpha_2\frac{u_2^2}{2}+gz_2\right) \tag{I.38}$$

The left hand side equation

$$3.486\times10^{-3}\,\frac{kg}{s}\left(\frac{0.05\times10^{5}\,\frac{kg}{ms^{2}}}{997\,\frac{kg}{m^{3}}}+2\frac{\left(0.0150\,\frac{m}{s}\right)^{2}}{2}\right)+\dot{W}_s \tag{I.39}$$

The right hand side equation

$$3.486\times10^{-3}\,\frac{kg}{s}\left(\frac{0.26\times10^{5}\,\frac{kg}{ms^{2}}}{997\,\frac{kg}{m^{3}}}+2\frac{\left(0.0314\,\frac{m}{s}\right)^{2}}{2}\right) \tag{I.40}$$

Equating left hand side equation to the right hand side equation and solving results in:

$$\dot{W}_s=0.63\text{W} \tag{I.41}$$

APPENDIX J

DATA RELATIVE TO CHAPTER 7

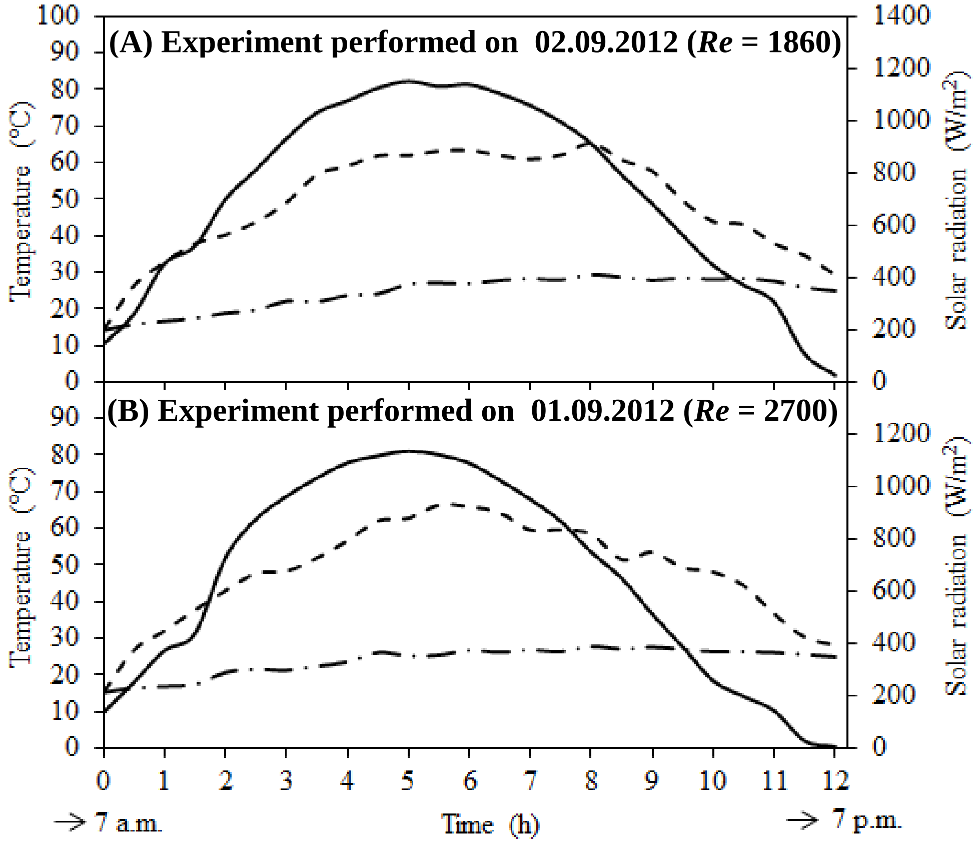

Figure J.1 The change in the air temperature (— · —), the ground temperature (– – –) and solar radiation (———) with time. The reactors contained water circulated at Reynolds number 1860 and 2700, in co-current flow to the cooling water. The start of the experiment (0^{th} hour) corresponds to 7 a.m. and the end of the experiment (12^{th} hour) corresponds to 7 p.m.

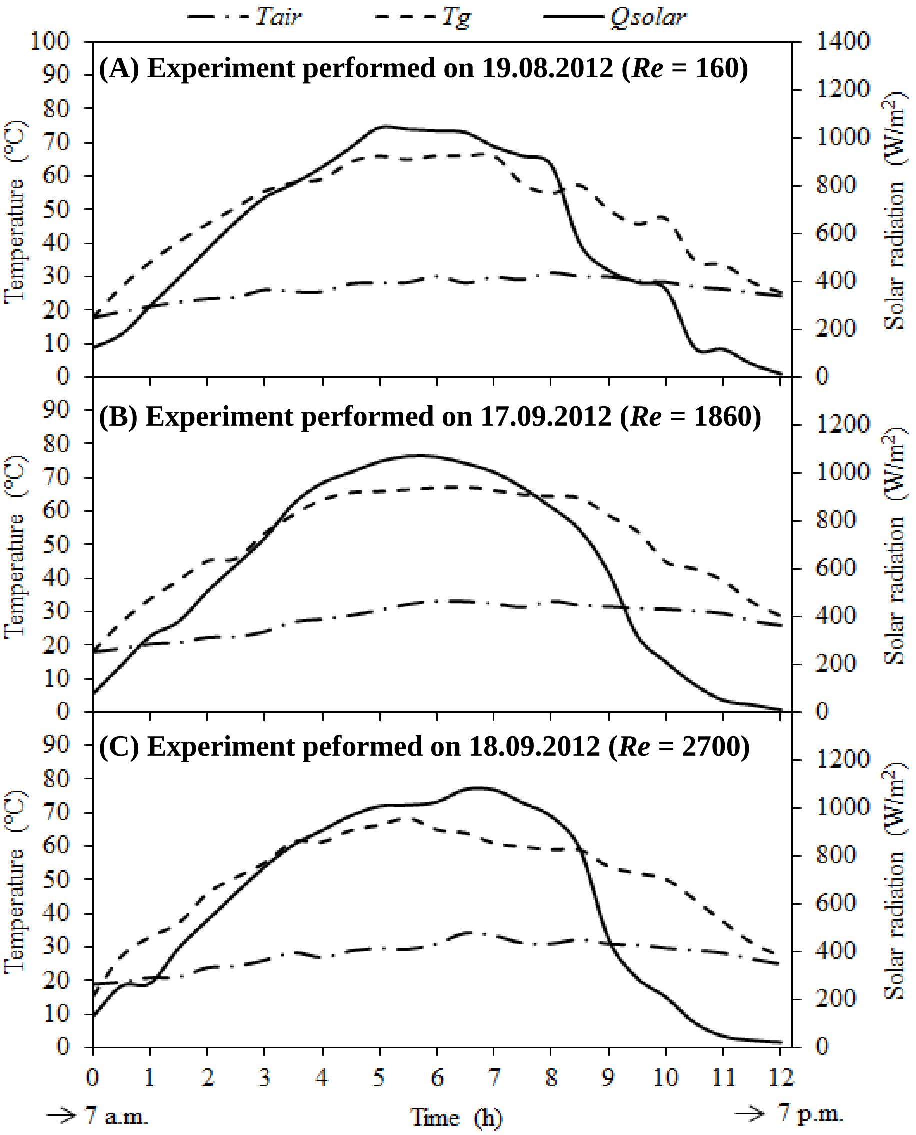

Figure J.2 The change in the air temperature (— · —), the ground temperature (– – –) and solar radiation (———) with time. The reactors contained water circulated at Reynolds number 1860 and 2700, in counter-current flow to the cooling water. The start of the experiment (0^{th} hour) corresponds to 7 a.m. and the end of the experiment (12^{th} hour) corresponds to 7 p.m.

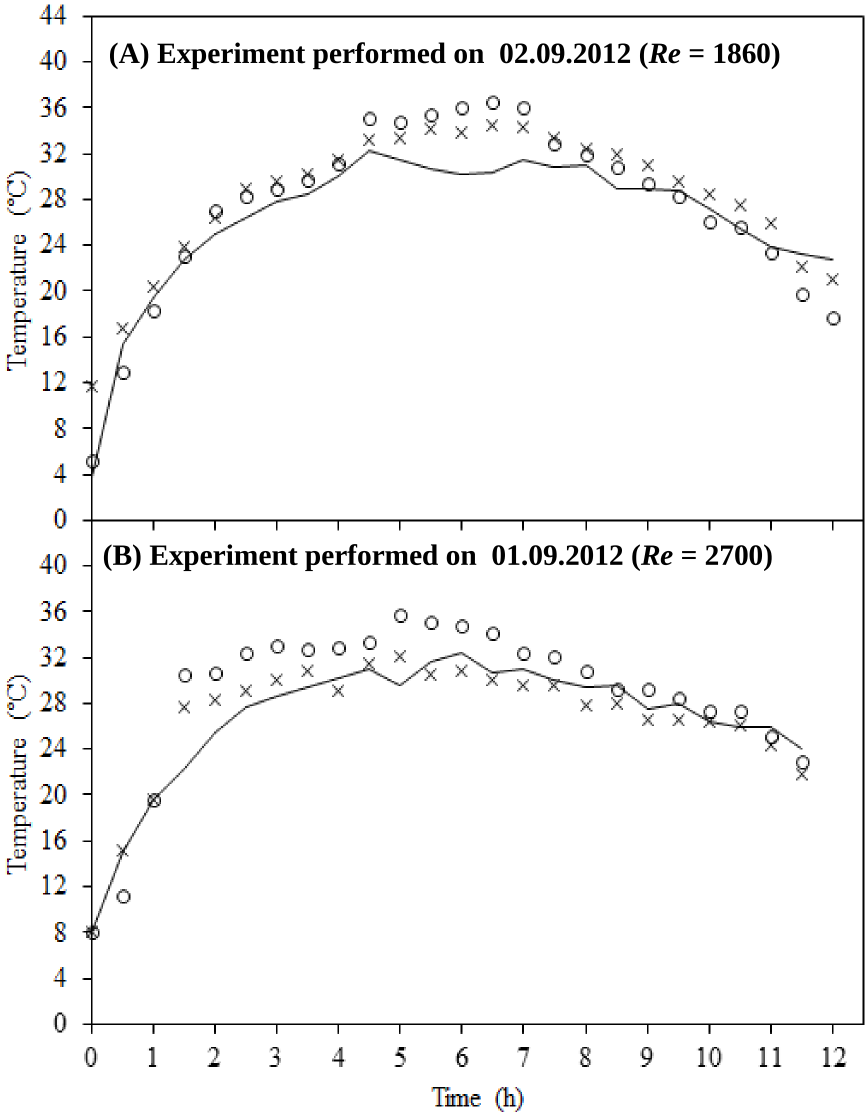

Figure J.3 Comparison of the changes in the reactor average temperatures T_{ave} (o), the reactor surface temperatures T_s (x) and the predicted (model) temperatures T_m (–) with time. The experiment was performed on the 28th of August, 2012.

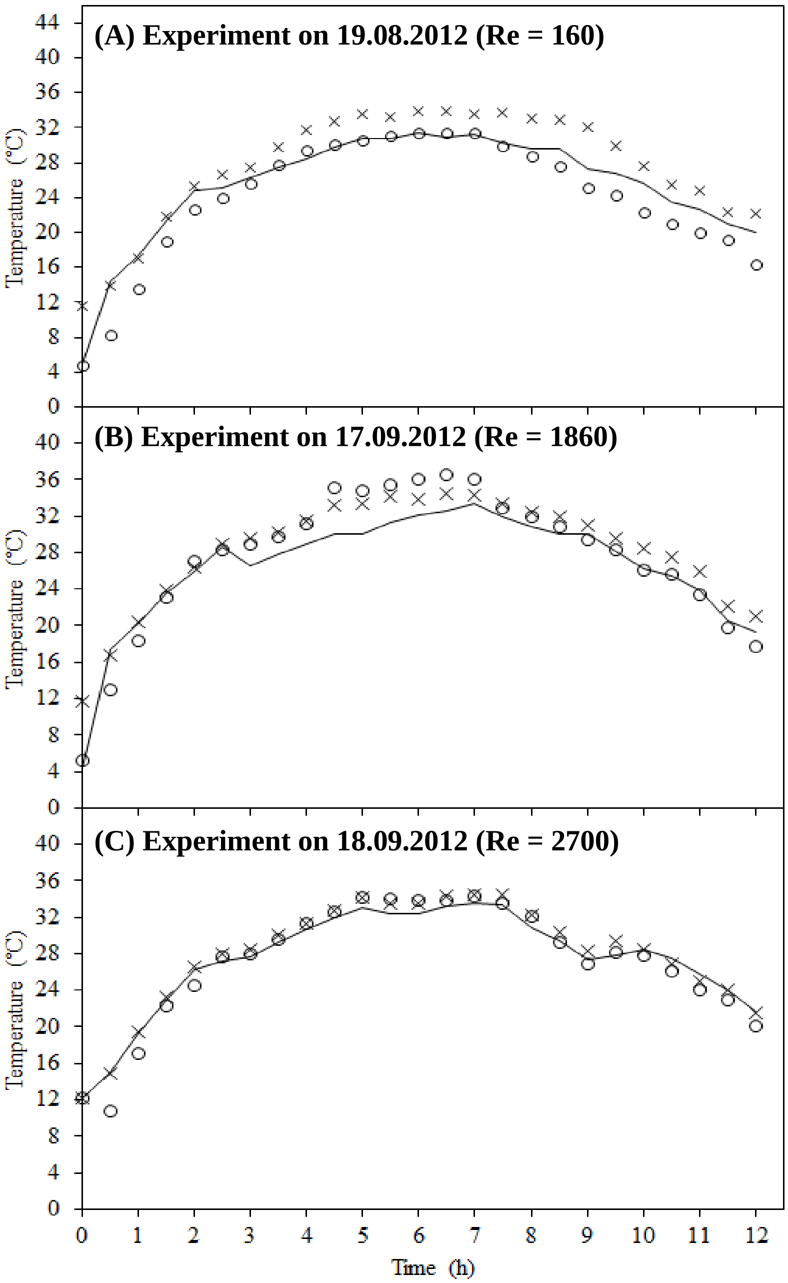

Figure J.4 Comparison of the changes in the reactor average temperatures T_{ave} (o), the reactor surface temperatures T_s (x) and the predicted (model) temperatures T_m (–) with time. The reactors were counter-currently cooled.

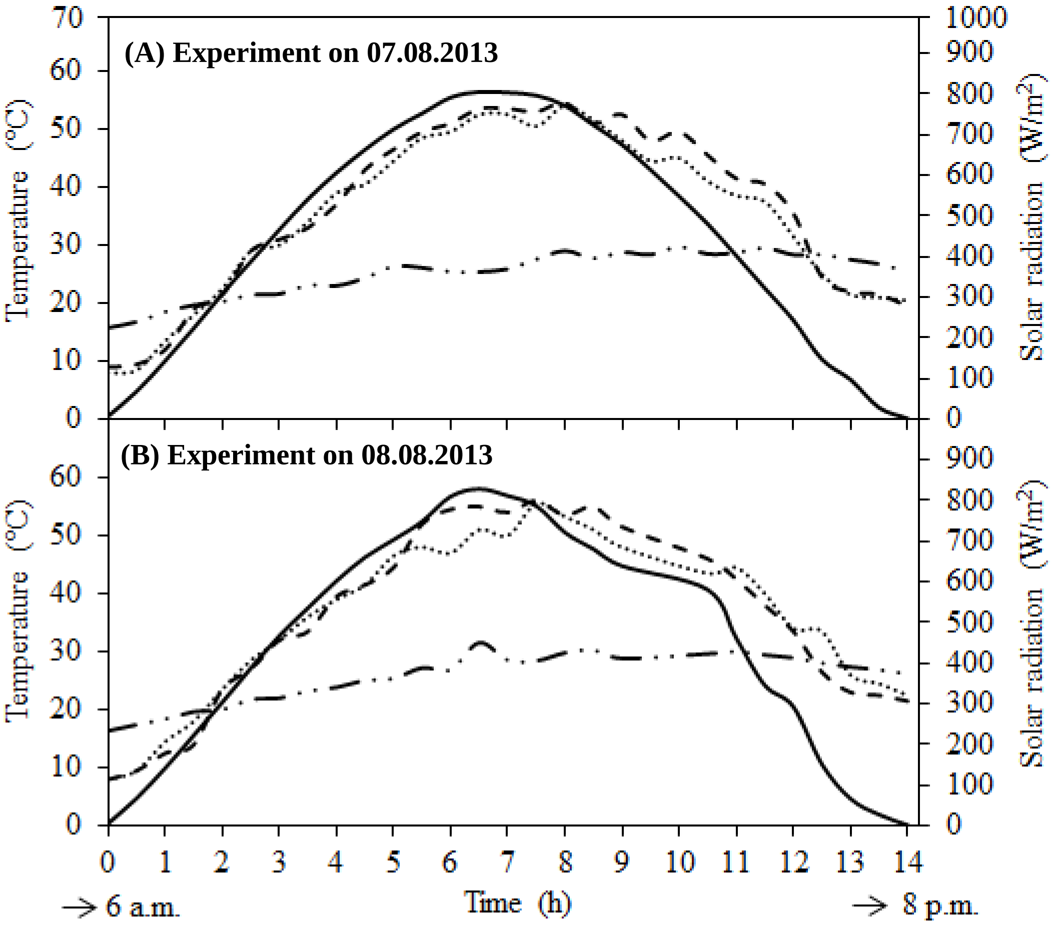

Figure J.5 The change in air temperature (— · · · -), the co-currently cooled reactor ground temperature (– – – –), counter-currently cooled reactor ground temperature (········) and solar radiation (——) with time. The experiments were carried out on the 7th and 8th of August, 2013. The start of the experiment (0th hour) corresponds to 6 a.m. and the end of the experiment (14th hour) corresponds to 8 p.m.

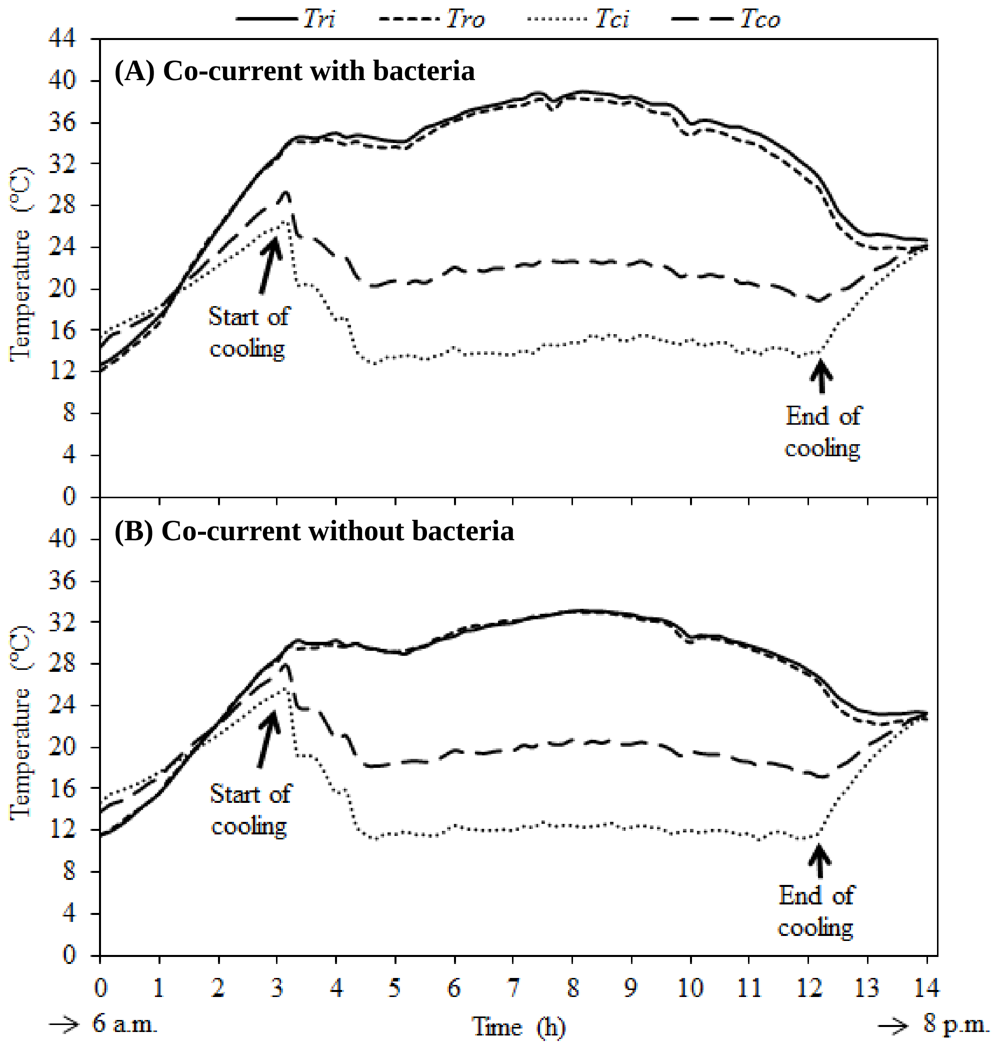

Figure J.6 Comparisons of the changes in the reactor inlet temperatures (T_{ri}, ——), the reactor outlet temperatures (T_{ro}, – –), the cooling water inlet temperatures (T_{ci},— —) and the cooling water outlet temperatures (T_{co}, ·····) with time. The experiments were performed on the 7th of August, 2013 using co-currently cooled reactors with and without *Rhodobactercapsulatus* YO3 cultures operated in outdoor conditions.

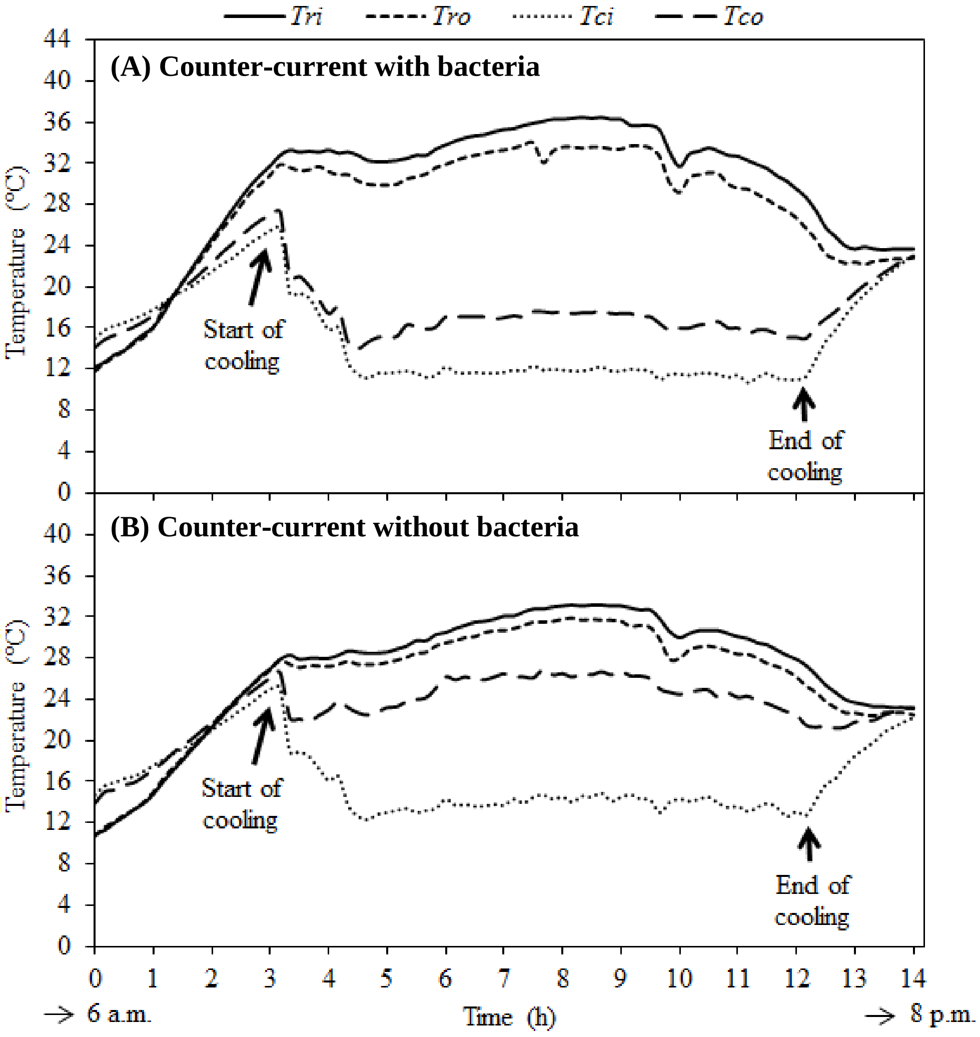

Figure J.7 Comparisons of the changes in the reactor inlet temperatures (T_{ri}, ——), the reactor outlet temperatures (T_{ro}, – –), the cooling water inlet temperatures (T_{ci},— —) and the cooling water outlet temperatures (T_{co}, ·····) with time. The experiments were performed on the 7th of August, 2013 using counter-currently cooled reactors with and without *Rhodobactercapsulatus* YO3 cultures operated in outdoor conditions.

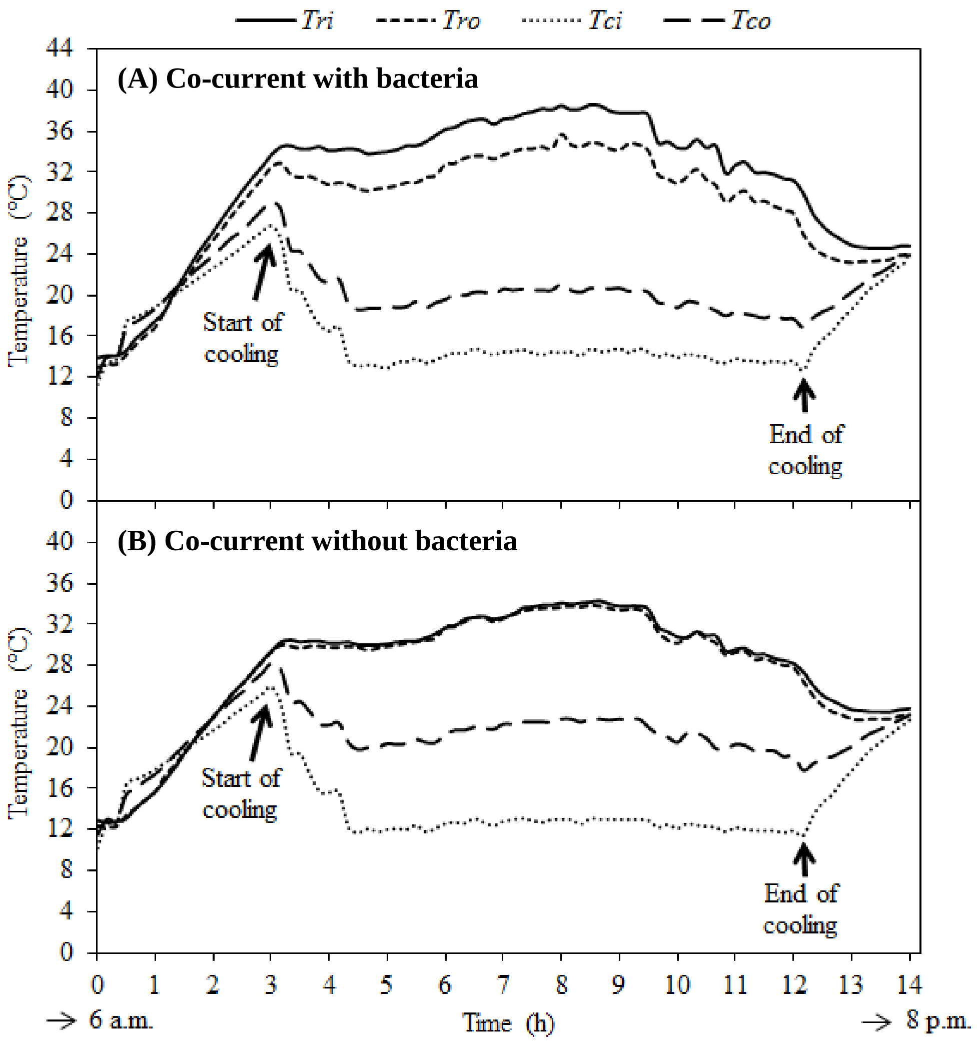

Figure J.8 Comparisons of the changes in the reactor inlet temperatures (T_{ri}, ——), the reactor outlet temperatures (T_{ro}, – –), the cooling water inlet temperatures (T_{ci},— —) and the cooling water outlet temperatures (T_{co}, ·····) with time. The experiments were performed on the 8th of August, 2013 using co-currently cooled reactors with and without *Rhodobactercapsulatus* YO3 cultures operated in outdoor conditions.

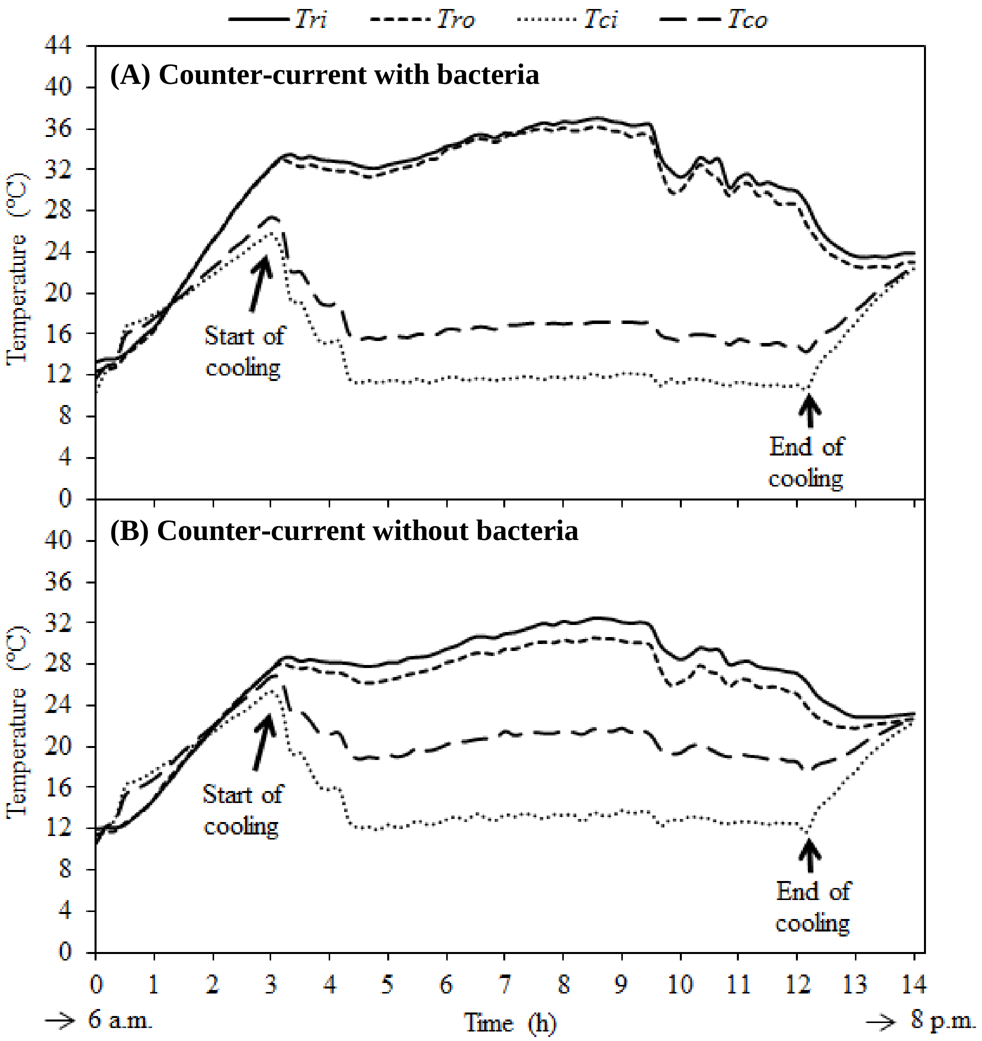

Figure J.9 Comparisons of the changes in the reactor inlet temperatures (T_{ri}, ——), the reactor outlet temperatures (T_{ro}, – –), the cooling water inlet temperatures (T_{ci},— —) and the cooling water outlet temperatures (T_{co}, ·····) with time. The experiments were performed on the 8th of August, 2013 using counter-currently cooled reactors with and without *Rhodobactercapsulatus* YO3 cultures operated in outdoor conditions.

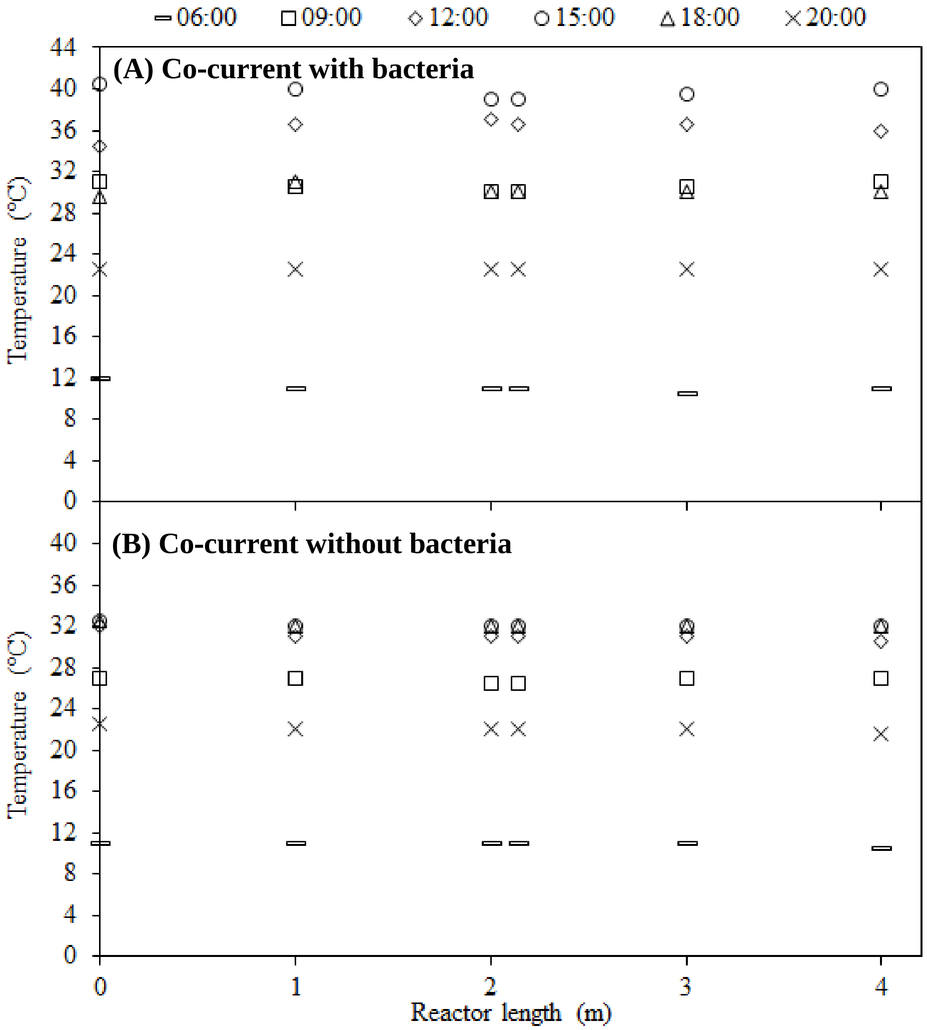

Figure J.10 The change in the surface temperature along the reactor tube at different times of the day. The experiments were performed on the 7th of August, 2013 using co-currently cooled reactors with and without *Rhodobacter capsulatus* YO3 cultures operated in outdoor conditions. (▭) 06:00, (□) 09:00, (◇) 12:00 p.m., (○) 15:00, (△) 18:00 and (×) 20:00.

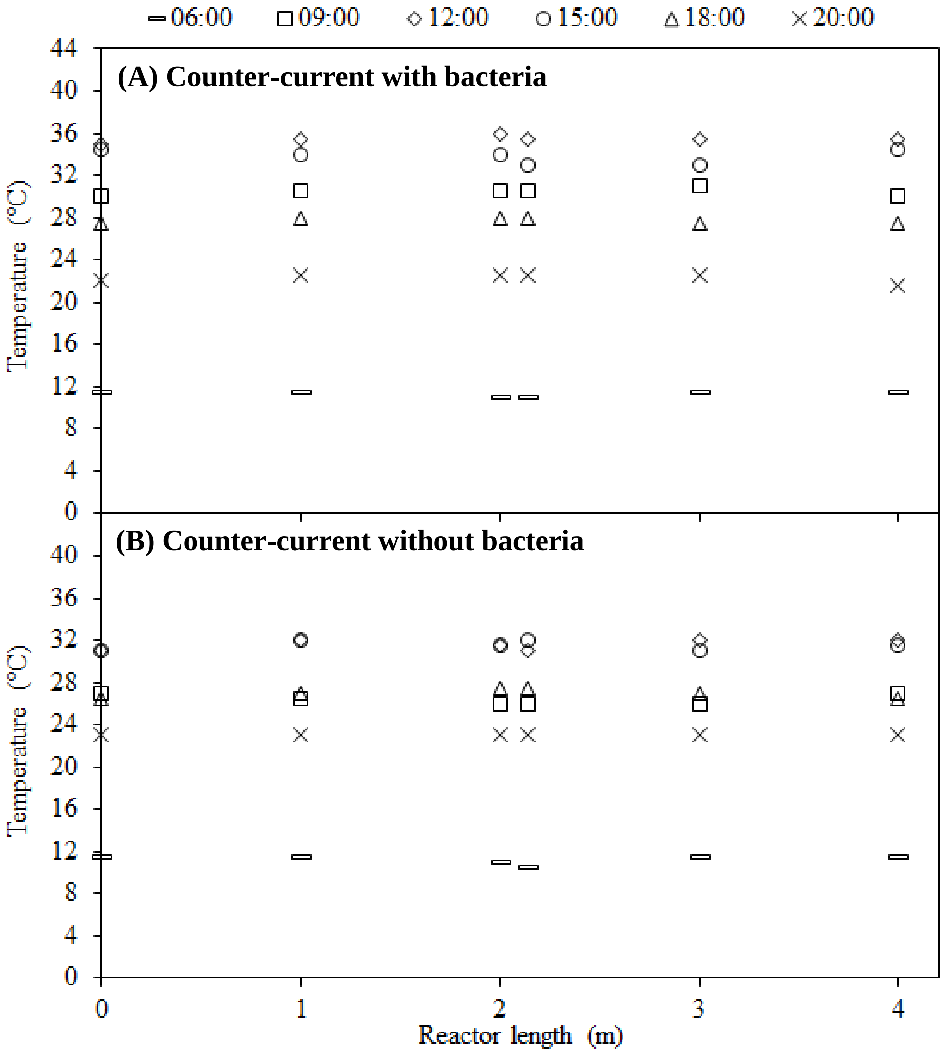

Figure J.11 The change in the surface temperature along the reactor tube at different times of the day. The experiments were performed on the 7th of August, 2013 using counter-currently cooled reactors with and without *Rhodobacter capsulatus* YO3 cultures operated in outdoor conditions. (▭) 06:00, (□) 09:00, (◇) 12:00 p.m., (○) 15:00, (△) 18:00 and (×) 20:00.

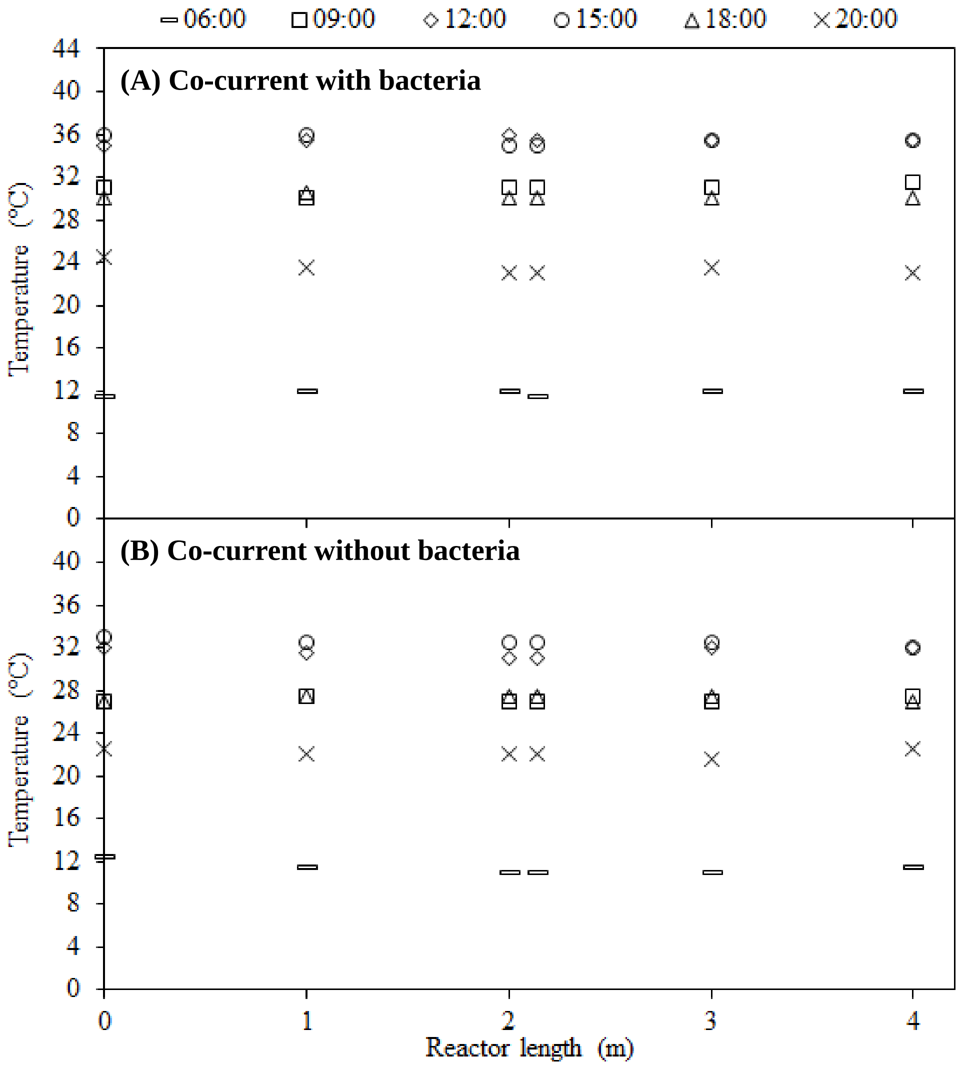

Figure J.12 The change in the surface temperature along the reactor tube at different times of the day. The experiments were performed on the 8th of August, 2013 using co-currently cooled reactors with and without *Rhodobacter capsulatus* YO3 cultures operated in outdoor conditions. (▭) 06:00, (□) 09:00, (◇) 12:00 p.m., (○) 15:00, (△) 18:00 and (×) 20:00.

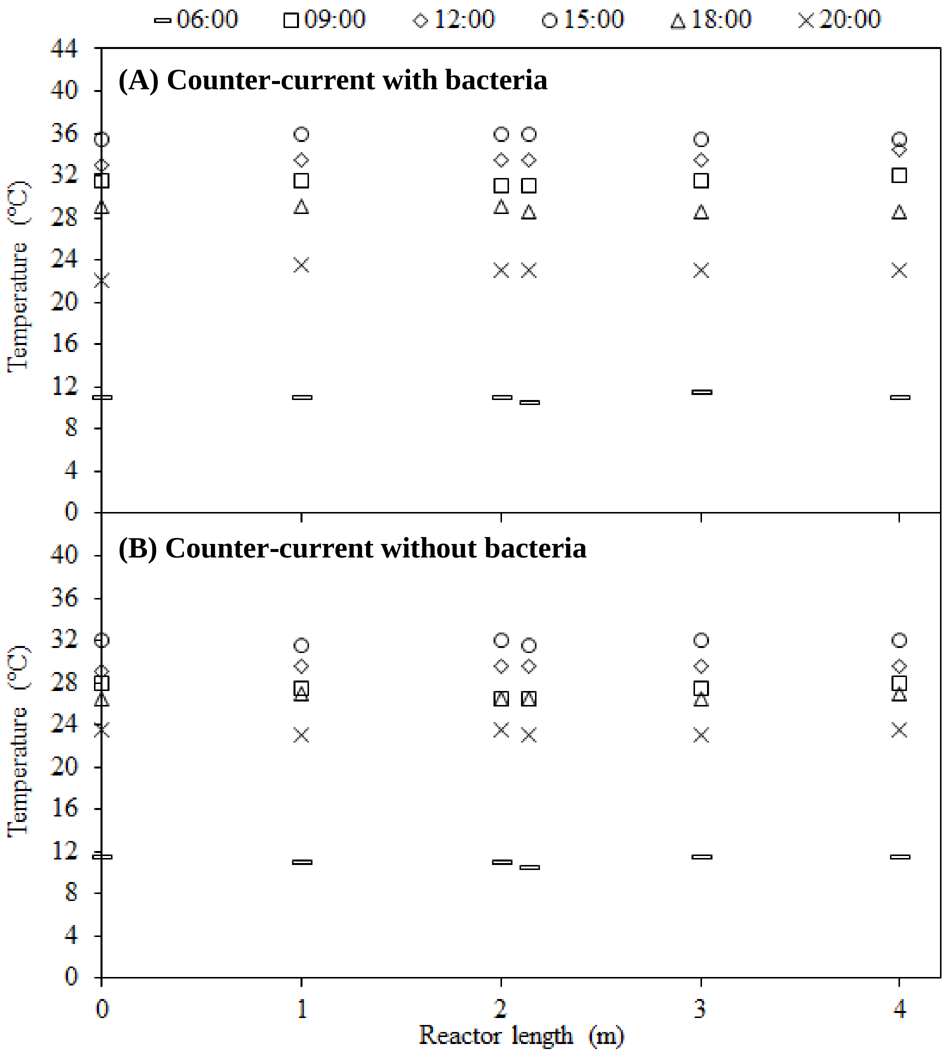

Figure J.13 The change in the surface temperature along the reactor tube at different times of the day. The experiments were performed on the 8th of August, 2013 using counter-currently cooled reactors with and without *Rhodobacter capsulatus* YO3 cultures operated in outdoor conditions. (▭) 06:00, (□) 09:00, (◇) 12:00 p.m., (○) 15:00, (△) 18:00 and (×) 20:00.

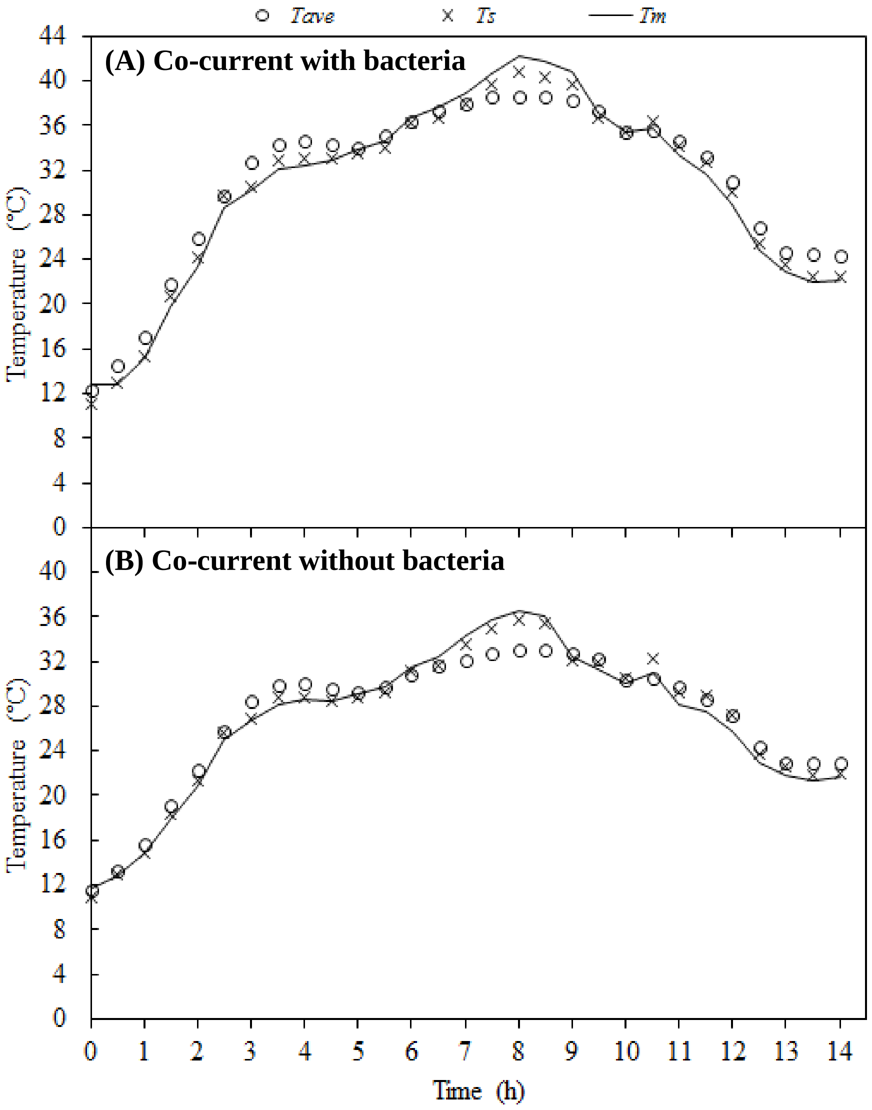

Figure J.14 Comparison of the changes in the reactor average temperatures T_{ave} (o), the reactor surface temperatures T_s (x) and the predicted (model) temperatures T_m (–) with time. The experiments were performed on the 7th of August, 2013 using co-currently cooled reactors with and without *Rhodobacter capsulatus* YO3 cultures operated in outdoor conditions.

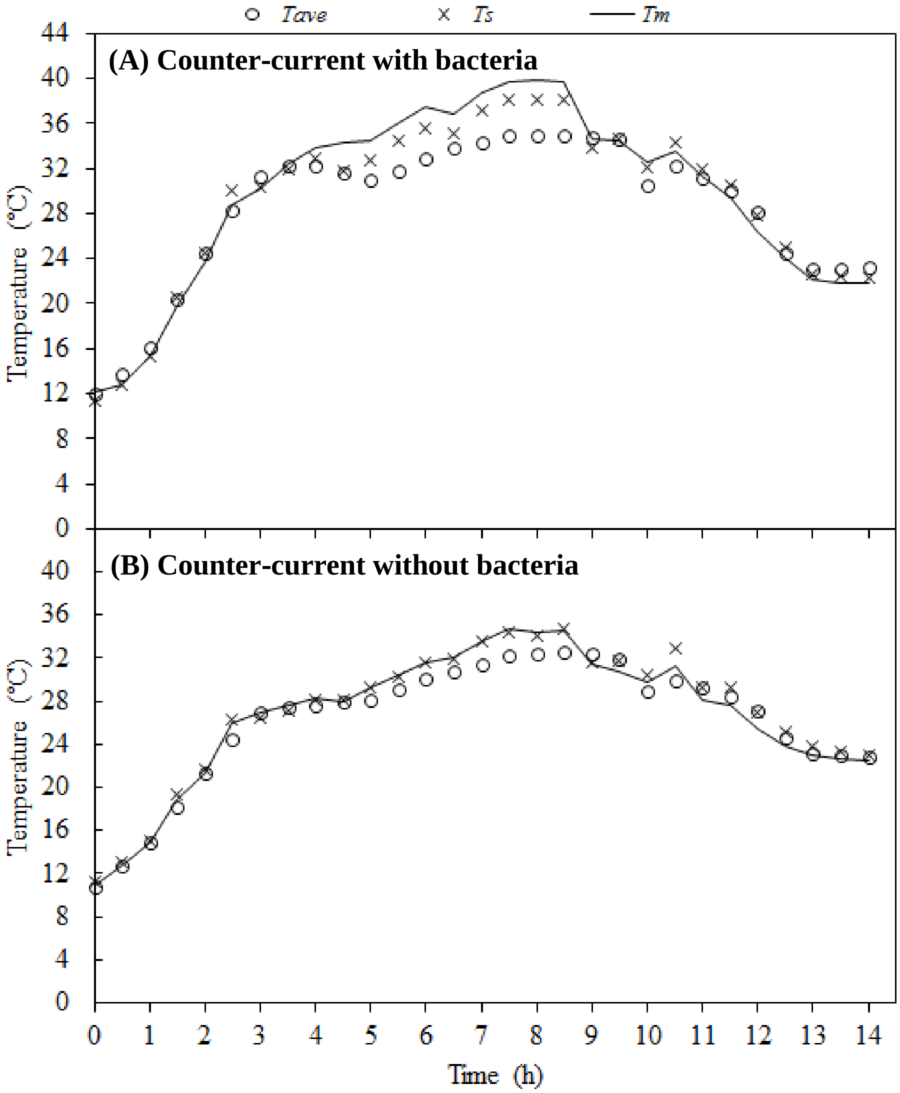

Figure J.15 Comparison of the changes in the reactor average temperatures T_{ave} (o), the reactor surface temperatures T_s (x) and the predicted (model) temperatures T_m (–) with time. The experiments were performed on the 7th of August, 2013 using counter-currently cooled reactors with and without *Rhodobacter capsulatus* YO3 cultures operated in outdoor conditions.

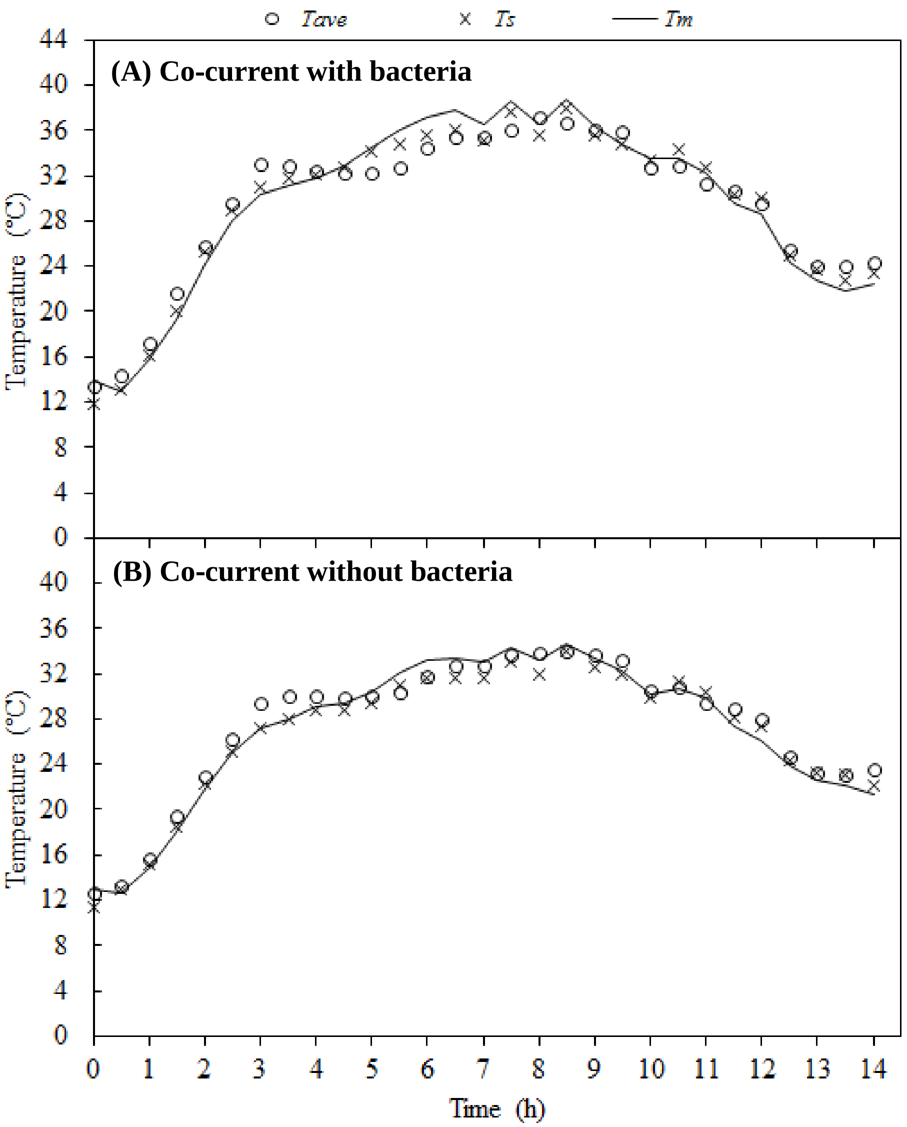

Figure J.16 Comparison of the changes in the reactor average temperatures T_{ave} (o), the reactor surface temperatures T_s (x) and the predicted (model) temperatures T_m (–) with time. The experiments were performed on the 8th of August, 2013 using counter-currently cooled reactors with and without *Rhodobacter capsulatus* YO3 cultures operated in outdoor conditions.

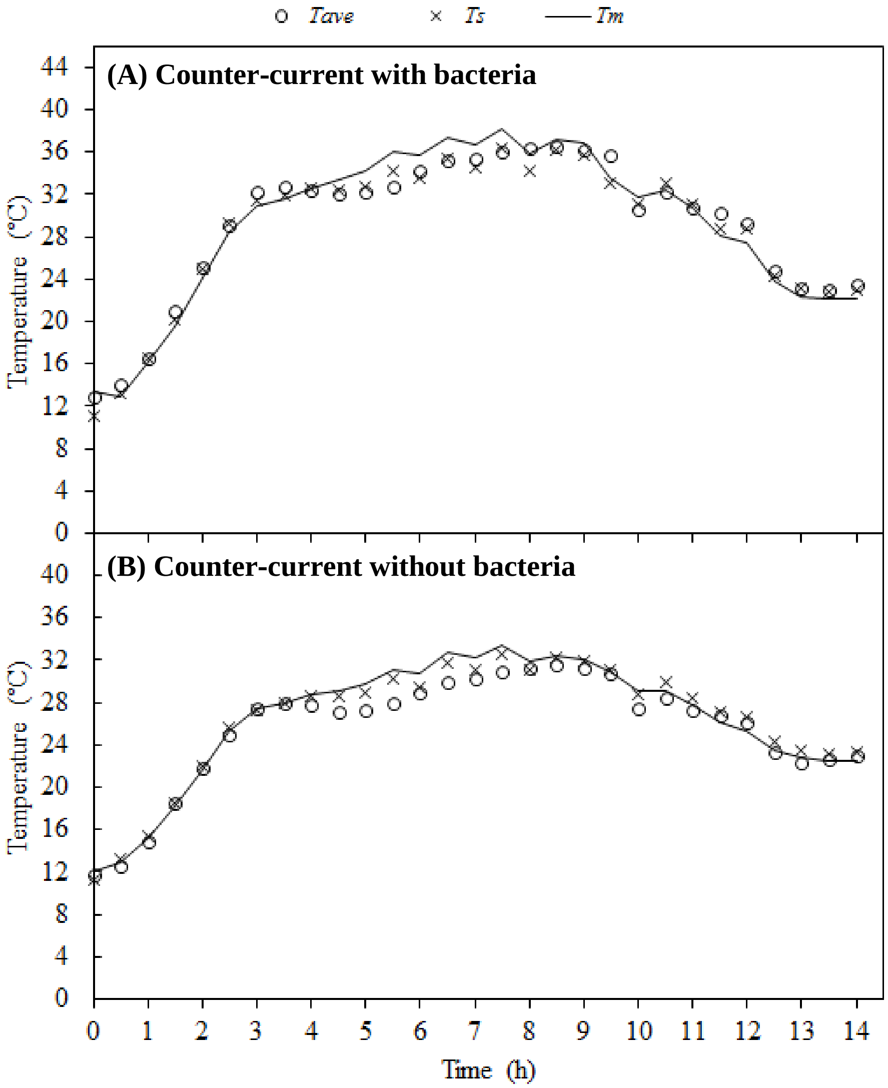

Figure J.17 Comparison of the changes in the reactor average temperatures T_{ave} (o), the reactor surface temperatures T_s (x) and the predicted (model) temperatures T_m (–) with time. The experiments were performed on the 8th of August, 2013 using counter-currently cooled reactors with and without *Rhodobacter capsulatus* YO3 cultures operated in outdoor conditions.

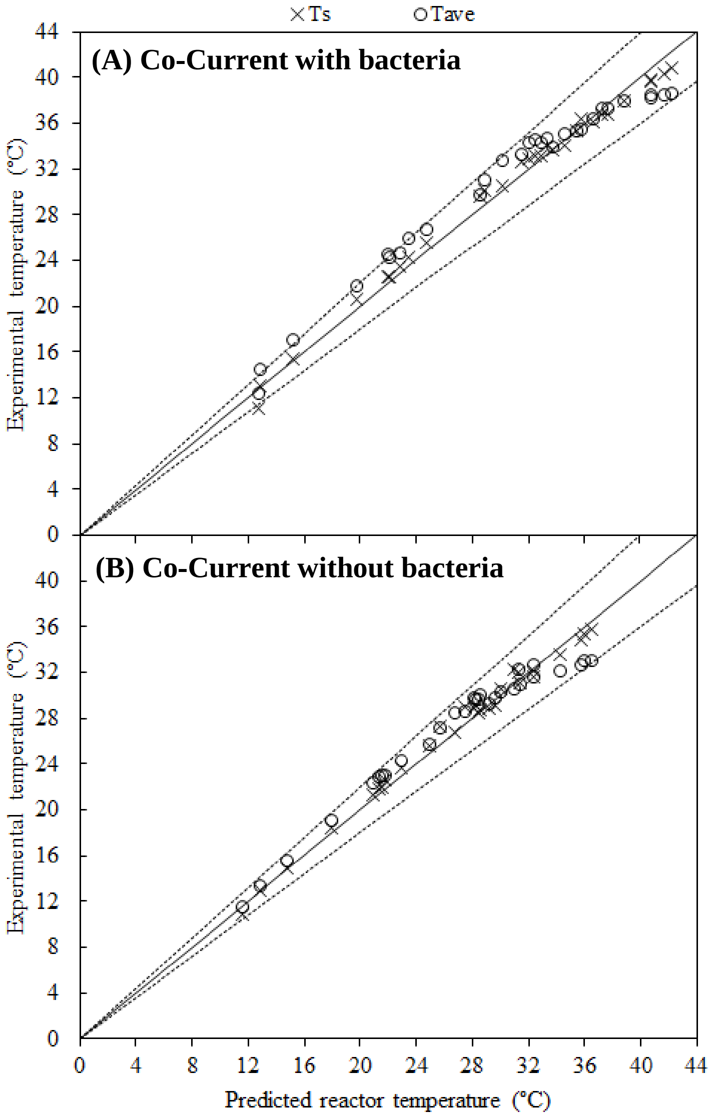

Figure J.18 Comparisons of the experimental reactor surface temperatures T_s (x) and the average reactor temperatures T_{ave} (o) with the predicted reactor temperatures. The dashed lines (·····) indicate the 10 % temperature error margin. The experiments were performed on the 7th of August, 2013 using co-currently reactors with and without *Rhodobacter capsulatus* YO3 cultures operated in outdoor conditions.

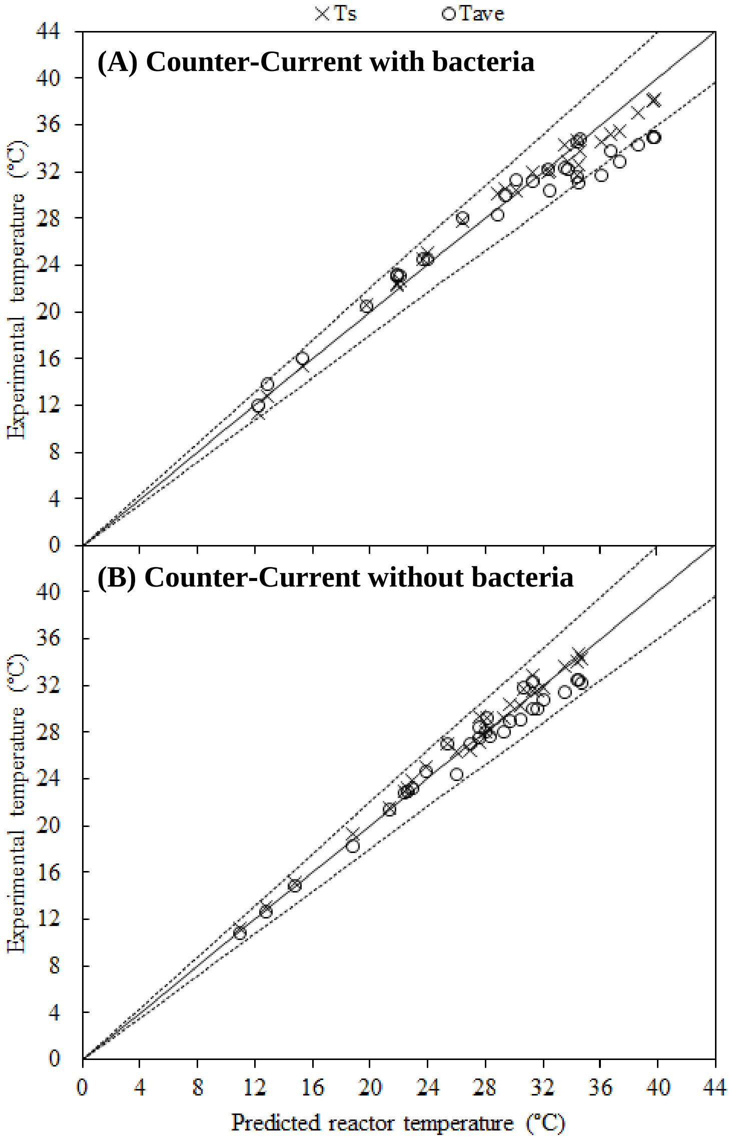

Figure J.19 Comparisons of the experimental reactor surface temperatures T_s (x) and the average reactor temperatures T_{ave} (o) with the predicted reactor temperatures. The dashed lines (·····) indicate the 10 % temperature error margin. The experiments were performed on the 7th of August, 2013 using counter-currently reactors with and without *Rhodobacter capsulatus* YO3 cultures operated in outdoor conditions.

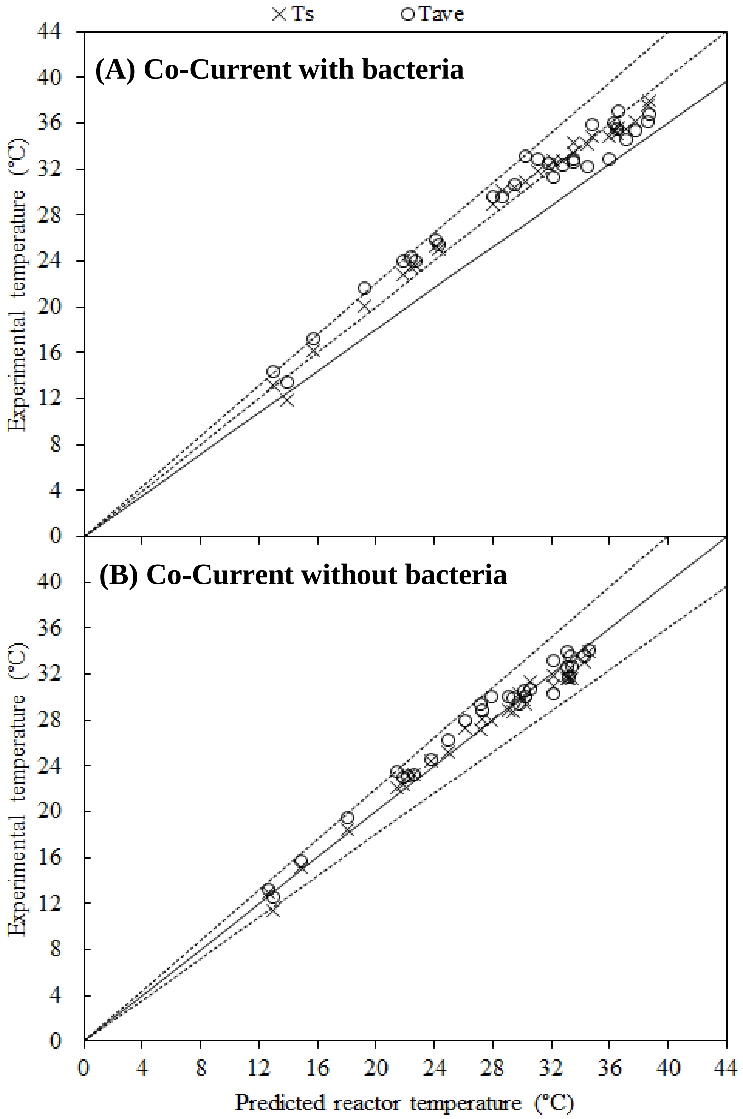

Figure J.20 Comparisons of the experimental reactor surface temperatures T_s (x) and the average reactor temperatures T_{ave} (o) with the predicted reactor temperatures. The dashed lines (·····) indicate the 10 % temperature error margin. The experiments were performed on the 8th of August, 2013 using co-currently reactors with and without *Rhodobacter capsulatus* YO3 cultures operated in outdoor conditions.

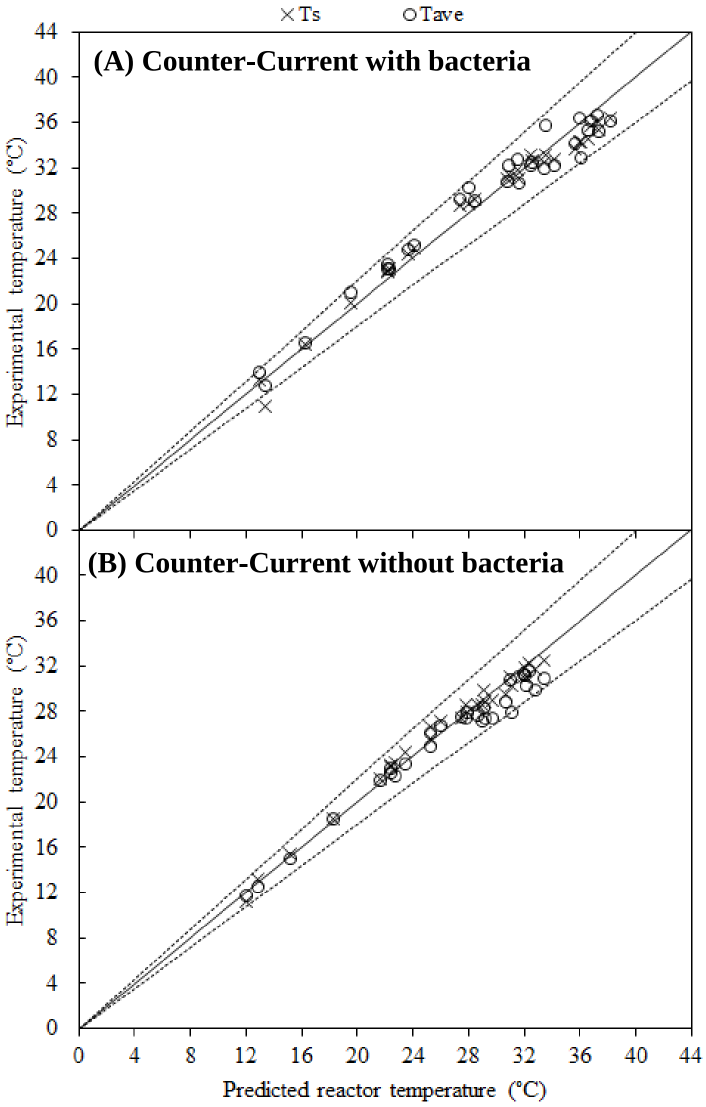

Figure J.21 Comparisons of the experimental reactor surface temperatures T_s (x) and the average reactor temperatures T_{ave} (o) with the predicted reactor temperatures. The dashed lines (·····) indicate the 10 % temperature error margin. The experiments were performed on the 8th of August, 2013 using co-currently reactors with and without *Rhodobacter capsulatus* YO3 cultures operated in outdoor conditions.

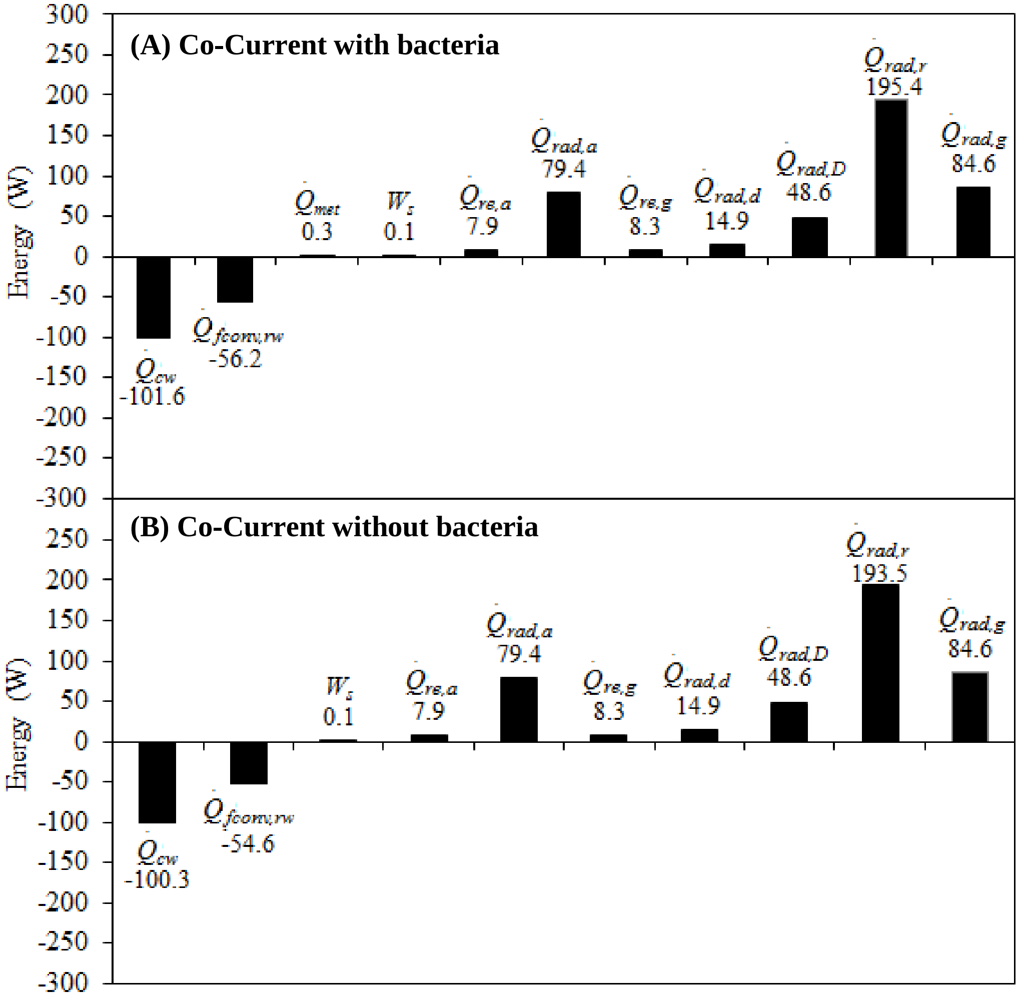

Figure J.22 Comparison of the energy gained or lost during the day time in the outdoor operated reactors. The experiments were performed on the 7th of August, 2013 using co-currently cooled reactors operated outdoors with and without *Rhodobacter capsulatus* YO3 cultures.

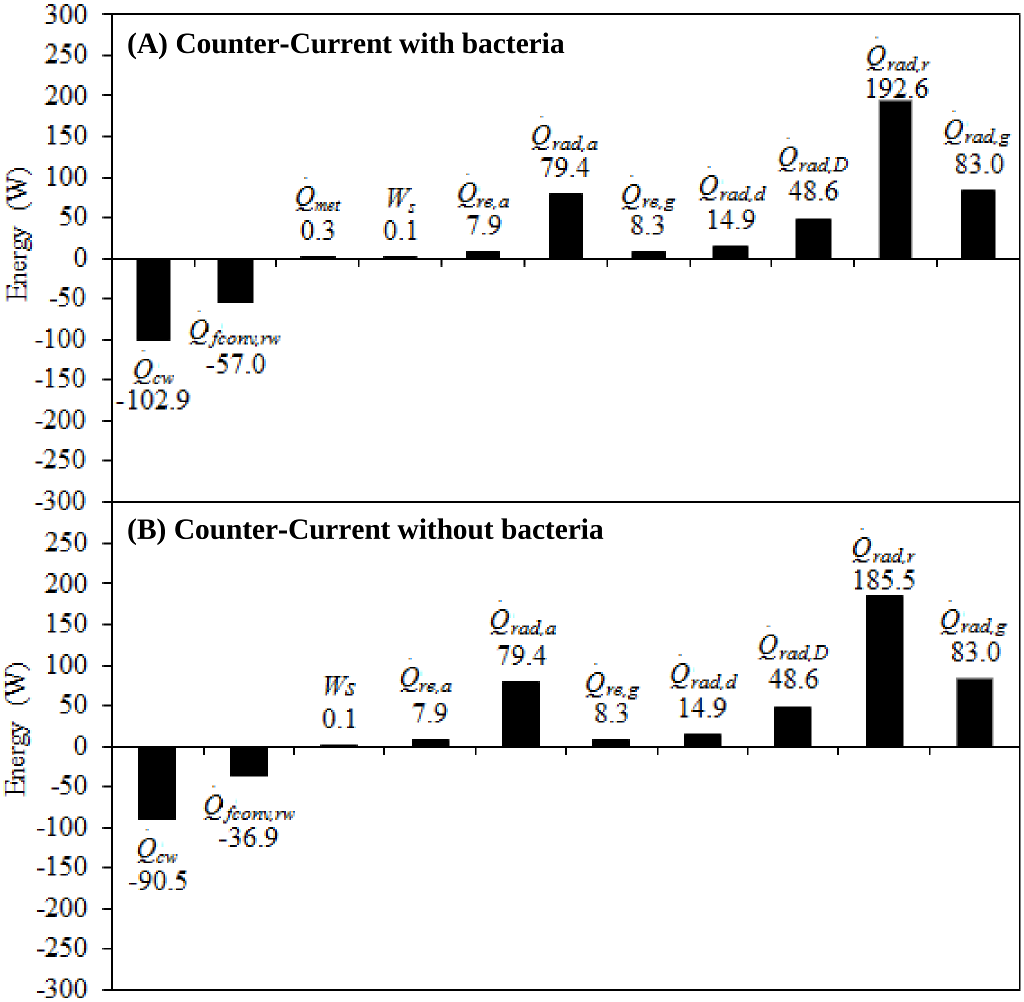

Figure J.23 Comparison of the energy gained or lost during the day time in the outdoor operated reactors. The experiments were performed on the 7th of August, 2013 using counter-currently cooled reactors operated outdoors with and without *Rhodobacter capsulatus* YO3 cultures.

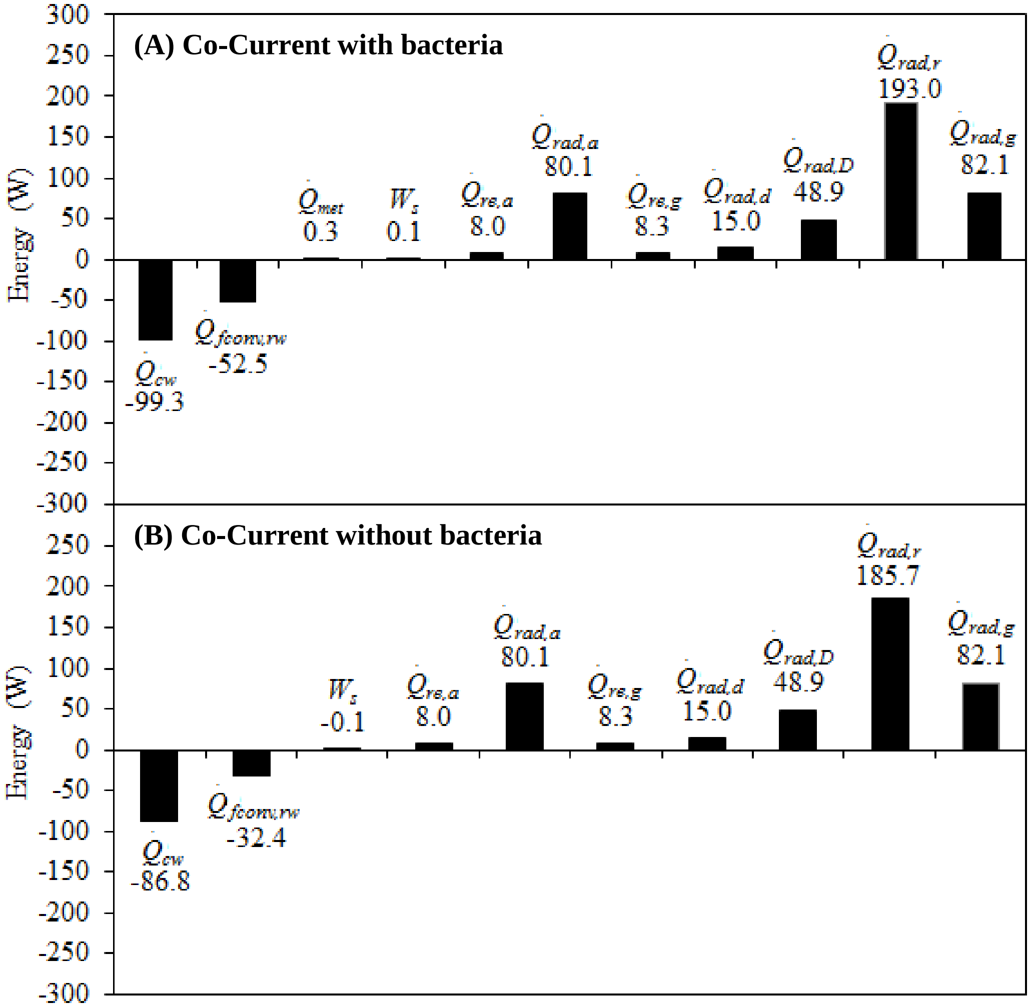

Figure J.24 Comparison of the energy gained or lost during the day time in the outdoor operated reactors. The experiments were performed on the 8th of August, 2013 using co-currently cooled reactors operated outdoors with and without *Rhodobacter capsulatus* YO3 cultures.

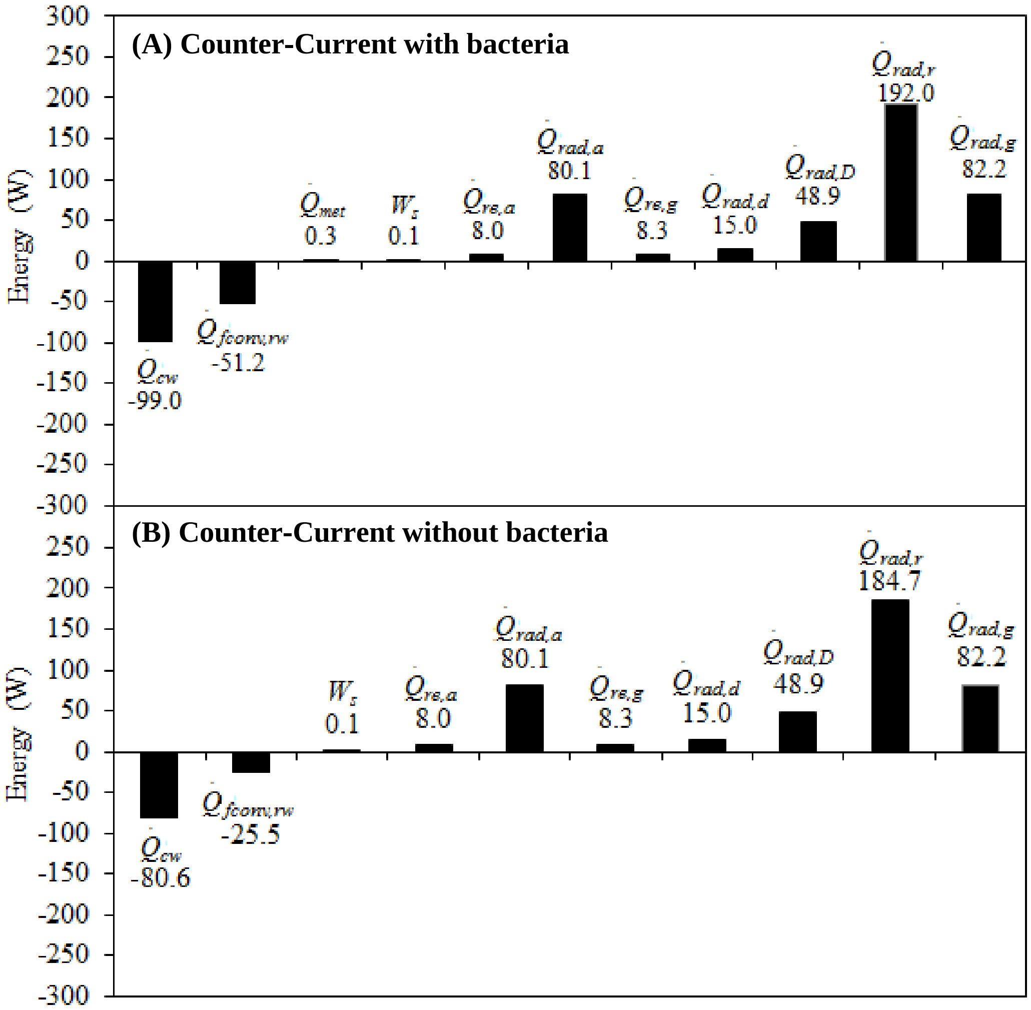

Figure J.25 Comparison of the energy gained or lost during the day time in the outdoor operated reactors. The experiments were performed on the 8th of August, 2013 using counter-currently cooled reactors operated outdoors with and without *Rhodobacter capsulatus* YO3 cultures.

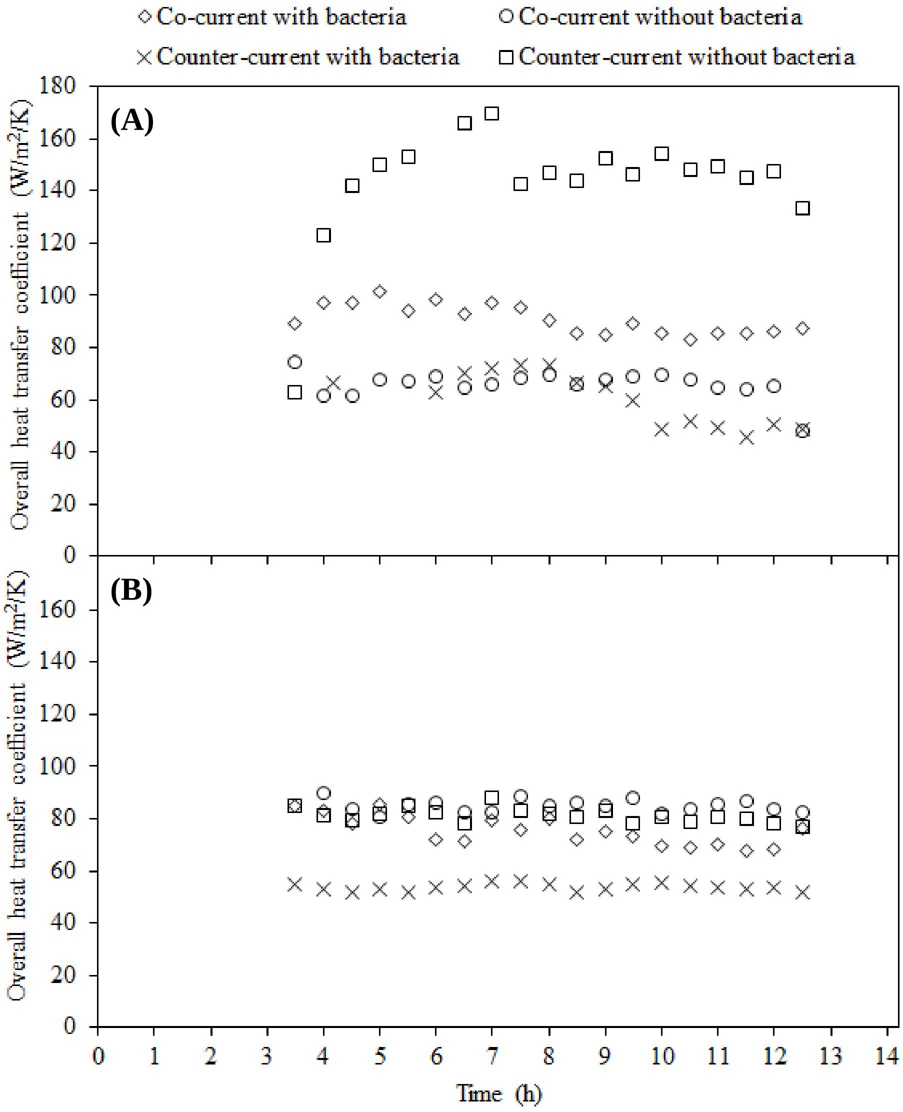

Figure J.26 Comparisons of the overall heat transfer coefficients between the medium in the reactors and the cooling water. The experiments were performed on the: (A) 7th of August, 2013 and (B) 8th of August, 2013 using reactors with and without *Rhodobacter capsulatus* YO3 cultures.

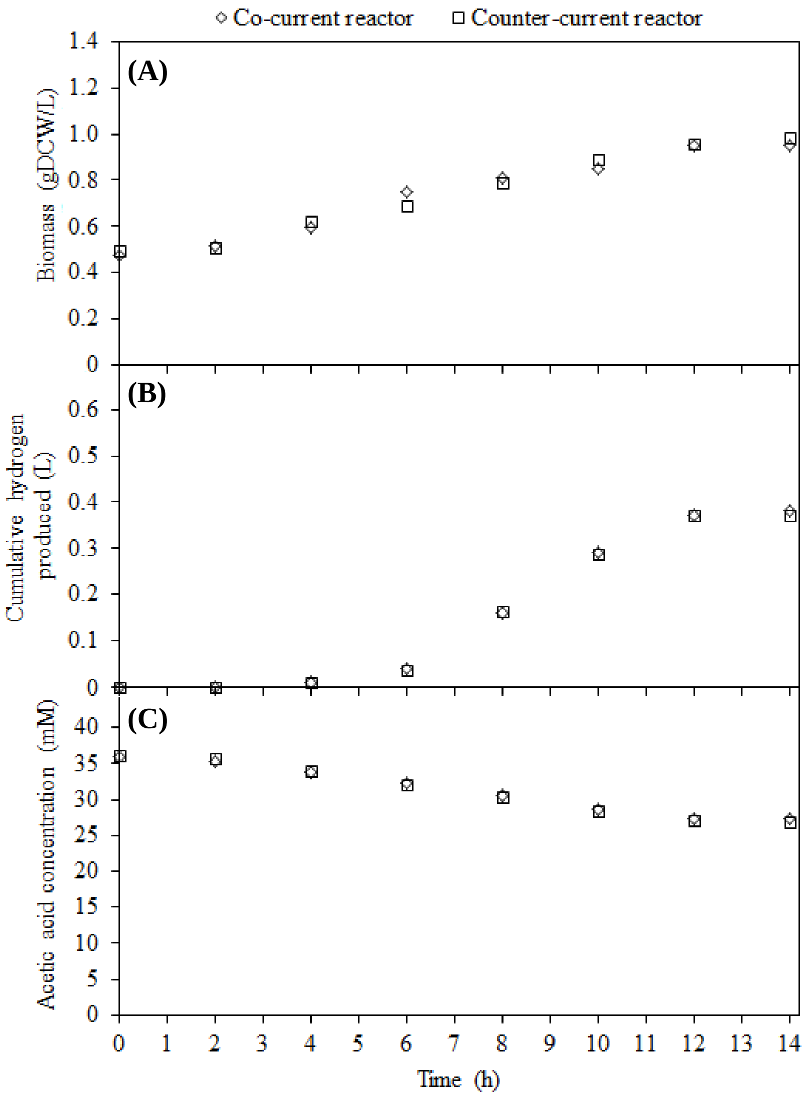

Figure J.27 The change in the biomass concentration, the cumulative hydrogen production and acetic acid concentration in the outdoor reactors with time. The experiments were performed on the 7th of August, 2013 using reactors operated outdoors with and without *Rhodobacter capsulatus* YO3 cultures. (A) Biomass growth, (B) Cumulative hydrogen produced and (C) Acetic acid consumption. (◊) Co-currently cooled reactor and (□) Counter-currently cooled reactor.

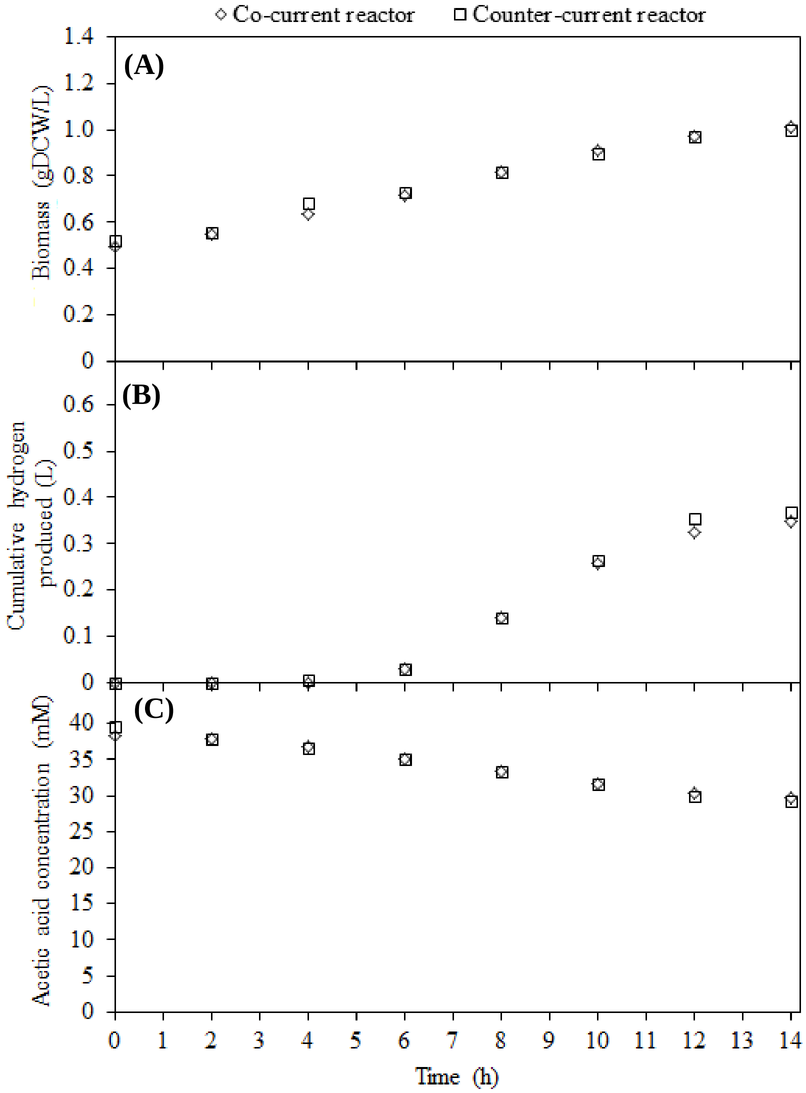

Figure J.28 The change in the biomass concentration, the cumulative hydrogen production and acetic acid concentration in the outdoor reactors with time. The experiments were performed on the 8th of August, 2013 using reactors operated outdoors with and without *Rhodobacter capsulatus* YO3 cultures. (A) Biomass growth, (B) Cumulative hydrogen produced and (C) Acetic acid consumption. (◊) Co-currently cooled reactor and (□) Counter-currently cooled reactor.

Table J.1 Summary of the results showing the acetic acid and glutamate consumption for growth, maintenance and hydrogen production by *Rhodobacter capsulatus* YO3. The experiment was performed on the 7th of August, 2013.

	Co-currently cooled reactor	**Conversion (%)**	**Counter-currently cooled reactor**	**Conversion (%)**
Biomass formed (mol)	0.067	n/a	0.068	n/a
Hydrogen formed (mol)	0.018	n/a	0.018	n/a
Acetate consumed (mol)	0.028		0.029	
• Hydrogen (mol)	0.0045	16	0.0044	15
• Growth (mol)	0.016	56	0.016	54
• Biosynthesis and maintenance (mol)	0.0076	28	0.0093	32
Glutamate consumed (mol)	0.0093	81	0.0095	82
Cumulative hydrogen produced (L)	0.38	n/a	0.37	n/a

Table J.2 Summary of the results showing the acetic acid and glutamate consumption for growth, maintenance and hydrogen production by *Rhodobacter capsulatus* YO3. The experiment was performed on the 8th of August, 2013.

	Co-currently cooled reactor	**Conversion (%)**	**Counter-currently cooled reactor**	**Conversion (%)**
Biomass formed (mol)	0.072	n/a	0.066	n/a
Hydrogen formed (mol)	0.016	n/a	0.018	n/a
Acetate consumed (mol)	0.027		0.033	
• Hydrogen (mol)	0.0041	15	0.0044	13
• Growth (mol)	0.017	62	0.015	47
• Biosynthesis and maintenance (mol)	0.0063	23	0.013	40
Glutamate consumed (mol)	0.010	79	0.0092	73
Cumulative hydrogen produced (L)	0.35	n/a	0.37	n/a

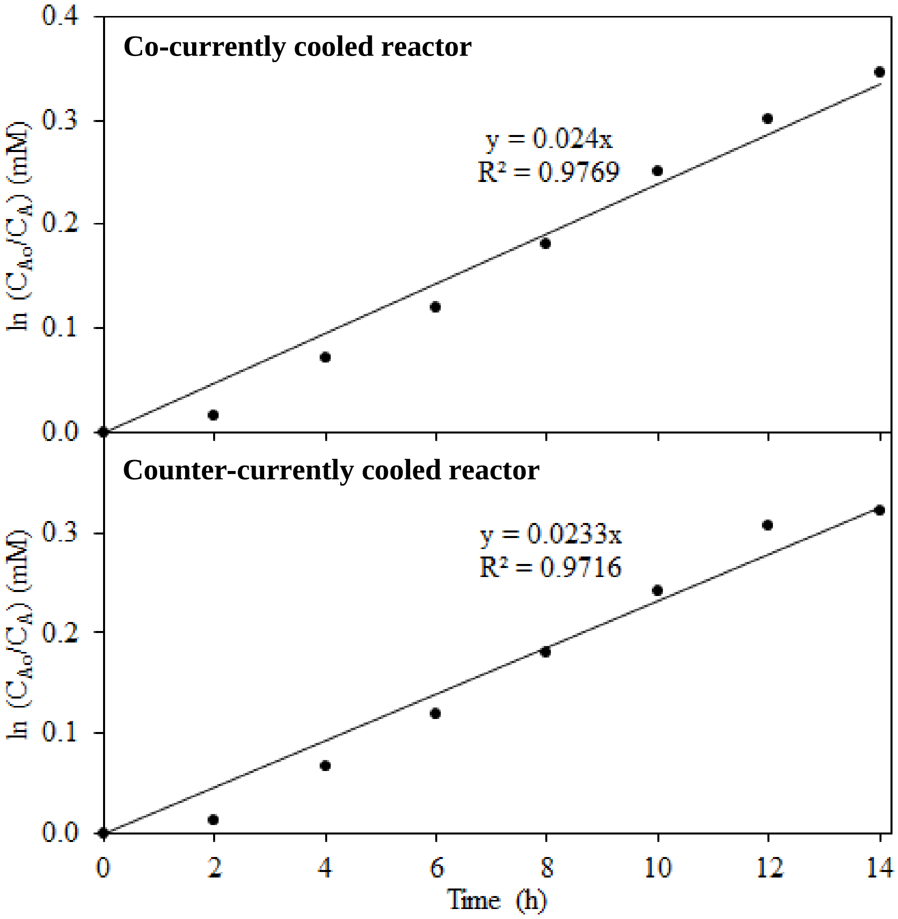

Figure J.29 The first order rate kinetics consumption of acetic acid by *Rhodobacter capsulatus* YO3 cultures grown in outdoor conditions. The experiments were performed on the 5th of August, 2013.

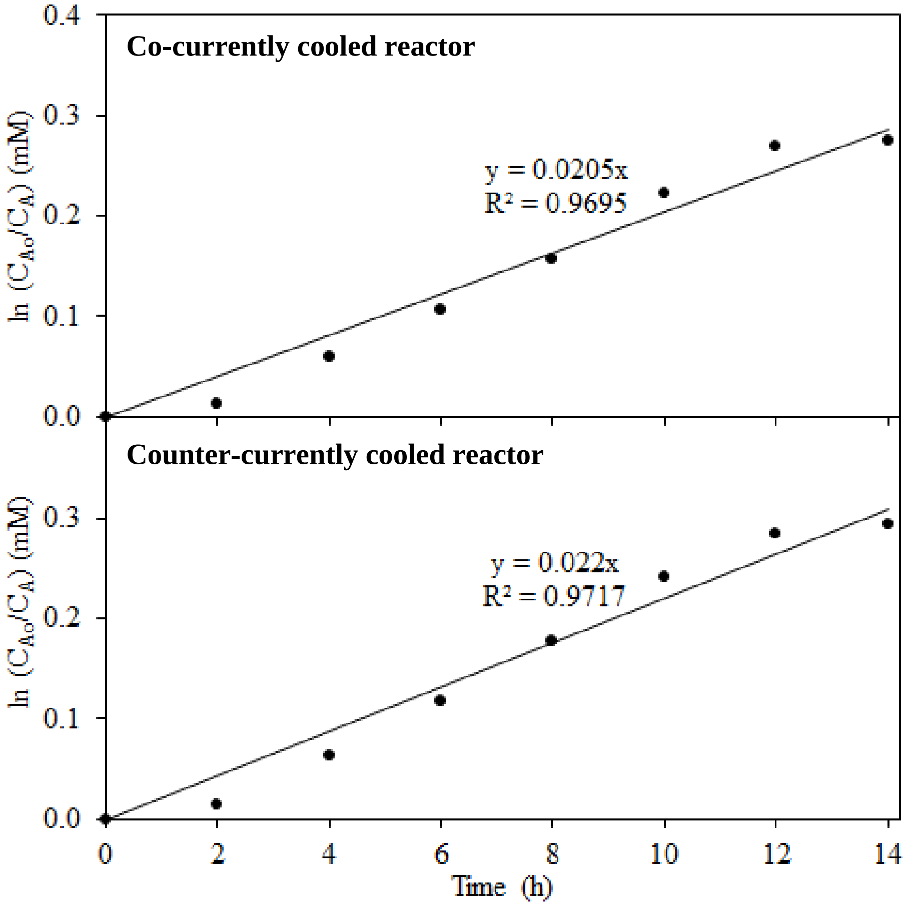

Figure J.30 The first order rate kinetics consumption of acetic acid by *Rhodobacter capsulatus* YO3 cultures grown in outdoor conditions. The experiments were performed on the 7th of August, 2013.

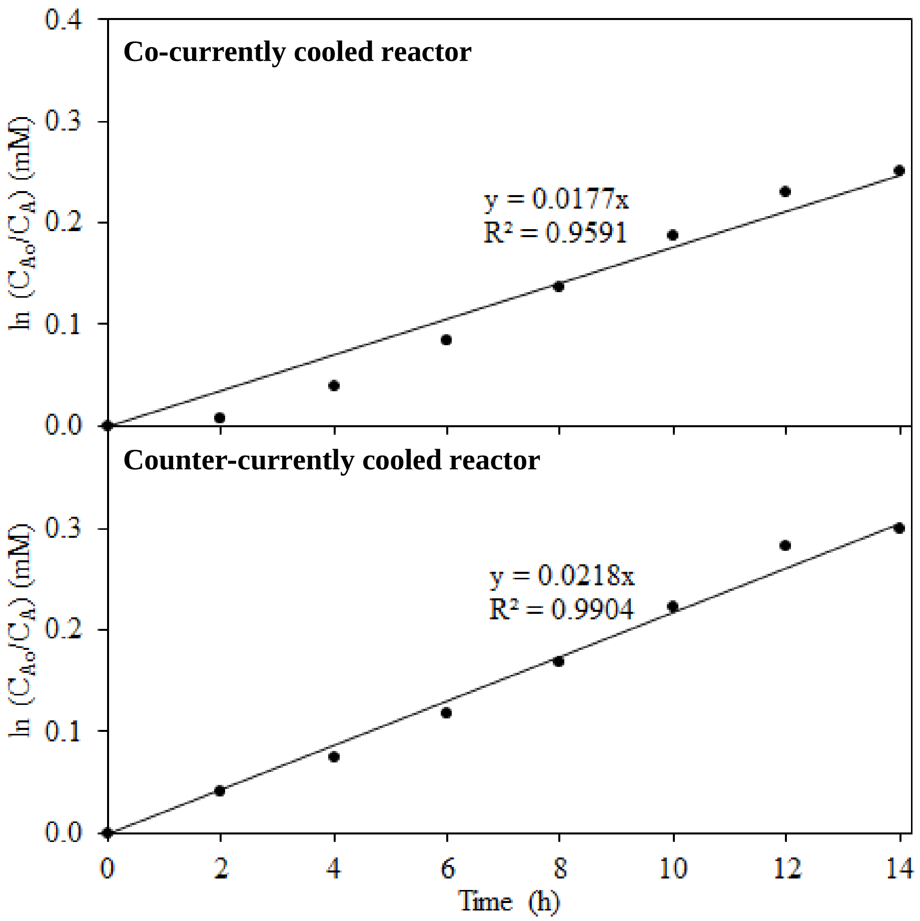

Figure J.31 The first order rate kinetics consumption of acetic acid by *Rhodobacter capsulatus* YO3 cultures grown in outdoor conditions. The experiments were performed on the 8th of August, 2013.

CURRICULUM VITAE

Personal Information

Surname, Name: Androga, Dominic Deo

Nationality: Ugandan

Date and Place of Birth: 18th September, 1984, Moyo, Uganda

Phone: (+90) 312 210 4397

email: dominicdeo@gmail.com

Education

Degree	Institution	Year of Graduation
PhD	METU Biotechnology	2014
Msc.	METU Chemical Engineering	2009
Bsc.	METU Chemical Engineering	2007
High School	Light Academy, Nairobi, Kenya	2001

Work Experience

Position	Place	Year
Research Scientist	METU, Hydrogen Research Laboratory, Ankara, Turkey	2007 – 2014
Intern, Chemical Engineer	Nakasero Soap Works Ltd., Kampala, Uganda	August 2006
Intern, Chemical Engineer	Tepe Betopan Inc., Ankara, Turkey	June and July, 2005

Scholarships

- **2003 – 2007** The Prime Ministry of Turkey Scholarship award for foreign nationals, Ankara, Turkey.
- **2009 – 2013** The Scientific and Technological Research Council of Turkey (TUBITAK) Scholarship award program (Code 2215) for foreign students, Ankara, Turkey.

Publications

Book Chapter

1. Androga, D.D, Özgür, E., Gündüz, U., Yücel, M., Eroglu, I., 2012, “Photofermentative hydrogen production in outdoor conditions”, In: Hydrogen Energy - Challenges and Perspectives. Editors: Minic, D., InTech, Rijeka, Croatia, 77 – 120.

Articles Published in International Journals

1. Androga, D.D., Sevinç, P, Koku, H., Yücel, M., Gündüz, U., Eroglu, I, 2014, “Optimization of temperature and light intensity for improved photofermentative hydrogen production using *Rhodobacter capsulatus* DSM 1710”, International Journal of Hydrogen Energy, 39:2472 – 2480.
2. Androga, D.D, Özgür, E., Gündüz, U., Yücel, M., Eroglu, I., 2012, “Amelioration of Photofermentative Hydrogen Production from Molasses Dark Fermenter Effluent by Zeolite-Based Removal of Ammonium Ion”, International Journal of Hydrogen Energy, 37:16421 – 16429.
3. Androga, D.D, Özgür, E., Gündüz, U., Yücel, M., Eroglu, I., 2011b, ‘‘Factors affecting the long-term stability of biomass and hydrogen productivity in outdoor photofermentation’’, International Journal of Hydrogen Energy, 36: 11369 – 11378.
4. Androga, D.D., Özgür, E., Eroglu, I., Gündüz, U., Yücel, M., 2011a, ‘‘Significance of carbon to nitrogen ratio on the long-term stability of continuous photofermentative hydrogen production’’, International Journal of Hydrogen Energy, 36: 15583 – 15594.

Conference Proceedings

1. Androga, D.D, Özgur, E., Eroglu, I., Gündüz, U., 2010, “Hydrogen Production by Photosynthetic Bacteria *Rhodobacter capsulatus* YO3 (hup^-) Strain on Acetate in Continuous Panel Photobioreactors”, In the 18th World Hydrogen Energy Conference, WHEC 2010: Parallel Sessions Book 2: Hydrogen Production Technologies–Part 1. Editors: Stolten, D., Grube, T.,

Forschungszentrum Jülich GmbH, Zentralbibliothek, Verlag, WHEC May 16th – 21st 2010, Essen, 17 – 22.

Articles in Preparations

1. Implementation and analysis of temperature control strategies for outdoor photobiological hydrogen production.
2. Dynamic modeling of temperature change in outdoor operated tubular reactors for biohydrogen production.

Conferences and Presentations

Poster Presentations

1. Sevinç, P., Androga, D.D., Eroglu, I., Gündüz, U., Yücel, M., "Optimization of Temperature and Light Intensity for Improved Photofermentative Hydrogen Production Using *Rhodobacter capsulatus* DSM 1710", 15th European Congress on Biotechnology, 23th – 26th September, Istanbul, Turkey.
2. Avcioglu, S.G., Androga, D.D., Uyar, B., Özgur, E., Gündüz, U., Yücel, M., Eroglu, I., "Continuous Hydrogen Production by *Rhodobacter capsulatus* on Acetate in Panel Photobioreactors in Outdoor Conditions", International Symposium on Biotechnology: Developments and Trends, 27th – 30th September, 2009, Middle East Technical University, Ankara, Turkey.

Workshops

1. Androga, D.D., Sevinç, P., Gürgan, M., Sağir, E., "1st German-Turkish Workshop on Biogas Research Turkey", Izmir, Ege University, 19th – 20th of October, 2011.

Oral Presentataions

1. Androga, D.D., Koku, H., Uyar, B., Eroglu, I., "Implementation and Analysis of Temperature Control Strategies for Outdoor Photobiological Hydrogen Production", The 20th World Hydrogen Energy Conference (WHEC), June 15th – 20th, 2014, Gwangju Metropolitan City, South Korea.

2. Androga, D.D., Özgür E, Eroglu I, Yücel M, Gündüz U., “Improvement of Integrated Dark-Photofermentation Biological Hydrogen Production Processes by Removing Ammonium Ion”, The International Conference on Hydrogen Production Technologies (ICH2P–11), June 19th – 22nd, 2011, Thessaloniki, Greece.
3. Androga, D.D, Özgür, E., Gündüz, U., Yücel, M., Eroglu, I., ‘‘Factors affecting the long-term stability of biomass and hydrogen productivity in outdoor photofermentation’’, The International Conference on Hydrogen Production Technologies (ICH2P–10), June 15th – 18th, 2010, Istanbul, Turkey.
4. Androga, D.D, Özgur, E., Eroglu, I., Gündüz, U., “Hydrogen Production by Photosynthetic Bacteria *Rhodobacter capsulatus* YO3 (hup$^-$) Strain on Acetate in Continuous Panel Photobioreactors”, The 18th World Hydrogen Energy Conference (WHEC), March 16th – 21st, 2010, Essen, Germany.
5. Avcioglu, S.G., Androga, D.D., Uyar, B., Özgur, E., Gündüz, U., Yücel, M., Eroglu, I., “Continuous Hydrogen Production by *Rhodobacter capsulatus* on Acetate in Panel Photobioreactors”, Paper presented in the VIII Hydrogen Power Theoretical and Engineering Solutions International Symposium (HYPOTHESIS) on hydrogen production conference, April 1st – 3rd, 2009, Lisbon-Portugal.